University of Reading

Developing a virus-like particle (VLP) Polio vaccine

Thesis submitted for a PhD

School of Biological Sciences

Sarah Altalhi

September 2025

Declaration of original authorship

I confirm that this is my own work and the use of all material from other sources has been properly and fully acknowledged.

Sarah Altalhi

Abstract

Poliovirus (PV) is a subtype of the enterovirus C species widely known as the agent responsible for poliomyelitis, a destruction of neurons that can result in paralysis and death. Control of the infection is achieved by vaccination with either a live-attenuated oral poliovirus vaccine (OPV) or an inactivated poliovirus vaccine (IPV), with global coverage reaching nearly 100%. As cases of the natural infection fall, the manufacture of the current vaccines, both of which rely of large-scale virus growth, present a biosafety risk and PV vaccines developed in the absence of live virus are desirable to address vaccine production to maintain PV global vaccination. Virus-like particles (VLPs), which are incapable of infection, made of the assembled viral capsid proteins synthesized in recombinant expression systems, represent a promising infection-free vaccine for PV. This study produced the capsid proteins VP0, VP1, and VP3 in *E.coli* and baculovirus expression systems and assessed both their expression levels and their ability to assemble into virus-like particles. To avoid protein aggregation in the *E.coli* system each protein was fused to the SUMO-tag and purified individually for SUMO tag removal and attempted VLP assembly. Novelly, *E.coli* strains were transformed with all three vectors simultaneously and processed similarly. Despite these modifications, SUMO tagged capsid proteins remained largely insoluble and the low levels present in the soluble fractions failed to be cleaved by the SUMO protease. In the baculovirus system the P1 precursor protein, co-expressed with 3C protease, gave rise to the authentic cleavage pattern and modification at both the N- and C- termini were investigated as a means to improve expression levels. A range of mutations aimed at optimizing the N-myristoylation reaction revealed several that were associated with increased levels of cleaved mature capsid proteins. Further, modification of the C-terminus, including short truncations of the VP1 sequence, was shown to benefit expression level. In a final study, mutations in VP4, previously reported in the live virus to abrogate the virus entry reaction, were investigated in the VLP system. Individual mutations at VP4 residues 24, 28 and 29 were shown to significantly alter expression levels and further analysis of these changes within the VP0 protein only were studied following VP0 fusion to Green Fluorescent Protein (GFP). The outcome of these studies showed that single residue changes in VP4 in the context of VP0 can significantly affect protein expression level and subcellular localization.

Overall, these studies suggest that optimization of the P1 sequence can improve the levels of PV protein expressed. However, when tested, the antigenicity of the PV VLPs detected was predominantly in the H (heated) rather than the N (native) form suggesting that none of the alterations tested resulted in a VLP conformation required for vaccine use.

Acknowledgements

I would like to express my deepest gratitude to Professor Ian Jones for his academic support, guidance, advice, and dedication throughout my studies. I am especially thankful to Dr. Jay Mulley for her assistance with this research project.

I gratefully acknowledge the financial support provided by the Ministry of Education in Saudi Arabia.

I would also like to thank the wonderful and supportive members of Professor Ian's group Silvia Loureiro, Sophie Jegouic, and Wafaa Aly for their technical support and help. My sincere thanks also go to my friends, Salihah Al Alyan and Iris Kabelo, for their kindness and cooperation.

Last but not the least, I wish to express my profound gratitude to my family: my father Hamed, my mother Aida, my husband Majed, my daughters Rima and Roaa, and my sons Muath and Mohannad. Your patience, love, and constant encouragement sustained me throughout this journey.

Table of Contents

List of Abbreviations

AcMNPV	*Autogapha californica* multi-nuclear polyhedrosis virus
BHK21	baby hamster kidney 21
BEVS	baculovirus expression vector system
BV	budded virus
CAd-V1	Canine Adenovirus Type 1
CNS	central nervous system
CSF	cerebrospinal fluid
CHO	Chinese hamster ovary
cVDPV	circulating vaccine-derived poliovirus
CV	coxsackievirus
CVB3	coxsackievirus B3
CAR	coxsackievirus-adenovirus receptor
CPE	cytopathic effect
CTL	cytotoxic T lymphocyte
DNA	deoxyribonucleic acid
EM	electron microscope
ER	endoplasmic reticulum
EV	enterovirus
ELISA	Enzyme-Linked Immunosorbent Assay
FACS	Fluorescence-Activated Cell Scanning
FMDV	Foot-and-mouth disease virus
gSTED	Gated-Stimulated Emission Depletion
GPEI	Global Polio Eradication Initiative
GST	glutathione S-transferase
GALT	Gut associated lymphoid tissue
HFMD	hand-foot-and-mouth disease
HAV	Hepatitis A virus
HBV	Hepatitis B virus
HBsAg	hepatitis B virus surface antigen
HCV	Hepatitis C virus
HEV	Hepatitis E virus
h	hours
HPV	Human papilloma virus
Ig	immunoglobulin

IgA	immunoglobulin A
IgG	Immunoglobulin G
IgM	Immunoglobulin M
IPV	inactivated polio vaccine
ICAM-l	inter-cellular adhesion molecule 1
INF	interferon
IRES	internal ribosome entry site
ICTV	International Committee on Taxonomy of Viruses
IHR	International Health Regulation
IPTG	isopropyl β-D-1-thiogalactopyranoside
kDa	kilodaltons
LLPS	liquid-liquid phase separation
MBP	maltose-binding protein
mRNA	messenger RNA
min	minutes
MVA	modified vaccinia virus Ankara
MW	molecular weight
MOI	multiplicity of infection
NIBSC	National Institute for Biological Standards and Control
NMT	N-myristoyl transferase
NTR	non-translated region
nOPV2-CD	Novel Oral Poliovirus Vaccine type 2 – CodonDeoptimized
NPVs	Nucleopolyhedroviruses
OBs	occlusion bodies
ODV	occlusion derived virus
ORF	Open Reading Frame
OD	optical density
OPV	oral polio vaccine
PAMPs	pathogen associated molecular patterns
PFU	plaque-forming units
PV	Poliovirus
PVR	poliovirus receptor
PCR	polymerase chain reaction
P1, P2 and P3	Polyprotein 1,2 and 3
PTMs	post-translational modifications
RT-PCR	reverse transcription polymerase chain reaction

RV	rhinovirus
RNA	ribonucleic acid
RdRp	RNA-dependent RNA polymerase
RT	Room temperature
s	seconds
SIgA	secretory Immunoglobulin A
SUMO	Small Ubiquitin-Like Modifier
SDS-PAGE	Sodium dodecyl sulphate polyacrylamide gel electrophoresis
TEM	Transition Electron Microscopy
UV	Ultraviolet
UTR	untranslated region
VAPP	Vaccine-associated paralytic polio
VDPV	vaccine-derived PV
VP	viral protein
VPg	viral protein genome-linked
VLP	Virus-Like-Particle
WB	Western blot
WPV1	Wild poliovirus 1
WT	wild type
WHO	World Health Organisation

Chapter 1 Introduction

1.1 Overview

Poliovirus (PV) was discovered by Landsteiner and Popper in 1909 and is one of the most famous viruses in history. In addition to the disease, it has played a fundamental role in virology as a model for studying the initiation of infection and the viral life cycles (Hogle, 2002). PV has a non-enveloped icosahedral protein capsid with a positive-sense (+ve) single stranded (ss) RNA genome (Blondel *et al.*, 2005). There are three different serotypes of Poliovirus, PV1, PV2, and PV3 belonging to the species Enterovirus C within the genus Enterovirus in the *Picornaviridae* family. PV is transmitted between people via the faecal-oral route and whilst the majority of infections are asymptomatic or mild, some infections can cause significant damage to motor neurons, leading to poliomyelitis (Baicus, 2012). Two effective polio vaccines, the Salk inactivated polio vaccine (IPV) and the Sabin oral polio vaccine (OPV), were developed in the 1950s and 1960s, respectively (Wimmer *et al.*, 1993) .While these two vaccines have been instrumental in reducing the number of PV infections worldwide since their implementation, wild PV remains endemic in Afghanistan and Pakistan. The attenuated PV in OPV can also mutate in rare cases leading to human-human transmission of vaccine-derived PV in under-immunized populations. According to the most recent update from the International Health Regulations (IHR), nine cases of wild poliovirus type 1 (WPV1) have been reported in 2025, with one case in Afghanistan and eight in Pakistan. As of the latest reporting period, a total of 67 cases of circulating vaccine-derived poliovirus (cVDPV) have been documented globally in 2025, comprising 65 cases of cVDPV type 2 (cVDPV2) and two cases of cVDPV type 3 (cVDPV3). No cases of cVDPV type 1 (cVDPV1) have been reported to date in 2025(IHR, 2025). These data underscore the continued need for sustaining global mass vaccination efforts against poliovirus.

The continued manufacture of current PV vaccines, which depends on large-scale production of live PV, raises considerable biosafety issues. Therefore, developing PV vaccines that do not require live viruses is crucial for maintaining global immunization efforts. VLP vaccines have been available for clinical use for years and are safe and effective against Hepatitis B (HBV), Human papillomavirus (HPV) and Hepatitis E (HEV) (Cutts *et al.*, 2007; Pushko *et al.*, 2007; Wu *et al.*, 2012). This study examines the expression of empty PV capsids in two chosen foreign expression system and examined potential enhancements in capsid yield that may also enhance immunogenicity, which could boost the expected acceptance of VLP as a candidate vaccine.

1.2 Classification of Poliovirus

Poliovirus (PV) is classified within the *Enterovirus* genus in the *Picornaviridae* family, which includes 63 genera and 147 species. Different species of Picornavirus cause infections in humans or other animals, which may be asymptomatic or lead to diseases that range from minor febrile illnesses to more severe diseases affecting the liver, heart, or central nervous system (ICTV, 2025). Most Picornaviruses cause infections in one or only a few host species, although there are a few notable exceptions with a broader host range including foot-and-mouth disease virus (FMDV, genus *Aphthovirus*) which has been isolated from at least 70 species of mammals, mainly cloven-hoofed animals such as cows, sheep, pigs, goats and deer. In addition to PV, other important human pathogens in the *Picornaviridae* family include hepatitis A virus, rhinoviruses, coxsackieviruses, echoviruses and enteroviruses **(Table 1)**.

There are a number of different human cell surface molecules that serve as viral receptors for viruses within the *Enterovirus* genus, although the specific receptors for many are not well known. The poliovirus receptor (PVR) is CD155, a cell surface glycoprotein involved in cell adhesion and immune modulation that is found on epithelial cells, neurons and some types of white blood cell. The coxsackievirus-adenovirus receptor (CAR) is the receptor for coxsackie B viruses, whilst inter-cellular adhesion molecule 1 (ICAM-l) is the receptor for “major-group" rhinoviruses, and Canine Adenovirus Type 1 (CAd-V1) uses the coxsackievirus and adenovirus receptor (CAR) (ICTV, 2025) .

Table 1. Classification of Picornaviruses that infect humans and the associated diseases they cause. CV: coxsackievirus; EV: enterovirus; E: echovirus; RV: rhinovirus; PV: poliovirus (Simmonds *et al.*, 2020).

Genus	**Species**	**Example Viruses**	**Associated Diseases**
Enterovirus	Enterovirus A	CVA2 → CVA8, CVA10, CVA12, CVA14, CVA16 EV-A71, EV-A76, EV-A89 → EV-A91, EV-A114, EV-A119 → EV-A121	Hand, foot, and mouth disease; viral meningitis
	Enterovirus B	CVA9; CVB1 → CVB6 E1 → E7, E9, E11 → E21, E24 → E27, E29 → E33 EV-B69, EV-B73 → EV-B75, EV-B77 → EV-B88, EV-B93, EV-B97, EV-B98, EV-B100, EV-B101, EV-B106, EV-B107, EV-B111	Myocarditis, pericarditis, aseptic meningitis
	Enterovirus C	CVA1, CVA11, CVA13, CVA17, CVA19 → CVA22, CVA24 EV-C95, EV-C96, EV-C99, EV-C102, EV-C104, EV-C105, EV-C109, EV-C113, EV-C116 → EV-C118 PV1 → PV3	Aseptic meningitis, hand-foot-and-mouth disease (HFMD) Acute respiratory illnesses (inc. pneumonia and bronchiolitis) Mild Febrile illness, Poliomyelitis
	Enterovirus D	EV-D68, EV-D70, EV-D94, EV-D111	Respiratory illness, acute flaccid myelitis, conjunctivitis

Genus	Species	Example Viruses	Associated Diseases
	Rhinovirus A	RV-A1, RV-A2, RV-A7 → RV-A13, RV-A15, RV-A16, RV-A18 → RV-A25, RV-A28 → RV-A34, RV-A36, RV-A38 → RV-A41, RV-A43, RV-A45 → RV-A47, RV-A49 → RV-A51, RV-A53 → RV-A68, RV-A71, RV-A73 → RV-A78, RV-A80 → RV-A82, RV-A85, RV-A88 → RV-A90, RV-A94, RV-A96, RV-A100 → RV-A109.	Common cold
	Rhinovirus B	RV-B3 → RV-B6, RV-B14, RV-B17, RV-B26, RV-B27, RV-B35, RV-B37, RV-B42, RV-B48, RV-B52, RV-B69, RV-B70, RV-B72, RV-B79, RV-B83, RV-B84, RV-B86, RV-B91, RV-B92, RV-B93, RV-B97, RV-B99, RV-B100 → RV-B106	Common cold
	Rhinovirus C	RV-C1 → RV-C57	Common cold
Hepatovirus	Hepatovirus A	HAV	Acute hepatitis

1.3 Structure of Poliovirus

Poliovirus is a small non-enveloped virion measuring about 27 nm in diameter, containing a single strand (ss) of positive polarity (+ve) RNA of 7500 nucleotides (nt) encapsidated within an icosahedral capsid composed of sixty copies of the polypeptides VP1, VP2, VP3 and VP4 as shown in **(Figure 1)** (Wimmer *et al.*, 1993b). The viral RNA serves as an mRNA and consists of a 742-nt 5′ untranslated region (5′ UTR), a single open reading frame encoding the viral polyprotein that is organized into three distinct regions termed P1, P2, and P3, a 68 nt 3′ untranslated region (3′ UTR), and a polyadenosine tract of various lengths (Burrill *et al.*, 2013a). The P1 region contains the four structural proteins VP4, VP2, VP3, and VP1, which come together to form the icosahedral capsid. The P2 and P3 regions encode the non-

structural proteins required for completion of the viral life cycle. Within the P2 region, three non-structural proteins (2A protease, 2B, and 2C) contribute to the restructuring of the host cell membranes during nucleic acid replication. The main proteins involved in replication of the RNA genome, 3C protease, 3D polymerase, and viral protein genome-linked (VPg) (3B; a structural protein) are in the P3 region (Minor, 2014).

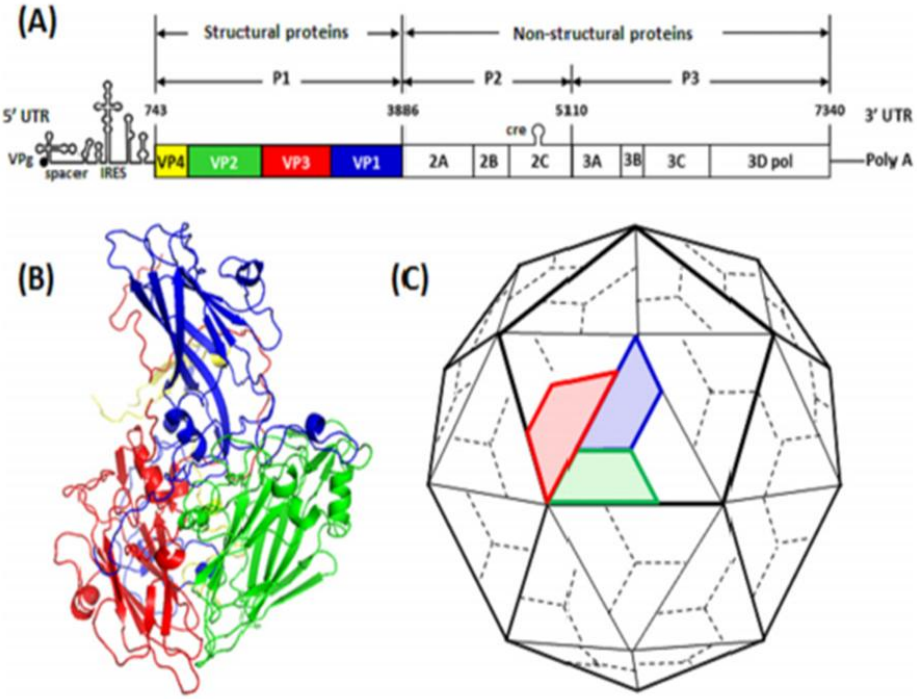

Figure 1. The structure of Poliovirus. A) Poliovirus genome structure; B) Ribbon diagram of poliovirus protomer; C) Model of poliovirus capsid formed by 60 pentamers, each formed from 5 protomers. Blue = VP1, Red = VP3, Green=VP2, Yellow=VP4. Drawings not to scale. Adapted from (Adeyemi *et al.*, 2017).

There are three serotypes of PV: PV1, PV2, and PV3 which have slight differences in the external capsid structure, within the region involved in binding to the cellular receptor that affects virus antigenicity; infection by one serotype therefore does not protect against infection by another serotype (Blondel *et al.*, 1998). There are four neutralizing antigen positions (N-AgI, N-AgII, N-AgIIIA and N-AgIIIB) within the PV capsid N-AgI, and N-AgIIIA are located in VP1 residues 90 - 104, 220 -222, and 286 - 290 respectively, N-AgII in VP2 residues 164 - 175, and N-AgIIIB in VP3 residues 58 - 60, and 71 - 79 (Rombaut *et al.*, 1990; Murdin *et al.*, 1992).

As discussed above, while the structure of the poliovirus particle and of VLPs has advanced considerably in recent years, the structure of VP4, either alone or as part of VP0, remains

largely unknown. Within the available virus structures (Belnap *et al.*, 2000), a short section of the N- and C-termini of VP4 can be seen underlying the protomer, but the majority of the chain, presumably including the section which might interact with RNA or an adjacent promoter, is not resolved. Generally speaking, the lack of a structure indicates a chain which is in constant movement and does not adopt a fixed position within the particle. This would be consistent with the finding that when subjected to folding software VP4 alone is predicted to be a natively unfolded protein with a tendency to undergo liquid-liquid phase separation (Vendruscolo & Fuxreiter, 2022a). Over the course of the studies in this thesis the bioinformatics approach to determining protein structure improved considerably with the development of Alphafold (Jumper *et al.*, 2021). The software uses a combination of sequence alignments and available structures to predict the structure of any sequence submitted. As there are no existing structures of VP4, for any picornavirus, the confidence associated with the use of AlphaFold to determine a VP4 structure will be low. However, the structure can usefully support speculation of how VP4 might act during assembly and provide a base for the comparison of sequence variants that have a biological effect. For this reason, the AlphaFold predicted structure of VP4 was determined **(Figure 2)**.

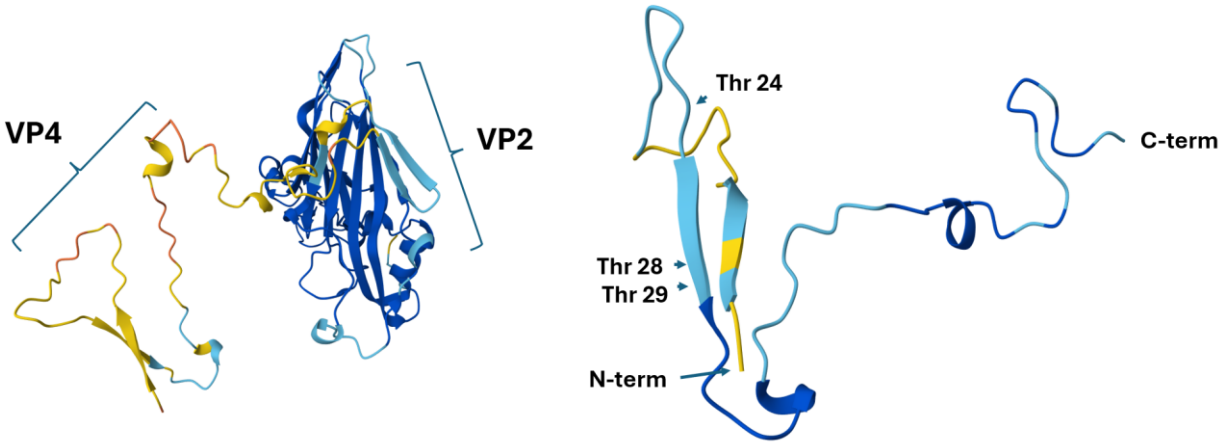

Figure 2. The AlphaFold predicted structure of poliovirus VP4. Left: The VP4 structure as part of VP0. Right: The VP4 structure predicted alone. Colours from dark blue to yellow indicate the confidence of the prediction from high to low. Marked residues feature later in the thesis.

The predicted structure of VP4 as part of VP0 clearly demonstrates the lack of confidence associated with the prediction. The VP2 domain is largely dark blue representing a very highly confident structure as a result of the many capsid structures already available. By contrast the VP4 domain is shown almost entirely in yellow indicating a very low confidence

in the structure. Interestingly confidence improves somewhat when the prediction is done for the VP4 chain alone, essentially an *ab initio* prediction with no available structural template. The N-terminal domain folds back on itself, placing the N-terminus itself, where the myristic acid would be pointing inward. This is very reminiscent of the classical Recoverin structure where the N-terminus is hidden in a hydrophobic groove to form a "calcium-myristoyl switch" which is released for membrane binding (Tanaka *et al.*, 1995). Another notable feature in the N-terminal domain is the short antiparallel β -sheet which is predicted with modest confidence. The inter-connecting strand between the sections of sheets has a very low confidence score possibly consistent with an ability to swing the N-terminal stand out when exposure of the myristate group is required. The remainder of the chain is random apart from a very short section of helix in the middle. It should be stressed again that there can be no certainty that these structural features actually form, especially in the interior of the virus or VLP capsid. Nevertheless, the structure acts as an anchor for the discussion of mutations later in this thesis.

1.4 Replication of Poliovirus

The replication cycle of poliovirus is rapid and productive, with roughly 8 hours elapsing from infection to the release of progeny virions following host cell lysis. During an infection, elevated levels of both the viral proteins and genetic material are synthesised (Burrill *et al.*, 2013). These allow the production of up to 10,000 virions per cell (Kew *et al.*, 2005). Levels of PVR protein expression are restricted to specific cells including vascular endothelial cells, spinal cord motor neurons, and immune cell subsets that correlate with PV dissemination sites (Li *et al.*, 2018). All three serotypes of poliovirus PV1, PV2, and PV3 bind the same receptor, and this interaction leads to uncoating and release of the +ve ssRNA into the cytoplasm (Hogle, 2002). PV enters the cell via an endocytic mechanism **(Figure 3)** and genome release occurs directly following virus particle internalization on the plasma membrane inside tightly sealed vesicles or membrane invaginations sited within 100–200 nm of the cell surface (Brandenburg *et al.*, 2007). Genome uncoating is unaffected by endosome acidification (Perez & Carrasco, 1993), and it is hypothesized that capsid destabilisation involves competition between receptor binding and a cellular lipid moiety, a pocket factor, inside VP1, located in a hydrophobic pocket directly under the floor of a depression around the 5-fold axis, known as the canyon (Rossmann, 1994).

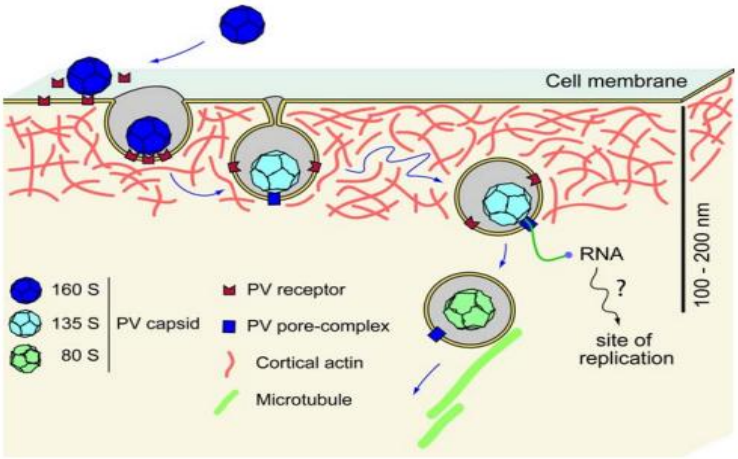

Figure 3. The mechanism of PV entry and uncoating. Binding of mature PV (160S) to the cellular receptor CD155 induces an expansion of the capsid to the 135S form, which is internalized by a mechanism that is clathrin-, caveolin-, flotillin-, and microtubule-independent but tyrosine kinase- and actin-dependent. The viral genome is released immediately following internalization into the endocytotic compartment, generally within 100–200 nm of the plasma membrane. The empty capsid (80S) is lost after the RNA genome is released (Brandenburg *et al.*, 2007).

Once released into the cytoplasm, the poliovirus genomic RNA functions as mRNA, most likely after removal of the 5'-terminal VPg by a cellular enzyme (Wimmer, 1982). Following that, the poliovirus internal ribosome entry site (IRES) initiates translation, resulting in the production of a single polypeptide that is subsequently processed by viral proteases into the mature viral proteins (Hellen *et al.*, 1989). The positive-sense genome is replicated by RNA-dependent RNA polymerase (RdRp) creating a negative-sense strand which is used as a template for genome replication (Schulte *et al.*, 2015). In the early stages of cleavage, the viral 2A protease cleaves the polyprotein, releasing the precursor protein myristoyl-P1 from the polyprotein. Then, the viral 3CD protease cleaves the P1 region, producing the capsid proteins VP1, VP3, and the immature capsid protein myristoyl-VP0. This cleavage allows the formation of the protomer (VP0, VP3 and VP1) which then produces the pentameric assembly intermediate, 12 of which then naturally assemble into an empty capsid containing the final sixty copies of each of VP1, VP3, and VP0 (Molla *et al.*, 1993). The cleavage of VP0 to produce VP4 and VP2 during maturation is linked to late steps in assembly and may necessitate encapsidation of the viral RNA (Wien *et al.*, 1996). In the final stage of poliovirus assembly, the empty capsids encapsidate the genomic RNA linked to the viral protein VPg (**Figure 4**) (Molla *et al.*, 1993).

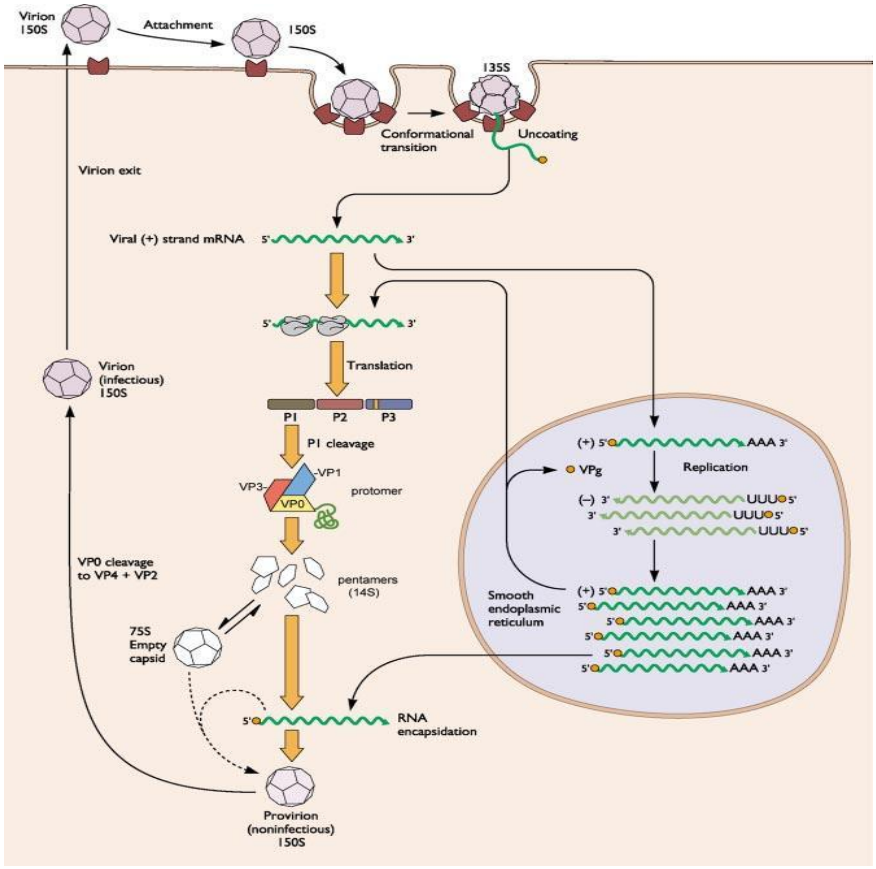

Figure 4. PV Replication Cycle. Poliovirus binds to the CD155 cell receptor, and the virion is taken up by endocytosis. The receptor interaction leads to uncoating and the +ssRNA is released into the cytoplasm of the cell. Translation of the single Open Reading Frame (ORF) leads to production of a single polyprotein that is subsequently cleaved by viral proteases 2A and 3CD. The positive-sense RNA is used as a template for synthesis of negative-strand intermediates, and this is used to produce many copies of positive-sense viral genomes. The viral structural proteins self-assemble first into protomers and then pentamers, and then then fully encapsidate a copy of viral genomic RNA. Progeny viruses are released following lysis of the host cell (Hogle, 2002).

1.5 N-Myristoylation of Poliovirus P1

Protein N-myristoylation describes the covalent binding of myristate, a 14-carbon saturated fatty acid, to the N-terminal glycine of eukaryotic and viral proteins Generally, N-myristoylation is an irreversible modification that happens to proteins while they are being translated, after an initial methionine residue is removed by cellular methionyl aminopeptidases exposing an N-terminal glycine **(Figure 5)** (Farazi *et al.*, 2001). A

significant number of viral and cell proteins undergo N-terminal myristoylation, which regulates their subcellular localisation and functionality through modifying protein-membrane and protein-protein interactions (Maurer-Stroh & Eisenhaber, 2004a).

N-myristoylation of the PV polyprotein occurs at the N-terminus of P1 in VP4, as is also the case in almost all Picornavirus genera, and it may play an essential role in their structure (Chow *et al.*, 1987). The structures of PV1(Chow *et al.*, 1987a), coxsackievirus B3 (CVB3) (Xiao *et al.*, 2005), and several other enteroviruses show a highly conserved arrangement of the myristic acid chain that is covalently linked to the N-terminus of VP4, although the orientation of the fatty acid chain from C14 to C11 may vary. The myristoyl groups initially aggregate around the icosahedral 5-fold axis and subsequently spread apart to include a twisted parallel β-tube formed by all five VP3 N-termini of a pentamer (Ramljak *et al.*, 2018a).

Two potential roles of myristoylation in the initial stages of particle formation have been suggested. Initially, myristoylated VP0 directs P1 to the membrane replication complex (Lee & Chow, 1992) and secondly, the myristic moiety may enhance protomer-protomer interactions essential for pentamer assembly (Ansardi *et al.*, 1992; Lee & Chow, 1992). The data relating to the necessity of myristoylation for assembly have changed in recent years and a more detailed discussion of these changes is found the Introduction to **Chapter 4**.

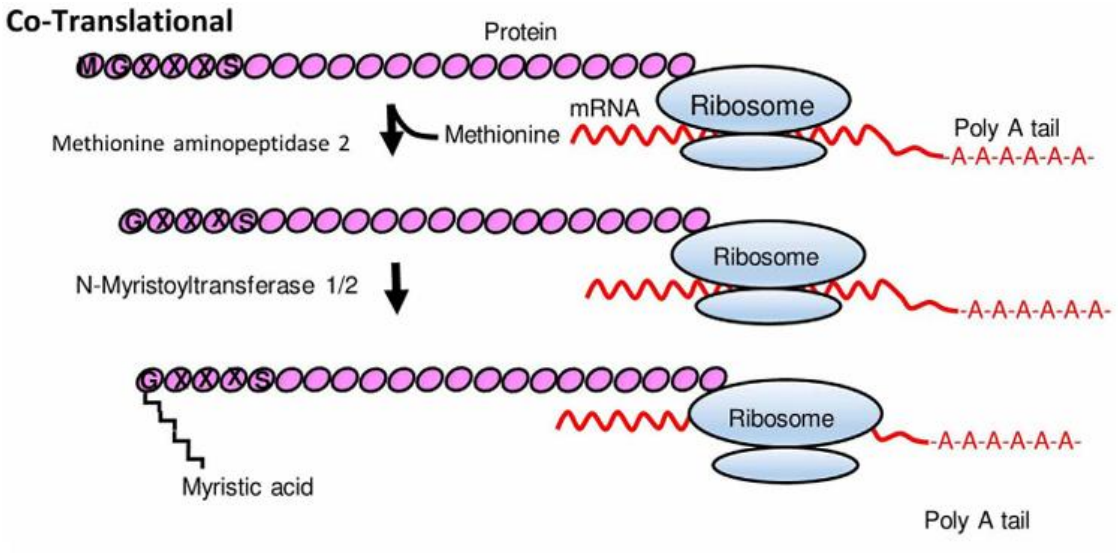

Figure 5. Co-translational myristoylation of proteins. Myristoylation involves the covalent attachment of the saturated 14-carbon fatty acid myristate to the N-terminal glycine residue following removal of the initial methionine residue (Kishore *et al.*, 2017).

1.6 Assembly of Poliovirus Capsid Proteins

The capsid proteins begin from the precursor polypeptide P1(97 kDa), which is initially cleaved to produce VP0 (37 kDa), VP3 (26 kDa), and VP1 (34 kDa), the three proteins that assemble to create the procapsid (Paul *et al.*, 1987). During maturation, VP0 is converted into VP2 (30 kDa) and VP4 (7 kDa), as discussed above. The protein shell gives an effective defence against physical and chemical degradation of the RNA genome. This is essential for the stability of the virus outside a host cell and for effective transmission via the faecal-oral route which may require long periods of survival in various environments.

The assembly of PV capsids results from consecutive steps in which the various intermediates are described by their antigenic or sedimentation profiles. The protomer, designated in Svedberg units is 5S while the pentamer has a sedimentation coefficient of 14S. The stability of the pentamer is greater than the protomer as a result of protein-protein interactions and the aggregation of myristate chains at the N-terminus of VP4 at the five-fold symmetry axis. The transition from the 14S pentamers, to the assembled but not yet mature 80S procapsid, and 160S mature capsids is dynamic, and the precise timing of RNA incorporation remains unclear(Hogle, 2002) **(Figure 6)**.

The cleavage of VP0 into VP2 and VP4 is rapid, one of the reasons it has been difficult to study and was originally suggested to require a conserved histidine residue (Basavappa *et al.*, 1994; Hindiyeh *et al.*, 1999). Mutational analysis indicated that the replacement of this histidine residue inhibits maturation cleavage while not affecting particle assembly or

genome packaging, leading to non-infectious particles that preserve uncleaved VP0 (Hindiyeh *et al.*, 1999). More recently, a model mechanism for the VP0 cleavage has been proposed in which the bound RNA allows the attainment of a stabilized intimidate 3D structure that is necessary for cleavage to occur (Kingston *et al.*, 2024).

Recent structural and biochemical studies have clarified that poliovirus assembly proceeds through parallel pathways, in which RNA-containing pentamers advance directly to the provirion, whereas RNA-free pentamers assemble into empty capsids that represent off-pathway products rather than true precursors of infectious virions. Cryo-EM analyses of enteroviruses, including poliovirus, have shown that these empty capsids lack the RNA-induced conformational transitions required for VP0 cleavage, consistent with their non-productive role in the assembly landscape (Liu *et al*., 2016).In contrast, genome-containing intermediates arise through selective recruitment of replication-competent RNA via defined packaging signals and cis-acting replication elements, which promote the formation of an RNA-stabilised intermediate necessary for maturation and efficient encapsidation (Wang *et al*., 2018). Together, these findings support a model in which genome packaging is integrated with ongoing RNA replication and capsid assembly, ensuring that only properly replicating genomes are incorporated into mature particles.

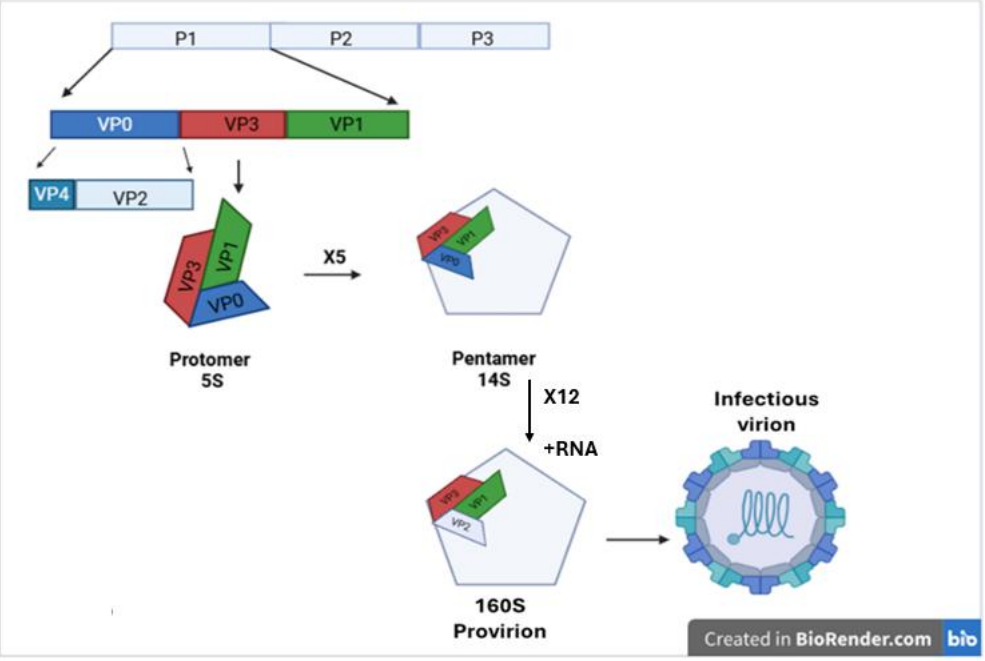

Figure 6. Poliovirus capsid assembly pathway. The process begins with the proteolytic processing of the P1 region of the polyprotein to generate protomers, each composed of VP0, VP3, and VP1. Five protomers associate to form a 14S pentamer, stabilized by protein-protein interactions and N-terminal myristoylation of VP4 at the five-fold axis. Twelve pentamers assemble into an 80S empty capsid, which lacks viral RNA. Genome encapsidation produces the 160S provirion, followed by VP0 cleavage into VP2 and VP4 a maturation step that increases capsid stability and yields the infectious mature virion.

It is important to recognise that capsid assembly in virus-infected cells differs fundamentally from assembly of recombinant VLPs produced by heterologous expression systems. In infected cells, capsid formation is tightly coupled to polyprotein processing, membrane-associated replication complexes, and requires N-terminal myristoylation of VP0 for pentamer stability. In contrast, recombinant VLP assembly occurs in the absence of these viral and cellular contexts, and certain requirements, such as the strict dependence on VP0 myristoylation may be reduced or bypassed due to differences in the expression environment and/or the assembly pathways used.

1.7 Antigenicity of Poliovirus

The initial stage of PV infection starts with the interaction of the virus with the CD155 receptor on the surface of a permissive cell. In the mature virion VP4 and the N-termini of VP1 to VP3 are situated on the inside surface of the PV capsid as shown by the original

crystal structure (Mendelsohn *et al.*, 1989). However, N-terminal peptides from both VP4 and VP1 are reversibly externalized at 37°C, a process known as “breathing”. They are also irreversibly externalised following receptor attachment (Li *et al.*, 1994). The details of this process have improved considerably in recent years, principally through the use of Cryo-electron microscopy which has been able to capture intermediates despite their transient existence. The conformational changes during infection that occur in the native 160S virion lead to the formation of the expanded 135S intermediate, also known as the A-particle, via am approximate 4% increase in the particle's diameter. This expanded form opens holes at the 2-fold and quasi-3-fold symmetry axes, and it is openings that accommodate the externalized N-terminal extensions of VP4 and VP1. These externalized polypeptides interact with the host cell membrane to form a pore (Panjwani *et al.*, 2014a) which facilitates the release of the viral RNA genome into the cytoplasm. The increased resolution of the native 160S form and the expanded 135S intermediate have revealed the EF loop of VP2 and the GH loop of VP3, previously poorly understood, have well-ordered conformations. Moreover, the studies have revealed that the 135S particle is a family of conformations, only the later of which are the forms which show the complete externalization of the N-terminus of VP1(Konopka-Anstadt *et al.*, 2020; Shah *et al.*, 2020). The same studies showed, for the first time, that a significant fraction of VP4 appears to remain associated with the viral genome inside the capsid during early stages of uncoating(Danthi *et al.*, 2003). This is relevant to the studies in Chapter 3, which were confounded by nucleic acid contamination of VP0 following bacterial expression. Recombinant VP1 and VP3 did not have similar nucleic acids contamination. The expansion of the particle that accompanies entry also has antigenic consequences. Each of the three serotypes of PV exist in two antigenic forms: 1) the “native” (N) form is infectious and presents conformational epitopes that are recognized by neutralizing antibodies and 2) the “heated” (H) antigenic form that lacks neutralizing epitopes, which encompasses naturally occurring empty capsid particles derived from N antigen following exposure to heat, UV radiation, or higher pH values (Breindl, 1971). The H (135S) particles are typically described as being unable to attach to susceptible cells and are considered non-infectious (Lonberg Holm *et al.*, 1975). They are also conformationally modified, having lost VP4 and irreversibly externalised the N terminus of VP1, resulting in slower sedimentation compared to the native virus (160S). The H particles exhibit heightened sensitivity to proteases and detergents compared to the native virus and can be easily differentiated from the native virus using immunological assays (Fricks & Hogle, 1990). Monoclonal antibodies were found that responded with the N antigen, the H antigen, or both N and H antigens in antigen blocking assays, demonstrating that the two particles possess both common and unique epitopes (Ferguson *et al.*, 1984). In *vitro*, three processes have been demonstrated to convert 160S virus into 135S particles: 1) binding of the native virus to the

poliovirus receptor on the cell surface at 37 ˚C during a natural infection (Fricks & Hogle, 1990); 2) incubation of the native virus with the soluble ectodomain of the receptor at 37˚C (Yafal *et al.*, 1993); and 3) heating 160S particles at 50˚C in the presence of divalent cations that stabilise the metastable 135S intermediate (Curry *et al.*, 1996). Importantly N particles play a central role in infection as they induce a strong neutralising antibody response while H particles fail to induce a neutralising antibody response **(Figure 7)**. The significance for this for vaccine development is obvious and is discussed further in the Introduction to **Chapter 5**.

(A)

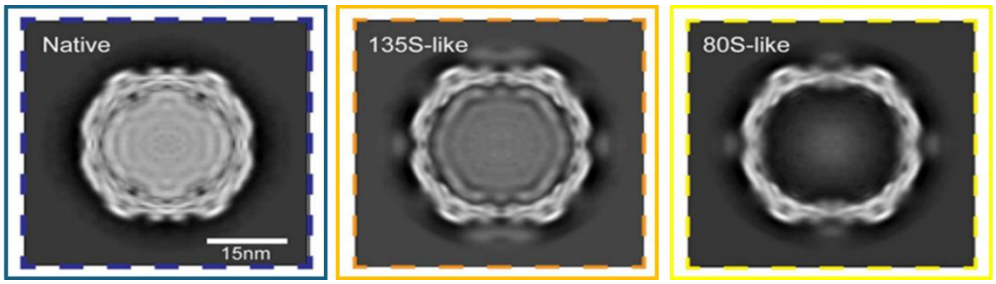

(B)

Characteristic	N Antigenic Form	H Antigenic Form
Infectivity	Infectious	Non-infectious
VP4	Present	Absent
Particles size	160S	135S
Antigenicity	Recognized by antibodies specific to infectious virus	Recognized by antibodies specific to empty capsids
Immune Response	Induces a strong neutralising antibody response	No neutralising antibody response

Figure 7. Conformational Forms of Poliovirus **A)** Using single-particle cryo-electron microscopy, the analysis includes 160S particles (blue edge), 135S-like particles (orange edge), and empty particles (yellow edge). **B)** A comparison of the Native (N) and Heated (H) antigenic forms of PV (Shah *et al.*, 2020).

Empty capsids produced in infected cells, as well as empty particles generated by heating mature virions, can undergo this conformational expansion and display H antigenicity, consistent with observations that RNA content does not alone determine antigenic state (Rombaut and Boeyé, 1982; Putnak et al., 1982; Basavappa et al., 1998). These findings

indicate that both RNA-containing and RNA-free particles are capable of adopting H-like conformations under appropriate conditions and that empty capsids should not be assumed to be exclusively N antigenic. Indeed, several recombinant systems yielding empty capsids have been described, with various levels of H and N reactivity ascribed to them **(Table 4)**.

1.8 Poliovirus Infections

Primary infection with poliovirus usually occurs in the mucosa of the nasopharynx and gastrointestinal tract where the virus multiplies in monocytes and then moves to the cervical and mesenteric lymph nodes to enter the blood, creating a transient viraemia lasting between 3 and 7 days. Viral particles are shed in faeces from infected individuals, with PV excretion starting immediately after infection and lasting approximately 7 weeks. PV particles can survive in the environment for up to two months and are transmitted via the faecal-oral route. However, the virus can also disseminate to secondary sites, including the central nervous system, where it may invade motor neurons and cause paralytic disease(Pfeiffer, 2010).

After the period of poliovirus of a typical infection, which is often from 7 to 14 days but may extend to 35 days, the following outcomes may occur: asymptomatic infection, mild illness (abortive poliomyelitis), aseptic meningitis (nonparalytic poliomyelitis), and paralytic poliomyelitis. In the case of abortive poliomyelitis, estimated to occur in 4-8% of PV infections, the most common symptoms are fever, headache, drowsiness, malaise, nausea, constipation, vomiting, and sore throat. Nonparalytic poliomyelitis occurs in 1-2 % of poliovirus cases, with symptoms including a high fever with anorexia, pharyngitis myalgia, vomiting and nausea, and neck stiffness with a headache (Melnick, 1996).

Paralytic poliomyelitis occurs in <1% of infections in which patients develop flaccid paralysis due to motor neuron damage when the virus spreads from the blood into peripheral neurons and then progresses to the central nervous system **(Figure 8)**. Flaccid paralysis occurs as a result of the virus causing extensive damage, essentially cytopathic effect, to the anterior horn cells in the spinal cord leading to their dysfunction. As the motor neurone cannot transmit signals to the muscle it innervates, muscular atrophy results. In the majority of cases of poliomyelitis, the lower limbs are affected hemi-laterally but in some cases the virus can continue spreading to posterior horn cells, thalamic and hypothalamic motor neurons to affect the respiratory centers causing bulbar poliomyelitis, which is fatal unless the infected individuals receive mechanical ventilation (Minor, 2014). Cells infected with PV undergo distinct morphological changes due to cytopathic effects, and there is an accumulation of microglia, plasma cells, and polymorphonuclear neutrophils at the site of infection.

Degeneration of axons may occur as infected cells get phagocytosed by macrophages (Gonzalez *et al.*, 2012).

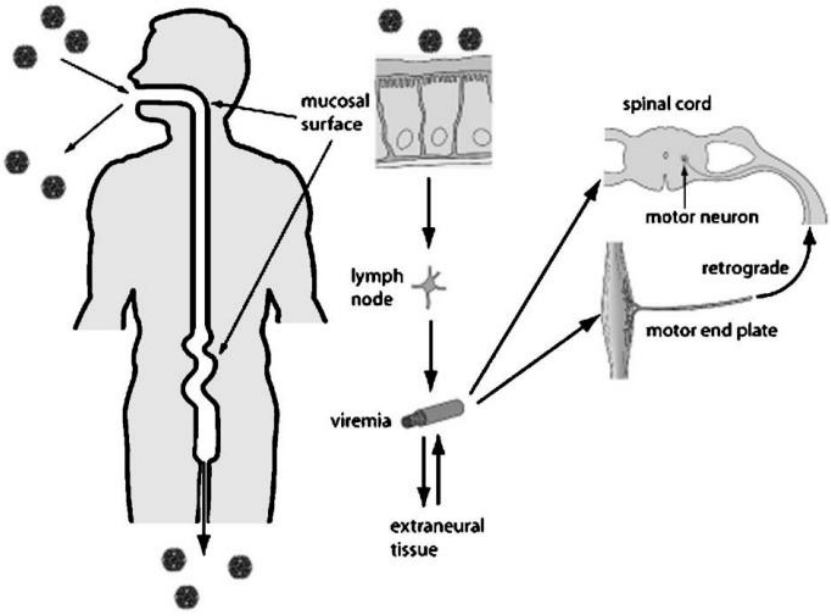

Figure 8. PV dissemination across the blood-nervous tissue barrier. PV multiplies in the gastrointestinal mucosa, infecting monocytes within gut associated lymphoid tissue (GALT) and in some cases may disseminate via the cervical and mesenteric lymph nodes to the bloodstream leading to viraemia. PV can bind CD155 receptors on peripheral neurons and migrate to the central nervous system via retrograde axonal transport (Racaniello, 2006).

1.9 Diagnosis of Poliovirus Infections

After showing symptoms, Poliovirus can be isolated from the faeces in cell culture (Gerloff *et al.*, 2018a) for up to 7 weeks and from the nasopharynx for five days. PV is seldom isolated from the cerebrospinal fluid (CSF) or serum, unlike most enteroviruses that cause paralysis (Muir *et al.*, 1993). Although the virus can be isolated more easily from the nasopharynx or faeces, the CSF displays an elevated protein concentration and pleocytosis (Kilpatrick *et al.*, 1996). Seroprevalence of neutralizing antibodies specific to PV1, PV2 or PV3 can be determined using viral neutralization assays in African green monkey kidney (Vero) cell culture (Reinheimer *et al.*, 2012). The most effective method for diagnosis of PV is reverse

transcription polymerase chain reaction (RT-PCR) after isolation of PV in cell culture, which can also be used to distinguish wild-type from vaccine-derived PV (VDPV) (Gerloff *et al.*, 2018).

1.10 Poliovirus Infection and Risk Factors

Poliovirus can infect people of all ages, but prior to the introduction of polio vaccinations most of those who contracted polio were over 5 years old and 25% over 15 years old. Since the introduction of the IPV and OPV polio, in regions where polio transmission still occurs most of the symptomatic cases occur in children under 5 years of age. This is because adults have acquired immunity through vaccination with OPV and IPV or wild poliovirus exposure (Nolan *et al.*, 1955). Another reason could be that adults are assumed to be more hygienic than children, and these aspects may reduce the spread of shed poliovirus (Gelfand *et al.*, 1959). In addition, malnourished children are also more susceptible to PV infections. The results of a study conducted in Pakistan showed that malnourished children are more likely to be infected with PV regardless of the multiple doses of OPV they received compared to normally fed children (Saleem *et al.*, 2015).

1.11 Immune Response to Poliovirus Infection

The immune response to viral infections includes the release of cytokines (particularly interferons), cytotoxic T lymphocyte (CTL) activation, and production of neutralising antibodies (Dotzauer, 2012). Type I IFNs induce the expression of major histocompatibility complex class I (MHC-I) on the cell surface and the activation of natural killer cells in the early stages of antiviral action (Baj *et al.*, 2015). In the case of PV infection, induction of innate immune responses is likely caused by PV-infected dendritic cells and macrophages (Wahid *et al.*, 2005) that produce IFN-γ. $CD4^+$ T cells specific to poliovirus substantially enhance the neutralising antibody response by delivering crucial helper signals to B cells, facilitating class switching and affinity maturation towards high-affinity serotype-specific neutralising IgG(Wahid *et al.*, 2005;Snyder *et al.*, 2025).

The initial line of defense to protect the intestinal epithelium against PV infection is dimeric mucosal IgA (SIgA), with a secreted monomeric form in serum (sIgA) important in protecting against infection of the CNS (Li *et al.*, 2020; Woof & Russell, 2011). The first antibody response on primary exposure to PV is an increase in anti-PV IgM antibodies, which appear approximately nine days after exposure and achieve their highest titer over a 4-week period before they disappear (Ogra *et al.*, 1968, 1971). Mucosal anti-PV SIgA is detectable in pharyngeal and stool samples one week after PV infection, while monomeric serum sIgA is

detectable 3 weeks after exposure. Roughly four weeks after infection both SIgA and sIgA reach their maximum levels, with SIgA at a higher level than sIgA (Nathanson, 2008). These antibodies reach their peak after 3-4 weeks post infection but can continue for years, perhaps for life (Paffenbarger *et al.*, 1961). Neutralizing serum antibodies are responsible for controlling viremia with circulating anti-PV antibodies, even at low levels (including passive immunization), preventing paralytic disease by stopping PV from crossing the blood-neurone barrier. The outcome of a PV infection is therefore largely determined by the speed and strength of the antibody response (Ogra *et al.*, 1971).

1.12 Prevention and Control

Implementation of personal and public sanitation, and isolation of PV infected patients, can help to reduce the spread of PV, but high population immunity through vaccination is required to prevent transmission (Duizer *et al.*, 2017). The first PV vaccine developed by Jonas Salk was the inactivated polio vaccine (IPV), produced by culturing wildtype PV in Vero cells and inactivated with formalin (Monto, 1999). Currently, IPV is produced by the purification and concentration of the inactive PV making the vaccine more potent (Minor, 2004). The vaccine is administered by intramuscular injection, raising serum IgM, IgG, and sIgA but not mucosal SIgA as full innate signaling requires an infection. This vaccine is safe and effective and can be used for people over the age of 50 years, immunosuppressed or pregnant(Kidd, 1996).

In 1962, the Salk vaccination was replaced with the Sabin trivalent live attenuated oral polio vaccine (OPV), which contains live attenuated strains of polioviruses 1, 2, and 3 (Kidd, 1996). The OPV strains were produced by passage of wild type PV in non-human primates and Vero cells (Avanzino *et al.*, 2018) leading to an accumulation of mutations and subsequently selecting attenuated viruses with low neurovirulence (Pliaka *et al.*, 2014). OPV is administered orally and generates an active localized infection in the pharynx and intestinal endothelium, resulting in mucosal SIgA production in addition to serum sIgA induction. Additionally, the attenuated virus is released in the faeces, which can spread to other unvaccinated individuals and contribute to herd immunity(Kidd, 1996) . OPV is recommended for infants starting at two months, with three doses separated by a one-month interval and is also given to pregnant women after the first three months of pregnancy (Harjulehto-Mervaala *et al.*, 1993). However, it is deemed not safe for immunocompromised patients and people in close contact with them (Kotton, 2008). The Global Polio Eradication Initiative (GPEI) aims to achieve high vaccination coverage in all regions and has successfully increased the number of vaccinated people to over 2.5 billion since it was

established in 1988 (Deressa *et al.*, 2020). However, the goal of eradication is still elusive, largely as the result of limited vaccination in areas of conflict (Lee *et al.*, 2025).

1.13 Disadvantages of current Polio vaccines

Whilst OPV has been used to greatly reduce the incidence of Polio globally due to humoral and mucosal immunity against poliovirus infection (Tano *et al.*, 2007), the vaccine can in rare cases lead to cases of vaccine-associated paralytic poliomyelitis (VAPP). This occurs when Sabin strains evolve toward more genetically stable variants during rapid replication, occasionally reverting to neurovirulent forms that can reach the CNS and induce paralysis that is clinically indistinguishable from wild poliomyelitis (Nkowane *et al.*, 1987). The risk of VAPP is approximately 1 in every 750,000 initial OPV doses, but the risk of paralysis due to immunization is estimated to be 1 in every 12 million people after two vaccination doses (Nkowane *et al.*, 1987). The PV3 OPV strain is most frequently associated with recipient VAPP, whereas the PV2 OPV strain is most commonly observed in immunocompromised individuals, and PV1 OPV strains are least frequently associated with cases of VAPP (Sutter *et al.*, 2018). Individuals with immunodeficiency disorders are at the increased risk of acquiring VAPP (Shahmahmoodi *et al.*, 2010) , and the risk also increases in under-immunized populations due to circulating vaccine-derived PV strains regaining neurovirulence as they replicate in multiple hosts (Tano *et al.*, 2007).

Recent developments in OPV design have yielded next generation live attenuated vaccine strains that maintain the immunogenic and manufacturing benefits of Sabin OPVs while greatly improving genetic stability. Novel Oral Poliovirus Vaccine type 2 - Codon Deoptimized (nOPV2-CD), created via codon deoptimization and UTR stabilisation, demonstrates comparable efficacy to Sabin OPV2 in inducing immunity while showing much enhanced resistance to reversion. Similar developments have enhanced this stabilisation strategy to produce safer OPV candidates for types 1 and 3, presenting a promising avenue for multivalent OPV formulations with lowered risk of vaccine-derived outbreaks(Konopka-Anstadt *et al.*, 2020; Yeh *et al.*, 2023).

Another potential risk of OPV is that the vaccine strains may recombine with other polioviruses or polio-like enteroviruses during co-infection, resulting in the emergence of novel neurovirulent chimeric viruses. Research in this process of genetic plasticity was stimulated by the appearance of dangerous recombinant circulating vaccine-derived polioviruses (cVDPVs), which were associated with poliomyelitis outbreaks in different regions of the world with limited vaccination coverage. The majority of these cVDPVs have mosaic genomes comprised of altered polio vaccine capsid sequences and partial or complete

non-structural sequences from other types of Enterovirus C, especially coxsackie A viruses (Combelas *et al.*, 2011; Muslin *et al.*, 2015).

Disadvantages are also associated with IPV, including limited vaccine supply due to poor yield of PV2 (Thomassen *et al.*, 2013). Although there is some evidence that IPV can reduce the quantity of virus shed, it does not induce enough intestinal mucosal immunity to eliminate faecal poliovirus shedding. The impact of IPV on poliovirus transmission in regions with widespread faecal-oral transmission is unknown, but it is likely to be limited when compared to OPV (Hird and Grassly, 2012). Another disadvantage of IPV is the requirement for large-scale culture of live PV in the manufacture process, which poses a risk of accidental release of PV which would pose a threat to under-immunized populations.

1.14 Virus-Like Particles (VLPs) as a Polio Vaccine Candidate

It would be ideal to develop a replacement vaccine for IPV and OPV that induces both neutralizing serum antibodies and mucosal antibodies without the need to culture live PV at any point of the manufacturing process. Viral-like particles (VLPs) are typically between 20-200 nm diameter that self-assemble from viral structural proteins (Pushko *et al.*, 2013). VLPs are characterized as enveloped or non-enveloped depending on the presence or lack of lipid envelopes and the existence of viral proteins assembled into one, two, or multiple layers, similar to the size and shape of the original viruses (Jeong & Seong, 2017). They can induce both cellular immune and humoral responses and can contain pathogen associated molecular patterns (PAMPs), leading to robust recognition by the immune system (Lee *et al.*, 2018; Mohsen *et al.*, 2018). VLPs are considered to be safe vaccines, particularly for immunocompromised or elderly people, as they lack the viral genome and therefore have no potential for replication within target cells (Balke & Zeltins, 2019). VLPs offer several advantages over traditional vaccine platforms, including enhanced stability under extreme environmental conditions such as elevated temperatures and variable pH (Aguado-Garcia *et al.*, 2022), as well as the ability to preserve native antigenic conformation more effectively than soluble antigens (Crisci *et al.*, 2012).

Various expression systems can be employed for the production of VLPs, including bacteria, insect cell lines (Joe *et al.*, 2020), yeast (Sailaja *et al.*, 2007), plants (Zhai *et al.*, 2019) and mammalian cell lines (Mohsen *et al.*, 2018). The manufacture of VLP vaccines generally involves 3 stages: primary processing (production), final treatment (purification) and formulation. Primary processing requires cloning of targeted viral structural genes and efficient production and self-assembly in a suitable expression system. After harvesting and lysing the cells, a clarification phase is performed to ensure that all contaminating cell debris is removed. To produce intact and pure VLPs, further purification methods such as ion-

exchange chromatography and ultracentrifugation are necessary. Polishing is the last purification step, which removes any remaining nucleic acids and host cell proteins. In the final step of the creation of VLP vaccines, formulation, and filter sterilization are carried out to provide a safe and effective vaccine **(Figure 9)** (Hillebrandt *et al.*, 2020)**.**

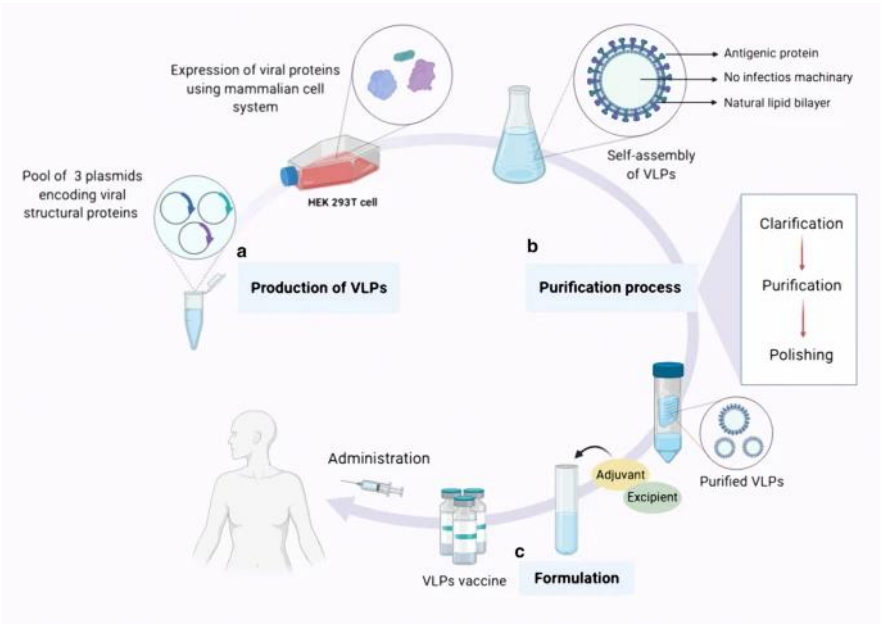

Figure 9. Stages in the manufacture of a VLP vaccine. a) Primary processing involves cloning of targeted viral genes and production of self-assembled VLPs in a suitable expression system, b) purification of VLPs and c) formulation of the VLPs into the vaccine product for distribution and administration (Nooraei *et al.*, 2021).

1.15 Expression Systems for VLP Production

Virus-like particles (VLPs) can be produced in various expression systems, including bacteria, yeast, insect, plant, and mammalian cells, each offering distinct advantages in scalability, post-translational modifications, and cost.

1.15.1 *E. coli* Expression System

E. coli is a popular host for recombinant protein production, preferred for its rapid growth rate, well-characterized genetics, and capacity to express proteins in large yields (Rosano & Ceccarelli, 2014). In *E. coli* systems, gene sequences encoding the target protein are introduced into plasmid vectors regulated by robust, inducible promoters (Studier, 2005). Several *E. coli* promoter systems have been implemented in vectors to enable control over the timing and level of gene expression, but the most commonly used are T7 and Ara **(Table 2).** However, *E. coli* lacks in the cellular machinery required for numerous eukaryotic post-translational modifications (PTMs) including glycosylation, phosphorylation, and ubiquitination that maybe required for the correct folding, stability, and biological function of various eukaryotic proteins (Bhatwa *et al.*, 2021).Relevant to the concept of PV VLPs, *E.coli* does not encode N-myristoyl transferase NMT so expressed proteins are not myristoylated. Nevertheless, several examples of picornavirus VLP assembly in *E.coli* have been published (Xiao *et al.*, 2016; Puckette *et al.*, 2017; Yu *et al.*, 2025) leading to the attempts to do the same for PV described in **Chapter 3**.

The main challenge for recombinant production in *E. coli* for VLPs is that high levels of expression frequently result in misfolded proteins and the formation of inclusion bodies. This limitation can be addressed by co-expressing modifying enzymes, such as glycosyltransferases for glycosylation or human kinases for phosphorylation, as effectively confirmed in modified *E. coli* or cell-free systems (Tokmakov *et al.*, 2012).

Several strategies can be employed to enhance solubility and improve folding including: 1) altering the culture conditions to reduce the rate of protein production (e.g. lowering temperature, reducing concentration of inducer, altering pH, addition of sorbitol, glycine betaine, sucrose, and raffinose); 2) use of solubility enhancing fusion tags such as maltose-binding protein (MBP) or glutathione S-transferase (GST); 3) codon optimization of the target gene to improve expression in *E. coli*; 4) co-expression of chaperones such as GroEL/GroES, DnaK/DnaJ/GrpE; 5) use of alternative host *E. coli* strains such as BL21(DE3) pLysS, Rosetta, or Origami; and 6) use of signal peptides to target the recombinant protein to the periplasm (Francis & Page, 2010; Marco, 2025) although many of

these may not be compatible with capsid assembly. An alternative strategy is to solubilize the recombinant protein from inclusion bodies (e.g. using urea or guanidine HCl) and refold *in vitro* (Alibolandi & Mirzahoseini, 2011) and this too has been applied to picornavirus VLPs (Lee *et al.*, 2009). These studies show that if post-translational modification, solubility and folding issues are either not a problem or can be overcome, the expression system is an efficient and flexible platform for recombinant protein production(Kaur *et al.*, 2018).

Table 2. The characteristics of *E. coli* promoter systems used for heterologous protein production.

Reference	Promoter System	Induction Method	Key Features	Expression Level
(Gronenborn, 1976)	lac	IPTG (0.05–2.0 mM)	Weak, inexpensive, regulated at low levels	Low–Medium
(Brosius *et al.*, 1985)	trc/tac	IPTG (0.05–2.0 mM)	Higher than lac, regulated, relatively costly	Moderate
(Studier & Moffatt, 1986)	T7	IPTG (0.05–2.0 mM)	Tight control, needs T7 polymerase strain	Very High
(Elvin *et al.*, 1990)	pL	Temperature shift (30–42°C)	Tight, no inducer, temperature-sensitive	Moderate
(Skerra, 1994)	tetA	Anhydrotetracycline (200 µg/L)	Tight, strain-independent, affordable	Medium–High
(Guzman *et al.*, 1995)	pBADara	L-arabinose (0.001–1.0%)	Tunable, dose-dependent, low basal level	Low–High
(Haldimann *et al.*, 1998)	pBADrha	L-rhamnose (0.2%)	Tight, tunable, no leakiness	Low–High

1.15.2 Baculovirus Expression System

Baculoviruses are classified within the family *Baculoviridae*, which, as per the latest report (ICTV), encompasses 85 acknowledged species categorised into four genera: *Alphabaculovirus* (Nucleopolyhedroviruses (NPVs) infecting *Lepidoptera*), *Betabaculovirus* (Granuloviruses (GVs) infecting *Lepidoptera*), *Gammabaculovirus* (NPVs infecting *Hymenoptera*), and *Deltabaculovirus* (NPVs infecting *Diptera*) (ICTV, 2025). NPVs generate polyhedral occlusion bodies (OBs) comprised of the protein polyhedrin, commonly encapsulating numerous occlusion-derived virions (ODVs), whereas granuloviruses (GVs) produce smaller granular occlusion bodies consisting of granulin, usually carrying a single ODV (Slack & Arif, 2007).

Baculoviruses have been successfully used as biopesticides because of their host specificity, safety for the environment, and ability to control insect populations in nature. In the early 1980's, baculoviruses were developed for use as an expression system due to advances in understanding the archetype baculovirus, *Autographa californica multiple nucleopolyhedrovirus* (AcMNPV) (Smith *et al.*, 1983). For the natural baculovirus replication cycle, there are two structurally distinct forms of the virus, budded virus (BV) and ODV, which occur as part of a biphasic replication cycle **(Figure 10)**. After a host larva consumes OBs, ODV are released in the alkaline midgut to initiate a primary infection of midgut cells. The form of virus released form these cells is the non-occluded BV which then spread to infect cells throughout the host larvae, disseminating BV from one tissue to another (Slack & Arif, 2007). Baculovirus gene expression is temporal, involving hierarchical expression of immediate early, delayed early, late, and very late genes. In the early stages of infection, nucleocapsids migrate through the cytosol to the plasma membrane to form BV, while in the very late stages, they stay in the nucleus to form ODV (Slack & Arif, 2007). ODV-producing nucleocapsids acquire an envelope through an unidentified process, which may involve nuclear membrane synthesis or a *de novo* process. ODVs are then occluded in a protein matrix made of either polyhedrin (for NPVs such as AcMNPV) or granulin (for GVs). As large amounts of these proteins are required, they are expressed at extremely high levels in the very late stage of infection by dedicated very late promoters whose activity depends on the earlier phases of gene expression. OBs protect ODV from environmental stress, particularly UV and desiccation, enabling them to persist in the environment until they are ingested by a new susceptible host while feeding(Hong *et al.*, 2023).

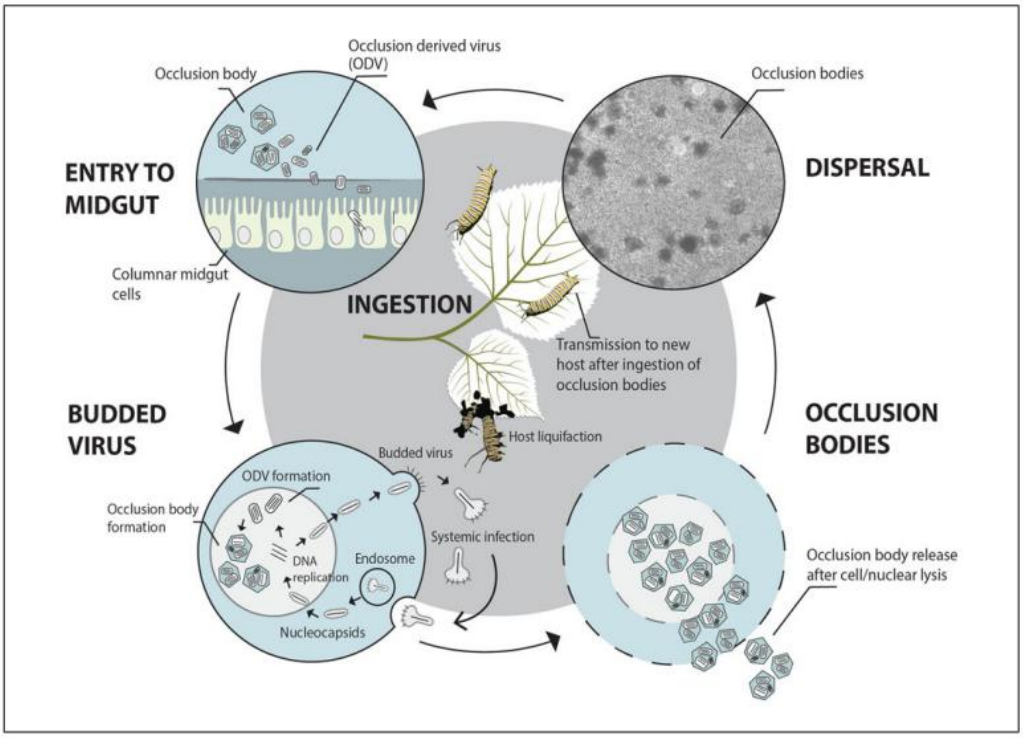

Figure 10. The Baculovirus Replication Cycle. Occlusion bodies (OBs) are accidentally consumed by insect larva and are solubilized by the alkaline pH of the insect midgut where they establish an infection. The ODVs penetrate the peritrophic membrane and fuse directly with the microvilli of columnar cells to release the baculovirus genome into the cytoplasm. The viral genome is transported to the nucleus where the baculovirus immediate early genes are transcribed by host RNA polymerase to initiate the infection. After the transcription of late genes 6 - 24 hours, budded viruses (BVs) are released by budding from the cell membrane. At the end of the very late phase (18 hours and beyond), nucleocapsids are retained in the nucleus, where they gain envelopes to form occlusion derived viruses (ODVs) and become embedded in a crystalline matrix protein (polyhedrin or granulin) to form OBs. Mature OBs are released by cell lysis, and due to their resilience to environmental stresses, they persist until they are consumed by a susceptible host (Chambers *et al.*, 2018a).

Whilst the *polh* gene, encoding polyhedrin, and the other highly expressed very late gene, p10 are necessary for horizontal transmission, they are not required to produce BVs and not required for successful infection in insect cell culture (Herniou *et al.*, 2003). The baculovirus expression vector system (BEVS) exploits this fact to produce recombinant proteins as recombinant genes can replace the *polh* or *p10* gene coding regions while retaining the extremely potent promoters to direct high level expression of foreign genes in virus-infected insect cells. Insect cells recognise and process signal peptides, facilitate oligomerization, and carry out the post-translational modifications like acylation, glycosylation, disulfide bond

formation, and phosphorylation, typical of eukaryotic cellsand comparable, but not identical, to those in mammalian cells (Sułek & Szuster-Ciesielska, 2025). BEVS can conveniently be scaled up in shaking cultures or bioreactors at 27°- 28°C in a serum-free medium (Chambers *et al.*, 2018a) and the system has been developed to allow the simultaneous expression of several foreign proteins within a single host cell, allowing for the spontaneous self-assembly of particles such as VLPs (Bissett & Roy, 2024; Sułek & Szuster-Ciesielska, 2025).

1.15.3 Plant Expression Systems

Recombinant proteins can also be produced in plants, referred to as "Molecular farming", which has been applied in the manufacture of medicinal products and industrial enzymes (Rybicki, 2020). Plant-based expression systems have gained significant interest as a flexible platform for the synthesis of virus-like particles (VLPs) as the rapid scalability offers the possibility of reduced manufacturing costs as well as the lack of contamination with mammalian pathogens or endotoxins (Buyel, 2024). As another eukaryotic protein synthesis system, plant-based expression systems are able to perform the post-translational modifications noted as sometimes necessary for protein folding and assembly (Mardanova *et al.*, 2024).

Vaccine proteins can be generated using stable transgenic plants, the standard method, or through transient expression (Chung *et al.*, 2022). Stable transgenic lines are generally established via biolistic transformation or *Agrobacterium tumefaciens*-mediated introduction of modified bacterial or viral vectors, resulting in genomic integration of the foreign gene (Kurup & Thomas, 2020). Conversely, transient expression entails the *Agrobacterium*-mediated introduction of expression vectors that stay episomal, allowing rapid but temporary expression of the target gene in the host cell (Canto, 2016). Engineered VLPs comprising animal or human virus capsid proteins that have been successfully produced in plant cells include the human norovirus capsid protein, HPV L1 protein, HBV core and surface antigens, HIV Gag protein, and influenza virus hemagglutinin protein (Rybicki, 2020). PV3 SktSC8 VLPs have also been produced in *Nicotiana benthamiana* and shown to induce significant neutralising antibody responses (Marsian *et al.*, 2017a).

1.15.4 Yeast Expression Systems

VLPs can be generated through recombinant protein expression in yeast cells, offering a more economical alternative to plants and mammalian expression systems. Genetic modification in yeast is well developed, and cells can grow to exceptionally high densities before the expression of recombinant proteins is activated. This enables commercial-scale fermenters to generate VLPs in substantial quantities. There is also a minimal risk of contamination by mammalian pathogens and bacterial endotoxin so VLPs from many viral families have successfully been generated in yeast (Brachelente *et al.*, 2023). *Saccharomyces cerevisiae* has been the preferred yeast used in biotechnological applications, although there are now multiple alternative yeast strains that have been effectively utilised to produce VLPs (Gnügge & Rudolf, 2017). Yeast expression systems have been used for the manufacture of several globally approved VLP vaccines including hepatitis B vaccines (Engerix-B, Recombivax HB), and vaccines that protect against cervical cancer caused by human papillomavirus (HPV, Gardasil® and Gardasil 9®) (Dorji *et al.*, 2021). The hepatitis B virus surface antigen (HBsAg) is the basis of hepatitis B VLP vaccines, the first to be approved for use in 1986, USA and has since been used worldwide (CE *et al.*, 1987). HBsAg was initially produced in *Saccharomyces cerevisiae* (Hsieh *et al.*, 1988) but is has been effectively expressed in multiple yeast expression systems including *Hansenula polymorph* (Xu *et al.*, 2014) and *Pichia pastoris*(Lünsdorf *et al.*, 2011; Zahid *et al.*, 2015). It is also possible to produce HBV VLPs in a cell-free *Pichia pastoris* system which could be used to speed up vaccine development (Spice *et al.*, 2020). The first malaria vaccine Mosquirix™, a VLP vaccine produced in *S. cerevisiae,* was also recently approved by the WHO to protect against malaria (Laurens, 2019). This vaccine contains *Plasmodium falciparum* circumsporozoite protein (CSP) and the T-cell epitope of CSP fused to HBsAg to form chimeric VLPs (Nooraei *et al.*, 2021).

The substantial advancement of molecular tools, such as synthetic promoters for precise expression control, genetically modified strains, and clustered regularly interspaced short palindromic repeats-Cas9 (CRISPR/Cas9) technology, has facilitated the creation of strains that are more efficient in VLP production for multiple yeast species (Gassler *et al.*, 2019). Overall, the yeast expression system combines the benefits of both *E. coli* and mammalian expression methods for VLP production, as yeast shows rapid growth with high yields of recombinant protein of acceptable quality for therapeutic applications.

1.15.5 Mammalian Expression Systems

Different mammalian cell lines, including, NS0, Chinese hamster ovary (CHO), murine myeloma (Sp2/0), murine C127, baby hamster kidney (BHK21), HEK293, and HT-1080, have been developed as potential sources for the manufacture of protein-based therapeutics for medical applications (Dumont *et al.*, 2016). Mammalian cell culture systems offer uniformity and adaptability throughout the development processes and are particularly suited to the expression of glycosylated proteins with lipid membrane compositions, analogous to those of the viral host. There are two strategies that can be used to produce VLPs in mammalian cell cultures. The traditional method involves the creation of a stable cell line in which a gene that encodes the protein of interest is integrated into the genome. Traditionally, transfection of a cell culture, succeeded by a single clone selection procedure to identify high producers to generate a stable cell line that produces VLPs, took around six months (Fontana *et al.*, 2015). However, the use of CRISPR-Cas and improved knowledge about chromosomal sites that are open to transcription offers a faster and surer approach in recent years (Taha *et al.*, 2022). The alternative approach is to use transient transfection, which is rapid, VLPs can be collected roughly 48 to 72 h post-transfection but not suited to continuous production (Cervera *et al.*, 2013). The method is appropriate for obtaining modest quantities of various VLPs, particularly during the initial study steps and is particularly beneficial when the wild-type antigen of interest requires numerous changes, or when one of the VLP proteins is toxic to the production cell line (Fuenmayor *et al.*, 2017).

Table 3: The different VLP production platforms with advantages and limitations.

Expression System	Advantages	Limitations
Bacteria	Low production cost - Scalable - Rapid growth - Simple modification– High level expression - Genetic stability	Recombinant proteins lack post-translational modifications - Poor immunogenicity - Poor solubility issues - endotoxins contamination by bacterial -
Yeast	Cost effective - No endotoxin contamination - Support protein folding- High-density fermentation.	VLP yield lower than *E. coli* - High mannose modification - Lack mammalian-limited Post-Translational Modifications
Insect cells	Transport and transfer significant amounts of DNA - High protein expression - Boost for eukaryotic protein post-translational modifications - Proper protein folding and assembly	Difficult to scale up -High production cost - Incomplete modification of proteins - Baculovirus contamination - Simpler N-glycosylation than mammalian cells
Mammalian cells	Perform proper folding, assembly, and post-translational modifications of proteins	High production cost -Require large-scale production facilities - Lengthy expression time - Low yield - Contamination by mammalian pathogens
Plant cells	Easy scalable – low production cost- Perform N-glycosylation - High expression - Correct folding and assembly	Lower yield than mammalian cells - Technical and regulatory issues

1.16 Production of PV VLPs Using Recombinant Protein Expression Systems

For many viruses, VLPs occur naturally as a consequence of the replication cycle, and this is also true for poliovirus (Minor *et al.*, 1980). This demonstrates that PV structural proteins are capable of self-assembly and that VLPs, also known as empty capsids, will assemble if the virus structural proteins are produced in a recombinant expression system at a level suitable for assembly. For PV this has been confirmed VLPs produced in yeast (Rombaut & Jore, 1997; Sherry *et al.*, 2020; Hong *et al.*, 2024), plants (Marsian *et al.*, 2017a), insect cells (Xu *et al.*, 2019), and mammalian cells (Ansardi *et al.*, 1991; Bahar *et al.*, 2021). PV VLPs are typically produced via the co-expression of the capsid precursor P1 and viral protease 3CD, resulting in the self-assembly of empty, non-infectious particles that retain morphological and immunological properties similar to native virions and capable of eliciting both B- and T-cell responses.

The first PV VLPs were generated in 1989 using a BEVS, whereby a plasmid encoding the complete 6.6 kb coding sequence of the PV3 Leon/37 strain was inserted into the baculovirus vector, leading to the production of RNA-free, non-infectious particles in insect cells. These particles, upon immunization in mice, induced antibodies against structural proteins, including neutralizing antibodies, demonstrating the immunogenic potential of empty capsids (Urakawa *et al.*, 1989). Similarly, in mammalian cells, expression of PV P1 and 3CD in HeLa cells resulted in the formation of capsid proteins VP0, VP3, and VP1, although the immune response to these particles was not tested (Ansardi *et al.*, 1991). The modified vaccinia virus Ankara (MVA) expression system in BHK-21 cells co-expressed the P1 and 3CD, testing different strategies to balance P1 expression and attenuate 3CD toxicity (Bahar *et al.*, 2021).

Yeast systems have been extensively used for PV VLP production. P1 and 3CD in an inducible *Saccharomyces cerevisiae* system were reported to generate immunogenic empty particles (Rombaut & Jore, 1997). More recently, using *Pichia pastoris*, co-expressed P1 and the viral protease 3CD using three separate expression cassettes was used to modulate the level of the potentially cytotoxic 3CD, crucial for P1 cleavage (Sherry *et al.*, 2020). Despite the VLPs demonstrating appropriate processing and structural integrity, no discernible N antigen was detected, suggesting that the particles were in a non-native H antigen form (Sherry *et al.*, 2020). In an extension of these studies, the viral 3CD protease was removed and the separation of the final capsid proteins achieved using the aphthovirus 2A peptide, allowing the protease-independent assembly of virus-like particles (Sherry *et al.*, 2023). More recently still high yields of N antigenic VLPs of PV2 were described from yeast using a combination of protease free expression and a stabilized P1 sequence (Hong *et al.*, 2024)

demonstrating a viable system for producing immunogenic vaccine quality PV VLPs. These recent advances have all used sequence variants of the database PV P1 sequences isolated following a study of poliovirus revertant and temperature sensitive variants to improve antigenic stability across all three PV serotypes (Fox *et al.*, 2017a). The result is a series of P1 sequences that carry multiple mutations engineered to stabilize empty capsids and provide enhanced N antigenicity. When the genetically modified PV3 (SktSC8) sequence was expressed in the plant *Nicotiana benthamiana* VLPs were still mostly in the native H antigenic conformation although they closely resembled the wild-type virus in cryo-EM analysis. However, these VLPs conferred protection in mice following a type 3 PV challenge, whereas VLPs derived from the wild-type PV3 construct did not (Marsian *et al.*, 2017a).

Similarly, when VLPs are evaluated following expression in four different systems: mammalian cells, yeast, insect cells, and plants, the N-antigenic content of VLPs of all three serotypes, including the stabilized PV3-SC8, was improved although the level varied with expression system and with PV serotype, PV2 being the least good (Sherry *et al.*, 2025).

Collectively, these studies demonstrate the feasibility of expressing immunogenic and structurally stable PV VLPs in multiple host platforms, highlighting their promise as safe and effective alternatives to traditional inactivated polio vaccines.

Table 4. Overview of recombinant poliovirus (PV) virus-like particle (VLP) expression strategies.

Host System	Expression Strategy	Protease / Processing	Antigenicity / Key Features	References
Insect cells (BEVS)	Baculovirus vector encoding P1 ± 3CD	3CD co-expression	Produces RNA-free, non-infectious particles; early VLPs mostly H-antigenic; immunogenic in mice	(Urakawa et al., 1989; Xu et al., 2019)
Mammalian cells (HeLa / BHK-21)	Transient or viral vector expression of P1 + 3CD	3CD co-expression	Produces VP0, VP1, VP3; early wild-type constructs often H/C-antigenic; 3CD cytotoxicity requires attenuation; immunogenicity variable	(Ansardi et al., 1991; Bahar et al., 2021)
Saccharomyces cerevisiae	Inducible co-expression of P1 + 3CD	3CD co-expression	Generates immunogenic empty capsids; early wild-type P1 may be H-antigenic; stable D-antigenic VLPs require engineered stabilizing mutations	(Rombaut & Jore, 1997)

Host System	Expression Strategy	Protease / Processing	Antigenicity / Key Features	References
Pichia pastoris	Multiple expression cassettes for P1 and 3CD / 2A peptide	3CD co-expression or 2A peptide	Protease-independent assembly achievable; early VLPs often H-antigenic; stabilized P1 sequence improves D-antigenicity and yield	(Sherry *et al.*, 2020; Sherry *et al.,* 2023; Hong *et al*., 2024)
Plants (Nicotiana benthamiana)	Transient expression of stabilized P1 ± 3CD	3CD co-expression	Stabilized P1 enhances D-antigenicity and immunogenicity; wild-type P1 yields mostly H-antigenic VLPs; protective in mice challenge	(Marsian *et al.,* 2017)

1.17 Aims of This Study

As discussed above, progress in the expression of PV VLPs that are of sufficient yield and quality to stimulate the immune system and induce a robust immune response has seen successive improvement in the last 5 years. However, variability in H/N ratios and cost of goods remain issues for future manufacture. Despite the reported success with other picornaviruses no report has yet demonstrated the production of PV VLPs in bacteria, although individual PV capsid proteins have been successfully expressed and purified (Uma *et al.*, 2016). If PV VLPs could be produced in *E. coli* the cost of PV vaccine production would fall, and the system could also allow a more high-throughput mutational investigation of sequence variation that could further improve PV VLP stability and antigenicity.

At its initiation, this project too had the aim of contributing data that could lead to improved VLPs, by developing a system to produce fully assembled PV VLPs in *E. coli* and to improve the yield and quality of PV VLPs produced using the BEVS in insect cells based on work completed by a previous student. The literature today would suggest that other systems, particularly yeast, may be already a highly productive solution but that was not the case when the work began. Accordingly, the first objective was to determine if high enough yields of soluble PV capsid proteins could be produced in *E. coli* to attempt *in vitro* assembly of VLPs. This work made use of the thermostabilised PV3 Saukett SC8 sequence carrying eight stabilising amino-acid substitutions that helped to maintain native antigenicity and enhance suitability for VLP-based vaccine development (Fox *et al.*, 2017) and the SUMO fusion expression system. A second objective was to improve the production of fully assembled PV VLPs in the BEVS by examining if further mutation of the P1 sequence was tolerated and could be useful for VLP production. This work used the stabilised PV1 P1 Mahoney SC6b sequence containing 6 mutations (Fox *et al.*, 2017) and included an investigation of the properties of novel PV mutations introduced for the first time into a VLP context. The work did not achieve all that was hoped for but has identified sequence changes that are permitted for VLP assembly. It is to be hoped that the combination of these with the better expression systems now described in the literature might lead to a better quality of VLPs and the development of a final candidate Poliovirus VLP vaccine.

Chapter 2 Materials and Methods

2.1 Materials

This section provides details of the bacterial strains, culture media, plasmids, recombinant baculoviruses, primers and antibodies used in this study.

2.1.1 *E. coli* Culture Conditions and Strains

E. coli was routinely cultured on Luria-Bertani (LB) broth (20g/L LB Lennox Fisher, pH 7.0), autoclaved at 121 °C for 15 min or LB solidified with 1% *w/v* agar at 37 °C. Antibiotics were added to media where necessary at the following concentrations: spectinomycin 100 μg/mL; ampicillin 100 μg/mL; kanamycin 40 μg/mL. The strains used in this study are listed in **Table 4.**

Overnight cultures were prepared by inoculating a single colony from an agar plate into 10 mL LB broth, supplemented with antibiotics if necessary for plasmid maintenance, and incubated at 37 °C with shaking at 250 rpm overnight. Overnight cultures were used to prepare stocks of strains in 15% *v/v* glycerol for long-term storage at -80 °C.

Table 5. *E. coli* strains used in this study.

Strain	Description	Source
5-alpha	*E. coli* cloning strain that has high efficiency in DNA transformation and - DH5α™ derivative Genotype*: fhuA2Δ(argF-lacZ)U169 phoA glnV44 Φ80Δ(lacZ)M15 gyrA96 recA1 relA1 endA1 thi-1 hsdR17*	NEB
Stellar cells	*E. coli* HST08 strain that has high transformation efficiency and lacks the genes responsible for cleaving methylated DNA (*mrr-hsdRMS-mcrBC* and *mcrA).* Genotype: F^-, *endA1, supE44, thi-1, recA1, relA1, gyrA96, phoA,* Φ80d *lacZΔM15,* Δ*(lacZYA-argF)* U169, Δ*(mrr-hsdRMS-mcrBC),* Δ*mcrA,* λ-	Takara Bio
BL21-AI	*E. coli* BL21-AI cells were engineered for applications that require strong, tightly controlled expression of toxic proteins from T7-promoter-based expression systems. The strain carries a chromosomal insertion of a cassette encoding T7 RNA polymerase (T7RNAP) in the *araB* locus of the *araBAD* operon to enable arabinose-inducible activation of T7 RNAP from the *araBAD* promoter. Genotype: F^- *ompT* $hsdS_B$ (r_B^-, m_B^-) *gal dcm araB*::T7RNAP-*tetA*	Invitrogen
BL21-DE3	*E. coli* BL21-DE3 is a strain of *E. coli* B that is used to express high levels of non-toxic proteins. The strain is a λDE3 lysogen; the integrated λ DE3 prophage carries the T7RNAP gene under the control of the lacUV5 promoter enabling induction by IPTG. Genotype: F^- *omp*T $hsdS_B$ (r_B^-, m_B^-) *gal dcm* (DE3)	Invitrogen

2.1.2 DNA Vectors and Plasmids

The pTriEx1.1 (EMD Chemicals Inc, 2011) **(Figure 11)** and pOPINE **(Figure 12)** vectors were used in this study because they enable highly efficient expression of recombinant proteins in multiple hosts due to the presence of multiple promoters upstream of the inserted sequence. Both vectors are designed for high-throughput expression in *E. coli*, insect, and mammalian cells by T7, P10, and CMV promoters, respectively. The feature of pTriEx1.1 vector (EMD Chemicals Inc, 2011) is a fixed C-terminal His-tag fusion allowing immediate detection and purification of the expressed protein via anti-His antibodies while feature of pOPINE (Berrow *et al.*, 2007) is the flexible tagging options that can be modified for either

N- or C-terminal fusions. Plasmids used in this study that were constructed using pTriEx1.1 are listed in **Table 5** and those constructed in pOPINE are listed in **Table 6**.

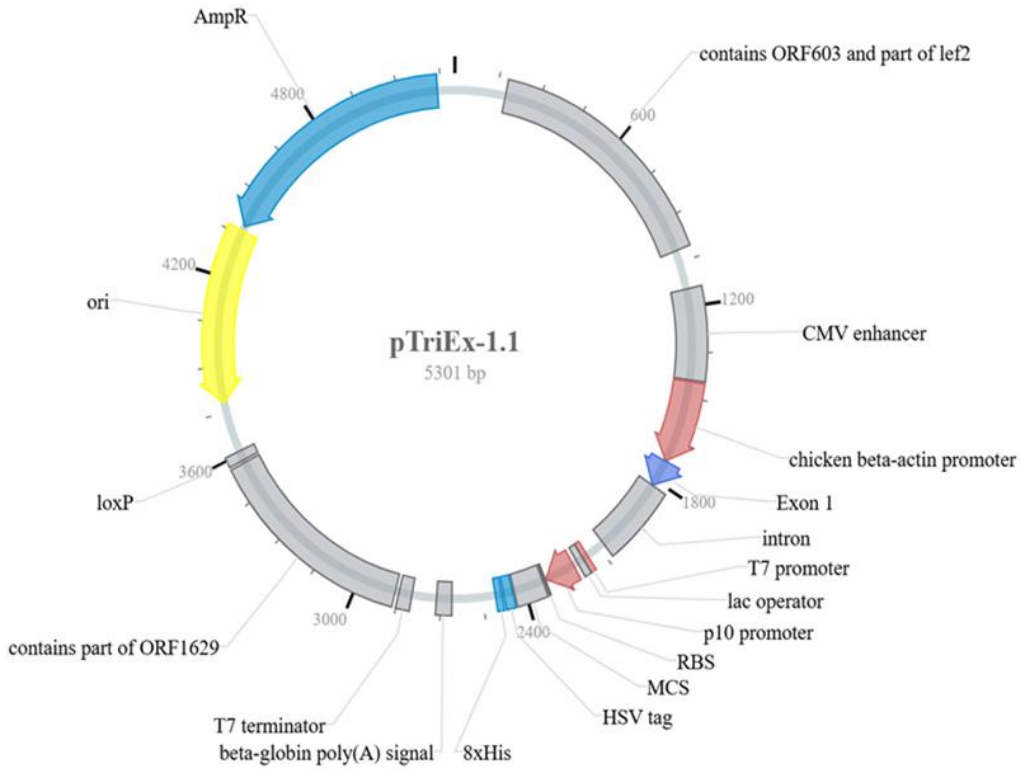

Figure 11. Map of the pTriEx1.1 vector. It is designed for tri-host protein expression in *E. coli*, insect cells (via baculovirus), and mammalian cells. Key vector elements include: T7 promoter for *E. coli* strains expressing, p10 promoter for baculoviral late promoter for strong expression in insect cells when using bacmid-based systems. CMV immediate-early promoter for mammalian cells expression, N-terminal His-Tag, HSV-tag, multiple cloning site (MCS), and ampicillin resistance gene for plasmid selection in *E. coli*. (EMD Chemicals Inc, 2011).

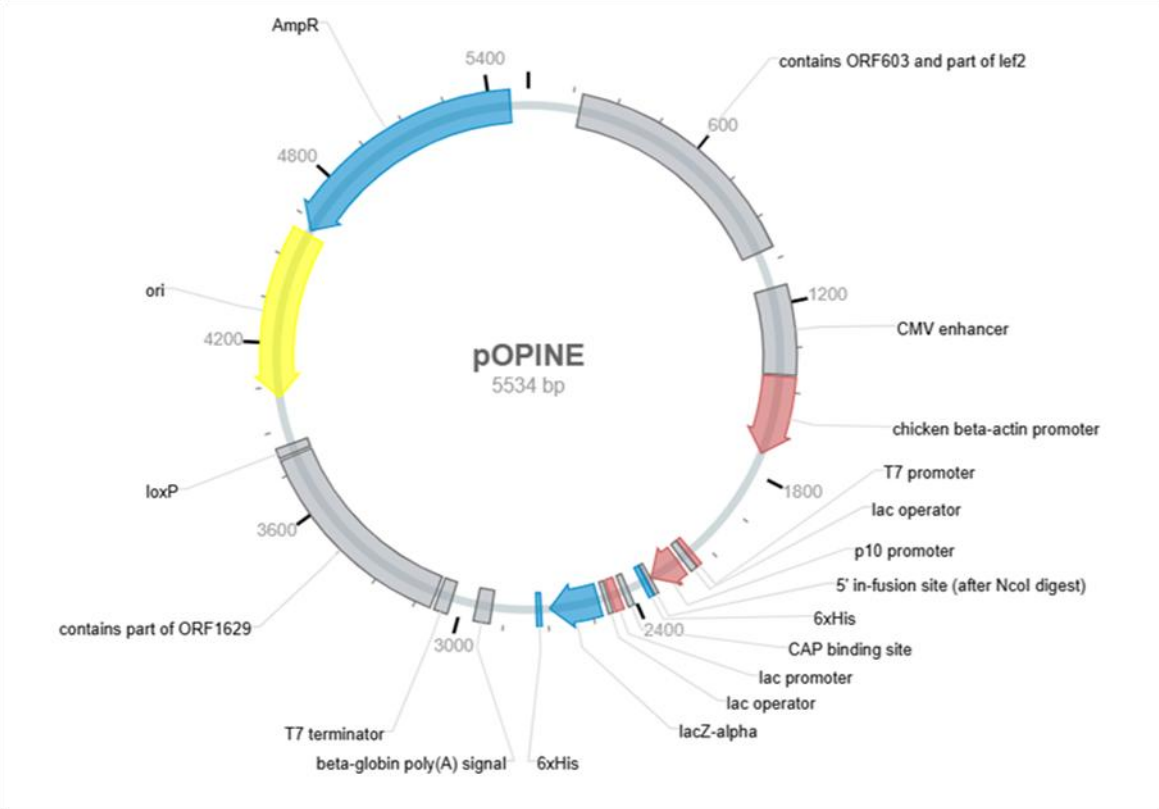

Figure 12. Map of the pOPINE vector. The vector includes the following elements: T7 in *E. coli*, p10 in insect cells independent of baculoviral infection and CMV in mammalian cells with ampicillin resistance gene, CAP binding site (catabolite activator protein) is a transcriptional activator in *E. coli* and His-tag (Berrow *et al.*, 2007).

Table 6. The mutants list for PV3 Saukett SC8 capsid proteins in pTriEX1.1 vector.

Plasmid	Description	Source
pTriEX1.1-SUMO-VP3 (KanR)	pTriEX1.1vector encoding SUMO (Small Ubiquitin-Like Modifier) tag cloning with VP3 and kanamycin resistant (kanR).	Mulley, G. unpublished
pTriEX1.1-SUMO-VP1 (AmpR)	pTriEX1.1vector encoding SUMO (Small Ubiquitin-Like Modifier) tag cloning with VP1 and ampicillin resistance marker (ampR)	Mulley, G. unpublished
pTriEX1.1-SUMO-VP0 (SpcR)	pTriEX1.1vector encoding SUMO (Small Ubiquitin-Like Modifier) tag cloning with VP0 and spectinomycin resistant (spcR)	Mulley, G. unpublished

Table 7. The N- terminus and C- terminus mutants list for PV1 Mahoney SC6b.

Plasmid	Description	Source
pOPINE Mahoney SC6b	pOPINEvector contains PV1 Mahoney P1+2A and frameshifted 3C with SC6b mutations	Host lab collaborator
pOPINE-Mahoney P1 VP4 Matrix	pOPINEvector contains PV1 Mahoney P1+2A and frameshifted 3C SC6b mutation with the myristoylation site from the HIV matrix protein (P17) inserted at VP4 N-terminus	This study
pOPINE-Mahoney P1 VP4 Marck	pOPINEvector contains PV1 Mahoney P1+2A and frameshifted 3C SC6b mutation with Marck as myristoylated proteins inserted at VP4 N-myristoylation	This study
pOPINE MahoneyP1VP4 Manduca	pOPINEvector contains PV1 Mahoney P1+2A and frameshifted 3C SC6b mutation with Manduca inserted at VP4 N-myristoylation	This study
pOPINE-Mahoney P1 VP4 ARF1	pOPINEvector contains PV1 Mahoney P1+2A and frameshifted 3C SC6b mutation with ARF1 inserted at VP4 N-myristoylation	This study
pOPINE-Mahoney P1 VP4 Recoverin	pOPINEvector contains PV1 Mahoney P1+2A and frameshifted 3C SC6b mutation with Recoverin as myristoylated proteins inserted at VP4 N-myristoylation	This study
pOPINE-Mahoney P1 VP4 opt1	pOPINEvector contains PV1 Mahoney P1+2A and frameshifted 3C SC6b mutation with opt1 inserted at VP4 N-myristoylation	This study
pOPINE-Mahoney P1 VP4 opt2	pOPINEvector contains PV1 Mahoney P1+2A and frameshifted 3C SC6b mutation with opt2 inserted at VP4 N-myristoylation	This study
pOPINE-Mahoney P1 VP4 opt3	pOPINEvector contains PV1 Mahoney P1+2A and frameshifted 3C SC6b mutation with opt3 inserted at VP4 N-myristoylation	This study
pOPINE-Mahoney P1 VP4 opt4	pOPINEvector contains PV1 Mahoney P1+2A and frameshifted 3C SC6b mutation with opt4 inserted at VP4 N-myristoylation	This study
pOPINE-Mahoney P1 VP4 opt5	pOPINEvector contains PV1 Mahoney P1+2A and frameshifted 3C SC6b mutation with opt5 inserted at VP4 N-myristoylation	This study
pOPINE-Mahoney P1 VP4 opt6	pOPINEvector contains PV1 Mahoney P1+2A and frameshifted 3C SC6b mutation with opt6 inserted at VP4 N-myristoylation	This study

Plasmid	Description	Source
pOPINE Mahoney P1 VP4 3C-0	pOPINEvector contains PV1 Mahoney P1 with 3C cleavage site positioned at the end of VP1.	Mai Uchida unpublished
pOPINE Mahoney P1 VP4 3C-5	pOPINEvector contains PV1 Mahoney P1with 3C cleavage site positioned at the end of VP1 and the last 5 amino acids of the VP1 C-terminus were deleted.	Mai Uchida unpublished
pOPINE Mahoney P1 VP4 3C-10	pOPINEvector contains PV1 Mahoney P1with 3C cleavage site positioned at the end of VP1 and the last 10 amino acids of the VP1 C-terminus were deleted.	Mai Uchida unpublished
pOPINEMahoney P1 VP1 3C-15	pOPINEvector contains PV1 Mahoney P1with 3C cleavage site positioned at the end of VP1 and the last 15 amino acids of the VP1 C-terminus were deleted.	Mai Uchida unpublished
pOPINE-Mahoney PV1 T24G	pOPINEvector contains PV1 Mahoney P1+2A and frameshifted 3C SC6b mutation that confers a threonine to glycine substitution at position 24 within VP4.	This study
pOPINE-Mahoney PV1 T28G	pOPINEvector contains PV1 Mahoney P1+2A and frameshifted 3C SC6b mutation that confers a threonine to glycine substitution at position 28 within VP4.	This study
pOPINE-Mahoney PV1 T29G	pOPINEvector contains PV1 Mahoney P1+2A and frameshifted 3C SC6b mutation that confers a threonine to glycine substitution at position 29 within VP4.	This study
pOPINE-Mahoney PV1 T24V	pOPINEvector contains PV1 Mahoney P1+2A and frameshifted 3C SC6b mutation that confers a threonine to valine substitution at position 24 within VP4.	This study
pOPINE-Mahoney PV1 T28V	pOPINEvector contains PV1 Mahoney P1+2A and frameshifted 3C SC6b mutation that confers a threonine to valine substitution at position 28 within VP4.	This study
pOPINE-Mahoney PV1 T29V	pOPINEvector contains PV1 Mahoney P1+2A and frameshifted 3C SC6b mutation that confers a threonine to valine substitution at position 29 within VP4.	This study
pTriEx1.1 Mahoney VP0-GFP	pTriEx1.1 vector contains VP0 of Mahoney SC6b PV1 with GFP sequence in the C-terminal to VP4	This study
pTriEx1.1 T24G Mahoney VP0-GFP	pTriEx1.1 vector contains T24G in VP0 of Mahoney SC6b PV1 with GFP sequence in the C-terminal to VP4	This study
pTriEx1.1 T28G Mahoney VP0-GFP	pTriEx1.1 vector contains T28G in VP0 of Mahoney SC6b PV1 with GFP sequence in the C-terminal to VP4	This study
pTriEx1.1 T29G Mahoney VP0-GFP	pTriEx1.1 vector contains T29G in VP0 of Mahoney SC6b PV1 with GFP sequence in the C-terminal to VP4	This study

Plasmid	Description	Source
pTriEx1.1 T24V Mahoney VP0-GFP	pTriEx1.1 vector contains T24V in VP0 of Mahoney SC6b PV1 with GFP sequence in the C-terminal to VP4	This study
pTriEx1.1 T28V Mahoney VP0-GFP	pTriEx1.1 vector contains T28V in VP0 of Mahoney SC6b PV1 with GFP sequence in the C-terminal to VP4	This study
pTriEx1.1 T29V Mahoney VP0-GFP	pTriEx1.1 vector contains T29V in VP0 of Mahoney SC6b PV1 with GFP sequence in the C-terminal to VP4	This study
pOPINE-Mahoney PV1 T24G 3C-0	pOPINE vector contains PV1 Mahoney P1 with T24G and 3C cleavage positioned at the end of VP1	This study
pOPINE-Mahoney PV1 T28G 3C-0	pOPINE vector contains PV1 Mahoney P1 with T28G and 3C cleavage positioned at the end of VP1	This study
pOPINE-Mahoney PV1 T29G 3C-0	pOPINE vector contains PV1 Mahoney P1 with T29G and 3C cleavage positioned at the end of VP1	This study
pOPINE-Mahoney PV1 T24V 3C-0	pOPINE vector contains PV1 Mahoney P1 with T24V and 3C cleavage positioned at the end of VP1	This study
pOPINE-Mahoney PV1 T28V 3C-0	pOPINE vector contains PV1 Mahoney P1 with T28V and 3C cleavage site positioned at the end of VP1	This study
pOPINE-Mahoney PV1 T29V 3C-0	pOPINE vector contains PV1 Mahoney P1 with T29V and 3C cleavage site positioned at the end of VP1	This study

2.1.3 Recombinant Baculoviruses

The recombinant baculovirus stocks were stored at 4°C.

Table 8. A list of recombinant baculovirus strains was made in this study.

Virus	Vector used	Description
Bac- PV1SC6b	pOPINE-Mahoney SC6b-P1 3C	Expresses the PV1 Mahoney SC6b P1 structural proteins, which are cleaved by 3C protease insect cells.
Bac- P1 3C Matrix	pOPINE-Mahoney P1 3C Matrix	Expresses the PV1 Mahoney SC6b P1 structural proteins, which are cleaved by 3C protease insect cells.
Bac- P1 3C Marck	pOPINE-Mahoney P1 3C Marck	Expresses the PV1 Mahoney SC6b P1 structural proteins, which are cleaved by 3C protease insect cells.
Bac-P13C Manduca	pOPINE Mahoney P1 3C Manduca	Expresses the PV1 Mahoney SC6b P1 structural proteins, which are cleaved by 3C protease insect cells.
Bac- P1 3C ARF1	pOPINE-Mahoney P1 3C ARF1	Expresses the PV1 Mahoney SC6b P1 structural proteins, which are cleaved by 3C protease insect cells.
Bac-P13C Recoverin	pOPINE-Mahoney P1 3C Recoverin	Expresses the PV1 Mahoney SC6b P1 structural proteins, which are cleaved by 3C protease insect cells.
Bac- P1 3C opt1	pOPINE-Mahoney P1 3C opt1	Expresses the PV1 Mahoney SC6b P1 structural proteins, which are cleaved by 3C protease insect cells.
Bac- P1 3C opt2	pOPINE-Mahoney P1 3C opt2	Expresses the PV1 Mahoney SC6b P1 structural proteins, which are cleaved by 3C protease insect cells.
Bac- P1 3C opt3	pOPINE-Mahoney P1 3C opt3	Expresses the PV1 Mahoney SC6b P1 structural proteins, which are cleaved by 3C protease insect cells.
Bac- P1 3C opt4	pOPINE-Mahoney P1 3C opt4	Expresses the PV1 Mahoney SC6b P1 structural proteins, which are cleaved by 3C protease insect cells.
Bac- P1 3C opt5	pOPINE-Mahoney P1 3C opt5	Expresses the PV1 Mahoney SC6b P1 structural proteins, which are cleaved by 3C protease insect cells.
Bac-P1 3C opt6	pOPINE-Mahoney P1 3C opt6	Expresses the PV1 Mahoney SC6b P1 structural proteins, which are cleaved by 3C protease insect cells.

Virus	Vector used	Description
Bac- P1 3C-0	pOPINE Mahoney P1 3C-0	Recombinant baculovirus to express PV1 Mahoney P1 3C-0 structural proteins.
Bac- P1 3C-5	pOPINE Mahoney P1 3C-5	Recombinant baculovirus to express PV1Mahoney P1 3C-5 structural proteins.
Bac- P1 3C-10	pOPINE Mahoney P1 3C-10	Recombinant baculovirus to express PV1 Mahoney P1 VP4 3C-10 structural proteins
Bac- P1 3C-15	pOPINE Mahoney P1 3C-15	Recombinant baculovirus to express PV1 Mahoney P1 VP1 3C-15 structural proteins
Bac- Mahoney PV1-P13C T24G	pOPINE- vector contains Mahoney PV1 P13C T24G sequence	Recombinant baculovirus to express Mahoney PV1 P1 T24G structural proteins cleaved by 3C
Bac- Mahoney PV1-P13C T28G	pOPINE- vector contains Mahoney PV1 P13C T28G sequence	Recombinant baculovirus to express Mahoney PV1 P1 T28G structural proteins cleaved by 3C
Bac- Mahoney PV1-P1 3C T29G	pOPINE- vector contains Mahoney PV1 P13C T29G sequence	Recombinant baculovirus to express Mahoney PV1P1 T29G structural proteins cleaved by 3C
Bac- Mahoney PV1 P1 3C T24V	pOPINE- vector contains Mahoney PV1 P1 3C T24V sequence	Recombinant baculovirus to express Mahoney PV1 T24V structural proteins cleaved by 3C
Bac- Mahoney PV1- P13C T28V	pOPINE- vector contains Mahoney PV1 P13C T28V sequence	Recombinant baculovirus to express Mahoney PV1 T28V structural proteins cleaved by 3C
Bac- Mahoney PV13C T29V	pOPINE- vector contains Mahoney PV1 P13C T29V sequence	Recombinant baculovirus to express Mahoney PV1 T29V structural proteins cleaved by 3C
Bac- Mahoney PV1 VP0-GFP	pTriEx1.1 vector contains Mahoney PV1 VP0-GFP sequence	Recombinant baculovirus to express Mahoney VP0-GFP structural proteins

Virus	Vector used	Description
Bac-Mahoney PV1 T24G VP0-GFP	pTriEx1.1 vector contains T24G Mahoney PV1 VP0-GFP sequence	Recombinant baculovirus to express T24G Mahoney VP0-GFP structural proteins
Bac- Mahoney PV1 T28G VP0-GFP	pTriEx1.1 vector contains T28G Mahoney PV1VP0-GFP sequence	Recombinant baculovirus to express T28G Mahoney VP0-GFP structural proteins
Bac-Mahoney PV1 T29G VP0-GFP	pTriEx1.1 vector contains T29G Mahoney VP0-GFP sequence	Recombinant baculovirus to express T29G Mahoney VP0-GFP structural proteins
Bac-Mahoney PV1 T24V VP0-GFP	pTriEx1.1 vector contains T24V Mahoney PV1 VP0-GFP sequence	Recombinant baculovirus to express T24V Mahoney VP0-GFP structural proteins
Bac-Mahoney PV1 T28V VP0-GFP	pTriEx1.1 vector contains T28V Mahoney VP0-GFP sequence	Recombinant baculovirus to express T28V Mahoney VP0-GFP structural proteins
Bac- Mahoney PV1 T29V VP0-GFP	pTriEx1.1 vector contains T29V Mahoney PV1 VP0-GFP sequence	Recombinant baculovirus to express T29V Mahoney VP0-GFP structural proteins
Bac-Mahoney PV1 P1-T24G 3C-0	pOPINE- vector contains Mahoney PV1 T24G 3C-0 sequence	Recombinant baculovirus to express Mahoney PV1 T24G 3C-0 structural proteins
Bac- Mahoney PV1 P1-T28G 3C-0	pOPINE- vector contains Mahoney PV1 T28G 3C-0 sequence	Recombinant baculovirus to express Mahoney PV1 T28G 3C-0 structural proteins
Bac-Mahoney PV1 P1-T29G 3C-0	pOPINE- vector contains Mahoney PV1 T29G 3C-0 sequence	Recombinant baculovirus to express Mahoney PV1 T29G 3C-0 structural proteins

Virus	Vector used	Description
Bac-Mahoney PV1 P1-T24V 3C-0	pOPINE- vector contains Mahoney PV1 T24V 3C-0 sequence	Recombinant baculovirus to express Mahoney PV1 T24V 3C-0 structural proteins
Bac-Mahoney PV1 P1-T28V 3C-0	pOPINE- vector contains Mahoney PV1 T28V 3C-0 sequence	Recombinant baculovirus to express Mahoney PV1 T28V 3C-0 structural proteins
Bac- Mahoney PV1 P1-T29V 3C-0	pOPINE- vector contains Mahoney PV1 T29V 3C-0 sequence	Recombinant baculovirus to express Mahoney PV1 T29V 3C-0 structural proteins

2.1.4 Primers

The oligonucleotide primers used in this study **(Table 8)** were purchased from Sigma-Aldrich at a concentration of 20 µM and stored at -20 °C. Primers for the recombinational cloning were designed using primer design tool from Takara Bio (Primer Design Tool for In-Fusion®,2025).

Table 9. Primers used in this study. Primers used for recombinational cloning of Poliovirus sequences contain a 5' region complementary to the vector insertion site up to the start codon of VP4 (underscore) and an identical 3' region to amplify the PV sequence (highlighted in bold).

Primer	**Sequence** **5'- 3'**
Matrix Fw_Main	TTACAATCAAAGGAGGTTACCATGGGTGCAAGAGCTTCCGTCTTGTC T**GTCGGAGCCCACGAAAACAGCAATGGCGCATAC**
ARF1 Fw_Main	TTACAATCAAAGGAGGTTACCATGGGTAACATCTTTGCTAATTTGTTC **GTCGGAGCCCACGAAAACAGCAATGGCGCATAC**
Manduca Fw_Main	TTACAATCAAAGGAGGTTACCATGGGCGGCCTCTTTTCTTACTTTCGT **GTCGGAGCCCACGAAAACAGCAATGGCGCATAC**
Recoverin Fw_Main	TTACAATCAAAGGAGGTTACCATGGGTAATTCCAAGAGTGGTGCGTT G**GTCGGAGCCCACGAAAACAGCAATGGCGCATAC**
opt1 Fw_Main	TTACAATCAAAGGAGGTTACCATGGGAAATGCAGCCGCGGCGC**GTC** **GCGTCGGAGCCCACGAAAACAGCAATGGCGCATAC**
opt2 Fw_Main	TTACAATCAAAGGAGGTTACCATGGGAAATGCTGCAAGCGCAGAGG AG**GTCGGAGCCCACGAAAACAGCAATGGCGCATAC**
opt4 Fw_Main	TTACAATCAAAGGAGGTTACCATGGGTAGTTCTAAATCAAAGCCAAA A**GTCGGAGCCCACGAAAACAGCAATGGCGCATAC**
opt5 Fw_Main	TTACAATCAAAGGAGGTTACCATGGGTTGTACTCTGTCAGCGGAAGA C**GTCGGAGCCCACGAAAACAGCAATGGCGCATAC**
Opt6 Fw_Main	TTACAATCAAAGGAGGTTACCATGGGTTGCAGGCAGAGCTCCGAAGA A**GTCGGAGCCCACGAAAACAGCAATGGCGCATAC**
Opt3 Fw_Main	TTACAATCAAAGGAGGTTACCATGGGAAATAGAGCAGCGGCCAGAC GC**GTCGGAGCCCACGAAAACAGCAATGGCGCATAC**

Primer	Sequence 5'- 3'
Marck Fw_Main	TTACAATCAAAGGAGGTTACCATGGGAGCACAGTTTTCTAAAACCGC C**GTCGGAGCCCACGAAAACAGCAATGGCGCATAC**
T28GF	GGAGGATCTACAATAAACTATGGAACAATAAATTATTATCGAG
T28GR	CTCGATAATAATTTATTGTTCCATAGTTTATTGTAGATCCTCC
T28VF	GGAGGATCTACAATAAACTATGTAACAATAAATTATTATCGAG
T28VR	CTCGATAATAATTTATTGTTACATAGTTTATTGTAGATCCTCC
T29GF	GGAGGATCTACAATAAACTATACAGTAATAAATTATTATCGAG
T29GR	CTCGATAATAATTTATTCCTGTATAGTTTATTGTAGATCCTCC
T29VF	GGAGGATCTACAATAAACTATACAGTAATAAATTATTATCGAG
T29VR	CTCGATAATAATTTATTACTGTATAGTTTATTGTAGATCCTCC
T24GF	GGAGGATCTGGAATAAACTATACAACAATAAATTATTATCGAG
T24GR	CTCGATAATAATTTATTGTTGTATAGTTTATTCCAGATCCTCC
T24VF	GGAGGATCTGTAATAAACTATGGAACAATAAATTATTATCGAG
T24VR	CTCGATAATAATTTATTGTTCCATAGTTTATTACAGATCCTCC
VP0_SGF	TTTACAATCAAAGGAGGTTACCATGGGAGCACAAGTCTCATCACAAA AAGTCGG
VP0_SGR	CTTGAATGGAGTAGAGGCCATGCCACTACCGCCTGAGCCTTGTAATC TGGGTAATGTGATG
VP0_SGF2	CATCACATTACCCAGATTACAAGGCTCAGGCGGTAGTGGCATGGCCT CTACTCCATTCAAG
VP0_SGR	ATGGTGATGATGGTGGTGGAGGTGCGCCTCGAGAGTTTCGG
T7 promoter (forward prime)	TAA TAC GAC TCA CTA TAG GG
Trix Down2 (reverse primer)	TCGATCTCAGTGGTATTTGTGAGC

2.1.5 Antibodies

All antibodies were stored at 4 °C for short-term use and at −20 °C for long-term storage.

Table 10. Typical antibody combinations for detecting specific antigens.

Antibody	Detection	Manufacturer
Anti-Poliovirus1 Antibody	Detection of PV1 VP1	Sigma-Aldrich- MAB8560
Mouse anti-baculovirus p39 sera	Detection of baculovirus p39	Host lab collaborator
Anti-poliovirus Blend Antibody	Detection all serotypes PV VP1	Millipore, Germany - MAB8566
Rabbit anti-VP1 sera poliovirus 1 Ab (R879) (at 1:500)	Detection of PV1 VP1	Host lab collaborator
Polyclonal Goat Anti-mouse Immunoglobulins/HRP,	Anti-mouse antibody conjugated with HRP	Dako, Denmark- P0447
Polyclonal Goat Anti-rabbit Immunoglobulins/HRP,	Anti-rabbit antibody conjugated with HRP	Dako, Denmark -P0448
Monoclonal Ab 234 PV1	N specific Ab for N/H ELISA	NIBSC, UK
Monoclonal Ab 1588 PV1	H specific Ab for N/H ELISA	NIBSC, UK
Anti-Mouse IgG (whole molecule)–FITC antibody produced in goat	Anti-mouse antibody conjugated with FITC	Sigma-Aldric (F0257)
HRP-conjugated Anti-6X His tag antibody	Detection of 6X His tag Synthetic peptide	Abcam(ab1187)
Rabbit anti-VP0 sera	VP0 detection	Host lab collaborator
Rabbit anti-VP3 sera	VP3 detection	Host lab collaborator

2.2 Methods

This section outlines the DNA methodologies, including the construction of expression vectors for insect cells, the production of recombinant proteins using *E. coli* and baculovirus expression systems, SDS-PAGE analysis, protein purification techniques, microscopy-based examination of VLPs, and antigenicity testing of VLPs.

2.2.1 Polymerase Chain Reaction (PCR)

The manufacturer's protocol for Phusion High-Fidelity PCR Master Mix with HF Buffer (ThermoScientific) was used for the PCR amplification reaction as it has a very low error rate. The reaction was prepared to contain 0.5 µM from forward and reverse primers, >5ng DNA template and adjusting to final volume 50 µl with Nuclease-free water. The reactions were placed in a thermal cycler (SensoQuest Labcycler, Geneflow). The PCR reaction was performed as follows: initial denaturation at 98°C for 30 seconds, and then 35 cycles of denaturation for 10 seconds at 98 °C, annealing for 30 seconds at 55°C - 64°C (depending on the annealing temperature of the different primer pairs) and an extension step for 1 minute 30 seconds at 72°C followed by a final extension for 10 minutes at 72°C. PCR products were then separated by agarose gel electrophoresis to ensure the correct size of the amplified products.

2.2.2 DNA Agarose Gel Electrophoresis

Agarose gel electrophoresis was used to purify and visualize DNA fragments. 0.8% w/v agarose gels were prepared by mixing agarose powder in 1X Tris-acetate-EDTA (TAE; National Diagnostic, US through Geneflow, UK) and heated in a microwave at full power for several minutes until fully dissolved. Then, after cooling to 45°C 1X Gel Red nucleic acid stain (Millipore) was added to the molten gel 10 µl per 100 ml and poured into a gel tray with an appropriate comb to set. Gels were placed in an electrophoresis tank (MultiSUB Midi Horizontal Gel Unit, Geneflow) filled with 1X Tris-acetate-EDTA (TAE) buffer (Thermo Scientific).

Samples were prepared by adding 8.3 µl DNA Gel Loading Dye (6X; Thermo Scientific) to 50 µl reaction. Then, 8 µl from each sample was loaded in the gel for imaging or 50 µl was loaded for gel extraction step. To determine the size of DNA fragments, 2 µl GeneRuler 1 kb Plus DNA Ladder (Thermo Scientific) was added to 5 µl TAE buffer before loading. Electrophoresis was performed at 90 V for 60 minutes. Gels were imaged using a G: BOX Chemi XL (Syngene).

2.2.3 Gel Extraction of DNA

PCR products were purified from agarose gels using the GeneJET Gel Extraction and DNA Cleanup Micro Kit (ThermoScientific) as per the manufacturer's protocol. A sterile scalpel was used to cut the DNA fragment from the agarose gel; 1 ml of binding buffer was added per mg of gel slice and then incubated for 10 min at 50-60 °C in a water bath. The solubilized gel solution was transferred to the purification column and centrifuged for 1 min at 4500 rpm. The sample was washed with a wash buffer to remove residual gel and centrifuged twice for 1 min. The column was then centrifuged to dry the membrane for 1 min and the DNA eluted into a new collection tube using 50 µL of elution buffer and centrifugation at 4500 rpm for 1 min. The DNA concentration was measured by Nanodrop spectrophotometer (ThermoScientific) and stored at -20 °C.

2.2.4 Restriction Digests

Plasmid DNA was linearised using the restriction endonucleases (ThermoFisher Scientific). Restriction endonucleases and buffers were purchased in the Fast Digest format (ThermoScientific). Reactions were made according to the flowing protocol: 2 µl 10x Fast Digest Green buffer, 500 ng plasmid DNA, 1 µl of each restriction enzyme, and adjusted to a final volume of 20 µLwith nuclease-free dH_2O. Reactions were incubated at 37°C for 30 min.

2.2.5 Recombinational Cloning

Recombinational cloning was used to clone the PCR amplified products into linearized vectors. There are several methods of recombinational cloning that enable site specific recombination of DNA fragments that are independent of the insert DNA sequence of interest, distinguishing it from traditional restriction enzyme-based cloning methods that rely on the presence of specific motifs (Park & LaBaer, 2006). Any two pieces of DNA with 15 bp of complementarity at their ends can be joined in a recombinational cloning reaction.

The regions of complementarity to the linearized vector were incorporated at the 5' end of the primers used to amplify the desired insert. PCR amplified products were cloned into the linearized vector using the NEBuilder HiFi DNA Assembly Kit with a 1:2 vector:insert ratio, 5 µL NEBuilder HiFi DNA Assembly Master Mix in a total volume of 10 µL. Reactions were incubated at 50 °C for 15 minutes incubation then placed on ice or stored at -20°C prior to transformation of 2.5 µLof the NEBuilder HiFi DNA Assembly reaction into 25 µL chemically competent *E. coli* cells.

2.2.6 Restriction-ligation Cloning

Purified PCR products were combined with linearized vectors in a 3:1 molar ratio with 1X T4 DNA Ligase Buffer and 1 unit of T4 DNA Ligase (ThermoScientific) in a total reaction volume of 20 µL. The reaction was incubated for 10 min at 22 °C. 1 - 5 µL of the mixture was transformed into 50 µL of *E. coli* chemically competent cells.

2.2.7 Competent *E. coli* Cells Preparation

The *E. coli* cell line was streaked on an LB-agar plate and incubated overnight at 37°C. The following day, 10 ml of LB medium were inoculated and incubated at 37°C with shaking at 250 rpm overnight. The culture was subcultured by diluting 1 ml overnight culture in 9 mL of fresh LB broth and incubated with shaking at 250 rpm, 37 °C until reaching an OD_{600} of 0.4-0.6. The culture was centrifuged at 4500 rpm for 10 min at 4°C and the supernatant discarded. The resultant cell pellet was placed on ice and gently resuspended in 4 mL of ice-cold 100 mM $CaCl_2$. Following a 15 min incubation on ice, the cells were centrifuged at 4500 rpm for 10 min at 4°C. The resultant cell pellet was resuspended in 100 µL of 100 mM $CaCl_2$. The chemically competent *E. coli* cells were stored at -80°C.

2.2.8 Transformation of Chemically Competent *E. coli* cells

Following addition of the cloning reaction mix, chemically competent cells were incubated on ice for 30 min, then heat shocked at 42 °C for 30 s, then placed back on the ice for 2 min. 200 µl SOC medium was added to recover the cells from heat shock and incubated at 37 °C for 1 h with shaking at 250 rpm. Transformations were plated on selective LB agar containing appropriate selective antibiotics and incubated at 37 °C overnight. Negative controls with linearized vectors only were also performed to ensure a low background of the undigested vector. Three transformants from recombinational cloning reactions were selected and inoculated in LB supplemented with appropriate antibiotics overnight to purify plasmids and confirm the correct constructs by Sanger sequencing.

2.2.9 Plasmid Purification

Plasmid DNA was extracted from 10 mL overnight *E. coli* LB cultures using the GeneJET Plasmid Miniprep Kit (Thermo Scientific), following the manufacturer's instructions. Cultures were centrifuged at 4,500 rpm for 15 min, the supernatant was discarded, and the resulting pellet

was resuspended in 250 µL of resuspension solution and vortexed thoroughly. Cells were lysed by adding 250 µL of lysis buffer and gently inverting the tubes five times. Subsequently, 350 µL of neutralization solution was added, and the mixture was centrifuged for 5min. The clarified supernatant was loaded onto a spin column to bind the plasmid DNA, followed by 1 min centrifugation. The column was washed twice and centrifuged for 1 min between each wash. Finally, 50 µL of elution buffer was applied to the column, incubated at room temperature for 2 min, and centrifuged for 2 min to elute the plasmid DNA. DNA concentration was measured by Nanodrop spectrophotometer (ThermoScientific), and samples were stored at −20 °C.

2.2.10 Quantification of DNA

The Nanodrop spectrophotometer (ThermoScientific) was used to measure the concentration of the purified plasmid and PCR products from 2 µl aliquots of sample. A suitable buffer (typically elution buffer) was used as a blank as per the manufacturer's protocol.

2.2.11 Colony PCR

Colony PCR is a technique employed to rapidly assess bacterial colonies produced during the transformation step of a molecular cloning process (Azevedo *et al.*, 2017). Each selected colony was boiled with 10 µl dH_2O at 95°C for 5 min and 1µl was then used as template DNA in the PCR reaction containing 0.5 µM forward primer, 0.5 µM reverse primer T7F2 (forward prime)Trix Down2 (reverse primer) and 25 µL DreamTaq PCR Master Mix (Thermo Scientific) to a final volume of 50 µL completed with nuclease-free water. The reactions were gently vortexed and spun down.Initial denaturation temperature 95°C for 1-3 min (1 cycle). Denaturation: 95°C for 30 s (25-40 cycles). Annealing temperature - 5°C for 30 s (25-40 cycles) Extension temperature 72°C for 1 min (25-40 cycles). Final Extension temperature 72°C for 5-15 min (1 cycle). PCR products were then separated by agarose gel electrophoresis to detect the presence of the expected inserts.

2.2.12 Sequencing DNA

Purified plasmid DNA (10 µL) with a concentration between 500-600 ng/µl was sent to Source Bioscience for Sanger sequencing. The T7 forward promoter primer was used to sequence inserts in the vector cloning site.

2.2.13 Production of VLPs using *E. coli* Expression System

Under the control of strong promoters such as the T7 promoter, *E. coli* expression systems can efficiently produce proteins in a cost-effective manner.

2.2.13.1. Induction of Protein Expression in Recombinant *E. coli*

E. coli strains carrying expression vectors were cultured overnight in LB medium supplemented with appropriate antibiotics with shaking at 250 rpm at 37°C. The following day, the cultures were diluted 1:100 in fresh LB medium containing 0.1% glucose (*v/v*) and incubated at 37 °C until reaching an optical density at 600 nm (OD_{600}) of 0.4–0.6 (approximately 2–3 h). Then, 1 mL of each uninduced culture was collected and centrifuged at 4500 rpm for 5 min and the supernatant discarded. The cell pellets were stored at -20°C for SDS-PAGE analysis. For the induction, IPTG was added to 1 mM to the remaining *E. coli* BL21-DE3 cultures, followed by incubation at 37°C with shaking for an additional 2 h. In the *E. coli* BL21-AI strain, 1 mM IPTG and 0.2% arabinose were added to regulate the expression of toxic proteins, with the additional arabinose required to activate expression of T7RNAP via the araBAD promoter and then incubated under the same conditions. Following the inductions, the absorbance measurements were taken (OD_{600}) using a spectrophotometer with 1 mL cuvettes, after diluting the cultures 1:10 in LB medium. In the last step, 1 mL samples from each induced culture were centrifuged at 4500 rpm for 5 min and the supernatant discarded, and the resulting cell pellets were stored at -20 °C for further analysis.

2.2.13.2. Solubility of Proteins in *E. coli*

To test the solubility of the recombinant proteins, cell pellets were resuspended in B-PER bacterial cell lysis buffer (Thermo Scientific -78243). The volume of B-PER lysis buffer was adjusted to account for the OD of culture and then incubated 15 min on ice, with intermittent vortexing. The lysed cells were centrifuged for 5 min at 12000 rpm to pellet insoluble fraction. The supernatant was collected in new tubes on ice and pellets were placed on ice and resuspended in an equivalent volume of 8M urea.

2.2.13.3. Extraction of Insoluble Recombinant Proteins from *E. coli* Inclusion Bodies

Pellets were resuspended in B-PER lysis buffer and incubated on ice for 15 min with intermittent vortexing. After incubation, the lysed cells were centrifuged at 4500 rpm for 15 min. The resulting insoluble pellets were extensively washed with 1x TBST, the pellets becoming progressively whiter with each wash. A final white pellet with no traces of brown was denatured using 1% Sodium Dodecyl Sulfate (SDS), (Invitrogen™ AM9822) at room temperature until fully clarified.

The samples were then centrifuged at 10,000 rpm for 20 min. The supernatants containing solublised protein were collected in new tubes and stored at 4 °C.

2.2.13.4. Purification of His-tagged Proteins Using Immobilised Metal Affinity Chromatography (IMAC)

Recombinant His-tagged proteins were purified using a His SpinTrap (Cytiva -28401353). The storage solution was removed, and the column was equilibrated by adding 600 µL of binding buffer (20 mM sodium phosphate, 500 mM NaCl, 20 mM imidazole, pH 7.4) then centrifuged for 30 s at 70 to 100 × g. The binding buffer was mixed with the clarified supernatant containing insoluble protein and incubated for 30 min at 4°C. 600 µL volumes of the sample were loaded to the column and centrifuged for 30 sec at 100 × g. The remaining samples were loaded in this way until all samples had been applied. The column was then washed by adding 600 µL binding buffer and centrifuging for 30 sec at 100 × g. Target proteins were eluted by adding 200 µL elution buffer (20 mM sodium phosphate, 500 mM NaCl, 500 mM imidazole, pH 7.4) to the column and centrifuging for 30 sec at 100 × g. The first elution of the purified sample was collected, and the elution step was repeated to obtain additional purified sample.

2.2.13.5. Proteolytic Removal of SUMO-tags from Recombinant Proteins

Following IMAC purification of SUMO-tagged proteins, the SUMO tags were removed using SUMO protease in the following reaction: purified recombinant SUMO-tagged protein, 10 units SUMO Protease (Invitrogen), 1X SUMO protease buffer +/- salt (both buffers supplied with the kit) and made to a final volume of 100 µl using sterile water. Reaction was mixed and 20 µl aliquots were incubated at varying temperatures (4°C, 16°C, 21°C and 30°) for 3 h.

2.2.14 Production of VLPs using the Baculovirus Expression System

The baculovirus expression system (BES) is an effective method for generating recombinant proteins, particularly in insect cells. It uses baculoviruses, particularly *Autographa californica multiple nucleopolyhedrovirus* (AcMNPV), as vectors for gene delivery into insect cells, resulting in increased production of the target protein(Bissett & Roy, 2024). The general methodology for the production of virus-like particles (VLPs) using the Baculovirus Expression System involves several key steps: gene cloning into a suitable baculovirus transfer vector; generation of recombinant bacmid DNA via homologous recombination following co-transfection of the transfer vector and baculovirus DNA into insect cells; amplification of viral stocks (P1, P2, etc.) to obtain high-titer recombinant baculoviruses; infection of insect cells for protein expression;

subsequent protein purification and analysis using SDS-PAGE; and finally, characterisation of the assembled VLPs **(Figure 13)**.

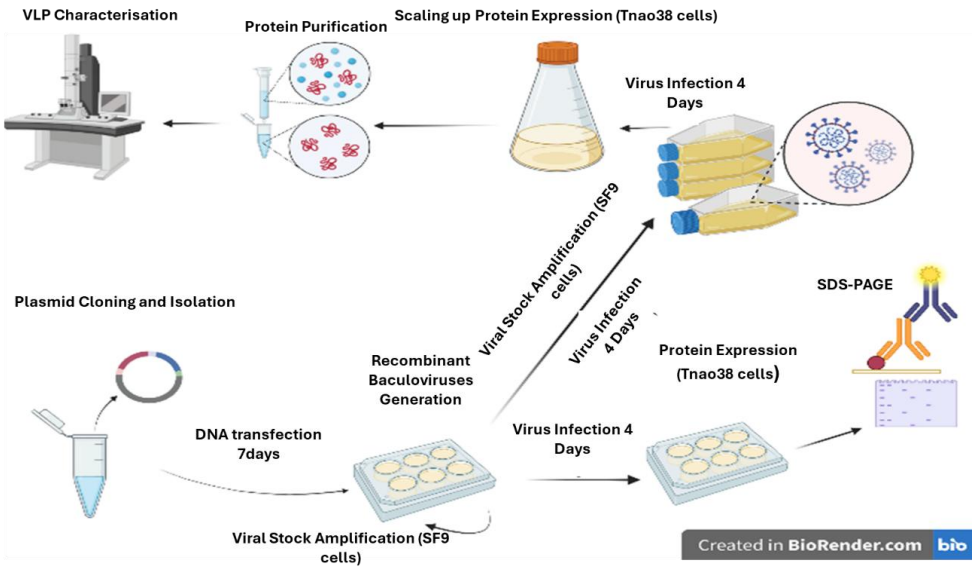

Figure 13. overview of the experimental workflow used in the baculovirus expression System. Plasmid was cloned and isolated from *E.coli*. DNA was transfected to *SF9* cells to produce recombinant virus stock. Tano38 was used for protein expression via infection by viral stock. SDS-PAGE was used to confirm production for the target protein. 30% Sucrose Cushion was used for large, infected cultures to purify the protein. VLPs were determined by TEM.

2.2.14.1. Culturing Insect Cells

Sf9 (Vaughn *et al.*, 1977) and Tano38 (Hashimoto *et al.*, 2010) insect cells were used to generate recombinant proteins by the Baculovirus Expression System.To start the culture, a frozen ampule of insect cells was rapidly thawed in a 37°C water bath. Once nearly thawed, the ampule was immersed in 70% ethanol to sterilize the exterior. The neck of the ampule was then broken, and the contents were transferred into a 25-cm² flask (Corning®) containing 4 ml of complete medium. The flask was gently rocked by hand to evenly distribute the cells and incubated at 27°C. After allowing the cells to attach for 2–3 h, the medium was replaced with 5 ml of fresh complete medium. The cultures were subsequently passaged every three days until 90% confluency was achieved. Once confluency was reached, the cells were subcultured into EX-CELL® 420 Serum-Free Medium (Sigma-Aldrich) supplemented with 2% fetal bovine serum (FBS) (Sigma-Aldrich) in sterile polycarbonate Erlenmeyer flasks (Corning®) with vented caps, at a density of 3–4× 10^5 cells/ml. The cultures were incubated at 27°C with shaking at 120 rpm for 3 days, or until 90% confluency was reached again.

2.2.14.2. Estimation of insect cell viability

Insect cell viability was estimated using trypan blue exclusion and an automated cell counter. A 10 µl aliquot of cell suspension was mixed with 10 µL of 0.4% trypan blue solution. The percentage of viable cells was determined using the Countess® Automated Cell Counter (Life Technologies).

2.2.14.3. Production of Recombinant Baculoviruses

Recombinant baculoviruses were created by transfecting *Sf9* cells with the FlashBAC™ GOLD (FBG, Oxford Expression Technologies) bacmid and an appropriately designed recombinant transfer vector. For each transfection, *Sf9* cells were seeded in a well of a 6-well tissue culture dish with a starting density of 1 x 10^6 cells/well then left for 20 min to adhere cells to the bottom of the wells. A transfection mix was prepared by combining 3 µL recombinant DNA vector (400-500 ng), 3 µL FBG bacmid DNA, and 6 µl nuclease-free water in a sterile PCR tube. A second PCR tube containing 8 µL lipofectin transfection reagent (ThermoScientific) and 4 µl nuclease-free water were prepared and the two solutions were mixed and incubated for 15 min at room temperature. The culture medium was removed from the well of the 6-well dish seeded with *Sf9* cells, and the cells were washed with 2 ml serum-free media. The transfection mixture (24 µL) was incubated for 15 min at RT and pipetted into 1 mL serum-free medium in a sterile microcentrifuge tube, and this was then added to the well containing the washed *Sf9* cells. The 6-well dish was incubated in a static incubator at 27°C overnight. The next day, the media was replaced with standard insect cell culture media containing 2% fetal bovine serum (FBS). The recombinant virus was harvested 7 days after the transfection day and centrifuged at 14500 rpm for 3 min. The supernatant containing recombinant baculovirus was collected as passage 0 (P0) and stored at 4°C (**Table 7)**. The titre of recombinant baculovirus was increased by using 0.1 ml P0 to infect *Sf9* cells seeded in six-well dishes at a starting density of 1 x 10^6 cells/well to obtain passage 1 (P1). P1 was used to obtain passage 2 (P2). This process was repeated until there was visible cytopathic effect (CPE) indicating the titer of recombinant baculovirus was high (~10^8 per ml).

2.2.14.4. Protein Expression Using Baculovirus Expression System

Following recombinant virus production, small-scale infections, six-well plates seeded with Tano38 cells were used to test the recombinant protein expression. Tano38 cells at 1×10^6 density (~50% confluence) were infected with 200 µL (10%) of recombinant virus stock. The infection was monitored using an inverted microscope. At 3 days post-infection, cells were collected from

each well by gentle pipetting and centrifuged at 5000 rpm for 5 min at RT. The resulting pellet was stored at –20 °C.

2.2.14.5. Scaling up Protein Expression

To purify virus-like particles (VLPs) a large volume of the recombinant virus was required to scale up the volume of infected insect cell culture to enable sufficient recombinant protein production. To amplify the recombinant baculovirus stock, *Sf9* cells were seeded into Greiner culture flasks (Corning®) to reach approximately 50% confluence (T25: 1×10^6 cells; T75: 9×10^6 cells; T175: 20×10^6 cells per flask). Recombinant baculovirus was added at 20 µL to T25, 50 µL to T75, and 100 µL to T175 flasks to initiate infection. The flasks were placed in a 27 °C incubator and checked visually every day using an inverted microscope (Leica, Germany) for CPE. The cells were gently tapped to dislodge the infected cells, transferred to 50 mL centrifuge tubes, and centrifuged at 4500 rpm for 15 min at 4 °C. The supernatants containing recombinant baculoviruses were collected in new 50 mL centrifuge tubes and stored at 4 °C.

To establish the infection for VLP production, a suspension culture of Tano38 cells (50 – 200 mL) was prepared in a sterile Erlenmeyer flask (Corning®) with 0.8×10^6 cells/ml and incubated one day to refresh the cells. Next day, the viability of cells was checked to ensure $1\text{-}2\times10^6$ cells/ml. Then the suspension culture was infected with 10 % of the total volume of virus stock and incubated for 3 - 4 days. The % of cell viability was estimated, with typical viability between 30-60% at 4 days pi. Cells were harvested by centrifugation at 4500 rpm for 15 min, 4 °C and cell pellets stored at -80 °C.

2.2.14.6. Baculovirus Stocks Titration

Baculovirus stock titration is the method for quantifying the quantity of infectious virus particle s in a baculovirus stock, usually represented as plaque-forming units (pfu) per millilitre. This step is necessary prior to baculovirus protein production as it allows precise regulation of the multiplicity of infection (MOI) to ensure that all cells in a culture are infected. Two methods are used for baculovirus titration in this study end-point dilution assay using Sf-9ET cells and viral plaque assay.

2.2.14.6.1 End-point Dilution Assay Using Sf-9ET Cells

End-point dilution assays were performed using Sf-9ET cells. (Hopkins & Esposito, 2009) researchers were developed the Sf-9ET cell line by transfecting Sf-9 cells with a plasmid encoding

the enhanced green fluorescent protein (eGFP) gene under the control of the baculovirus polyhedrin promoter. In the absence of baculovirus infection, eGFP is not expressed; however, upon infection, viral early proteins activate the polyhedrin promoter, leading to eGFP expression. Infected cells form distinct fluorescent foci that are readily visible under a fluorescence microscope (Hopkins & Esposito, 2009).

Baculovirus titrations were conducted in sterile, transparent, flat-bottom 96-well plates (Thermo Fisher) by recording GFP-positive wells at each virus dilution to determine viral titer. Sf-9ET cells were seeded at 7.5×10^4 cells per well in 100 µL of serum-free medium supplemented with 2% fetal bovine serum (FBS; Sigma-Aldrich). Cell suspensions were dispensed into wells using a multichannel pipette, and plates were incubated at 27 °C. The following day, 100 µL of medium was removed from each well and replaced with 100 µL of fresh medium containing 2% FBS. Each recombinant baculovirus stock was diluted 1:1000 in serum-free medium, and 100 µL of the diluted virus was added to the first wells in triplicate after medium removal. Two-fold serial dilutions were performed across the plate. Plates were placed in a humidified airtight box and incubated at 27 °C for 3 days. GFP expressions were quantified using an EVOS inverted microscope (Thermo Fisher). The dilution at which GFP fluorescence is no longer detectable is defined as the endpoint.

2.2.14.6.2 Viral Plaque Assay

Sf9 cell suspensions cultured in EX-CELL® 420 serum-free medium supplemented with 2% fetal bovine serum (FBS) were used to establish monolayers in 6-well tissue culture plates. Cells were seeded at 1×10^6 cells/mL and allowed to settle and attach for 20 min at RT. The medium in each well was then replaced with 1 mL of fresh EX-CELL® 420 medium containing 2% FBS. To initiate infection, the medium from the first well was removed, and recombinant baculovirus stocks were diluted 1:100 in serum-free medium as a starting dilution. Ten-fold serial dilutions were performed across the plate. The plate was incubated at room temperature for 1 h to allow viral adsorption, after which the medium was removed from all wells.

A 1.4% low-temperature gelling (LTG) agarose solution was prepared and cooled to hand-warm temperature. It was then mixed with an equal volume of EX-CELL® 420 medium supplemented with 2% FBS (final composition: 50% LTG, 50% medium, 2% FBS). Two milliliters of this overlay mixture were quickly added to each well and allowed to solidify. Once the gel had set, 1 mL of medium containing 2% FBS was gently layered on top of each well. Plates were incubated at 27 °C for 4 days. Each viral plaque, formed from a single infectious particle, was counted to calculate the viral titer or selected for isolation to generate a new viral stock.

2.2.14.7. Purification of PV VLPs

The methods in this section described especially for insect cell expressed VLPs.

2.2.14.7.1 Lysis of Insect Cells

To purify VLPs from insect cells, baculovirus infected cell pellets were resuspended with lysis buffer which continued 50 mM HEPES buffer (Sigma-Aldrich), 500 mM NaCl, 1 cOmplete™ ULTRA protease inhibitor tablet (Roche, Switzerland), and 200 µg/mL Benzonase (DNAse recombinantly produced in the host Lab). The cells were incubated on ice for 3 h to lyse cells with occasional vortexing. Lysed cells were centrifuged for 45 min at 15000 rpm and 10 °C to clarify the lysate and remove all the residual cell debris. The supernatant was then used to purify VLPs.

2.2.14.7.2 Ultracentrifugation

Two types of ultracentrifugation, velocity centrifugation and isopycnic centrifugation were used. Velocity centrifugation separates particles based on differences in size and shape, which influence their sedimentation rate; sucrose gradients are commonly employed for this method. In contrast, isopycnic centrifugation separates particles according to their buoyant density OptiPrep density gradients were used in this project. During centrifugation, particles migrate to the point where their buoyant density equals that of the surrounding gradient. At this isodensity point, no further migration occurs. A 30% sucrose cushion was used because assembled capsids can migrate through this dense layer to the bottom of the centrifuge tube, while smaller or unassembled components are excluded and remain above. This approach serves as a preliminary selection step prior to the final gradient-based purification.

2.2.14.7.3 30% Sucrose Cushion

Density gradient ultracentrifugation was used to concentrate and purify VLPs from baculovirus-infected insect cell lysates. The sucrose cushion is a pre-clean step of the sample to avoid gradient overloading. A preliminary crude purification of VLPs was made using a 30% (w/v) sucrose cushion because assembled capsids can move through this sucrose layer to the bottom of the centrifuge tube. The clarified lysate was loaded on the 30% sucrose layer by using Ultra-Clear ultracentrifuge tubes (Beckman) in the SW32 rotor to 38.5 ml capacity. After 250 ml of infected Tano38 culture was lysed. Volume of 34 mL clarified lysate was loaded into 38 mL SW32Ti Beckman centrifuge tubes, and 3 mL of 30% sucrose (w/v) in Hepes buffer was carefully added to the bottom of each tube using a syringe. The tubes were centrifuged at 28,000 rpm for 5 h at 10 °C. After centrifugation, the supernatant was decanted, and the resulting pellet was resuspended in 1 mL of lysis buffer (50 mM Hepes, 500 mM NaCl, 1% NP-40, supplemented

with protease inhibitors and Benzonase). The suspension was incubated overnight at 4°C. The resuspended pellet was centrifuged in a microcentrifuge at 15,000 rpm for 45 min at 4°C. The supernatant was collected, and the pellet was washed a second time by adding 0.2–0.5 mL of lysis buffer, incubating on ice for 1h at RT, and centrifuging again. The second supernatant was collected and pooled with the first supernatant to concentrate the VLPs**.** This combined supernatant was used as the load for the density gradient and stored at 4 °C.

2.2.14.7.4 20-45% Discontinuous OptiPrep Density Gradient

OptiPrep offers higher resolution to separate VLPs from host proteins and non-assembled particles based on their unique density. A 20–45% discontinuous OptiPrep density gradient was prepared in a size 14 mL SW40 Beckman centrifuge tube by layering 2 mL of 45%, 40%, 35%, 30%, 25%, and 20% OptiPrep solutions gently (Sigma-Aldrich), starting with the most concentrated (45%) at the bottom. Approximately 200 µL of buffer was removed from the top of the tube, and 1–1.2 mL of the sample was loaded. The gradient was centrifuged for 24 h at 36,000 rpm and 10 °C. The gradient was fractionated by collecting 1–1.2 mL from the top, continued by 1 mL fractions down to the bottom of the tube. A 10 µL aliquot from each fraction was analysed by Coomassie-stained SDS-PAGE, and the fractions were also subjected to Western blot analysis.

2.2.14.7.5 15-45 % Sucrose Gradient

The combined supernatant was layered onto a linear 15–45% sucrose. Ultracentrifugation was performed at 30,000 rpm for 24 hours at 4 °C. The gradient was fractionated by sequentially collecting 1–1.2 mL from the top, followed by 1 mL fractions to the bottom of the tube. A 10 µL aliquot from each fraction was analyzed by SDS-PAGE with Coomassie staining, and Western blot analysis was also performed.

2.2.15 Protein Analysis

A commonly used method for protein analysis is sodium dodecyl sulfate-polyacrylamide gel electrophoresis (SDS-PAGE). It is used to separate proteins based on their molecular weight, allowing assessment of protein purity, integrity, and expression levels.

2.2.15.1. Sodium Dodecyl Sulfate–Polyacrylamide Gel Electrophoresis (SDS-PAGE)

To prepare cell pellets for SDS-PAGE, *E. coli* induction pellets were resuspended in PBS, with the volume adjusted based on the optical density (OD) of each culture to normalize sample loading. Insect cell pellets, obtained from a single well of infected cells in a 6-well plate, were resuspended in 100 µL PBS for *Sf9* cells and 200 µL for Tnao38 cells. For SDS-PAGE analysis, 5 µL of the insect cell suspension was mixed with 35 µL of PBS and 10 µL of 4× Bolt™ LDS sample buffer (Invitrogen, USA) containing 5% (v/v) 2-mercaptoethanol in a PCR tube.

The samples were vortexed and briefly centrifuged then incubated at 100°C for 10 min to completely denature the sample. For the purpose of reducing viscosity, the samples were vortexed again and briefly centrifuged. A Bolt™ 4-12% Bis-Tris Plus 10-well gel (Invitrogen) was assembled in a dual mini gel tank (Life Technologies) filled with 1x Bolt™ MES SDS running buffer (Invitrogen). 7µL BLUeye Pre-Stained Protein Ladder (Geneflow S6-0024) was loaded in the first well as a marker and 50 µL samples were loaded per well. Samples were separated at a constant voltage of 200 V for approximately 30 min until the dye front reached the bottom of the gel. Proteins were then visualized by Coomassie stain and/or Western blot.

2.2.15.2. Coomassie Brilliant Blue Staining of Proteins

Following separation by SDS-PAGE, proteins were visualised using Coomassie blue dye. 5 mL from a solution of Coomassie Brillant Blue R-250 (0.025% w/v), 45% v/v methanol, and 10% v/v glacial acetic acid) was used to stain the gels at RT on a rocking platform (25 rpm) for 30 min. The gel was then washed at room temperature with a destaining solution (10 % v/v methanol, 10 % v/v glacial acetic acid) on the rocking platform (25 rpm) for 10 min. The washing process was repeated several times until the protein bands became clear. Gels were imaged using a G: BOX Chemi XL (Syngene).

2.2.15.3. Western Blot

A piece of Immobilon-P transfer membrane (Merck Millipore, US) was prepared by soaking in 100% methanol for 2 min and then washing in 1X Tris-glycine electroblotting buffer (National Diagnostics, US). The SDS-PAGE gels were electroblotted onto the prepared Immobilon-P transfer membrane (Merck Millipore, US) for 1 h and 30 min at 150 mA in a semi-dry Western blotting apparatus (ATTO, Japan) assembled as follows: Three pieces of Whatman™ 3MM Chromatography Paper (GE healthcare, US) were soaked in 1X Tris-glycine electroblotting buffer

and layered into the apparatus, followed by the pre-washed transfer membrane, the gel was placed on top of the membrane and layered with another three pieces of Whatman™ 3MM Chromatography Paper soaked in 1X Tris-glycine electroblotting buffer. Following the transfer, the membrane was incubated overnight in either 5% non-fat milk in 1x TBST, or Pierce™ Protein-Free Blocking Buffer (Thermo Scientific Pierce, US) for at least 1 h at RT or overnight at 4 °C. The membrane was washed three times (5 min each) with 1 x TBST to remove any excess carryover from the blocking step. After that, the membrane was incubated for 1 h at room temperature with the primary antibody on the rocking platform (25-30 rpm) in the same buffer used in the blocking step. Following incubation, the membranes were washed three times (5 min each) with 1x TBST buffer. A secondary antibody conjugated with horseradish peroxidase (HRP) was used to detect the primary antibody. The specific combinations of primary and secondary antibodies used for each antigen are listed in (**Table 9)**. The membrane was incubated for 1h at room temperature with the secondary antibody**.** On the rocking platform (25-30 rpm) in the same buffer used in the blocking step. The membranes were washed another three times (5 min each) with 1x TBST buffer to remove any unbound antibodies. Equal volumes of reagents A (0.25 ml) and B (0.25 ml) ECL Western Blotting Substrate (Pierce™) were applied to the membrane for 1 min, the excess solution was then drained off the membrane and the luminescence from the proteins bands imaged using a G: BOX Chemi XL (Syngene).

2.2.16 Electron Microscopy

Transmission electron microscopy (TEM) was used to visualize and analyse purified VLPs. To bind the VLPs to copper grids by drop casting and negatively stain with uranyl acetate, a 2 µL droplet of VLP sample was pipetted onto a small piece of parafilm next to 2 x 2 µL droplets of phosphate buffer (pH 7.2-7.4) and a 2 µL droplet of 2 % (w/v) uranyl acetate (0.45 µm filtered). The back of a formvar/carbon 300 mesh copper grid (Sigma-Aldrich) was gently floated on each droplet of liquid for 5 min in turn, starting with the VLP sample, then the 2x phosphate buffer washes and finishing with the uranyl acetate stain. Excess liquid was removed with filter paper after each step, without allowing the sample to dry. The grid was placed in a grid box and then analysed using a JEM-2100Plus LaB6 TEM (CFAM, University of Reading).

2.2.17 Fluorescence Microscopy

To visualise fluorescence in Tano38 cells infected with recombinant baculoviruses engineered with green fluorescent protein (GFP), the surface of a Nunc glass-bottom dish (ThermoScientific,

150680) was pre-treated with 200 µL of 0.01% poly-L-lysine (Sigma-Aldrich) for 10 min to improve cell adhesion to the glass surface and subsequently dried for 10 min after removing the poly-L-lysine solution. Ao38 cells were seeded onto the treated dish at a density of 1×10^6 cells per well and infected with 200 µL of recombinant baculovirus stock. The culture was maintained at 27 °C, and images were captured on the second day post-infection at 60× magnification at 488 nm by an EVOS microscope (ThermoFisher).

2.2.18 Antigenicity test

Antigenicity for PV was assessed by measuring two forms: the native (N) form and the heated (H) form, using monoclonal antibodies.

2.2.18.1. Enzyme-linked Immunosorbant Assays (ELISA)

A non-competitive sandwich ELISA was used to quantity the amount of N-antigen relative to H-antigen in purified VLP samples. Flat-bottom clear nonsterile high-binding 96-well plates immune (Thermofisher) were coated with 50 µL monoclonal capture antibodies specific to either the N-antigen (mAb234) or H-antigen (mAB1588) of PV1 capsids proved by National Institute for Biological Standards and Control (NIBSC) diluted at 1:500 in Carbonate-Bicarbonate Buffer (containing both sodium carbonate (Na_2CO_3) and sodium bicarbonate ($NaHCO_3$) with pH of 9.6) then incubated overnight at 4 ◦C.

The next day, the plates were washed three times with PBST (phosphate buffer + 0.05% Tween20 buffer) before adding 200 µL Pierce™ Protein-Free Blocking Buffer (Thermo Scientific Pierce) to each well and incubating for 1 h at RT. The plates were washed three times with PBST buffer. The European IPV standard (NIBSC code: 12-104) and the lysate samples expressed PV1 VLPs were diluted to 1:10 in blocking buffer as the starting dilution, and then a 2-fold dilution series was made in the appropriate wells (50 µL/well) with technical triplicates and incubated for 2 h at RT. The plates were washed with PBST three times and 50 µL of a 1:500 dilution of the antibody specific to PV1, R879 (Host lab collaborator), made in PBST (phosphate buffer + 0.05% Tween20) buffer was added to each well and incubated for 1 h at RT. The plates were washed three times with PBST and then 50 uL of a 1:1000 dilution of a polyclonal goat anti-rabbit HRP conjugated antibody (P0448, Dako) made in blocking buffer was added to the wells and incubated at RT for 1 h. The plates were washed three times with PBST.

Colorimetric detection was achieved by adding 50 µL TMB Stable (Thermofisher, US) to each well and incubating for 30 min at RT in the dark. The reaction was stopped by adding 50 µL of

250 mM H_2SO_4 and the absorbance was read at 440 nm using a spectrophotometer (Tecan, Spark). OD vs serial dilution graphs were plotted after exporting the result to Excel.

2.2.18.2. Flow Cytometry

A 6-well tissue culture plate (Falcon) was seeded with Tnao38 cells at a density of 1×10^6 cells per well. Each well, except one designated as an uninfected control, was inoculated with 200 µL of recombinant baculovirus stock and incubated at 27 °C for four days. Following incubation, the cells were harvested via centrifugation at 4500 rpm for 15 min, and the resulting pellets were washed with 1 mL of 1× phosphate-buffered saline (PBS).

The eBioscience™ Intracellular Fixation & Permeabilization Buffer Set (Invitrogen, Cat:88-8824-00) was employed to permeabilize and fix cells for intracellular staining. The cell pellets were resuspended in the fixation buffer and incubated overnight at 4 °C on a tube rocker (Thermofisher). The next day, the samples were centrifuged at 400–600 × g for 5 min at RT, the supernatant was discarded and 200 µL of 1× Permeabilization Buffer was used to resuspend the cell pellets. After a 10 min incubation on the rocking platform at RT, the samples were centrifuged at 400–600 × g for 5 min at RT.

To block nonspecific binding, 1 mL of blocking buffer (PBS containing 3% bovine serum albumin [BSA] and 0.1% sodium azide) was added to the pellets and incubated for 35 min on a tube rocker at RT. The samples were then centrifuged at 600xg for 5 min, and the cell pellets were resuspended in blocking buffer containing a 1:500 dilution of primary antibody specific to the PV1 N-antigen (mAb234) or H-antigen (mAB1588) and incubated for 1 h on the rocking platform at RT. The samples were centrifuged at 600xg for 5 min and cell pellets resuspended in 1ml blocking buffer to wash the cells. This washing process was repeated another 2 times prior to labelling with the secondary antibody.

Cell pellets were then incubated with 500 µL of a 1:1000 dilution of anti-mouse FITC-conjugated secondary antibody prepared in blocking buffer. This step was performed under the same conditions as the primary antibody incubation and followed by three additional washes with blocking buffer. Finally, the cell pellets were resuspended in 500 µL of PBS and transferred to flow cytometry tubes (Falcon) for the measurement of FITC-A fluorescence. The FITC-A channel of the C6 Plus Flow Cytometer was used to detect the samples, and the data were analyzed using BDC Sampler Plus software. The conventional gate used to distinguish the FITC-A -negative (V1-L) from the FITC-A -positive (V1-R).

Chapter 3 Expression of The Poliovirus Capsid Proteins in *E. coli*

3.1 Introduction

The *E. coli* expression system is a multifaceted platform extensively used in the pharmaceutical, food, and biotechnology sectors due to its rapid doubling time of roughly 20 minutes in cost-effective media under tightly regulated conditions (Kaur *et al.*, 2018). The first human protein generated via genetically engineered DNA in *E. coli* was somatostatin in 1977, followed quickly by human insulin in 1978 which was the first recombinant drug to be approved for clinical use (Goeddel *et al.*, 1979). By 2003, almost 80% of the protein structures deposited in the Protein Data Bank (PDB) were produced in *E. coli* systems (Terpe, 2006). The efficacy of *E. coil* in expressing foreign genes mostly depends on the inducible lac operon, which is modulated by the lactose analogue, isopropyl-β-D-thiogalactoside (IPTG), a powerful inducer (Donovan *et al.*, 1996).

Although it has many benefits, high production of recombinant proteins in *E. coli* often leads to the formation of inclusion bodies, insoluble cytoplasmic aggregates of misfolded and denatured protein without biological activity (Vallejo & Rinas, 2004). Multiple strategies have been established to improve the solubility of recombinant proteins in *E. coil*, including the optimisation of culture conditions, co-expression of molecular chaperones, reduction of induction temperature, early-log phase induction, fusion tags, and decreased IPTG concentration (Studier, 2005). When inclusion bodies form, the recovery of biologically active protein typically necessitates solubilisation under denaturing conditions followed by a carefully optimised refolding process (Singh *et al.*, 2015). Common solubilising agents include chaotropic compounds such as 6–8 M urea, guanidine hydrochloride, and Sodium Dodecyl Sulfate (SDS) to fully unfold the protein (Palmer & Wingfield, 2012; Singh *et al.*, 2015)

E. coli has been used in vaccine development to generate the first VLP vaccine, Hecolin, produced using this platform for hepatitis E virus (HEV) that was licensed for mass vaccination in China in 2012. Whilst there are currently no other approved VLP vaccines produced in *E. coli*, several studies have demonstrated effective VLP production using this expression system for foot-and-mouth disease virus (FMDV) which belongs to the *Picornaviridae*. This involved expressing FMDV capsid subunits as fusion proteins tagged with the Small Ubiquitin-Like Modifier (SUMO) to improve solubility and folding. The SUMO tag, featuring a hydrophilic external surface and a hydrophobic core, acts as a nucleus for correct folding by stabilising target proteins in solution and reducing misfolded products which can prevent aggregation (Butt *et al.*, 2005; Marblestone *et al.*, 2006; Judy & Kishore, 2019; Nazir *et al.*, 2024). Production of FMDV

VLPs was accomplished by co-expression of SUMO-tagged fusions of the capsid proteins VP0, VP1, and VP3 within the same host cell followed by purification and proteolytic removal of the SUMO-tags to enable VLP assembly *in vitro* (Guo *et al.*, 2013; Xiao *et al.*, 2016; Xiao *et al.*, 2021). Whilst there are currently no studies reporting production of Poliovirus VLPs in *E. coli*, immunogenic poliovirus type 3 (PV3) VLPs have been successfully produced in *Nicotiana benthamiana* plants for both the wildtype PV3 Saukett serotype and the stabilized mutant Sc8 (Marsian *et al.*, 2017b). PV VLPs have also been expressed in yeast (Rombaut & Jore, 1997; Sherry *et al.*, 2020; Hong *et al.*, 2024), insect cells (Y. Xu *et al.*, 2019) and mammalian cells (Ansardi *et al.*, 1991; Bahar *et al.*, 2021), suggesting that the cellular environment compatible with assembly may be very broad.

Building on these approaches, in this Chapter a method was designed to investigate if it is possible to produce Poliovirus VLPs in *E. coli* as this would be a cheaper and easier method at large-scale. Specifically, three plasmids based on the pTriEx expression vector, each containing a different antibiotic resistance marker, were constructed to enable production of SUMO-tagged PV3 Saukett Sc8 capsid proteins SUMO-VP0, SUMO-VP1, and SUMO-VP3. Several strategies were employed to enhance the yield of soluble recombinant proteins with the expectation that the optimization steps would improve the recovery of assembled Poliovirus VLPs from the *E. coli* expression systems.

3.2 Validation of Vectors for Recombinant Expression of SUMO-tagged Capsid Proteins

pTriEx1.1 is a DNA vector that enables expression of recombinant proteins in three different expression systems: 1) *E. coli*; 2) the baculovirus expression system; and 3) mammalian cells. The standard vector has an ampicillin resistance marker (amp^R), but prior to this project kanamycin resistant (kan^R) and spectinomycin resistant (spc^R) versions of this vector were constructed using PCR and In-fusion cloning (Mulley, G. unpublished). These were used to produce three constructs encoding SUMO-tagged versions of the mature PV3 Saukett SC8 capsid proteins (Fox *et al.*, 2017),VP0, VP1, and VP3 (Mulley, G. unpublished). At the start of this project the pTriEX1.1-SUMO-VP3 (Kan^R), pTriEX1.1-SUMO-VP1 (Amp^R) and pTriEX1.1-SUMO-VP0 (Spc^R) strains were recovered from -80°C stocks on selective LB agar plates and cultured overnight in LB with the appropriate antibiotic. Plasmid DNA was purified and sent to Source BioScience for Sanger sequencing. This verified that the constructs contained the correct PV3 sequences and that the N-terminal SUMO tag, which also contains a His-tag to enable detection and purification using Anti-6X His tag antibody, was in frame (**Figure 14)**.

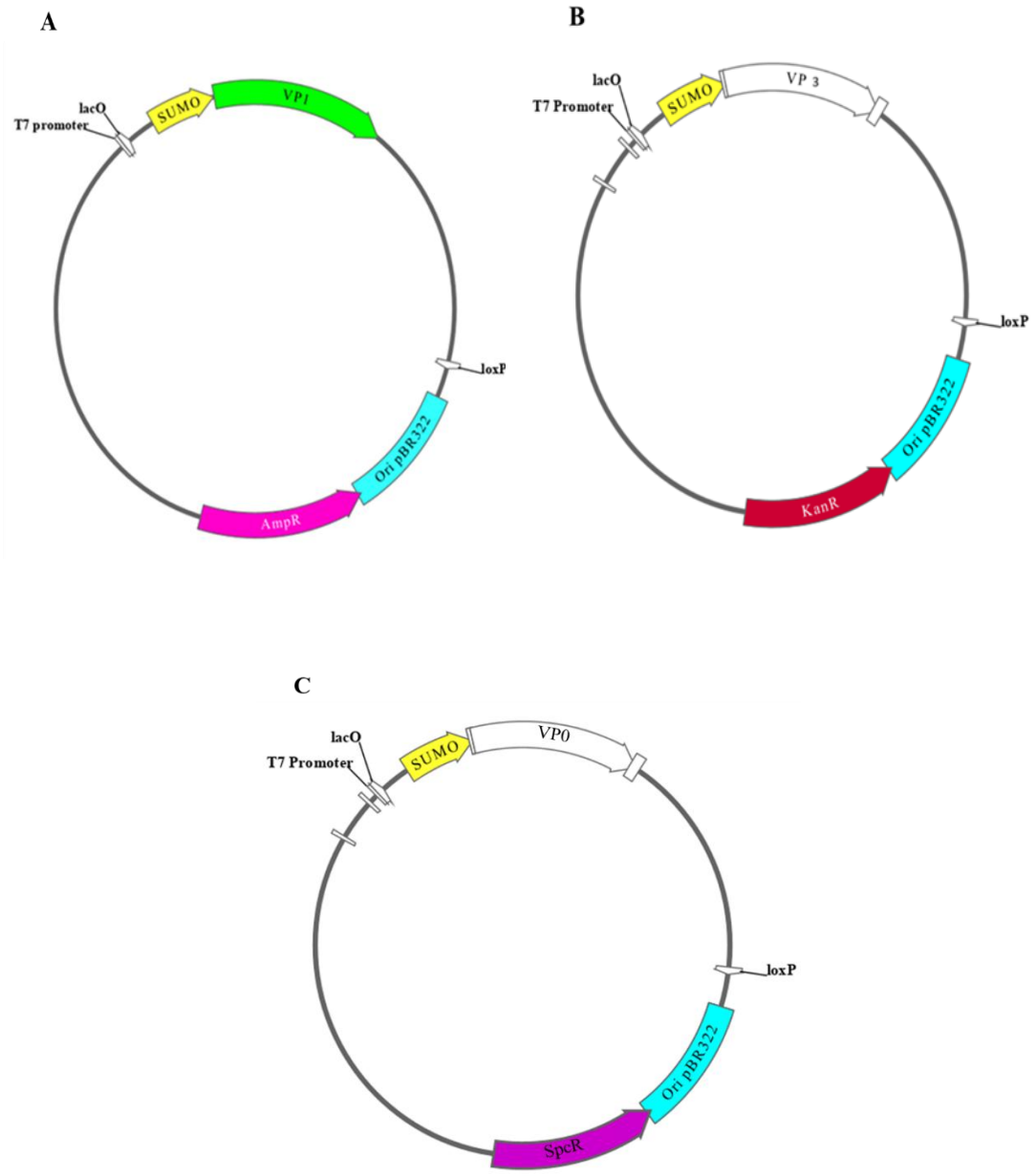

Figure 14. Maps of the recombinant plasmids, A) pTriEx-SUMO-VP1, B) pTriEx-SUMO- VP3 and C) pTriEx-SUMO-VP0 showing the selective marker for each plasmid and T7 promoter.

3.3 Comparison of Expression of SUMO-tagged PVs Capsid Proteins in *E.coli* BL21- DE3 and BL21- AI

The recombinant plasmids pTriEx-SUMO-VP0, pTriEx-SUMO-VP3, and pTriEx-SUMO-VP1 were transformed into two different strains of chemically competent *E. coli*, BL21-DE3 and BL21-AI, to determine which produces higher levels of expression of the SUMO-tagged PV3 capsid proteins. BL21-DE3 is a strain of *E. coli* B that carries the lambda DE3 prophage with the T7 RNA polymerase under the control of the lacUV5 promoter and it is induced by IPTG. It is also deficient in two proteases, lon and OmpT, which can help reduce degradation of recombinant proteins. The BL21-AI strain also lacks these two proteases but contains a chromosomal insertion of T7 RNA polymerase in place of *araB* placing it under the control of the arabinose-inducible *ara*BAD promoter. This enables much tighter control over the level of gene expression than is the case with IPTG induction and it can even be used to obtain high yields of toxic proteins.

Transformations were plated on selective agar containing ampicillin 100 μg/mL (for pTriEx-SUMO-VP1), spectinomycin 100 μg/mL (for pTriEx-SUMO-VP0), or kanamycin 40 μg/mL (for pTriEx-SUMO-VP3), and incubated overnight at 37°C. A single colony from each transformation plate was inoculated into LB medium supplemented with the respective antibiotic and cultured overnight at 37°C with shaking. Glycerol stocks were subsequently prepared from these overnight cultures.

The expression of PV3 Saukett SC8 capsid proteins pTriEx1.1-SUMO-VP0, pTriEx1.1-SUMO-VP3, and pTriEx1.1-SUMO-VP1 was assessed in BL21- DE3 and BL21- AI *E. coli* strains. Cultures of *E. coli* strains were grown overnight in LB medium with spectinomycin (100 μg/mL), ampicillin (100 μg/mL), or kanamycin (40 μg/mL) as appropriate at 37°C with shaking. The following day, cultures were diluted into fresh LB medium containing 0.1% glucose and incubated at 37°C until reaching an optical density (OD600) of 0.4–0.6, which required approximately 2–3 hours. Uninduced samples were collected before induction by centrifuging 1 mL of culture and the cell pellets were stored at -20°C.

For induction, 1 mM IPTG was added to the *E. coli* BL21-DE3 cultures. In the *E. coli* BL21-AI strain, 1 mM IPTG and 0.2% arabinose were added to regulate the expression of toxic proteins, with arabinose activating the araBAD promoter to induce T7 RNA polymerase. The cultures were incubated at 37°C with shaking for 2 h. Following the induction, 1 mL samples from each culture were collected, centrifuged, and the resulting cell pellets were stored at -20°C.

The uninduced and induced cell pellets were used to prepare samples for SDS-PAGE analysis. HRP-conjugated Anti-6X His tag antibody (ab1187) was used to detect the SUMO/His-tagged

capsid proteins **(Figure 15)**. For *E. coli* BL21-DE3, there were no bands observed for the empty vector control pTriEx-SUMO in the uninduced sample and after 2 h induction. A weak band at ~43 kDa was observed for pTriEX1.1-SUMO-VP3 before induction and this was much stronger after 2 h induction, corresponding to the expected molecular weight (MW) of VP3 (26 kDa) combined with the SUMO tag (17 kDa). Bands at 51 kDa were observed for pTriEX1.1-SUMO-VP1 in both the uninduced and induced samples, consistent with the calculated MW of VP1 (34 kDa) plus the SUMO tag. A band was observed in both the uninduced and induced samples at 54 kDa for pTriEX1.1-SUMO-VP0, which matches the expected MW of VP0 (37 kDa) with the SUMO tag.

For *E. coli* BL21-AI, there were either no, or very faint bands detected in the uninduced samples **(Figure 15)**, indicating much tighter regulation of recombinant protein expression in this strain compared to BL21-DE3. Induction for 2 h produced consistent levels of expression for all constructs in BL21-AI including the pTriEx-SUMO control which had failed to express in *E. coli* BL21 DE3. These Western blot results confirmed the accurate expression of the SUMO-tagged PV3 Saukett Sc8 VP0, VP1, and VP3 capsid protein in *E. coli*. The BL21-AI strain was selected for use in further experiments due to the tighter level of regulation and consistent levels of capsid protein expression.

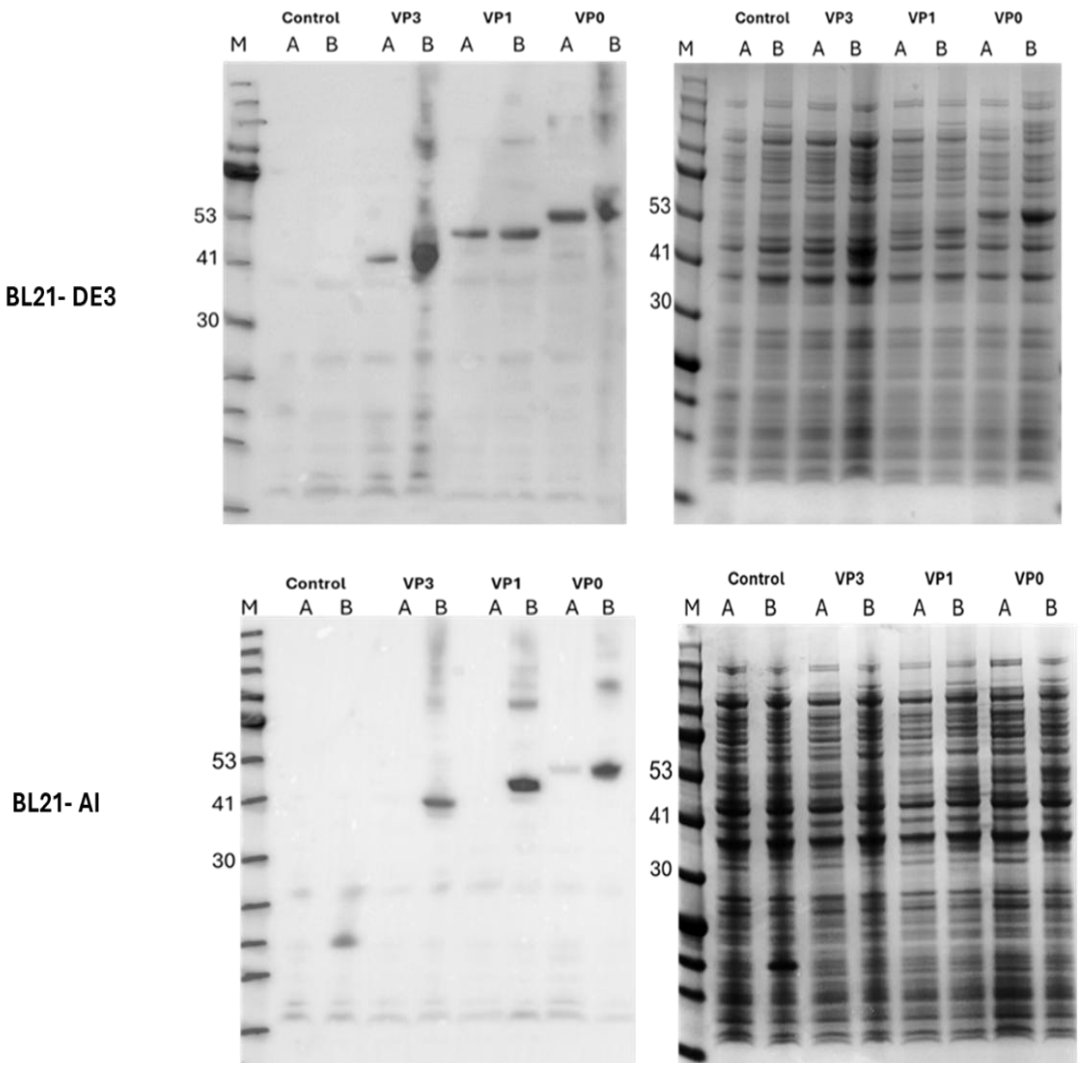

Figure 15. Comparison of expression of the SUMO-tagged PV3 Saukett SC8 capsid proteins in two different *E.coli* strains (BL21-DE3 and BL21-AI). Samples were loaded on 4-20% gels and proteins separated by SDS-PAGE for 30 min at 200V. SUMO-tagged proteins were detected by Western blot (left) using an HRP-conjugated Anti-6X His tag antibody (ab1187). Duplicate gels were Coomassie stained to detect all visible proteins (right). Lanes labelled "A" contain cells from uninduced samples, while lanes labeled "B" represent cells after 2 h induction in 1 mM IPTG (+ 0.2% arabinose for BL21-AI). Control: pTriEx-SUMO; VP3: pTriEx-SUMO-VP3; VP1: pTriEx-SUMO-VP1; VP0: pTriEx-SUMO-VP0. Molecular weight markers (M): BLUeye Pre-Stained Protein Ladder (Geneflow) with selected sizes indicated in kilodaltons (kDa).

3.4 Optimisation of Solubility of SUMO-tagged PV3 Capsid Proteins Expressed in Individual Strains of *E. coli* BL21-AI

Protein solubility often presents significant challenges in *E. coli* expression systems and is a critical factor that can lead to failure of recombinant protein production. Solubility is affected by a complicated interaction of the structure of the target protein and the external experimental conditions. External factors, including the selection of vector, host strain, incubation temperature, concentration of inducer, and culture media composition, significantly influence the solubility and yield of the generated protein (Rosano & Ceccarelli, 2014). A number of studies have described various molecular strategies to produce difficult proteins in *E. coli* expression systems by optimising critical parameters, including cultivation temperature, inducer concentrations at induction, and the incorporation of additives in the culture medium (García-Fraga *et al.*, 2015).

To optimise the yield of soluble SUMO-tagged PV3 Saukett SC8 capsid proteins produced in *E. coli* BL21-AI, 2 h inductions were performed under three different conditions: 37 °C with 1 mM IPTG and 0.2% arabinose, 25 °C with 1 mM IPTG and 0.2% arabinose, and 25 °C with 0.2 mM IPTG and 0.04% arabinose. The cell pellets were resuspended in the B-Per lysis buffer to lyse the cells and release soluble proteins. Following centrifugation, the supernatant was transferred to fresh tubes (soluble fraction) and pellets were resuspended in 8M urea (insoluble fraction). Samples were run on duplicate gels to separate proteins by SDS-PAGE, with one gel stained using Coomassie and the other used to perform a Western blot. SUMO-tagged capsid proteins were detected using HRP-conjugated Anti-6X His tag antibody (ab1187).

SUMO-VP3 was partially soluble when expressed at 37 °C with 1 mM IPTG and 0.2% arabinose, but SUMO-VP1 and SUMO-VP0 were only detected in the insoluble fraction **(Figure 16)**. Decreasing the induction temperature from to 25 °C increased the yield of soluble SUMO-VP3, but reducing the concentration of the inducer from 1 mM IPTG + 0.2% arabinose to 0.2 mM IPTG + 0.04% arabinose did not provide any further increase in the level of soluble protein. Neither lowering the temperature nor reducing the concentration of inducer improved the solubility of SUMO-VP1 and SUMO-VP0, with both proteins expressed at high levels but almost 100% in the insoluble fraction in all conditions.

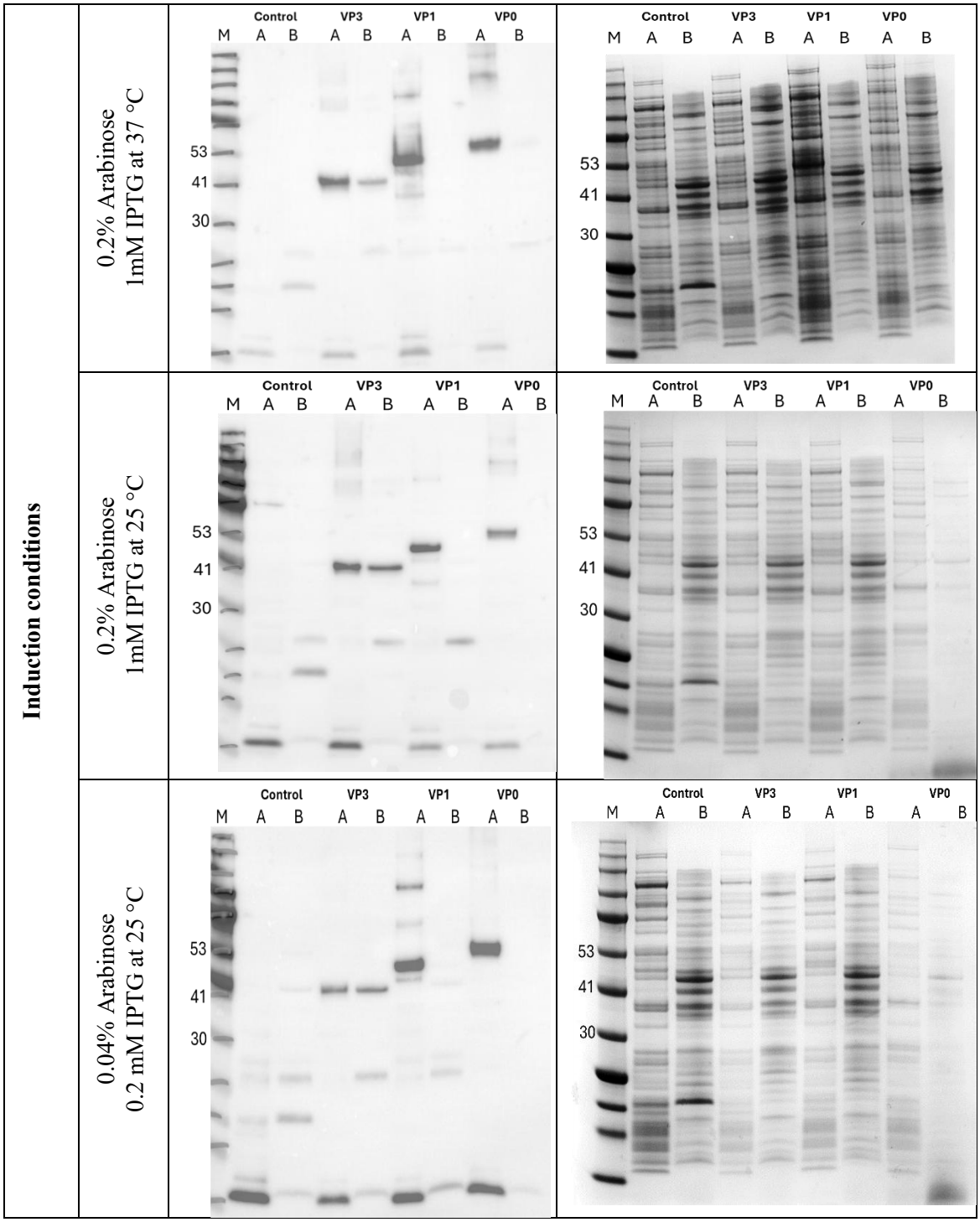

Figure 16. Comparison of solubility of SUMO-tagged PV3 Saukett SC8 capsid proteins in three different conditions. Samples were loaded on 4-20% gels and proteins separated by SDS-PAGE for 30 min at 200V. SUMO-tagged proteins were detected by Western blot (left) using an HRP-conjugated Anti-6X His tag antibody (ab1187). Duplicate gels were Coomassie stained to detect all visible proteins (right). A: insoluble fractions; B: soluble fractions. Control: pTriEx-SUMO; VP3: pTriEx-SUMO-VP3; VP1: pTriEx-SUMO-VP1; VP0: pTriEx-SUMO-VP0. Molecular

weight markers (M): BLUeye Pre-Stained Protein Ladder (Geneflow) with selected sizes indicated in kilodaltons (kDa).

3.5 Extraction of SUMO-tagged PV3 Capsid Proteins from Inclusion Bodies

Wang *et al.,* 2023 had previously demonstrated that it was possible to assemble FMDV capsids from recombinant proteins they had extracted from inclusion bodies (Wang *et al.*, 2023). Given the insolubility of the SUMO-tagged PV3 Saukett SC8 capsid proteins, a similar procedure was followed to extract from inclusion bodies. 100 mL culture was induced with 1 mM IPTG and 0.2% arabinose at 37°C and the cell pellets were resuspended in B-PER lysis buffer and centrifuged. The insoluble pellets were washed in 1x Tris-buffered saline (TBS) containing 2% Tween 20 (TBST) until they became white. The final white pellet was denatured using 1% SDS at room temperature until fully clarified. The samples were then centrifuged at high speed. The clear supernatants were prepared for Western blot analysis which confirmed that all proteins were successfully solubilized with 1% SDS **(Figure 17)**, with a very dark band at 51 kDa for SUMO-VP1, a clear band at 43 kDa for SUMO-VP3 but only a very faint band for SUMO-VP0 at 54 kDa.

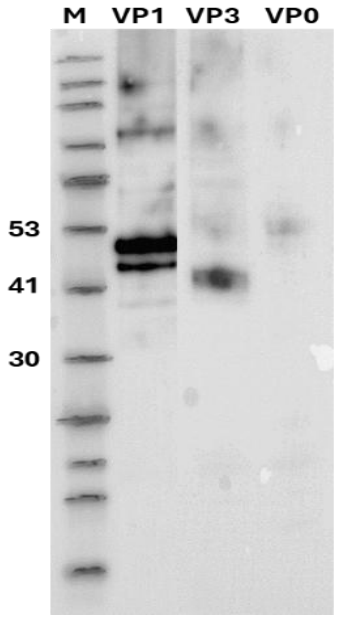

Figure 17. Western blot analysis of SUMO-tagged PV3 Saukett SC8 capsid proteins following extraction from inclusion bodies using 1% SDS. Detection was performed with an HRP-conjugated Anti-6X His tag antibody (ab1187). VP3: SUMO-VP3; VP1: SUMO-VP1; VP0: SUMO-VP0. Molecular weight markers (M): BLUeye Pre-Stained Protein Ladder (Geneflow) on the left side of the gel in kilodaltons (kDa).

3.6 Purification of SUMO-tagged PVs Capsid Proteins

The SDS-solubilised SUMO-tagged capsid proteins were then purified with a His SpinTrap using immobilized metal ion affinity chromatography (IMAC). Protein concentrations were measured using a NanoDrop spectrophotometer (Thermo Scientific). The concentrations of VP1, VP3, and VP0 were 26.484 mg/mL, 18 mg/mL, and 15 mg/mL, respectively. Samples were stored at −20 °C. The successful purification was confirmed by SDS-PAGE and Coomassie-staining **(Figure 18)**.

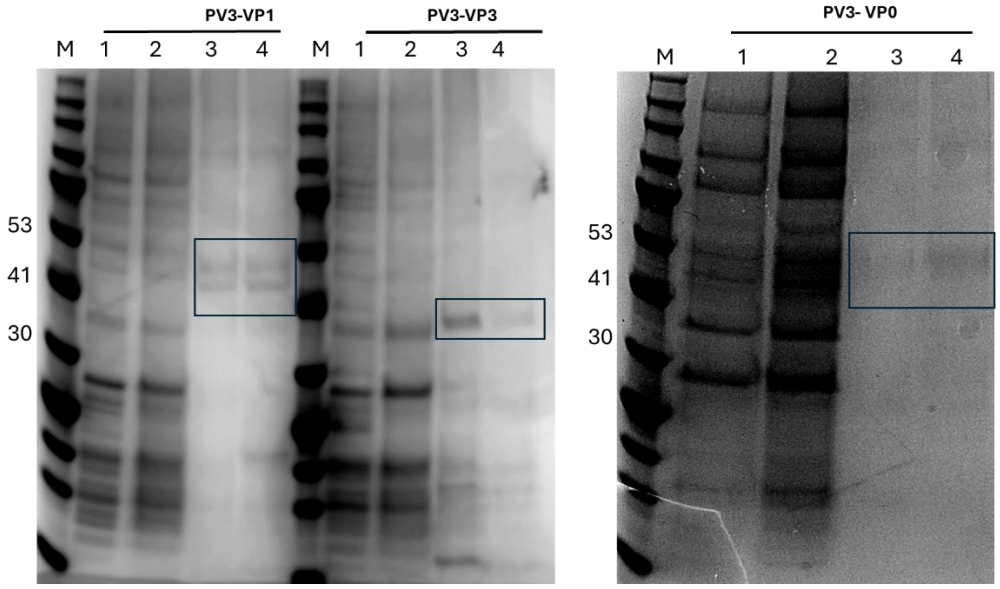

Figure 18. Purification of SUMO-tagged PV3 Saukett SC8 capsid proteins using immobilized metal ion affinity chromatography. Proteins were separated by SDS-PAGE and stained using Coomassie. 1: lysed cells prior to purification; 2: flow through from His column during washing step; 3: elution 1; 4: elution 2. Molecular weight marker (M): BLUeye Pre-Stained Protein Ladder (Geneflow) with selected sizes indicated in kilodaltons (kDa).

The same samples above for purified recombinant VP1, VP3, and VP0 proteins were analysed on agarose gels to assess potential contamination with nucleic acids. The analysis revealed that VP0 preparations were confounded by co-purified nucleic acids following bacterial expression, whereas VP1 and VP3 showed less nucleic acid contamination **(Figure 19)**.

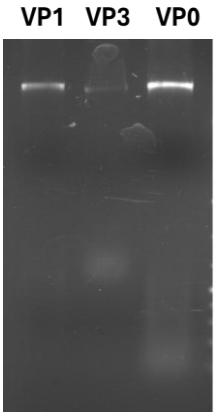

Figure 19. Agarose gel analysis of purified recombinant VP1, VP3, and VP0 proteins to assess nucleic acid contamination.

3.7 Protease Removal of SUMO tag from PV3 Saukett Sc8 Capsid Proteins

It is necessary to remove the SUMO tag from the Poliovirus capsid proteins to avoid disruption of the assembly process (Li *et al.*, 2024; Y. Xiao *et al.*, 2016). The purified SUMO-tagged PV3 Saukett Sc8 proteins were treated with SUMO Ubl-specific protease 1 (Ulp1) for 3 h at 4°C, 16°C, 24°C and 30°C. Samples were then analysed by Western blot **(Figure 20)** which showed successful cleavage of the SUMO tag from VP1 and VP0, with the loss of the band representing the SUMO-tagged capsid and the appearance of a band of the expected molecular weight for SUMO tag at 17 kDa following cleavage. However, there was no cleavage of SUMO-VP3 as indicated by the presence of a band at 43 kDa, and this was not resolved by performing the reaction in protease buffers with altered concentrations of salt.

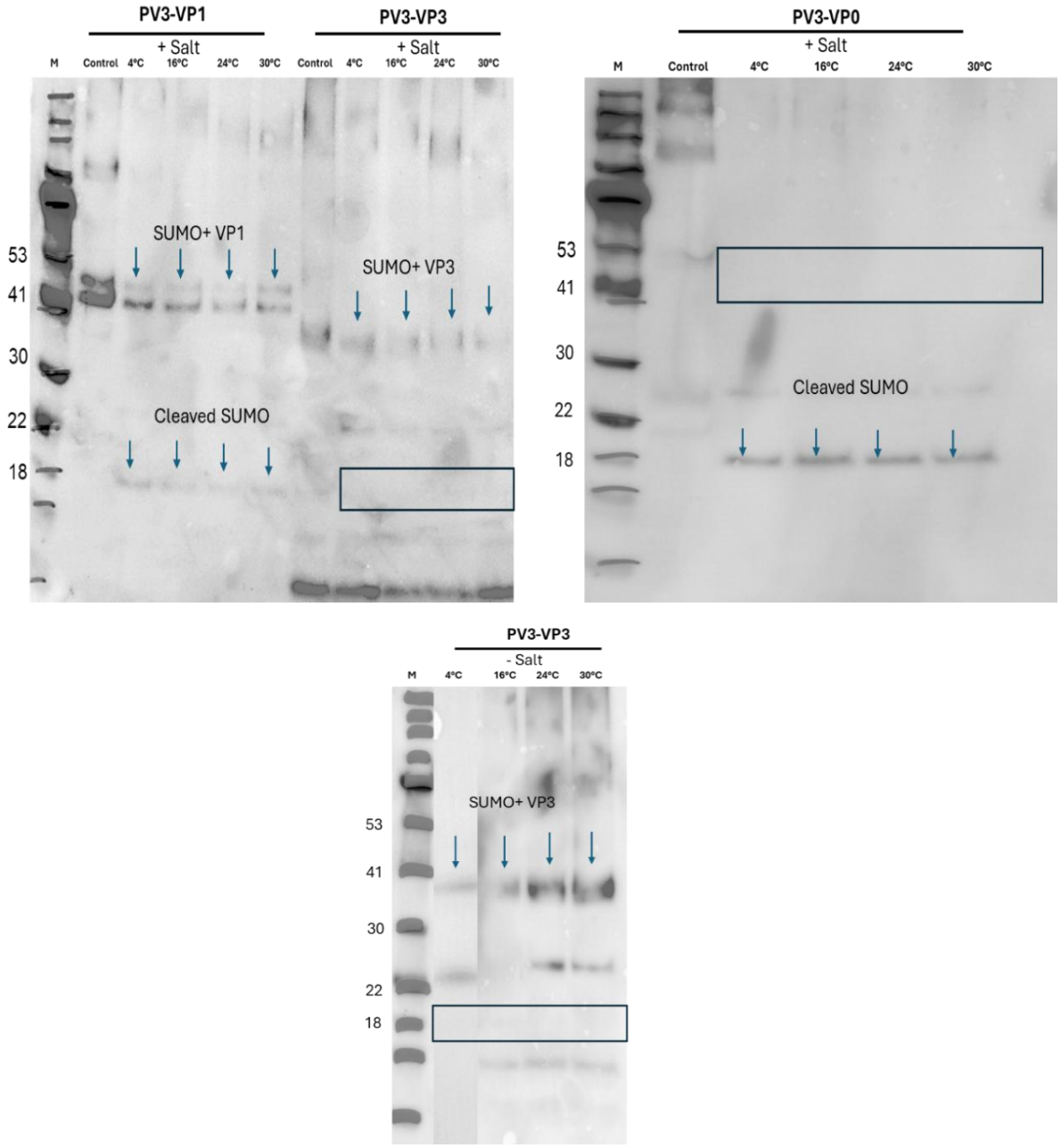

Figure 20. Removal of SUMO tags from PV3 Saukett SC8 capsid proteins using SUMO Ulp1 protease. The samples treated with SUMO protease were incubated at different temperatures for 3 h in the standard SUMO protease buffer containing 150 mM NaCl (+ salt). VP3 was treated with SUMO protease in the buffer lacking NaCl (- salt) due to unsuccessful cleavage in the standard buffer. Control = samples without SUMO protease. Some expected bands did not appear but were marked in the WB. The cleavage SUMO tag is 17 kDa. Molecular weight markers (M): BLUeye Pre-Stained Protein Ladder (Geneflow) with selected size markers indicated in kilodaltons (kDa). The figure is a composite image which combines lanes from separate experiments done under the same conditions. The lanes are labeled and the experimental conditions detailed in both the images and the legend.

3.8 Triple Transformation of *E. coli* BL21-AI with VP0, VP3, and VP1 Constructs

Whilst the results of this study so far have demonstrated that the individual SUMO-tagged capsid proteins can be purified from inclusion bodies and the SUMO-tag can subsequently be removed from SUMO-VP0 and SUMO-VP1, the SUMO tag could not be cleaved from SUMO-VP3 following purification from inclusion bodies and so it was not possible to attempt to assemble Poliovirus VLPs *in vitro* . Guo and colleagues, (Guo *et al.*, 2013; Y. Xiao *et al.*, 2016) successfully produced high yields of FMDV VLPs by co-expressing the SUMO-tagged capsid proteins within the same host cell, which they reported was a necessary strategy to increase their solubility (Guo *et al.*, 2013; Xiao *et al.*, 2016; Xiao *et al.*, 2021). To determine if this could also improve the yield of SUMO-tagged Poliovirus PV3 Saukett Sc8 capsid proteins, the recombinant plasmids pTriEx-SUMO-VP0, pTriEx-SUMO-VP3, and pTriEx-SUMO-VP1 were transformed into the same BL21-AI strain.

The starting point for this was the *E. coli* strain BL21-AI carrying pTriEx-SUMO-VP0, which was grown overnight culture in LB supplemented with spectinomycin (100 μg/mL) to maintain the plasmid. The next day, the culture was subcultured in fresh LB containing spectinomycin (100 μg/mL) and incubated at 37°C to an OD_{600} of 0.4-0.6 was reached. The culture was then centrifuged, and the resulting pellet was placed on ice and gently resuspended in 4 mL of ice-cold 100 mM $CaCl_2$. After incubating on ice for 15 minutes, the cells were centrifuged, and the pellet was resuspended in 100 μL of 100 mM $CaCl_2$. The cell suspension was split into two 50 μL aliquots, one as a control and the other was transformed with 2.5 μL of pTriEx-SUMO-VP3.

For VP3 transformation, 2.5 μL of the VP3 plasmid was added to 50 μL of competent *E. coli* BL21-AI cells. The cells were incubated on ice for 30 minutes, heat-shocked at 42°C for 30 seconds and then returned to ice for 2 min. Subsequently, 200 LB medium was added for cell recovery, followed by incubation at 37°C for 1 h with shaking. The transformations were plated on selective LB agar containing kanamycin (40 μg/mL) and spectinomycin (100 μg/mL) and incubated overnight at 37°C. Negative controls with only the VP0 plasmid were also plated to ensure no background growth.

The next day, three colonies containing both pTriEx-SUMO-VP0 and pTriEx-SUMO-VP3 were selected and inoculated in LB medium supplemented with spectinomycin (100 μg/mL) and kanamycin (40 μg/mL) for overnight incubation at 37°C with shaking. The following day, the same process was repeated to prepare chemically competent *E. coli*. The overnight culture was subcultured in LB with spectinomycin (100 μg/mL) and kanamycin (40 μg/mL) and incubated at 37°C until reaching an OD_{600} of 0.4-0.6. After centrifugation, the pellet was resuspended in 4 mL

of ice-cold 100 mM $CaCl_2$ and incubated on ice for 15 min. The cells were centrifuged and resuspended in 100 µL of 100 mM $CaCl_2$, then split into two 50 µL aliquots, one for the control and the other was transformed with 2.5 µL of pTriEx-SUMO-VP1. Transformants were plated on selective LB agar containing kanamycin (40 µg/mL), ampicillin (100 µg/mL), and spectinomycin (100 µg/mL) and incubated overnight at 37°C. The negative control containing pTriEx-SUMO-VP0 and pTriEx-SUMO-VP3 was included to ensure the antibiotic selection was effective.

On the following day, three colonies containing pTriEx-SUMO-VP0, pTriEx-SUMO-VP3 and pTriEx-SUMO-VP1 were selected and grown in LB medium with kanamycin (40 µg/mL), ampicillin (100 µg/mL), and spectinomycin (100 µg/mL) and incubated overnight at 37°C with shaking. Glycerol stocks were prepared from these overnight cultures and stored at -80°C.

3.9 Co-expression of The Three SUMO-tagged PV3 Capsid Proteins in *E. coli* BL21-AI

A subculture of the *E. coli* BL21-AI strain carrying pTriEx-SUMO-VP0, pTriEx-SUMO-VP3 and pTriEx-SUMO-VP1 was induced using 1 mM IPTG and 0.2% arabinose for 3 hours. Subsequent Western blot analysis confirmed that SUMO-VP0, SUMO-VP1, and SUMO-VP3 were expressed in equal amounts in this strain **(Figure 21).**

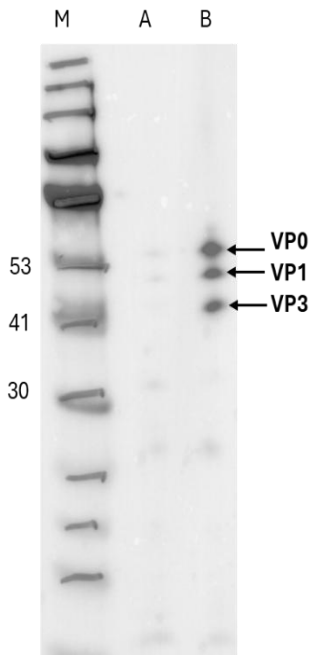

Figure 21. Expression of SUMO-tagged PV3 Saukett SC8 capsid proteins in single strain of *E. coli* BL21-AI. Proteins were separated from crude cell lysates by SDS-PAGE and detected using an HRP-conjugated Anti-6X His tag antibody (ab1187) by Western blot. A: uninduced sample; B: following induction with 1 mM IPTG and 0.2% arabinose in LB at 37 ° C for 3 h. M: BLUeye Pre-Stained Protein Ladder (Geneflow) molecular weight markers are indicated in kilodaltons (kDa).

3.10 Optimisation of Solubility of SUMO-tagged PV3 Capsid Proteins Co-expressed in a Single Strain of *E. coli* BL21-AI

To optimise the yield of soluble SUMO-tagged PV3 Saukett SC8 capsid proteins co-expressed in the single strain of *E. coli* BL21-AI, 2 h inductions were performed under four conditions: 37 °C with 1 mM IPTG and 0.2% arabinose, 37 °C with 0.2 mM IPTG and 0.04% arabinose, 25 °C with 1 mM IPTG and 0.2% arabinose, and 25 °C with 0.2 mM IPTG and 0.04% arabinose. The cell pellets were resuspended in B-Per lysis buffer to lyse the cells and release soluble proteins. Following centrifugation, the supernatant was transferred to fresh tubes (soluble fraction) and pellets were resuspended in 8M urea (insoluble fraction). Samples were run on duplicate gels to separate proteins by SDS-PAGE, with one gel stained using Coomassie and the other used to perform a Western blot. SUMO-tagged capsid proteins were detected with HRP-conjugated Anti-6X His tag antibody (ab1187).

Similar amounts of the three SUMO-tagged PV3 Saukett SC8 capsid proteins were produced in the *E. coli* BL21-AI strain carrying pTriEx-SUMO-VP0, pTriEx-SUMO-VP3 and pTriEx-

SUMO-VP1 when the induction was carried out at 37°C, regardless of the inducer concentration, but were only detected in the insoluble fraction **(Figure 22).** None of the three SUMO-tagged PV3 Saukett SC8 capsid proteins were detected in either the soluble or insoluble fractions when the inductions were performed at the lower temperature 25 °C **(Figure 22).**

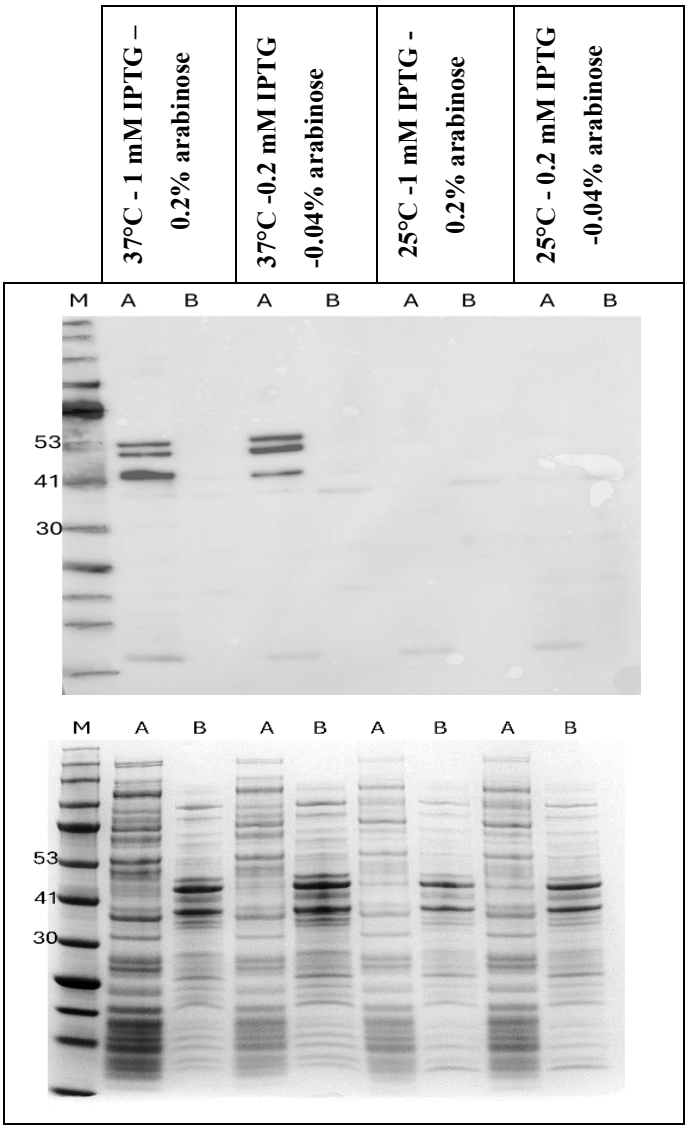

Figure 22. Comparison of solubility of SUMO-tagged PV3 Saukett SC8 capsid proteins co-expressed in *E. coli* BL21-AI carrying pTriEx-SUMO-VP0, pTriEx-SUMO-VP3 and pTriEx-SUMO-VP1 under different induction conditions. Samples were loaded on 4-20% gels and proteins separated by SDS-PAGE for 30 min at 200V. SUMO-tagged proteins were detected by Western blot (top) using an HRP-conjugated Anti-6X His tag antibody (ab1187). A duplicate gel was Coomassie stained to detect all visible proteins (bottom). A: insoluble fractions; B: soluble fractions. Molecular weight markers (M): BLUeye Pre-Stained Protein Ladder (Geneflow) with selected sizes indicated in kilodaltons (kDa).

3.11 Extraction of SUMO-tagged PV3 Capsid Proteins Co-expressed in *E. coli* BL21-AI from Inclusion Bodies

As the SUMO-tagged PV3 Saukett SC8 capsid proteins could only be produced in the insoluble fraction despite co-expressing all the constructs in the same strain, extraction was attempted using a similar approach to that used for their extraction from the individual BL21-AI strains carrying only one plasmid.

A 100 mL culture of the *E. coli* BL21-AI strain carrying pTriEx-SUMO-VP0, pTriEx-SUMO-VP3 and pTriEx-SUMO-VP1 were induced using 1 mM IPTG and 0.2% arabinose at 37°C. The cell pellet was processed to extract the inclusion bodies in 1% SDS and this was then purified with a His SpinTrap using immobilized metal ion affinity chromatography (IMAC). The concentration of purified proteins was measured using a NanoDrop spectrophotometer (Thermo Scientific). The concentration of VP1, VP3, and VP0 co-expressed in *E. coli* were 26.4 mg/mL. Samples were stored at −20 °C. The SDS-solubilised SUMO-tagged capsid proteins after purification were analysed by SDS-PAGE, Coomassie staining and Western blot.
The results in **Figure 23**, visible bands of VP1, VP0 and VP3 are observed in purified proteins lanes 4 and 5 which approved successful purification for all 3 proteins together from BL21-AI.
.

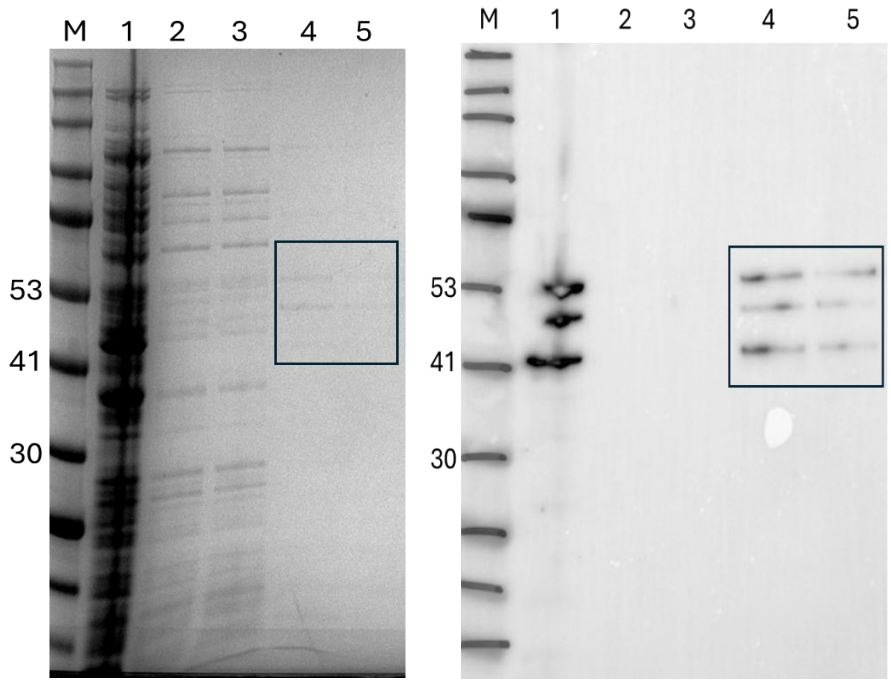

Figure 23. Purification of SUMO-tagged capsid proteins VP0, VP1, and VP3 (PV3 Saukett SC8) from triple strain BL21-AI using immobilized metal ion affinity chromatography. Proteins were separated by SDS-PAGE and stained using Coomassie Brilliant Blue (left) and Western blot (Right). 1: lysed cells prior to purification; 2: flow through from His column during washing step; 3: elusion 1; 4: elution 2. Molecular weight marker (M): BLUeye Pre-Stained Protein Ladder (Geneflow) with selected sizes indicated in kilodaltons (kDa).

3.12 Protease Removal of SUMO Tag from Triple Strain BL21-AI

The co-purified SUMO-tagged PV3 Saukett Sc8 proteins were treated with SUMO protease Ulp1 following the manufacturer's protocol. The reaction was carried out for 3 h at 4°C, 16°C, 24°C and 30°C in the supplied buffer with and without 150 mM NaCl and subsequently analysed by Western blot **(Figure 24)**. The anti-His antibody did not detect any protein at the expected molecular weight of the SUMO tag, (17kDa). This indicates that SUMO protease was unable to cleave the SUMO tag from any of the PV3 Saukett Sc9 capsid proteins regardless of the incubation temperature and NaCl concentration of the SUMO protease buffer.

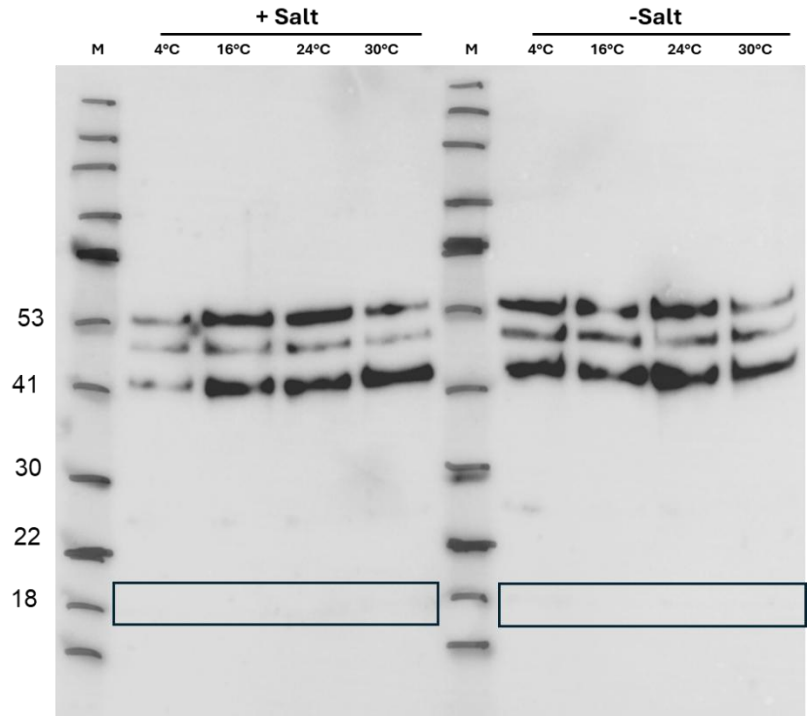

Figure 24. SUMO protease treatment of the co-purified SUMO-tagged PV3 Saukett Sc8 capsid proteins. SUMO protease reactions were incubated at different temperatures for 3 h. +Salt: SUMO protease buffer containing standard NaCl concentration 150 mM; -Salt: SUMO protease buffer lacking NaCl. Samples were loaded on 4-20% gels and proteins separated by SDS-PAGE for 30 min at 200V. SUMO-tagged proteins were detected by Western blot (top) using an HRP-conjugated Anti-6X His tag antibody (ab1187). Molecular weight markers (M): BLUeye Pre-Stained Protein Ladder (Geneflow) with selected sizes indicated in kilodaltons (kDa).

3.13 Discussion

This study aimed to co-express poliovirus type 3 (PV3, Saukett SC8 strain) capsid proteins VP0, VP1, and VP3 in *E. coli* using a T7-based expression system, with the goal of improving solubility via N-terminal fusion to SUMO. The inducible T7 expression system is widely employed for recombinant protein production in *E. coli*, and prior studies have reported successful co-expression of foot-and-mouth disease virus (FMDV) capsid proteins using similar approaches (Guo *et al.*, 2013; Xiao *et al.*, 2016, 2021). Here, each capsid gene was cloned into a pTriEx1.1 vector carrying distinct antibiotic resistance markers to enable simultaneous induction in a single *E. coli* strain.

A primary challenge in expressing viral capsid proteins in *E. coli* is their tendency to misfold and aggregate into inclusion bodies, leading to poor solubility. The SUMO tag, due to its hydrophilic and structurally ordered surface, has been reported to enhance solubility and promote proper folding of aggregation proteins (C. Der Lee *et al.*, 2009). This approach has been validated in other systems, such as the successful solubilization of SUMO-MMP13 in yeast (Malakhov *et al.*, 2004).The expression was assessed in two *E. coli* strains: BL21-DE3, commonly used for high-yield expression of non-toxic proteins, and BL21-AI, which allows tighter expression control for potentially toxic gene products under T7 promoter systems. BL21-AI was ultimately selected based on higher expression levels of VP0, VP1, and VP3.

To optimise soluble expression, induction parameters were varied across temperature and IPTG concentrations, as excessive induction levels are known to cause metabolic stress and protein misfolding (Mühlmann *et al.*, 2017; Sergeev *et al.*, 2024). Three conditions were tested: 37°C with 1 mM IPTG and 0.2% arabinose; 25°C with 1 mM IPTG and 0.2% arabinose; and 25°C with 0.2 mM IPTG and 0.04% arabinose. While VP3 was partially soluble, VP0 and VP1 remained largely insoluble under all conditions. These results, consistent with previous observations (Ponte-Sucre *et al.*, 2021), indicate extensive aggregation and formation of inclusion bodies.

A similar strategy was employed for PV3, following the successful *in vitro* assembly of FMDV VLPs from inclusion body derived capsid proteins (Wang *et al.*, 2023). A key distinction in our approach was the use of SUMO-fused VP0, VP1, and VP3 to enhance solubility prior to folding and assembly in *E. coli*. However, for native VLP formation to occur, SUMO tags must be cleaved, as they interfere with essential capsid protein interactions (Guo *et al.*, 2013a). Proteins were extracted from denatured inclusion body pellets using 1% SDS and subsequently purified by His-tag affinity chromatography. As a result of losses, the final yield of each recombinant capsid protein was low. Based on the fact that proteins could be observed directly on induced gels (e.g. Figure 15) the primary expression yield was high, >1mgs per liter of induced culture.

However the final yields prior to attempted SUMO protease digest was ~micrograms, reflecting the inherent challenges of expressing viral capsid proteins in *E. coli*. An additional complication was observed with VP0, which exhibited nucleic acid contamination following bacterial expression, whereas VP1 and VP3 showed less contamination. This finding is notable in light of previous work by (Karunatilaka *et al.*, 2021a), which demonstrated that a significant fraction of VP4 remains associated with the viral genome during the early stages of uncoating. Thus, the observed nucleic acid contamination of VP0 may represent a related phenomenon, complicating interpretation of the expression and purification results **(Figure 18) (Figure 19)**. Cleavage was attempted using Ulp1 SUMO protease under a range of salt and temperature conditions. As shown in (**Figure 20)**, VP0 was completely undetectable after cleavage, VP1 was only partially processed, and VP3 remained uncleaved. This likely reflects the inability of Ulp1 to recognise the SUMO domain under non-native folding conditions (Marblestone *et al.*, 2006).

To further assess the potential for soluble co-expression, a triple expression strain (BL21-AI) was generated. However, solubility remained poor even under optimised induction parameters with co-expression of all three capsid proteins **(Figure 21)**. Proteins were again purified from denatured inclusion bodies, but, as before, there were low levels of each capsid protein in the soluble fractions and SUMO tag cleavage remained ineffective, likely due to conformational constraints imposed by aggregation.

Although SDS is not recommended as a detergent for the lysis of induced cultures as it can interfere with the subsequent IMAC chromatography, low levels of SDS (<0.3%) are compatible and that cold storage of SDS solubilized proteins results in an SDS precipitate that, once removed by centrifugation, leaves a level in solution that does not interfere with the IMAC process (Schlager *et al.,* 2012). The recombinant capsids proteins described here required SDS for solubility but were then stored at 4 degrees and clarified prior to the IMAC step. This undoubtedly explains why the IMAC was successful here but it should be noted that no optimization of SDS level and removal was done and that investigation of these parameters could yet rescue the expression ff PV capsid proteins in *E.coli*. Overall, expressing PV VLPs in *E. coli* made progress in the experiments described here but requires new strategies to enhance soluble capsid protein production by minimizing the complexity and costs associated with denaturing inclusion bodies and purification steps.

Chapter 4 Optimization of PV1 P1 to Enhance Expression of Capsid Proteins in Insect Cells

4.1 Introduction

The baculovirus expression vector system (BEVS) was first used in 1983 (Smith *et al.*, 1983). BEVS allows the rapid and effective generation of helper-free recombinant viruses which express high levels of recombinant protein as part of their replication cycle. Various improvements to enhance protein yield have been described over the years since its introduction (Chambers *et al.*, 2018b) and the system has produced many recombinant vaccines (Hong *et al.*, 2023) including Cervarix®, the VLP based vaccine for Human Papillomavirus, produced by BEVS and licensed for commercial use (Felberbaum, 2015). The expression of PV empty capsids requires the mature components of the structural polyprotein (P1),which are VP0, VP3 and VP1 (Jiang *et al.*, 2014). Typically these are produced by co-expression of the P1 precursor with the 3C protease, often as a 3CD protein, reflecting the polyprotein processing that occurs in PV infected cells(Ypma-Wong *et al.*, 1988). As reviewed in the **Introduction**, a number of expression systems have been used successfully to produce PV VLPs **(Table 4)** using this type of approach, including mammalian, yeast and plant (Sherry *et al.*, 2025). Recently, a new design which does away with the need for the 3C protease was shown to be very productive in yeast, producing vaccine quality VLPs for PV2 serotypes (Hong *et al.*, 2024a). The BEVS system too has been used to demonstrate the assembly of high quality VLPs that can induce an immune response characteristic of protection against PV infection (Xu *et al.*, 2019). In the BEVS case however, contamination with BV particles is a significant issue for commercial production. Recent developments in the BEVS system may circumvent this in future designs (Oosten *et al.*, 2025), but currently residual baculovirus particles represent a limit to system use for PV VLPs. One approach that could improve this would be modifications to the current construct to improve expression level, as the higher the VLP production the lower the relative level of baculovirus contamination. Accordingly, this chapter examines alterations to the P1 sequence that may influence expression level, beginning with changes at the N-terminus which encodes the post-translational modification of myristoylation. A second reason for these studies is the changing nature of the field regarding the requirement of myristoylation for capsid assembly. The N-terminal glycine of P1, which is exposed following N-methionine processing, is covalently modified with myristic acid, a 14-carbon aliphatic chain as a result of recognition of the myristoylation consensus sequence (MGXXXS/T) by the cellular N-myristoyl transferase (NMT). During replication of wild poliovirus, the myristoylation process takes place co-translationally and was originally reported as crucial for productive infection (Ansardi *et al.*, 1992), with myr-negative mutants showing flaws in assembly (Marc *et al.*, 1989). In the mature virion particle, the myristic acid moiety has

been suggested to play a structural role (Lee & Chow, 1992) although at the time of publication the precise function of this lipid moiety in the poliovirus replication cycle was unclear (Moscufo *et al.*, 1991; Martín-Belmonte *et al.*, 2000). More recently however, re-investigation of its role has suggested its action is more related to the entry reaction than to assembly (Panjwani *et al.*, 2014; Ramljak *et al.*, 2018). The hydrophobic myristic acid chain embeds in the host cell membrane, following VP4 movement in the virus particle after receptor engagement as part of the pore formation required for genomic RNA transfer into the cytoplasm. As VLPs only undergo an assembly reaction, never cell entry, the requirement for myristoylation, or for a particular myristoylation signal, may be less stringent than once supposed. Indeed, for the related FMDV picornavirus, assembly of capsids from non-myristoylated VP0 has been reported (Puckette *et al.*, 2017; Li *et al.*, 2024).

Protein N-myristoylation involves the attachment of myristate via an amide linkage to the amino group of a glycine residue at the N-terminus of eukaryotic and viral proteins. In the PV structure, the myristate functional group of VP4 is located close to the virus particle's 5-fold axis and participates, along with the 5-fold-related N-termini of VP4 and VP3, in a β-tube which has a unique shape (Chow *et al.*, 1987b). Elsewhere, N-myristoyl proteins serve a variety of functions often associated with an “in” conformation locating the group in a hydrophobic pocket that prevents interaction with the membrane, and an “out” conformation that causes membrane binding (Patwardhan & Resh, 2010; B. Wang *et al.*, 2021). N-myristoylation is an irreversible protein modification that follows methionyl aminopeptidase removal of the initiator methionine residue and is catalyzed by the enzyme N-myristoyl transferase (NMT). NMT is found in all eukaryotes but not in prokaryotes, with most mammalian cells expressing two isozymes, NMT1 and NMT2, with slightly different substrate specificity (Seaton & Smith, 2008). Many viruses encoded proteins that are myristoylated (Maurer-Stroh & Eisenhaber, 2004b) and inhibition of NMT function can have an anti-viral effect (Priyamvada *et al.*, 2022). In the case of the PV-related rhinoviruses, the inhibition of NMT using a small fragment inhibitor prevents virus assembly and subsequent cytopathic effect in cell culture (Mousnier *et al.*, 2018). This would confirm a late role in the virus life cycle in addition to the very early role during virus entry, when the N-terminus of VP4 engages the host cell membrane to form a pore through which the RNA genome enters the cytoplasm (Panjwani *et al.*, 2014).

PV is one of the oldest described human infections (Mehndiratta *et al.*, 2014) and P1 myristoylation has evolved to use human NMTs. In the case of recombinant VLPs however, P1 is expressed in non-human cells. The fact that PV VLPs have been expressed in many eukaryotic cell backgrounds (plant, yeast, insect) shows that NMT origin is not a restriction for N-terminal peptide recognition and myristoyl transferase activity. However, as N-myristoylation is likely to be a rate-limiting step following P1 translation, and that the actual sequence recognized by NMT

may not be essential for assembly, it may be possible to modify the sequence so that it is better recognized by NMT present in the expression host. To emphasize this point, the alignment of human and insect cell NMTs (**Figure 25**) shows considerable variation supporting the hypothesis that they may have preferred peptide substrates while maintaining the MGXXXS/T consensus. Optimizing the consensus for the resident enzyme could lead to a higher level of modified P1 and thus higher yield of VLPs.

To examine this possibility, a number of sequence variants of the N-myristoylation signal were substituted for the resident PV sequence, and their effect on insect cell expression of PV proteins was assessed. Among 11 variants tested, several were found to function more effectively and improved the synthesis of the P1 protein and its cleaved mature capsid proteins.

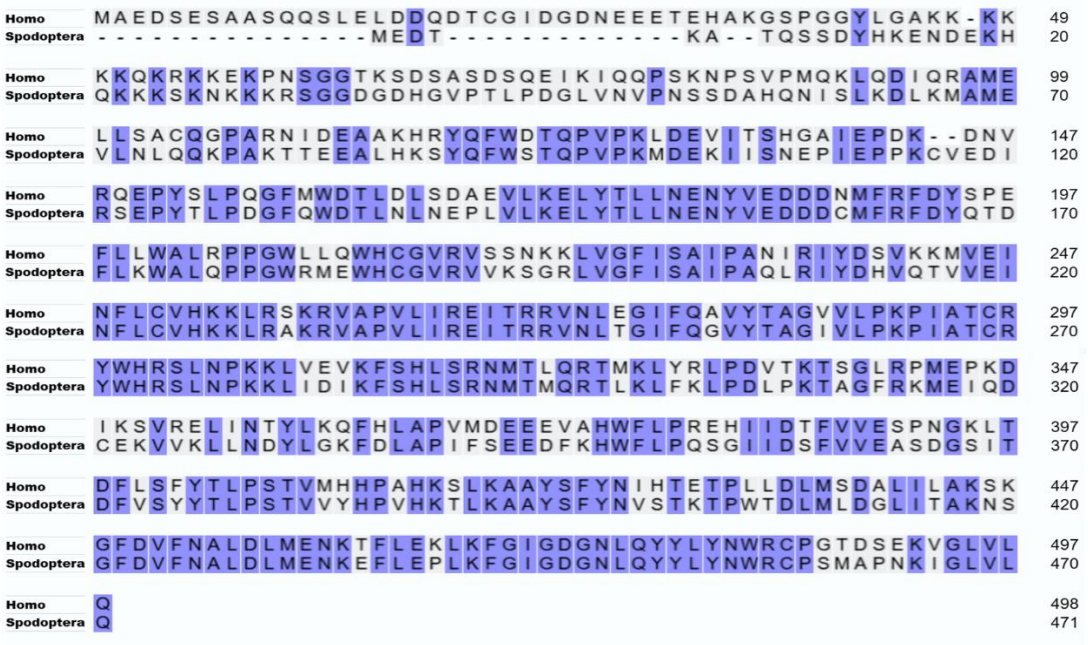

Figure 25. A BLAST alignment of NMT sequences from human (AAH06376.1 – *Homo sapiens*) and insect cells (XP_022821279.1 – *Spodoptera litura*) highlighting the sequence variation between the two species (non-highlighted).

4.2 Design and Construction of PV1 Myristoylation Substrate Peptide Mutations

Eleven different myristoylation sites were chosen based on a review of the literature. They vary from peptide sequences found in well characterized myristoylated proteins such as Recoverin and MARCK kinase, viral sequences such as HIV matrix protein (P17), a *bona fide* insect example sequence found in an insect species (the Tobacco hornworm) and a series of synthetic sequences that were described during a comparative study of the optimal peptide substrate specificity used by NMT in yeast and human cells (Rocque *et al.*, 1993). The entire set is described in **Table 9.**

The resident myristoylation peptide sequence of poliovirus type 1 Mahoney was exchanged for each of the chosen sequences virtually and then the back-translated to the optimal *Sf9* codon sequences and appended to primer sequence that was homologous to the PV1 Mahoney Sc6b sequence used in this study (Fox *et al.*, 2017). The corresponding oligonucleotides were introduced into the PV sequence by PCR with a reverse primer sited just downstream of a unique BseJI site to generate an amplicon of 1658 bp. The forward primers were designed to also overlap the vector sequence upstream of the N-terminal VP4 sequence to enable recombination with the parental pOPINE-PV vector **(Figure 26)**. using in-Fusion technology. The PCR products for the eleven N-terminal mutations were produced with the high fidelity Phusion enzyme and analyzed by agarose electrophoresis, confirming the correct amplicon size of 1658 bp **(Figure 27)**. After agarose gel electrophoresis, the PCR products were purified using GeneJET Gel Extraction Micro Kit and quantified using a Nanodrop spectrophotometer.

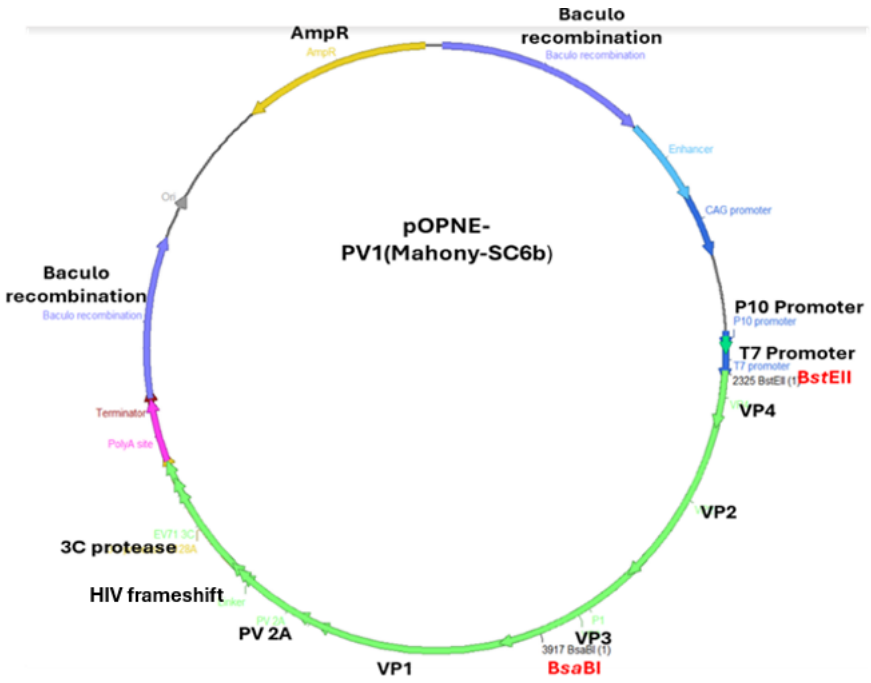

Figure 26. Plasmid map for pOPINE Mahoney Sc6b showing the complete Poliovirus PV1 Mahoney P1 sequence and 3C protease, separated by a HIV ribosomal frameshift element, assembled into the pOPINE vector. The *Bst*EII (*Eco*91I) and *Bsa*BI (*Bse*JI) restriction sites used in cloning are highlighted. The P10 promoter required for expression in insect cells is also shown.

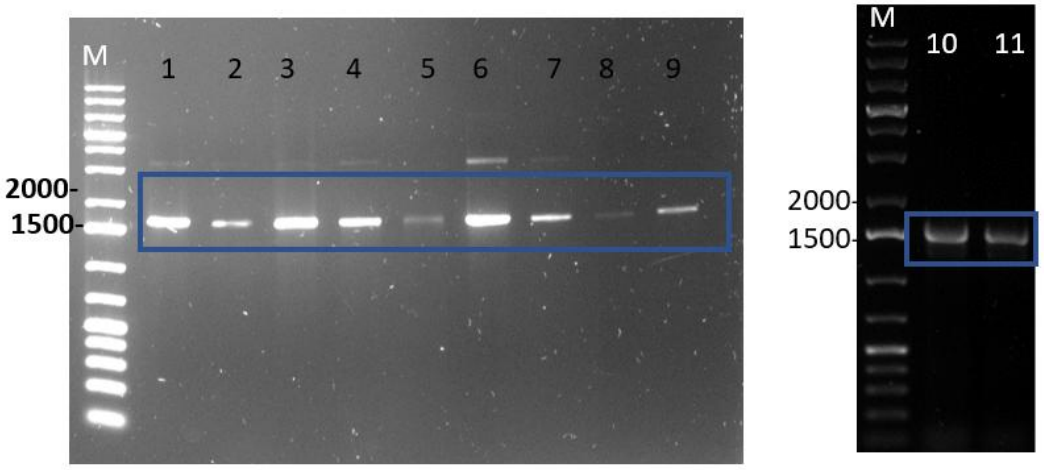

Figure 27. PCR was used to amplify a 1658 bp fragment from the P1 sequence of PV1 using pOPINE Mahoney Sc6b pDNA as a template in order to introduce 11 different myristoylation peptide sequences in the 5'-region of P1. M: GeneRuler 1 kb Plus DNA Ladder (Thermo Scientific™).

A linearised pOPINE Mahoney SC6b vector was produced by double digestion with enzymes *Bst*EII (*Eco*91I) and *Bsa*BI (*Bse*JI), and the 7256 bp band was purified using a gel extraction kit (ThermoFisher) after agarose gel electrophoresis **(Figure 28)**. The eluted DNA was quantified using a Nanodrop spectrophotometer and used for infusion cloning reactions with each of the purified PCR products.

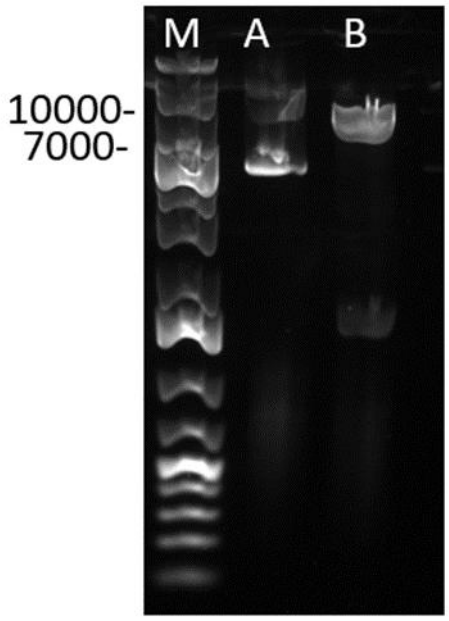

Figure 28. Agarose gel electrophoresis of pOPINE PV1 Mahoney Sc6b vector: lane A undigested plasmid DNA. lane B double digest of plasmid DNA using two enzymes Eco91I and BseJI showing correct size for linearized vector fragment, 7256 bp. Lane M: GeneRuler 1 kb Plus DNA Ladder (Thermo Scientific™).

Each purified PCR product was mixed with the linearized pOPINE Mahoney Sc6b in an in-fusion cloning reaction using NEBuilder HiFi DNA Assembly kit according to the manufacturer's instructions. The reaction mixture was transformed into competent *E. coli* cells and plated on selective agar containing ampicillin and incubated overnight**.** A separate transformation using the linearised DNA plasmid was used as a control. Three colonies were randomly selected from each transformation plate, transferred to LB with ampicillin, and grown overnight at 37°C with shaking. Plasmid DNA was extracted from the three candidates and sent to Source BioScience for Sanger sequencing **(Figure 29)**.

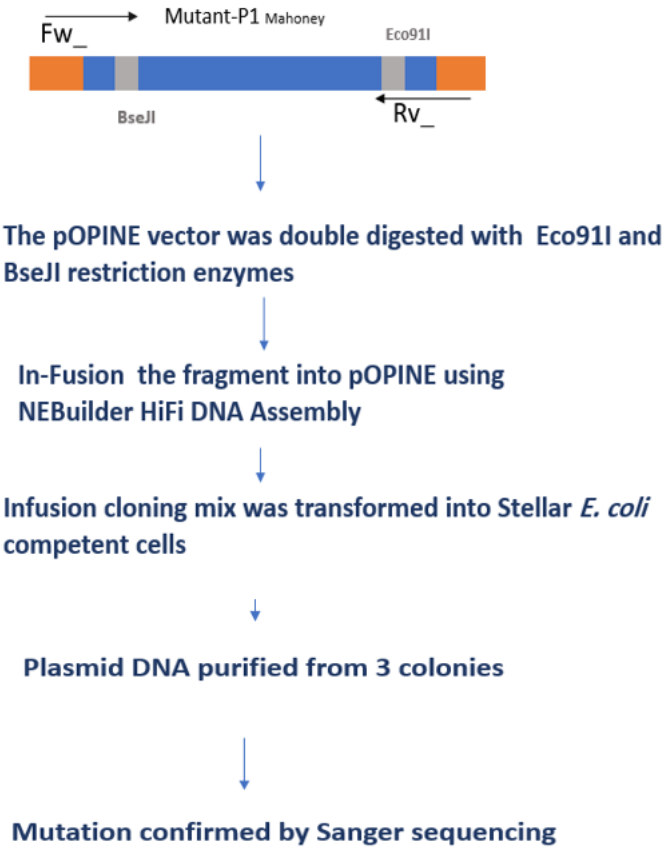

Figure 29. A flow diagram of the steps used to create the mutant Poliovirus Mahoney P1 sequences.

The sequences obtained were aligned to the parental DNA sequence using DNA Dynamo (Blue Tractor Software), and a single sequence adopted as representative of each mutant. These were translated to protein sequences and a multiple sequence alignment done using Clustal Omega(Goujon *et al.*, 2010; Sievers *et al.*, 2011). The alignment confirmed the correct mutations within the first 8 amino acids of P1 in all cases, which matched the expectation of the sequences designed **(Figure 30)**. No other changes were apparent in the P1 sequence as far as the read allowed.

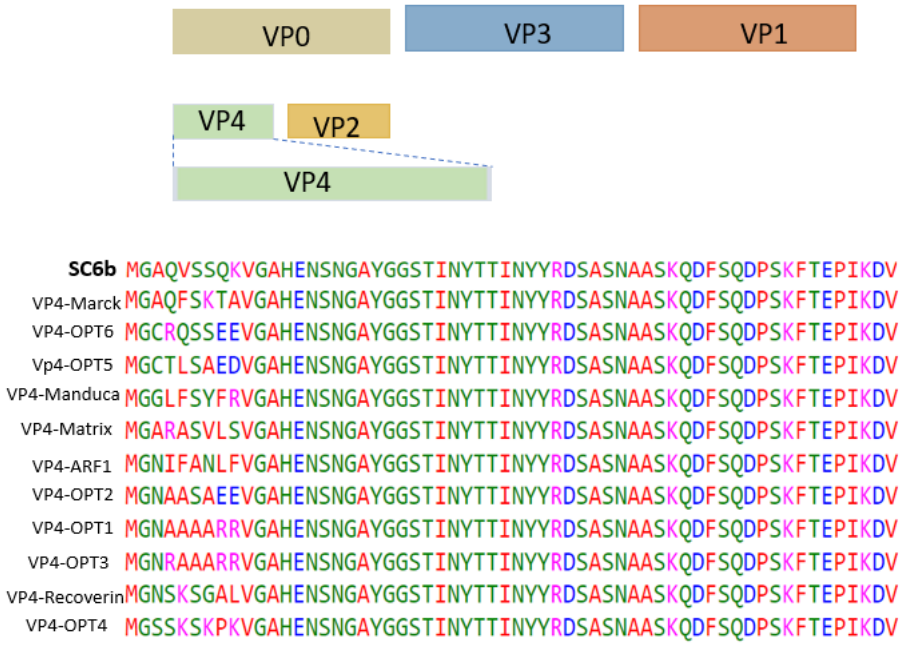

Figure 30. Alignment of eleven N-myristoylation mutations with the parental PV1 sequence using Clustal Omega.

4.3 Comparing Expression of VP1 in P1 N-myristoylation Mutants

The sequence verified plasmids encoding Poliovirus 1 Mahoney SC6b, both parental and mutant, were used to generate recombinant baculoviruses. The transfer vector and baculovirus DNA were transfected into insect *Sf9* cells using a standard transfection agent where recombination occurs between the transfer vector sequences and those of the virus genome leads to the production of recombinant baculovirus containing the PV sequences within the baculovirus genome and under the control of the p10 promoter. The recombinant baculoviruses generated after transfection were subjected to several rounds of virus passage in *Sf9* cells to produce high titer stock as described in section 2.2.14.3. The control Bac-GFP recombinant virus was also amplified to serve as an infection control. Following amplification small-scale cultures of Tnao38 cells infected with each recombinant baculovirus and examined by WB to confirm PV protein expression. A six-well dish was seeded with $1x10^6$ Tnao38 cells per well and allowed to settle as a monolayer before being infected with 200 µl of each recombinant baculovirus stock, and incubated for 4 days at 27°C. Each well of infected cells was harvested, centrifuged and the infected cell pellets were used to prepare samples for SDS-PAGE and Western blot. Following transfer, the Blots were incubated with the anti-Poliovirus 1 Antibody (MAB8560, Sigma-Aldrich) and then an anti-mouse -HRP conjugate to detect VP1. The membrane was finally incubated with a chemiluminescence substrate and imaged. To ensure equivalent loading the VP1 expression levels were normalized to the level of p39, the major baculovirus capsid protein, by a parallel blot using anti P39 antibody and the relative expression level was calculated by densitometry using Image J **(Figure 32)** (Schneider *et al.*, 2012). The 34 kDa VP1 band was identified in all tracks except the negative control with significantly different intensities **(Figure 31)**. Notably, the parental construct bearing the original PV1 myristoylation gave a relatively weak signal as did the Myr peptides from the HIV matrix protein, ARF and Recoverin (lanes 1, 2, 4 respectively). Intermediate intensities were apparent for the peptides from Opt1, Opt4, MARCK and Opt 3 (lanes 5, 7, 10, 11 respectively), and high intensity bands were observed for the peptides labeled Manduca, Opt 2, Opt 5 and Opt 6 (lanes 3, 6, 8, 9 respectively). No construct failed to express VP1 but some residual P1 precursor was present in some tracks, notably those with the high intensity VP1 bands. These data suggest that altering the myristoylation recognition peptide can significantly improve the expression of P1 and the cleaved mature capsid proteins.

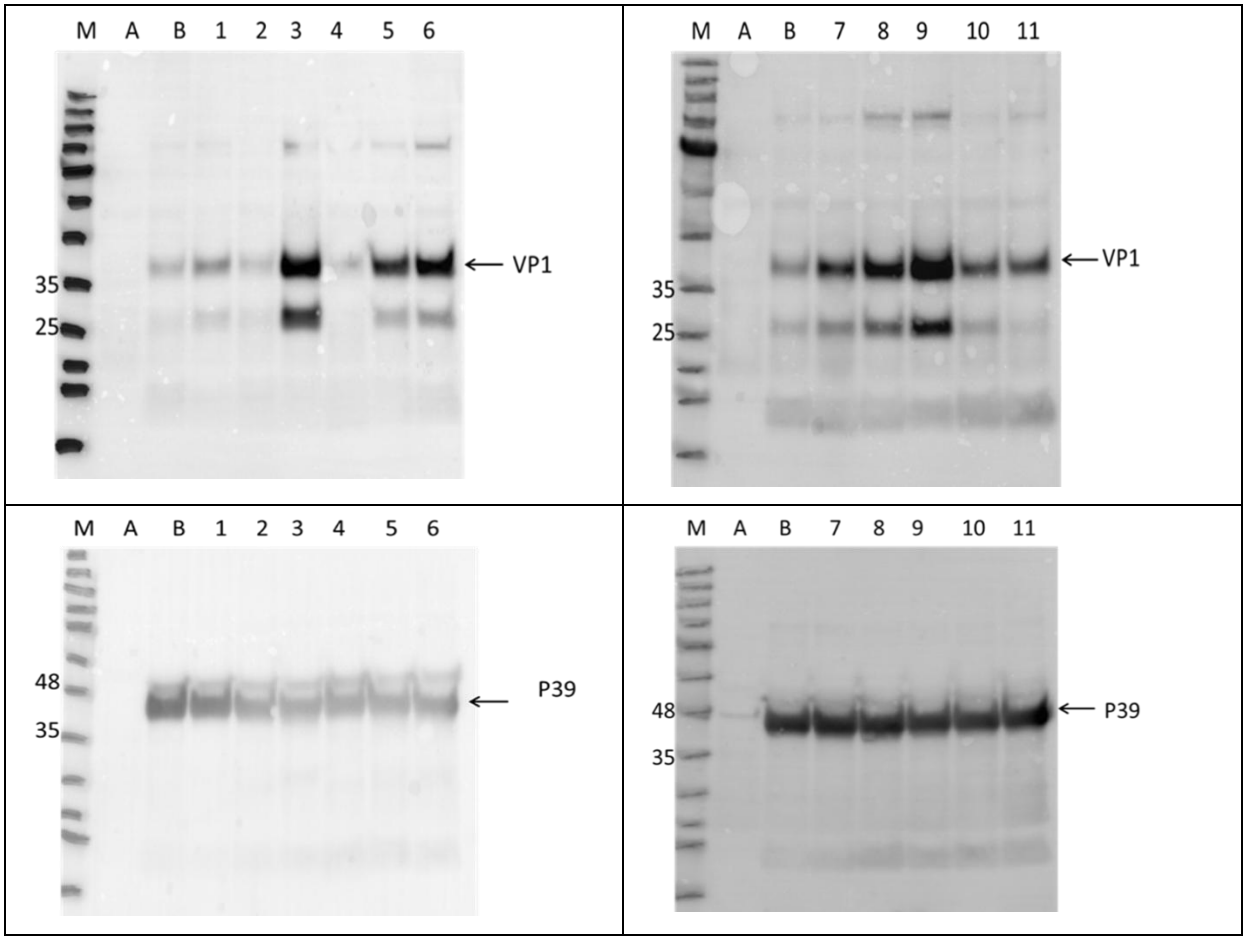

Figure 31. PV antibody detected recombinant PV expression in a small scale from Tnao38 insect cells by Western blot analysis. Lane A is uninfected cells used as a negative control; Lane B is WT PV used as a positive control, and Lanes 1 to 11 showed a different level intensity of expression for Bac_PV1 P1 N-myristoylation mutations. PV1-Matrix (Lane 1), PV1-ARF1 (Lane 2), PV1-Manduca (Lane 3), PV1-Recoverin (Lane 4), PV1-opt1 (Lane 5), PV1-opt 2 (Lane 6), PV1-opt4 (Lane 7), PV1-opt5 (Lane 8), and PV1-opt6 (Lane 9) PV1-Marck -2(Lane 10) and PV1-opt3-2 (Lane 11) .P39 was detected with anti-P39 and showed the same intensity for P39 production by Baculovirus. (M) makers on the left of the gel are shown molecular weight for protein in kilodaltons (BLUeye Pre-Stained Protein Ladder- Geneflow S6-0024).

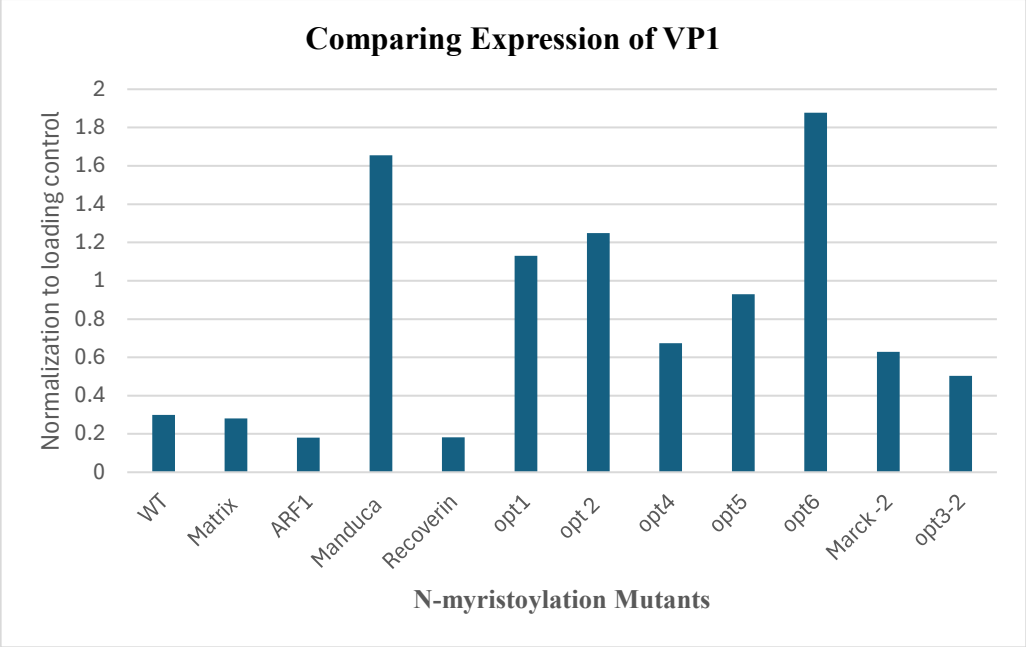

Figure 32. Expression of VP1 in Tnao38 cells with various N-myristoylation mutants. VP1 expressions were quantified and normalized to loading control (P39). Image J was used to measure band intensity. Results indicate variable expression levels depending on the N-myristoylation. Manduca and opt6 mutants showing the highest expression, while ARF1 and Recoverin yielded the lowest.

4.4 Modification of the N-terminus of P1 Does Not Abrogate VLP Assembly

Improving the level of P1 and mature cleaved capsid proteins necessary for poliovirus VLP assembly by modification of the myristoylation recognition peptide is an interesting way forward for improved yields overall. However, such a modification could not be used if it was incompatible with subsequent VLP assembly. Accordingly, to ensure that VLP assembly was not compromised by the sequence changes made a single mutant was selected for amplification and expression at a large scale and processed for VLPs.

Density gradient ultracentrifugation was used to fractionate VLPs from the opt6 variant following a 250 ml Tano38 infection with PV1-opt6. Cells were lysed with lysis buffer (see section 2.2.14.7.1) and centrifuged at 15,000 rpm to obtain a clarified lysate. The supernatant was then layered on top of a 30% sucrose cushion and centrifuged at 28K rpm for 5 h to pellet large, assembled material from the soluble insect cell proteins (see section 2.2.14.7.3). The pellet was resuspended in lysis buffer overnight at 4°C and re-clarified at 15,000 rpm for 15 minutes at 4°C to obtain a VLP enriched supernatant. VLPs were finally fractionated on a 20-45% linear discontinuous OptiPrep density gradient as described in section 2.2.14.7.4. and spun for 24 hours at 36K rpm. The gradient was fractionated by hand from the top of the tube and each fraction processed for SDS-PAGE and Western Blot in order to determine the presence of VP1 using MAB8560 as before **(Figure 33)**. VP1 was present in the clarified lysate used as the load and peaked in fractions 4 and 5 of the gradient. Some VP1 signals were present in other fractions suggesting a level of unassembled, or partially assembled VLP and showed a second minor peak in fraction 9, probably representing aggregated material. Fractions 4 and 5 were pooled and concentrated using 1ml spin-filters with a cut-off value of 500,000 kDa.

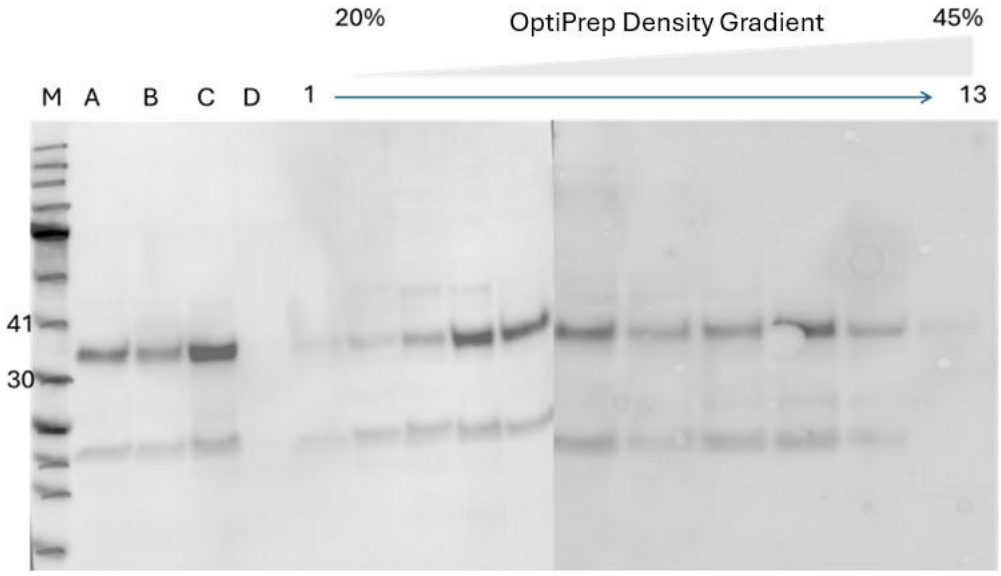

Figure 33. The purified VLPs from Tnao38 cells infected with PV1-opt6 recombinant baculovirus underwent Western blot analysis. Lane A was clarified lysate; lane B was the 30% sucrose cushion fraction and lane C was the gradient load. Lane D was the sample taken from the discard after concentrating the protein to confirm the efficiency of the concentration step. A total of 13 fractions were run on 2 gels (Bolt™ 4-12% Bis-Tris Plus Gels–ThermoFisher). VP1 reactivity peaked in fractions 4 and 5, while the (M) markers on the left of the gel represent the BLUeye Pre-Stained Protein Ladder (Geneflow S6-0024), with molecular weights indicated in kilodaltons (kDa).

4.5 Transmission Electron Microscopy

TEM imaging can show particle size and state, with VLPs having a unique icosahedral shape with an empty interior, sometime penetrated with stain. The pooled and concentrated samples, from fractions 4 and 5 from the 20-45% sucrose gradient, were adsorbed to EM grids and stained with 1% uranyl acetate (see 2.2.16). PV VLPs, with typical empty capsids imaged in the literature were present on the grid (Hogle *et al.*, 1985). Stain penetration was consistent with empty PV capsids, but the calculated size was ~34 nm, which is slightly larger than the expected size for PV itself (~27-30nm). The data confirms the ability of the myristoylation mutant to assemble into VLPs but suggests the particles might be slightly expanded. In addition, there is some background of smaller material on the grid. Whether this derives from the VLPs or was background material carried over in the purification process was not investigated **(Figure 34)**.

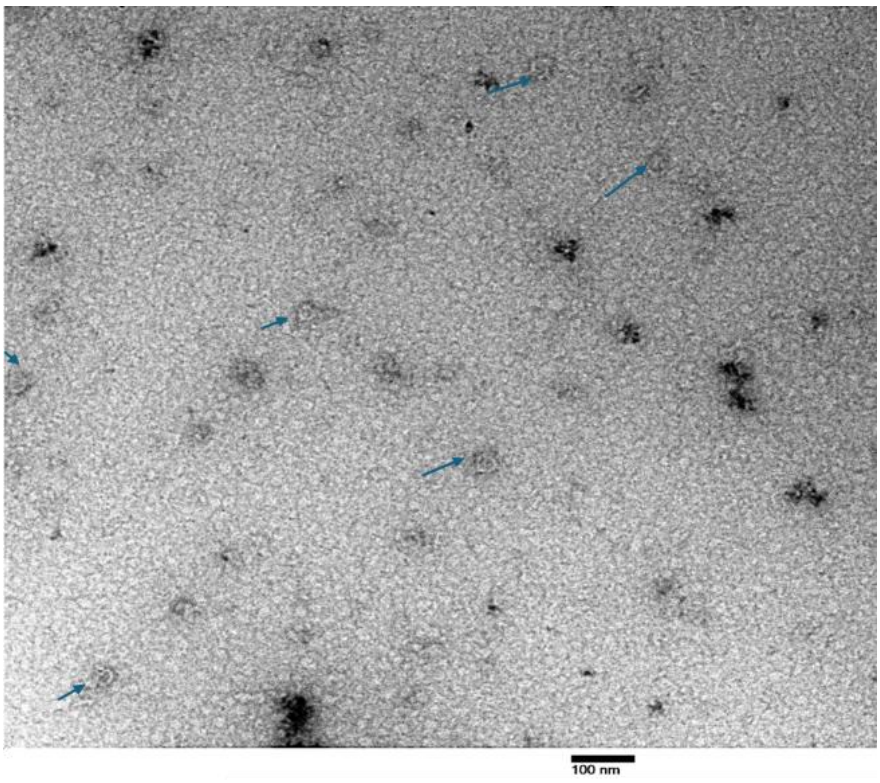

Figure 34. Transmission electron microscopy of uranyl acetate negative stained VLPs produced in Tnao38 cells infected with bac-opt6 recombinant baculovirus. The blue arrow indicates the VLPs. The scale bar is 100 nm.

4.6 The Expression for VP1 in P1 C-terminal Mutants

As described in the **Introduction**, the basic construct used for the production of poliovirus VLPs in this thesis is built in an analogous way to that described for the expression of Foot and Mouth Disease Virus VLPs (Porta *et al.*, 2013; Kotecha *et al.*, 2015). The original design, made by a previous graduate student, used sequences encoding the P1 protein and the 3C protease connected via a frameshift sequence to produce a monocistronic transcript under control of the baculovirus P10 promoter (Uchida, 2019). It was later shown that the end of VP1 was incompletely processed and that although VLPs assembled, the ragged C-terminus led to poor antibody recognition in VLP ELISAs (Sherry *et al.*, 2023). To correct this, the construct was altered to include the full 2A coding region downstream of the P1 sequence, as is the case in the virus genome. In FMDV, cleavage of P1 and P2 is achieved by the 2A peptide, an 18-residue sequence that causes an unusual co-translational peptide-bond-skipping event that results in termination of translation at the end of VP1 (Rao *et al.*, 2025). In PV however the equivalent cleavage is achieved by the 2A protease, which is similarly sited but much larger, 149 residues. During virus infection the 2A protease has been found to also cleave host cell proteins involved in the interferon response, contributing to immune evasion, which may partly explain why it is used in place of a 2A peptide (Feng *et al.*, 2014; Kastan *et al.*, 2021). This design resulted in authentic P1 cleavage, but the overall expression level was reduced substantially when compared to the previous design, possibly reflecting toxicity from 2A proteolytic cleavage of insect host cell proteins. To circumvent this problem new constructs were assembled in the host laboratory, but their characterization was not completed. They are included here as they also modify the P1 coding region to try and recover expression level. In these constructs a second copy of the 3C cleavage site from the PV VP3/VP1 junction, is introduced at the end of VP1. Eight residues, ALAQ/GLGQ are used, four from either side of the Q/G cleavage site to ensure efficient 3C recognition, meaning that the final 4 residues at the C-terminus of VP1 will be different from the WT sequence (ALAQ instead of LTTY). However, in the PV structure the last 12 amino acids of VP1 lie outside of the classic “jellyroll fold” of the mature picornavirus capsid proteins and are relatively unstructured (Basavappa *et al.*, 1994) so the identity of the final 4 residues may not be critical. Because of this C-terminal flexibility, three further constructs were also tested, in each case moving the 3C cleavage site back by 5 residues. Following these changes, the sequence reverts to the frameshift and 3C coding sequence described in the original constructs (Uchida, 2019), no 2A protease sequence is present. To ensure the constructs were as described they were first sequenced using a 3C reverse primer and the encoded VP1 protein translated (**Figure 35**).

(A)

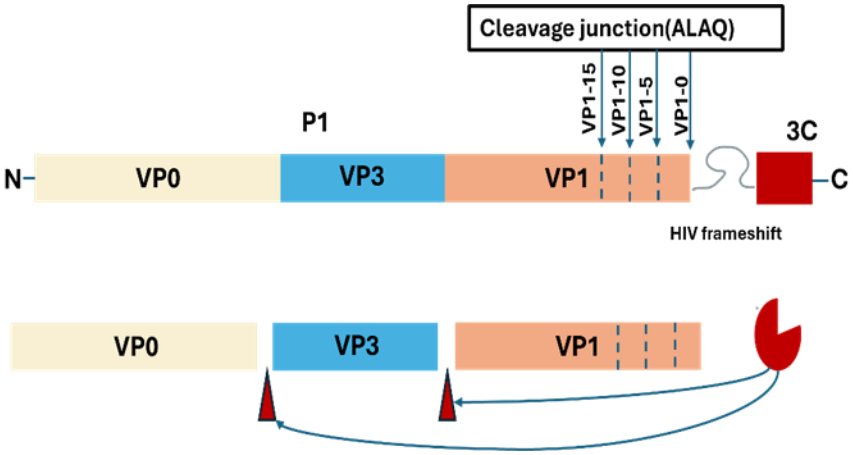

(B)

PV1 Mahoney VP1	GLGQMLESMIDNTVRETVGAATSRDALPNTEASGPTHSKEIPALTAVETGATNPLVPSDTVQTRHVVQHRSRSESSIESFFARGAC VTIMTVDNPASTTNKDKLFAVWKITYKDTVQLRRKLEFFTYSRFDMELTFVVTANFTETNNGHALNQVYQIMYVPPGAPVPEKW DDYTWQTSSNPSIFYTYGTAPARISVPYVGISNAYSHFYDGFSKVPLKDQSAALGDSLYGAASLNDFGILAVRVVNDPNPTKVTSKI RVYLKPKHIRVWCPRPPRAVAYYGPGVDYKDGTLTPLSTKDLTTY
PV1 Mahoney VP1-0	.....RVYLKPKHIRVWCPRPPRAVAYYGPGVDYKDGTLTPLSTKDALAQ
PV1 Mahoney VP1-5	.....RVYLKPKHIRVWCPRPPRAVAYYGPGVDYKDGTLTPALAQ
PV1 Mahoney VP1-10	.....RVYLKPKHIRVWCPRPPRAVAYYGPGVDYKDALAQ
PV1 Mahoney VP1-15	.....RVYLKPKHIRVWCPRPPRAVAYYGPGALAQ
PV1 Mahoney VP3/VP1 cleavage junction	ALAQ/GLGG

Figure 35. (A) Schematic representation of the 3C protease cleavage site in all C-terminal VP1 deletion mutants. In the VP1-0 construct, the cleavage junction (ALAQ) is positioned at the C-terminus of VP1, while in the VP1-5, VP1-10, and VP1-15 mutants, the cleavage site is progressively shifted upstream by 5, 10, and 15 amino acids, respectively. **(B)** The presence of the novel 3C cleavage sites and the truncation of the C-terminus of VP1 (indicated) was as described and the transfer vectors were used to produce recombinant baculoviruses as described in section 2.2.14.3. Plasmid DNA was mixed with linearized baculovirus DNA and transfected into insect *Sf9* cells to obtain recombinant baculovirusesBac-P1 VP1 3C-0, Bac-P1 VP1 3C-5, Bac-P1 VP1 3C-10, and Bac-P1 VP1 3C-15 all as VP1 C-terminal mutations.

Protein expression was done in small-scale cultures of Tnao38 cells as before. A six-well dish was seeded with $1x10^6$ Tnao38 cells per well and allowed to form a monolayer before the PV1 recombinant baculovirus stock was added. The plate was then incubated for 4 days at 27°C, the infected cells harvested by centrifuge and the infected cell pellets analyzed by WB using the anti-

Poliovirus 1 antibody MAB8560 from Sigma-Aldrich **(Figure 36**). VP1 signal was detected at ~34 kDa. Small reductions in the apparent MW were apparent for each of the truncation mutants, easily observed by a comparison of the -0 mutant with the -15 (lanes 1 and 4 respectively). It is also clear that the level of expression was substantially higher than the parental (2A encoding) construct (lane B). Blotting the same samples for the baculovirus capsid protein p39 showed all infections to be at an equivalent level, therefore the different levels of PV antigen expression are not due to different levels of baculovirus infection **(Figure 36)**. To ensure equivalent loading, VP1 expression levels were normalized to those of p39, the major baculovirus capsid protein, using a parallel blot probed with an anti-p39 antibody. Relative expression levels were then quantified by densitometry with ImageJ **(Figure 37)** (Schneider *et al.*, 2012) .

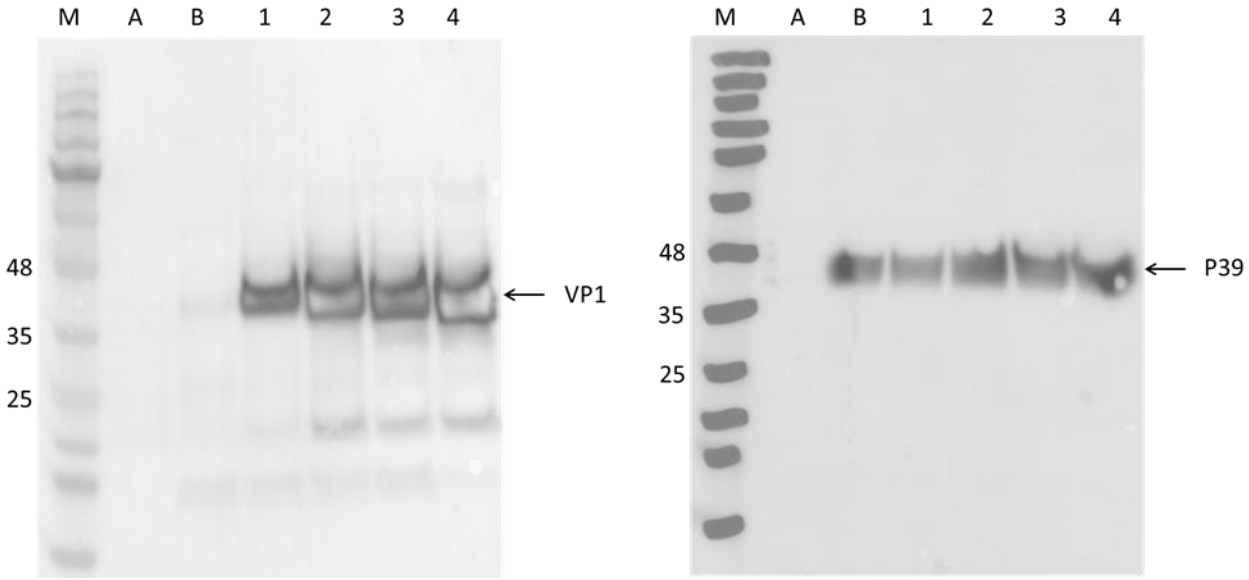

Figure 36. Upper panel. PV antibody detection of recombinant PV protein in Tnao38 insect cells by Western blot. Lane A is uninfected cells used as a negative control; Lane B is WT PV used as a positive control and lanes 1 to 4 are the -0, -5, -10 and -15 VP1 truncations. Lower panel. P39 was detected with anti-P39 and showed the same intensity for all infections. (M) makers on the left of the gel are shown molecular weight for protein in kilodaltons (BLUeye Pre-Stained Protein Ladder- Geneflow S6-0024.

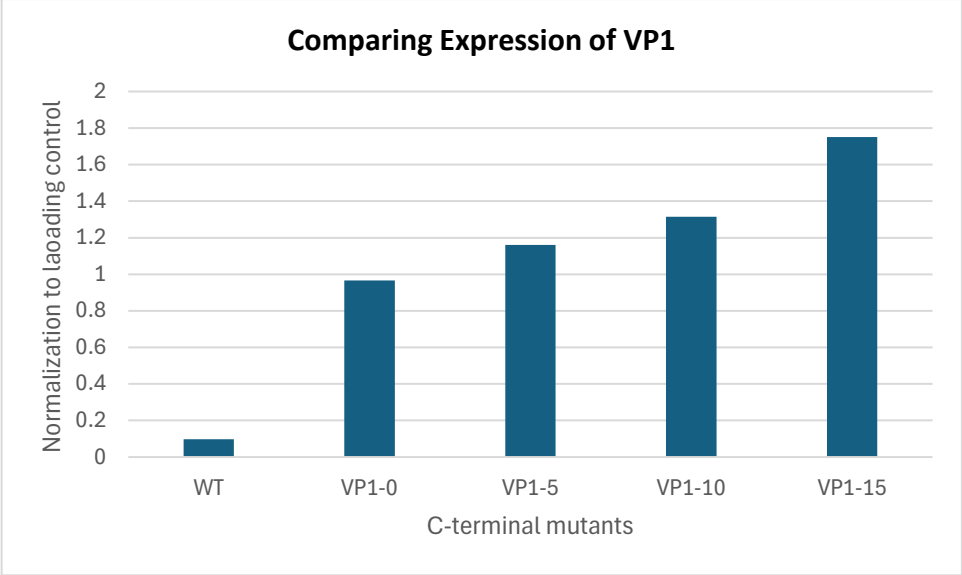

Figure 37. Expression of VP1 in Tnao38 cells with different C-terminal mutants. Protein expression was quantified by measuring band intensity using ImageJ and normalized to P39 as a loading control. Results indicate that VP1 expression varies depending on the C-terminal sequence, with the highest expression observed in VP1-15 and the lowest in VP1-5.

To confirm that expression of PV1 VP0, VP3, and VP1 was consistent across all 3C constructs (VP1-0, VP1-5, VP1-10, and VP1-15), small-scale cultures of Tnao38 cells were infected with each recombinant baculovirus and analysed by Western blot. A six-well plate was seeded with 1×10^6 Tnao38 cells per well, allowed to adhere as a monolayer, and infected with 200 µL of each baculovirus stock. Cells were incubated for four days at 27 °C, harvested, centrifuged, and the resulting pellets were processed for SDS-PAGE and Western blotting. Following transfer, three blots were prepared: one incubated with anti-Poliovirus 1 antibody (MAB8560, Sigma-Aldrich) to detect VP1 then anti-mouse HRP-conjugated secondary antibody was used. A second with rabbit anti-VP0 sera antibody to detect VP0, and a third with rabbit anti-VP3 sera antibody to detect VP3. These were followed by incubation with HRP-conjugated polyclonal goat anti-rabbit immunoglobulins. Finally, the membranes were incubated with a chemiluminescent substrate and imaged. Bands corresponding to ~37 kDa (VP0), ~26 kDa (VP3), and ~34 kDa (VP1) were detected in all samples, confirming successful expression of VLP components in all C-terminal deletion mutants, although the strength of antibody binding was relatively poor for both rabbit sera **(Figure 38)**. As expected of the genetic design, the VP1 band decreased in size with the extent of the C-terminal deletion as above while the sizes of both VP0 and VP3 remained constant. Poliovirus chimeras have been described previously but only by engineering major antigenic site 1 with relatively short peptide sequences (Martin *et al.*, 1988; Rose *et al.*, 1994), so the shortening of the C-terminus of VP1 is new. It was of interest therefore to examine these constructs further for VLP assembly.

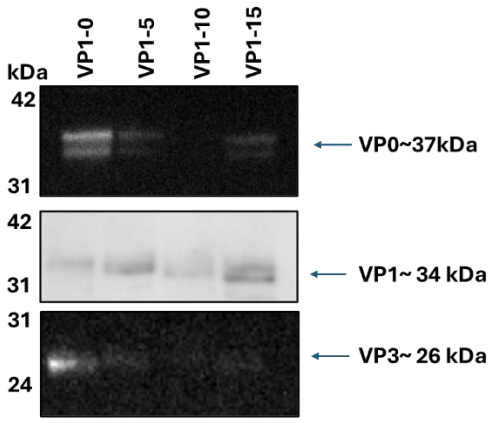

Figure 38. Western blot analysis of *Tnao*38 cells infected with recombinant baculoviruses shows expression of PV1 structural proteins VP0, VP1, and VP3, as detected using specific anti-PV1 antibodies. Markers to the left of the blots are in kilodaltons.

4.7 Effect C-terminal Deletion of PV VP1 on VLP Formation

As shown above, removal of the sequence encoding the 2A protease and substitution with a well cleaved 3C cleavage site resulted in improved levels of P1 synthesis. Analysis of the expressed products showed a truncated VP1 protein, depending on the position of the cleavage site, but unchanged VP0 and VP3 suggesting that processing remained competent for the assembly of VLPs. However, for the increase in P1 expression to lead to increased VLP yield the changes made must not interfere with VLP assembly. To evaluate this, two of the 3C VP1 mutants, VP1-0 and VP1-15 were selected for large-scale amplification, expression and subsequent VLP characterisation. These two mutations were chosen as they represent the extremes of the deletion made **(Figure 36)**. The -0 3C protease cleavage site is essentially at the VP1 C-terminus formed by 2A cleavage while the -15-residue position represents a new boundary, not previously investigated for compatibility with VLP formation.

VLPs generated from the VP1-0 and VP1-15 mutants were subjected to velocity gradient ultracentrifugation to assess particle assembly. *Sf9* cells were used for high-titre baculovirus amplification, followed by infection of 250 ml cultures of Tnao38 cells. Infected cells were lysed (Section 2.2.14.7.1), and lysates were clarified by centrifugation at 15,000 rpm. The resulting supernatants were layered onto a 30% sucrose cushion and centrifuged at 28,000 rpm for 5 h.

Pellets were resuspended overnight in lysis buffer at 4 °C, re-clarified at 15,000 rpm for 15 minutes, and subjected to 15–45% linear sucrose gradient ultracentrifugation at 36,000 rpm for 24 h (Section 2.2.14.7.5).Gradients were manually fractionated from the top, and 1 ml aliquots from each fraction were analysed by spectrophotometry at OD_{280} and Western blot.

Analysis of the gradient profile for total protein content by OD_{280} showed a high absorbance at the top of the gradient (fractions 1–3), consistent with the majority of soluble proteins not incorporated into any form of higher molecular weight assembly. A secondary peak was observed at the bottom, corresponding to aggregated material **(Figure 39)**.

Western blotting using MAB8560 confirmed the presence of VP1. For both VP1-0 and VP1-15, VP1 peaked in fractions 12 and 13, corresponding to the VLP-containing region. Signals in fractions 1-7 likely represent unassembled or partially assembled proteins. The finding of assembling VLPs for the VP1-15 mutant is new and may a secondary VP1 signal was also observed in fractions 3–7, indicating the presence of aggregated VP1 material or misassembled particles.

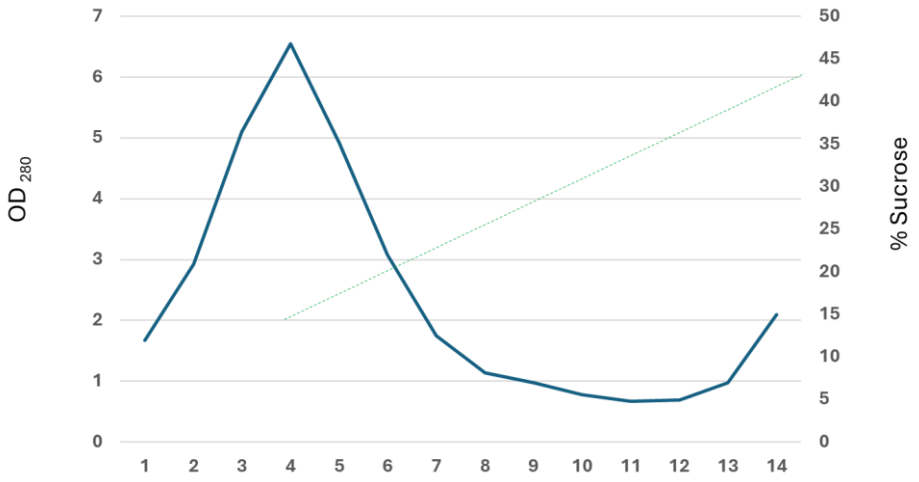

Figure 39. OD_{280} measurements of sucrose gradient fractions from Tnao38 cells infected with recombinant baculovirus expressing C-terminal VP1 deletion mutant (VP1-15). A strong OD_{280} signal was observed at the top and bottom of the gradient, corresponding to the soluble and aggregated proteins respectively. Assembled VLPs were detected in the denser region of the gradient, with peak absorbance in fraction 12.

(A)

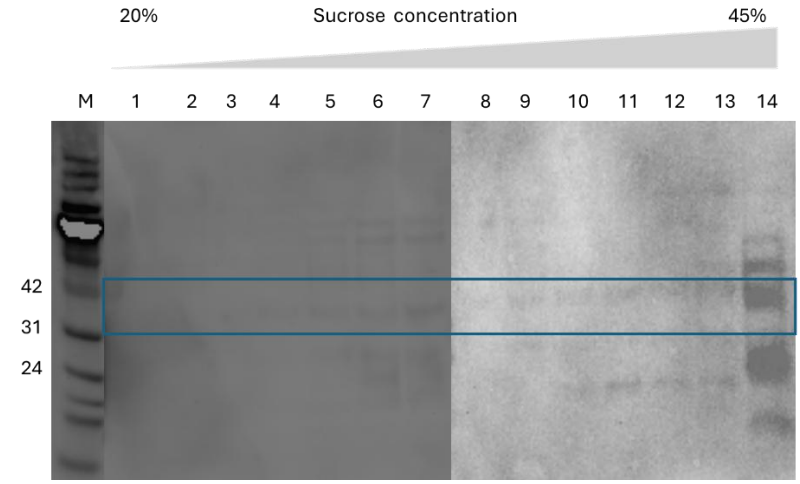

(B)

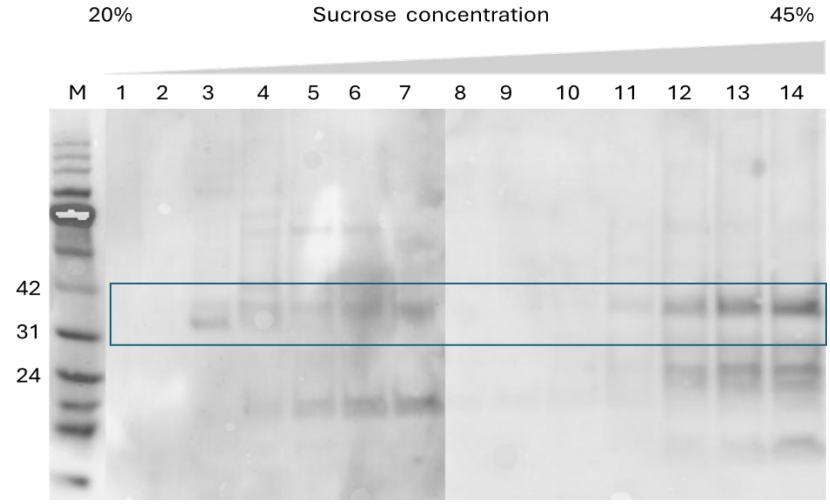

Figure 40. VLPs were purified from Tnao38 cells infected with recombinant baculovirus of C-terminal deletion mutations and analyzed by Western blot. A) PV1-VP1-0. B) PV1-VP1-15. A total of 14 fractions were run on 2 gels (Bolt™ 4-12% Bis-Tris Plus Gels –ThermoFisher). VP1 reactivity peaked in fractions 12 - 14. The (M) markers on the left of the gel represent the BLUeye Pre-Stained Protein Ladder (Geneflow S6-0024), with molecular weights indicated in kilodaltons (kDa).

4.8 N/H Flow Cytometry

The issue of N/H antigenicity for PV was discussed in the **Introduction** and as noted, the use of the Sc6b sequence isolated by (Fox *et al.*, 2017a) can result in excellent levels of N reactivity. However, predominantly H reactivity can remain if the expressed VLPs remain in the expanded 135S state, either because of the expression background used or of the methods used during VLPs isolation. Despite the use of the Sc6b sequence, the WT VLPs formed in this work were largely in the H antigenic form (Uchida, 2019). However, it was possible that the changes made at both the N- and C- termini described in this chapter could improve N reactivity. To investigate this Tnao38 cells in 6-well plates were harvested after 4 days of incubation with Bac-PV1P1-3C, which contains the modification in N-myristoylation and C-terminal mutations and processed for antibody staining. Uninfected cells were used as a negative control. For intracellular protein staining, the cell pellets were resuspended in a fixation buffer, followed by the addition of Permeabilization Buffer to the cells. After a blocking step, the monoclonal antibodies for N and H from NIBSC were added to the pellets, followed by an anti-mouse FITC-conjugated labelling Ab.

Pellets were resuspended in PBS and transferred to flow cytometry tubes for the measurement of FITC-A fluorescence by a C6 Plus Flow Cytometer. The results were blotted by BD CSampler Plus, the H antibody labeled VLPs in red and the N VLPs in green. The percentage of the cells above a threshold set by the highest fluorescence signal from the control cells (black) was calculated using the gating function and is shown the top right quadrant of each plot. The level of antigen recorded by H antibody staining was broadly in agreement with the WB results (denatured antigen) already described, i.e. the myristoylation mutants Opt6 and Manduca were more highly expressed than the WT or the other Myr mutants. Similarly, the -15 C-terminal deletion was more highly expressed that the -10, -5 or -0 variants. However, the N-reactivity was poor throughout the experiment, barely rising above the fluorescence associated with the control cells in any of the samples tested **(Figure 41)**.

(A)

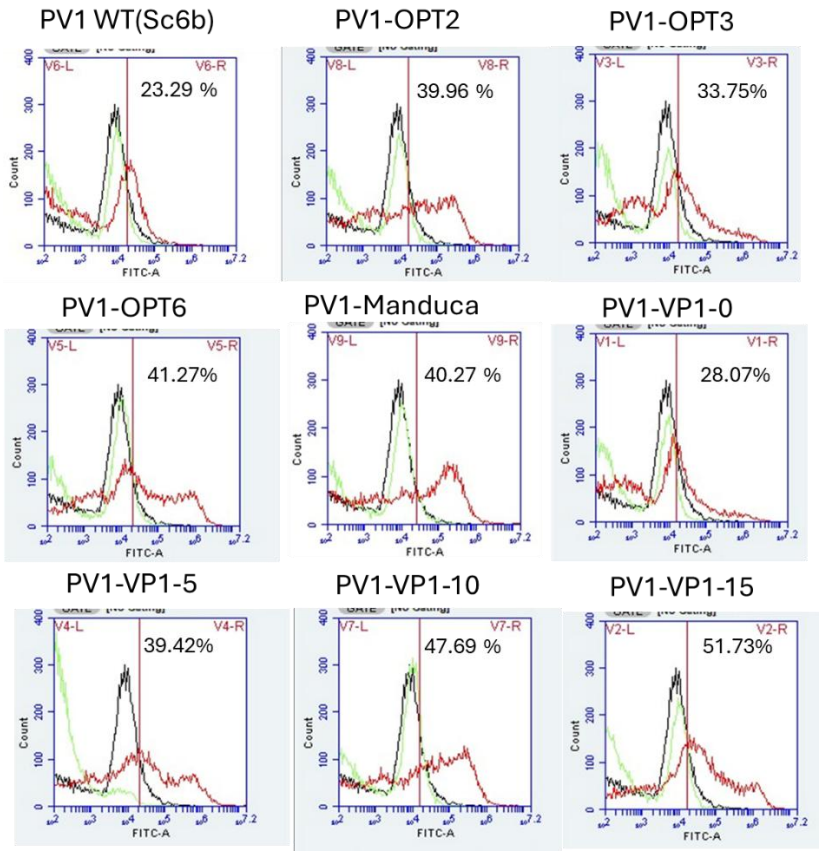

(B)

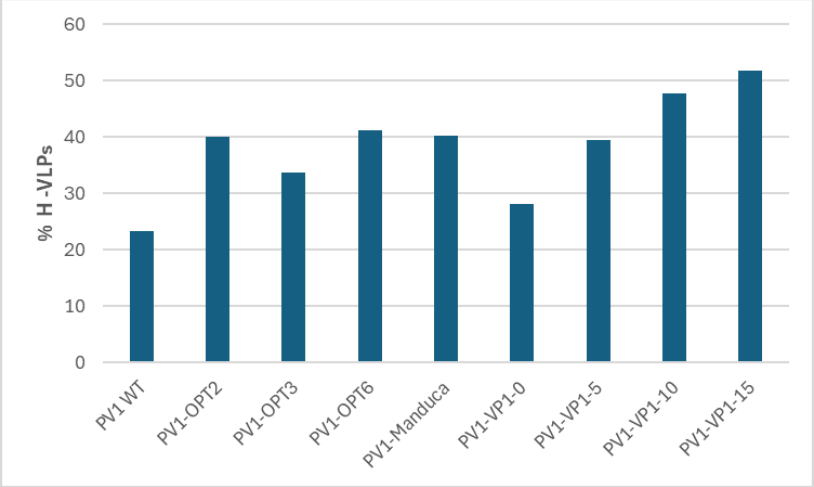

Figure 41. N/H flow cytometry results of Tnao38 cells infected with PV1 SC6b Mahony wild type, PV1 N-terminal mutants and PV1 C-terminal mutants. Cells were analysed for fluorescence intensity in the FITC-A channel. **A**- BDC Sampler Plus software indicates a variety of H VLPs (red line) comparison to the negative control of uninfected cells (black line) while for N VLPs (green line) insignificant change was noted. The vertical demarcations (V1-L, V1-R) indicate the conventional gate used to distinguish the FITC-A -negative (V1-L) from the FITC-A -positive

(V1-R). Peaks that shift further to the right represent signals, whereas peaks overlapping the control uninfected cells (black line) reflect the absence of signal. **B** - The percentage of H-VLP-positive cells within the V1-R (FITC-A-positive) gate was calculated, demonstrating varying levels of H-VLP expression among the samples.

4.9 N/H ELISA

The poor N reactivity observed above could be the result of the assay format used, i.e. that the N-antibody used is incompatible with staining PV antigen in fixed and permeabilized cells. To address this possibility, ELISA was also performed. For these tests only the N-myristoylation (PV1-OPT6) and C-terminal mutations (PV1-VP1-0) were selected, as they had a good expression for VLPs. 50 ml of Tnao38 cells were infected and followed by a 4-day incubation period with the required Bac-PV1P1-3C mutants. Cells were harvested and lysed to extract the VLPs, following the instructions provided in section 2.2.14.7.1.

The antigenicity of PV VLPs was then analysed by a non-competitive sandwich enzyme-linked immunosorbent assay (ELISA). The immunosorbent plate wells were coated with capture antibodies, which were monoclonal antibodies for N and H from NIBSC. Then, the IPV standard as a positive control for N antigen and PV VLPs samples was applied. Then, poliovirus 1 Ab (R879) as the detection Ab was added to each well. Conjugated secondary anti-rabbit Ab was added to the wells for enzyme-substrate interaction. The antibodies and techniques were detailed in **Table 9**.

While H-antigen again mirrored the know overall expression level for the WT and Opt6 samples, N antigenicity was relatively flat (**Figure 42)** panels top right and bottom left). In the case of the -0 mutant both antibodies tracked together, and the absolute OD was low, suggesting background binding. The overall OD for the IPV sample was even lower and did not follow the dilution curve again suggesting only background binding **(Figure 42)** panels bottom right and top left). The results confirmed H- but not N- antigenicity although in the absence of the +ve control (IPV N) any conclusion regarding N reactivity is not valid.

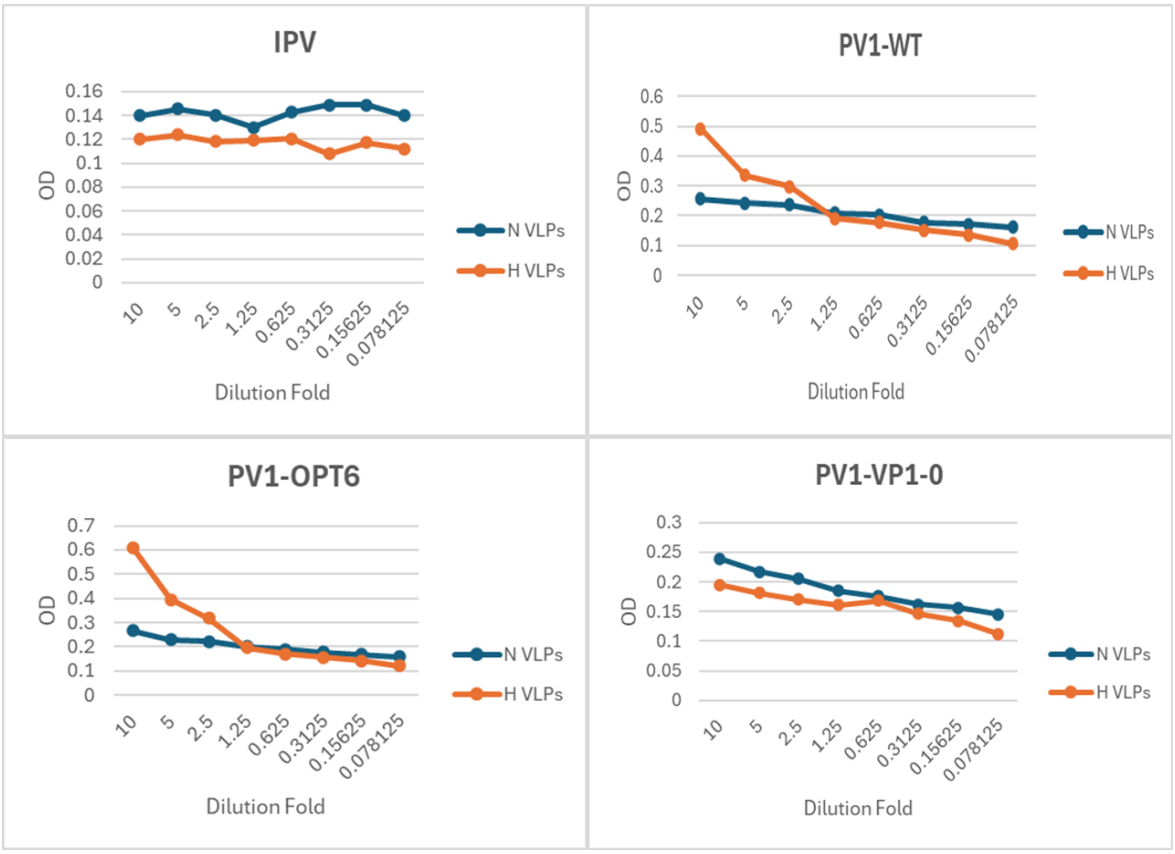

Figure 42. ELISA analysis of European IPV standard (NIBSC code: 12-104) and PV VLPs expressed in insect cells detected by N/H-specific antibodies. Triplicates of IPV and VLP samples were analyzed. IPV standard and PV VLPs samples started with a dilution from 1/10, and the dilution was completed with a 2-fold series. O.D. readings were reached as non-significant and unchanged through the later dilutions in IPV and PV VLP samples. The samples were WT (wild-type VLPs), OPT6 as N-myristoylation and VP1-0 as C-terminal mutations.

4.10 Discussion

The data presented in this chapter investigated modification of the P1 sequence to improve expression levels and lead to higher yields of VLP. A limit of the baculovirus system is that the transcription unit used for expression is fixed and the promoters used, the very late promoters such as the polyhedrin and P10 promoters, are already the strongest available. Moreover, the P1 sequence used was already codon optimized to allow efficient translation leaving modification of the coding region itself as the only option for further improvements. The extent to which P1 can be successfully modified is largely unknown as the focus of most expression studies is the generation of wild type rather than modified VLPs. However, previous work such as the isolation of the Sc6b sequence used here demonstrates that modification is not only possible but can benefit the VLP formed (Fox *et al.*, 2017). To further investigate possible changes that might improve VLP yield, the N-myristoylation site of VP4 was targeted with the suggestion that this may not be the optimum for use in insect cells and that a modified site could enhance the production of P1 protein by providing a substrate for NMT that is better suited to the insect cell enzyme. As previously noted, this post-translation step is likely to be rate limiting (Ansardi *et al.*, 1992b) and, as PV has evolved in a mammalian background it is likely the NMT recognized peptide is not optimal for the insect cell enzyme. A series of alternate NMT peptides were obtained from the literature, all spanning the first 8 amino acids of the VP4 region and were introduced into the PV SC6b sequence by re-PCR of the coding region using 5' primers that incorporated the required changes followed by in-fusion cloning of the eleven modified amplicons back into the original vector. The in-fusion fragments used allowed the change of the eight amino acids as shown in (**Figure 31**), all of which were confirmed by DNA sequencing prior to expression studies. Following the cloning of the complete sequenced mutants into the pOPINE vector, the baculovirus expression system in insect cells was used to express the modified N- terminal sequences resulting in P1 with different expression levels in infected insect cells (**Figure 32**), vindicating the hypothesis that optimized NMT binding could improve translation levels overall. Detection of expression was achieved with a VP1 antibody which also showed no change in the processing pattern (P1 to VP0, VP3 and VP1) following the changes made. These data confirm that N-myristoylation plays a role in the synthesis of the P1 region for PV (Corbic *et al.*, 2018). The data also revealed less favorable NMT peptides which resulted in lower levels of VP1 (**Figure 32**). The effect was specific to the expressed PV sequence as probing the blots for the level of baculovirus infection with the p39 antibody showed the same level for all mutations. VLP assembly was not affected by the changes made, as expected of a sequence that is found inside the assembled capsid. The VP1 signal precipitated through a 30% sucrose cushion and 20-45% discontinuous OptiPrep density gradient consistent with a high molecular weight complex. VP1 band intensity reached a maximum in fractions 4 and 5, which were also positive based on TEM

imaging. Some signal was also present in the lighter fractions consistent with some non-assembly of VLPs (**Figure 33**). The observed VLPs were expanded, ~ 36nm in size (**Figure 34**), and further work is necessary to investigate the reasons behind the expanded VLPs and also assess the quality of the VLPs as a suitable vaccine candidate.

The limitations of any structural interpretation of VP4 were outlined in the **Introduction**, but as the Opt6 and Manduca Myr sequences offered improved expression levels their AlphaFold structures were derived and compared **(Figure 43)**. Both sequences folded into structures that were very similar to the WT sequence (cf. Figure 2) suggesting the exact N-terminus plays little role in guiding the folding of VP4.

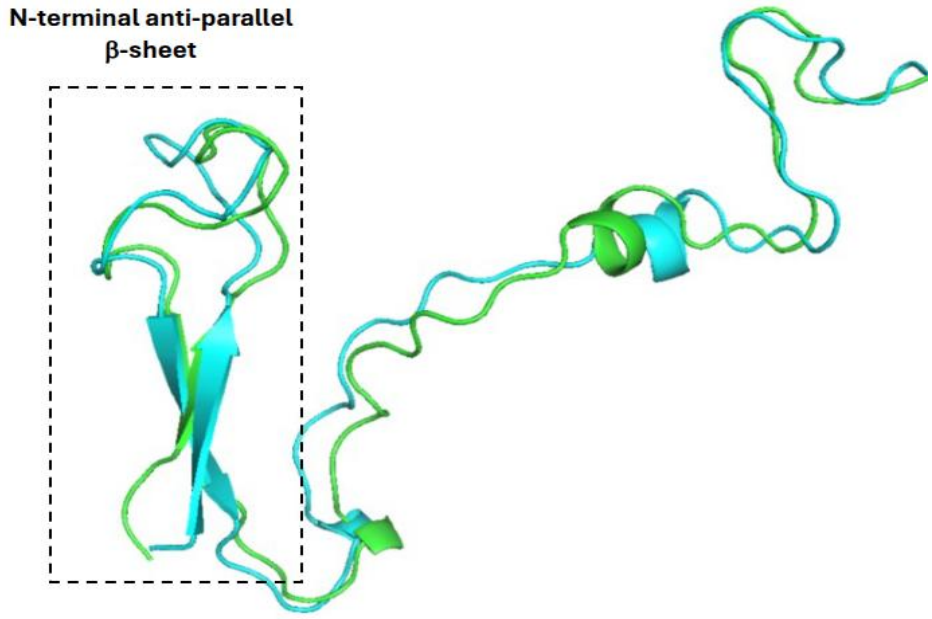

Figure 43. The AlphaFold predicted structures of the Opt6 (cyan) and Manduca (green) VP4 sequences. The structures were loaded from the AF generated pdb files into PyMol and the align function chosen. N-terminus at the left, C-terminus at the right. In particular the folding of the beta opposing beta strand and their interconnect loops are very similar despite the sequence changes made.

The same approach, mutation of PV sequence followed by retest of expression level was also applied to the C-terminus of P1 for the reasons outlined in the text and showed that deletion of 10 or 15 residues resulted in higher levels of VP1 (**Figure 36**).

The expression of PV1 capsid proteins (VP0, VP3, VP1) in the P1 C-terminal mutants was consistent across all 3C constructs (VP1-0, VP1-5, VP1-10, and VP1-15), indicating that the introduced mutations did not impair polyprotein processing (**Figure 38**). The assembly of PV

VLPs was supported by the detection of VP1 in high-density fractions (12–14) following 20–45% sucrose velocity gradient centrifugation (**Figure 40**), suggesting successful formation of high molecular weight complexes consistent with VLPs. The variation in VP1 band intensity across fractions, with the strongest signals in fractions 12–14, further supports efficient VLP assembly in these constructs. As expected, velocity gradient centrifugation placed assembled VLPs in the denser, lower fractions. However, VP1 signal was also detected in lighter fractions at the top of the gradient, consistent with the presence of unassembled or partially assembled capsid proteins.

To establish the antigenicity of VLPs, the change from the native N antigenic form (N Ag) to the non-native form (H Ag) was examined. Recombinant VLP vaccines have to maintain N antigenicity because H-type particles cannot generate a protective immune response. Flow cytometry and ELISA were used to test N and H Ag. The flow cytometry results (**Figure 41**) indicated varying levels of H Ag in SC6b Mahoney wild-type, N-terminal mutant VLPs and C-terminal mutant VLPs compared to the negative control (uninfected cells), whereas N Ag expression remained largely unchanged. ELISA results (**Figure 42**) demonstrated O.D. values remaining stable and non-significant across two-fold dilutions in both IPV and poliovirus -0 VLP samples. It is worth noting that the standard ELISA format for H and N antigen used a non-discriminatory coating antibody to capture PV antigen (Adeyemi *et al.*, 2017) that is then probed with either the H- or N-specific layer. Unfortunately, for the course of this study Mab1588 was absent from the NIBSC products catalogue and could not be obtained elsewhere. A number of gifted antibodies were tested for a capture role, but none proved satisfactory, leaving the H- and N-specific capture the only option for the ELISA. Overall, the true N status of the VLPs produced remains unresolved. Previous work has suggested that N-myristoylation of -VP4 may affect the assembly of VLPs (Moscufo *et al.*, 1991) but more recently that view has been questioned (Corbic Ramljak *et al.*, 2018). Overall, the critical role for myristoylation in the assembly of PV VLPs requires more analysis and the various mutants described, with lower and higher levels of synthesis, may allow a novel approach to this.

In conclusion, changes of the myristoylation sequence modified the PV P1 production level in the insect cell by the baculovirus expression system suggesting it as a general method for improved expression. More generally the approach of modified P1 sequence followed by re-analysis can now be applied throughout the P1 sequence to optimize the synthesis of viral proteins and maximize their self-assembly into PV VLPs.

Chapter 5 The Role of Site-Specific Changes in VP4 in The Expression of PV1 VLPs

5.1 Introduction

The current view of the PV entry process is outlined in the **Introduction** and has been pieced together by stepwise improvements in the resolution of the derived structures for PV particles, often arrested in the entry reaction (Hogle, 2002), supported by biochemical studies of individual capsid proteins, especially VP4 (Panjwani *et al.*, 2014; Panjwani *et al.*, 2016). To recap, binding of the virus to the cellular receptor, CD155 occurs in the "canyon" depression that surrounds the 5-fold axis of the virus particle and causes a slight expansion of the virus particle. This early binding has not yet committed the virus to disassembly but further expansion, along with loss of the VP1 pocket factor that stabilizes the particle, leads to the formation of the "A" particle which sediments in gradients at 135S, compared to the 160S of the native virus, and represents the end of the expansion process and the formation of a structure primed for genome release and eventual particle dissolution (Shah *et al.*, 2020). As this process progresses, the N-terminus of VP1 relocates from near the 5-fold axis and emerges from the expanded particle at the 2-fold axis, as does the N-terminus of VP4 whose myristic acid moiety embeds into the host cell membrane to form a pore through which the genome enters the cell cytoplasm (Panjwani *et al.*, 2014; Panjwani *et al.*, 2016; Shah *et al.*, 2020). The relevance of this transition to the field of PV VLPs is that structures that mimic the 160S particle are immunogenic whereas those that mimic the 135S particle are not. Experimentally, 160S particles can be converted to 135S particles by incubation with soluble receptor but also by heating, which converts the "native" (N) particle to the "heated" (H) variant. The nomenclature is synonymous with the earlier designation of C and D antigens, taken from the gradient fraction numbers containing the 135S and 160S particles, respectively. N to H conversion also occurs spontaneously during virus preparation and vaccine preparations are assessed for N antigen content before use. The USFDA accepted levels for trivalent IPV are 40 N-antigen units of Type 1, 8 N-antigen units of Type 2, and 32 N-antigen units of Type 3 (Bravo *et al.*, 2020). As a result of the global eradication campaign, the PV2 component was removed from the vaccine in 2016 (Blake *et al.*, 2018) although evidence for its continued spread has led to the need to stockpile PV2 vaccine is case of widespread recurrence (Harutyunyan *et al.*, 2023). Any successfully developed recombinant PV vaccine will also need to meet the criteria for the minimum accepted levels of N antigen and the **Introduction** outlined the sequence and formulation changes that have been investigated to improve the relative N/H ratio, including the isolation of the PV1 Mahoney Sc6b sequence used here and in a number of other recombinant studies (Sherry *et al.*, 2025). Despite these changes the N/H ratio remains variable, depending on

the serotype and the expression system used (Marsian *et al.*, 2017a) and genetic changes that result if a particle fixed in the N antigenic form remain elusive.

Prior to the current level of understanding of the structural changes that accompany PV particle expansion and the entry reaction, the processes involved were investigated through a combination of mutagenesis and the selection of viral mutants with altered receptor binding properties (Racaniello, 1996). Among those studies it was noted that mutations in VP4 could inhibit a late stage of the virus entry reaction (Moscufo *et al.*, 1993). In particular, changes at residue 28, normally threonine to glycine, serine, or valine (4028T.G, 4028T.S, and 4028T.V) led to various phenotypes when compared to the wild-type Mahoney strain. Specifically, the entry-defective mutant (4028T.G) was unable to release its genome into the cytoplasm, whereas the other mutants showed various levels of genome delivery (Danthi *et al.*, 2003). The (4028T.G) mutant was later shown to have altered membrane binding properties suggesting that VP4 played a role in the formation of ion channels (Tosteson *et al.*, 2004). Today, this mutation would be interpreted as preventing or restricting the movement of the VP4 N-terminus through the expanded 2-fold axis so that the pore required for genome transfer fails to form. In the context of WT virus this renders the mutation non-viable, but in the context of VLPs the lack of viability and inability to release the genome into the cytoplasm during the entry step associated with 4028T.G is irrelevant. Conversely, restricting the conformational flexibility mapped to threonine-28 in VP4 could be advantageous in that it is possible that a modified capsid with this mutation could freeze the capsid in the native 160S conformation, corresponding to a higher yield of N antigen material from PV1 VLPs. To examine this possibility, 4028T.G and 4028T.V were substituted for the WT PV sequence in the context of PV1 VLPs and the effect on expression evaluated. Other VP4 mutations described as altering but not aborting virus entry, at the 24 and 29 positions in VP4 were also replaced with glycine and valine (Danthi *et al.*, 2003;Tosteson *et al.*, 2004). In addition to examining the role of these mutations in P1 expression and processing the VP0 domain carrying each variant was expressed as a GFP fusion protein. A VP0-EGFP fusion protein has been used in another study, to evaluate the role of PV capsid proteins in the cellular autophagy pathway (Zimina *et al.*, 2021), and their use here was to allow a simple visualization of any gross effect the mutations might have on expression level or protein distribution with the expressing cell. The synthesis of the P1 protein of PV with the highlighted mutations in VP4 was achieved by PCR mutagenesis as before but, based on the expression level data in **Chapter 4**, the SC6b variant with the C terminus of VP1 defined by the inclusion of a 3C cleavage site, the -0 variant, was used as in addition to the parental P1 sequence. It was hoped that a re-investigation of these historical mutations in a VLP rather than live virus background might provide a promising and underexplored route to improve the quality of PV1 VLPs.

5.2 Design and Construction of PV1 Site-Specific Mutations

Site-specific mutagenesis of the sequence encoding PV VP4 to introduce the changes described by (Danthi *et al.*, 2003; Tosteson *et al.*, 2004) was done by an overlap PCR approach **(Figure 44)**. A short fragment from the 5' end of the coding sequence was produced by the T7 forward primer combined with a mutagenic reverse primer binding in the VP4 region. A long overlap fragment was produced by a complimentary forward mutagenic primers and a 3' reverse primer binding at the end of the P1 coding region. In both cases there are sufficient bases at the ends of the fragment for them to be assembled together, and with the pOPINE vector, using the infusion ligation independent cloning method. The DNA fragments were amplified by PCR utilizing the forward and reverse primers detailed in **Table 8** and using the PV1- Mahoney SC6b sequence in pOPINE, WT or the -0 variant, as a template using a PCR reaction as follows: initial denaturation at 98°C for 30 seconds, and then 35 cycles of denaturation for 10 seconds at 98 °C, annealing for 30 seconds at 63°C and an extension for 1 minute 30 seconds at 72°C followed by a final extension for 10 minutes at 72°C.

Six different versions of the site-specific mutations in the VP4 region, targeting threonine at positions 24, 28, and 29 individually substituted with glycine or valine were produced in this way. The resulting PCR products for the six mutations were analyzed by agarose gel electrophoresis, confirming the expected fragment sizes of 1500 bp and 300 bp.

(A)

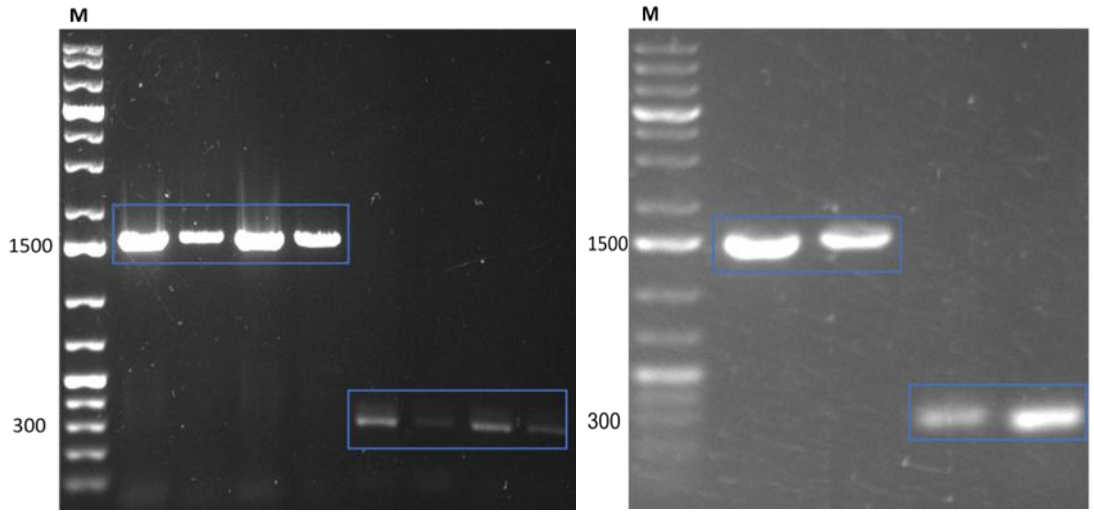

(B)

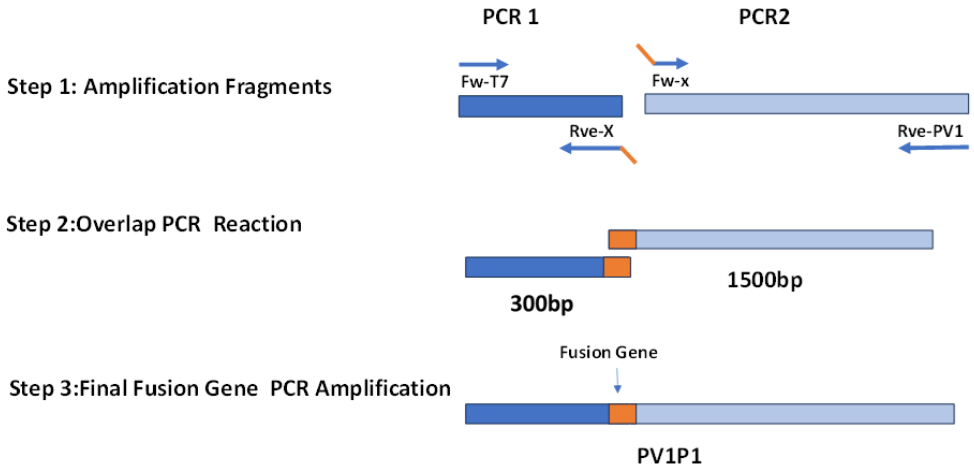

Figure 44. A) PCR amplification of two DNA fragments, 1500 bp and 300 bp in size, was performed from the PV1-Mahoney SC6b sequence to introduce six distinct versions of site-specific mutations in the VP4 region. M: GeneRuler 1 kb Plus DNA Ladder (Thermo Scientific™). **B)** Diagram overview of the generation of PV1P1 with a site -mutagenic reverse primer binding in the VP4 region by overlapping PCR.

The 1500 bp and 300 bp PCR products were purified using a gel extraction kit (ThermoFisher) following agarose gel electrophoresis **(Figure 44)** and quantified with a Nanodrop spectrophotometer. The two purified DNA fragments were then used for overlapping cloning into the linearized pOPINE Mahoney SC6b vector, following the protocol provided by the NEBuilder HiFi DNA Assembly kit.

The assembly mixture was transformed into NEB 5-alpha competent *E. coli* cells, plated on selective agar containing ampicillin, and incubated overnight at 37°C. A separate transformation using the linearized DNA plasmid served as a control. Three colonies were randomly selected from each transformation plate, transferred to LB medium containing ampicillin, and cultured overnight at 37°C with shaking. Plasmid DNA was extracted from these three candidates and submitted to Source BioScience for Sanger sequencing with the T7F primer which binds upstream of the PV P1 sequence. The resulting confirmed sequences were aligned and translated with the reference DNA sequence using DNA Dynamo (Blue Tractor Software), to confirm the presence of glycine or valine at positions 24, 28, and 29 in VP4 **(Figure 45).**

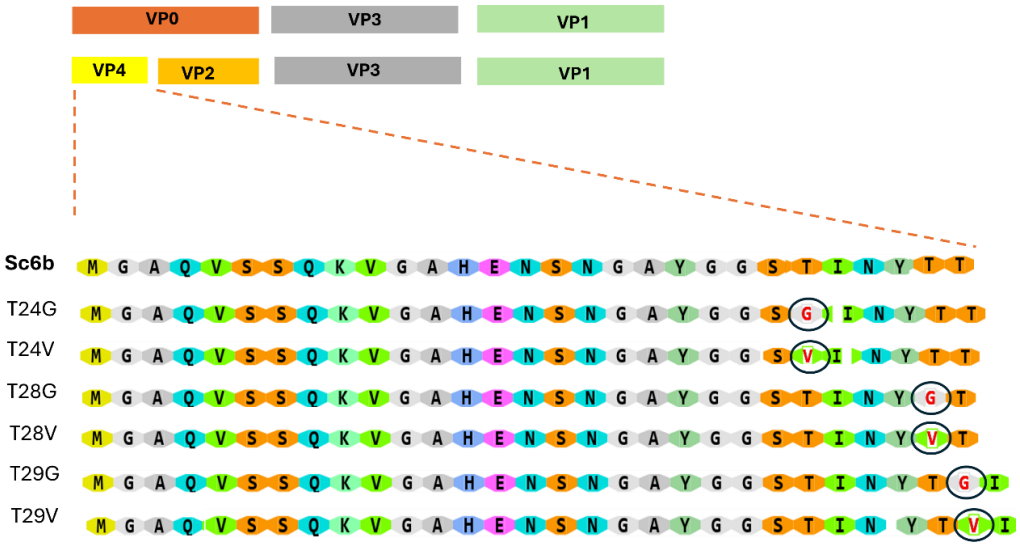

Figure 45. Alignment of the translated proteins showing the WT (SC6b) PV sequence and the site-specific mutations in the VP4. Produced using DNA Dynamo (Blue Tractor Software).

5.2.1 Expression of PV1 Site-Specific Mutants Recombinant Virus in Insect Cells

Plasmids encoding both wild type and mutant forms of Poliovirus 1 Mahoney SC6b with the site-specific mutants described were used to generate recombinant baculoviruses. The transfer vector and baculovirus DNA were co-transfected into *Sf9* insect cells using a standard transfection procedure as described in section 2.2.14.3 with recombination between the transfer vector sequences and the baculovirus genome allowing reconstruction of a circular infectious virus genome. This resulted in the production of recombinant baculoviruses carrying the Poliovirus 1 Mahoney SC6b VP0 mutations, under the control of the p10 promoter. Recombinant baculovirus stocks (Bac-PV1P1-x) for each mutation were generated after transfection and subsequent virus passage in *Sf9* cells.

Following the procedures outlined in section 2.2.14.4, small-scale cultures of Tnao38 cells infected with the recombinant baculoviruses were analyzed for protein expression via Western blot (WB). A six-well plate was seeded with $1x10^6$ Tnao38 cells per well, infected with 200 µl of recombinant baculovirus stock, and incubated for 4 days at 27°C. Cells from each well were harvested, pelleted by centrifugation, and prepared for WB analysis. Anti-Poliovirus 1 antibody (MAB8560, Sigma-Aldrich) was used to detect VP1 **(Figure 46)**, revealing a weak 34kDa band of varying intensity, consistent with the predicted molecular weight of VP1and confirming the successful expression of the mutant sequences for all mutations.

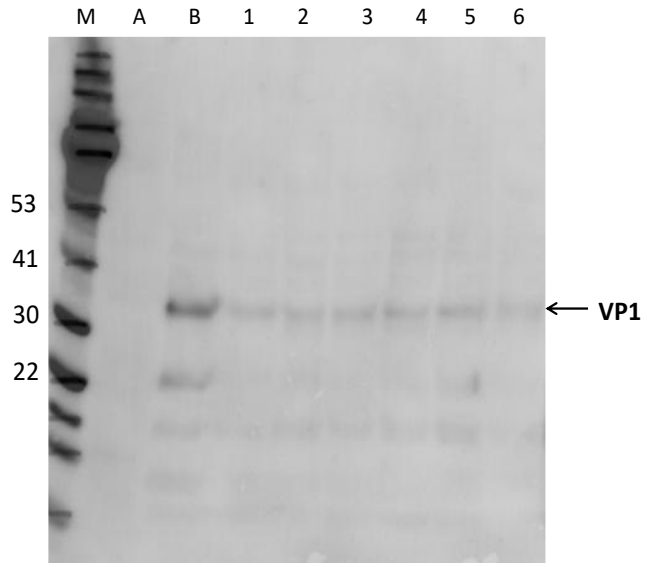

Figure 46. Detection of recombinant Poliovirus expression in Tnao38 insect cells using Western blot analysis with an anti-Poliovirus antibody. Lane A represents uninfected cells serving as a negative control, while Lane B contains wild-type Mahoney SC6b as a positive control. Lanes 1 to 6 display varying expression levels of the VP4 site-specific mutants, 24G, 24V, 28G, 28V, 29G and 29V respectivley. Molecular weight markers (M) on the left side of the gel represent protein sizes in kilodaltons (BLUeye Pre-Stained Protein Ladder, Geneflow S6-0024).

5.2.2 N/H Flow Cytometry for Site-Specific Mutants

The mutations described, it was argued, could alter the breathing of the PV particle and influence the relative level of H/N reactivity. To assess this N/H flow cytometry was done as described in section 2.2.18.2. Tnao38 cells were seeded in 6-well plates at a density of 1×10^6 cells per well and infected with 200 µL of viral stock, with one well serving as an uninfected control. After 4-days incubation at 27°C, the cells were harvested washed with PBS and repelleted. For intracellular staining, the eBioscience™ Intracellular Fixation and Permeabilization Buffer Set was used. Pellets were fixed overnight at 4°C, permeabilized, and blocked with PBS containing 3% BSA and 0.1% sodium azide. Cells were then stained with primary antibodies against poliovirus antigens N (PV1-234) and H (PV1-1588) at a 1:500 dilution, followed by a FITC-conjugated anti-mouse secondary antibody at a 1:1000 dilution. After washing, the cell pellets were resuspended in PBS and transferred to flow cytometry tubes for analysis of the FITC-A fluorescence using a C6 Plus Flow Cytometer. Data were acquired with the BD CSampler Plus software, revealing distinct fluorescence intensities corresponding to the H form of VLPs (red curve) at different levels, calculated as the % of cells above an arbitrary cut-off of 10^4 fluorescence units. Staining the cells for the N form (green curve) showed minimal binding overall although the green peaks were shifted marginally to the right in the panel for 28G. However, the H binding score was also highest for this mutant (29%) suggesting the marginal improvement in N binding is more probably a consequence of better expression overall than a true shift form H to N antigenicity (**Figure 47)**.

(A)

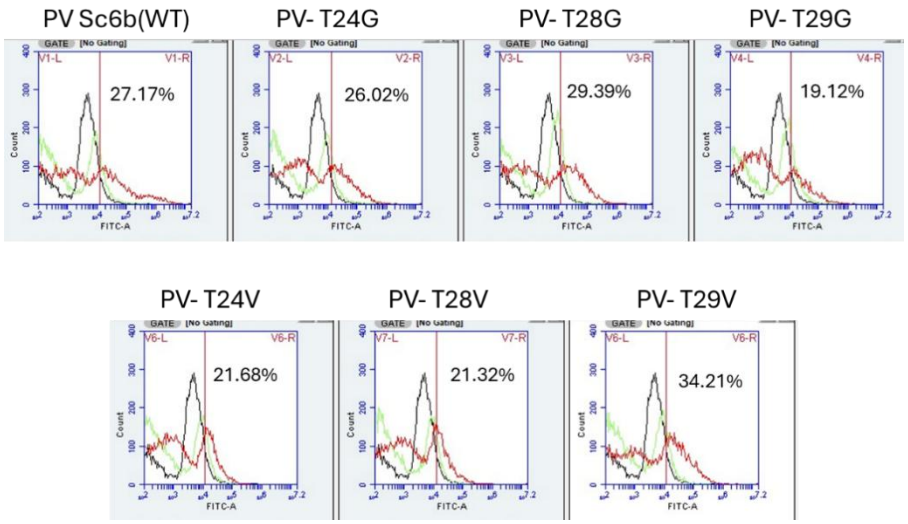

(B)

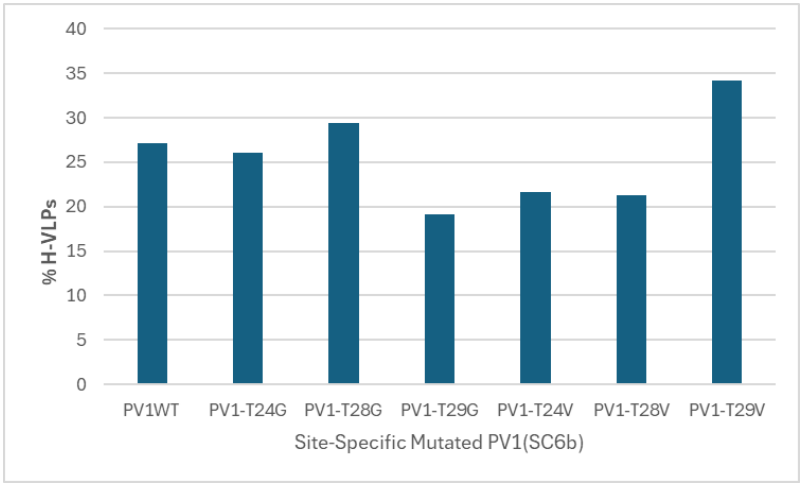

Figure 47. N/H flow cytometry results of Tnao38 cells infected with PV1 SC6b Mahony wild type and site-specific mutants. Cells were analysed for fluorescence intensity in the FITC-A channel. **A**) BDC Sampler Plus software indicates a variety of H VLPs (red line) comparison to the negative control of uninfected cells (black line) while for N VLPs (green line) insignificant change was noted. The vertical demarcations (V1-L, V1-R) indicate the conventional gate used to distinguish the FITC-A -negative (V1-L) from the FITC-A -positive (V1-R). Peaks that shift further to the right represent signals FITC-A, whereas peaks overlapping the control uninfected cells (black line) reflect the absence of signal. **B**) The percentage of H-VLP-positive cells within the V1-R (FITC-A-positive) gate was calculated, demonstrating varying levels of H-VLP expression among the samples.

However, despite the positive expression of each of the mutants described, there are difficulties with interpreting some of the data obtained. By Western blot the expression level of each mutant was reduced when compared to the WT, which itself was poorly expressed (see **Chapter 4**). By FACS, which measures antibody binding to non-denatured antigen the level of H antibody binding varied but, with the exception of 28G, was also reduced in each mutant when compared to the WT. At this low level of binding, it is doubtful that any N reactivity would be apparent, even if present.

5.3 Construction of PV1 Site-Specific Mutations in VP1-0 (C-Terminal Deletion)

PV1 site-specific mutations expression were enhanced by constructing the PV1 site-specific mutation PV VP1-0 (C-terminal 3C mutation) which was described in Chapter 4. To assess if improved expression levels would allow N-reactivity to be detected the same mutants described in the WT sequence above were recloned into the -0 variant sequence and expression and antibody reactivity was re-assessed. DNA fragments containing each of the mutations were produced by double digestion with two enzymes *Bst*EII (*Eco*91I) and *EcoRI,* producing a ~300bp fragment encoding the N-terminal region of P1 including the VP0 sequence changes. Then, 7000 bp vector and 300 bp mutant fragments for the 6 site mutations were purified using a gel extraction kit (ThermoFisher) after agarose gel electrophoresis **(Figure 48)** and quantified using a Nanodrop spectrophotometer. This linearized vector was used in DNA ligation reactions, reconstituting the transfer vector necessary for baculovirus formation but now with each VP0 mutation appended to the truncated (no 2A) PV P1 sequence.

The DNA ligation for site-specific mutations in the VP4 region in PV1-Mahoney SC6b (VP1-0 C-terminal deletion) as vector was done as described in section 2.2.6. The reaction mixture was transformed into competent *E. coli* cells and plated on selective agar containing ampicillin and incubated overnight. A separate transformation using the linearised DNA plasmid only was used as a control. Three colonies were randomly selected from each transformation plate, transferred to LB with ampicillin, and grown overnight at 37°C with shaking. Plasmid DNA was extracted from the three candidates and sent to Source BioScience for Sanger sequencing **(Figure 49)**. The T7F Primer was used to sequence the DNA, with reads of ~1000bps crossing the introduced mutations. The sequences were aligned and translated using DNA Dynamo (Blue Tractor Software to confirm correct mutations **(Figure 49)**.

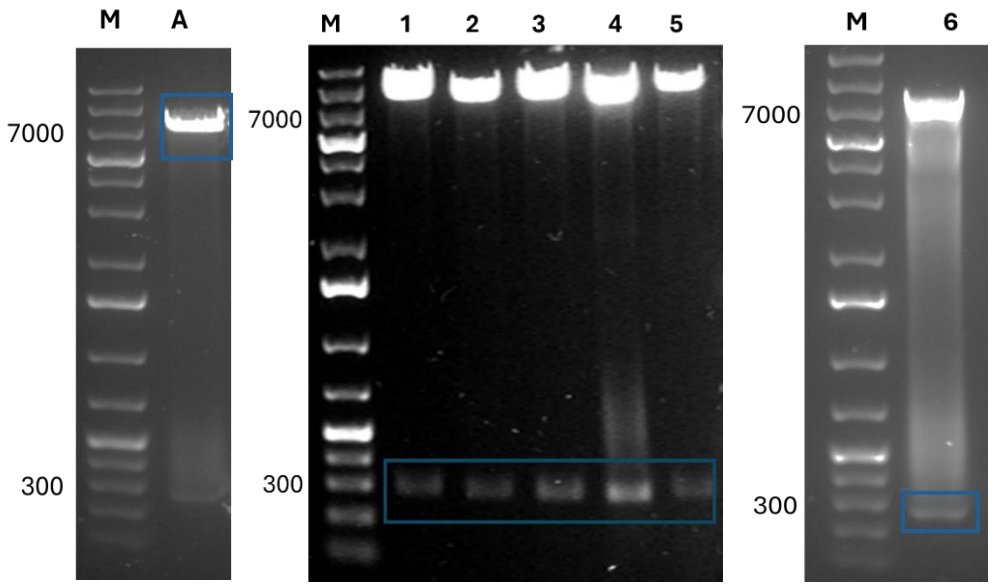

Figure 48. As a preparation step before the DNA ligation for site-specific mutations in the VP4 region in PV1-Mahoney SC6b (VP1-0 C-terminal deletion) as vector. Two DNA fragments of pOPINE PV1 Mahoney Sc6b vector after double digest of pDNA using two enzymes BstEII (Eco91I) and EcoRI. lane A VP1-0 the C-terminal mutation and 1 to 6 are PV1 site-specific mutations in VP4 pDNA showing correct size for linearized fragments 700bp for vector and 300bp for 6 site mutations. The DNA fragments that were used for ligation are marked on the gel. Lane M: GeneRuler 1 kb Plus DNA Ladder (Thermo Scientific™).

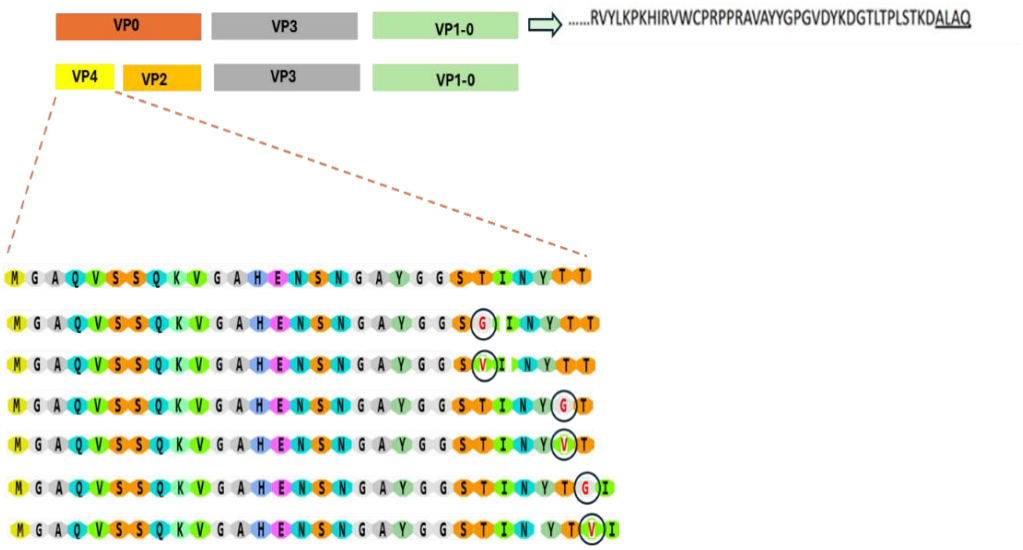

Figure 49. Alignment of translated proteins showing the wild-type (SC6b) PV sequence and site-specific mutations in VP4 of PV1-Mahoney SC6b (VP0 C-terminal deletion) used as the vector. The alignment was generated using DNA Dynamo (Blue Tractor Software).

5.3.1 Expression of Site-Specific Mutated PV1-Mahoney SC6b (VP1-0 C-Terminal Deletion) as a Recombinant Virus in Insect Cells

Recombinant baculoviruses (Bac-PV1P1) expressing site-specific VP4 mutations in the PV1 Mahoney SC6b (VP1-0 C-terminal deletion) were generated via recombination in *Sf9* insect cells using DNA plasmids and a baculovirus bacmid as before. High-titer viral stocks were obtained through consecutive passages. For expression analysis, Tnao38 cells were seeded in six-well plates at 1 × 10^6 cells per well and infected with 200 µL of each recombinant baculovirus. Following a 4-day incubation at 27°C, cells were harvested by centrifugation, and protein expression was evaluated by Western blotting as described in section 2.2.15.3.

VP1 was detected using the anti-Poliovirus 1 antibody MAB8560 from Sigma-Aldrich **(Figure 50)**. Visible bands were detected at 34kDa, which is the same calculated for VP1 MW. The different levels of expression protein were shown by bands that appeared with different densities at the same volume of samples. Lane2 (T28G) and lane 4 (T24V) showed the lowest level of expression. Lane3 (T29G) showed the highest level of expression. The baculovirus capsid protein p39 was detected by anti-p39 in all infections at the same level, therefore different levels of PV antigen expression are not due to different levels of baculovirus replication infection **(Figure 50)**. These results confirm successful expression of the correct sequences for all PV1 for the VP0 site-specific mutations in the PV1-Mahoney SC6b VP1-0 3C mutant.

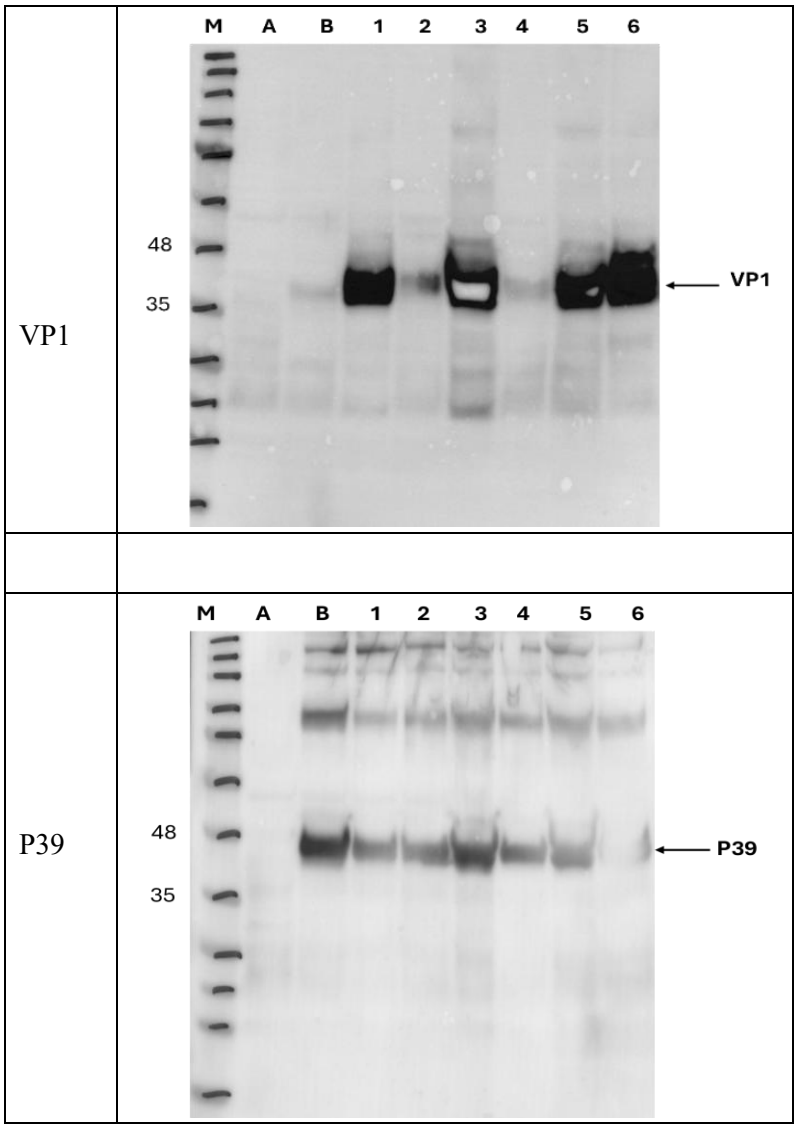

Figure 50. Using VP1 (MAB8566) antibody to detect recombinant PV expression in Tnao38 insect cells by Western blot analysis. Lane A is uninfected cells used as a negative control; Lane B is wild PV used as a positive control, 1-T24G 2-T28G, 3- T29G, 4-T24V, 5-T28V and 6-T29V Lanes showed a different level intensity of expression for Bac_ PV1-Mahoney SC6b (VP1-0 C-terminal deletion) with site-specific mutations. P39 was detected with anti-P39 and showed the same intensity for P39 production by Baculovirus. (M) makers on the left of the gel are shown molecular weight for protein in kilodaltons (BLUeye Pre-Stained Protein Ladder- Geneflow S6-0024).

5.3.2 N/H Flow Cytometry Analysis of PV1 Site-Specific Mutations in (VP1-0 C-Terminal Deletion)

Tnao38 cells in 6-well plates infected with PV1 SC6b Mahony wild type and site-specific mutants in VP1-0 vector were also used for N/H Flow cytometry as described in section 2.2.18.2. The cell pellets were resuspended in PBS and transferred to flow cytometry tubes for analysis of FITC fluorescence using the C6 Plus Flow Cytometer. The results **(Figure 51)**, analysed using BD CSampler Plus, revealed varying levels of the H form of VLPs (red line), whereas little to no change was observed for the N VLPs (green line) as compared to uninfected cells (black line).

(A)

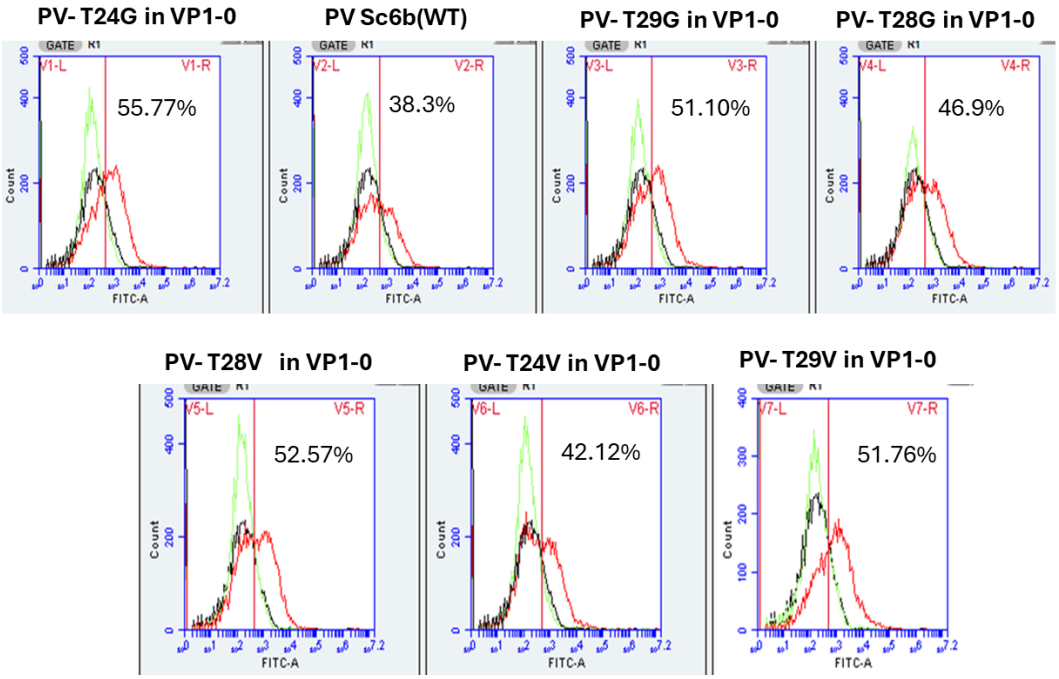

(B)

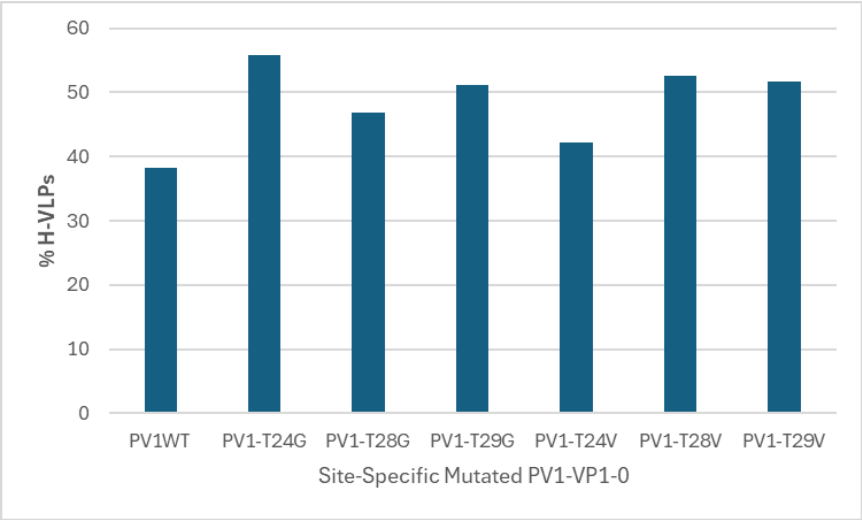

Figure 51. N/H flow cytometry results of Tnao38 cells infected with PV1 SC6b Mahony wild type and site-specific mutants in VP1-0 vector. Cells were analysed for fluorescence intensity in the FITC-A channel. **A)** BDC Sampler Plus software indicates a variety of H VLPs (red line) comparison to the negative control of uninfected cells (black line) while for N VLPs (green line), almost no change was observed. The vertical demarcations (V1-L,V1-R) indicate the conventional gate used to distinguish the FITC-A -negative (V1-L) from the FITC-A -positive (V1-R) populations. Peaks that shift further to the right represent signals FITC-A, whereas peaks overlapping the control uninfected cells (black line) reflect the absence of signal. **B)** The

percentage of H-VLP-positive cells within the V1-R (FITC-A-positive) gate was calculated, demonstrating varying levels of H-VLP expression among the samples.

5.4 Design and Construction of PV1 VP0 -GFP with Site-Specific Mutations

Green fluorescent protein (GFP) is widely utilized as a molecular tool for visualizing spatial and temporal dynamics of protein expression in *vivo*. GFP was used in this study to investigate whether variations at specific mutations within VP4 result in differential GFP fluorescence intensity and distribution, potentially reflecting changes in protein stability or ability to locate to different cellular organelles. To construct the PV1 VP0 -GFP mutations two DNA fragments were overlapped by seamless PCR and cloned into the pTriEx™-1.1 vector. The fragments comprised VP0 with each site-specific mutation in VP4 and a fragment encoding the "staygold" version of GFP (Hirano *et al.*, 2022). The VP0 DNA fragments were amplified via PCR, using the forward and reverse primers listed in **Table 8**, with the PV1-Mahoney SC6b sequence and six variants of site-specific mutations as templates to make seven different fragments of VP0. The GFP fragment was amplified using the primers detailed in **Table 8**, with pTriEx™-1.1 GFP serving as the template. The PCR was carried out under the following conditions: initial denaturation at 98°C for 30 seconds, followed by 35 cycles of denaturation at 98°C for 10 seconds, annealing at 63°C for 30 seconds, and extension at 72°C for 1 minute 30 seconds, concluding with a final extension at 72°C for 10 minutes. The amplified PCR products for the WT and six mutations (**Figure 52)** were confirmed by agarose gel electrophoresis, yielding the expected fragment sizes of 1000 bp for VP0 and 700 bp for GFP.

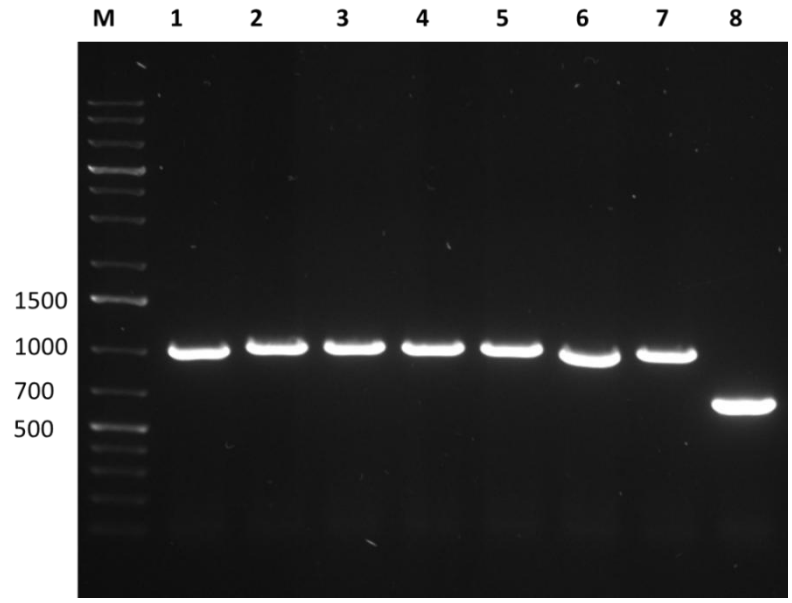

Figure 52. PCR amplification of two DNA fragments, 1000 bp for VP0 with site-specific mutations in VP4 (Lanes 1to7) and 700 bp for GFP (Lane 8) were performed from the PV1-Mahoney SC6b sequence to introduce seven distinct versions of VP0. M: GeneRuler 1 kb Plus DNA Ladder (Thermo Scientific™).

DNA of PV1 VP0-GFP containing site-specific mutations into the pTriEx™-1.1 vector was performed as described in section 2.2.5. The assembly mixture was transformed into NEB 5-alpha competent *E. coli* cells, plated on ampicillin-selective agar, and incubated overnight. A control transformation using only the linearized plasmid DNA was included. Three colonies were randomly selected from each plate, inoculated into LB broth containing ampicillin, and cultured overnight at 37 °C with shaking. Plasmid DNA was extracted from these colonies and submitted to Source BioScience for Sanger sequencing **(Figure 53)**. The T7F primer was used for sequencing, generating ~1000 bp reads spanning the introduced mutations. Sequence data were aligned and translated using DNA Dynamo (Blue Tractor Software) to confirm the presence of the intended mutations **(Figure 53)**.

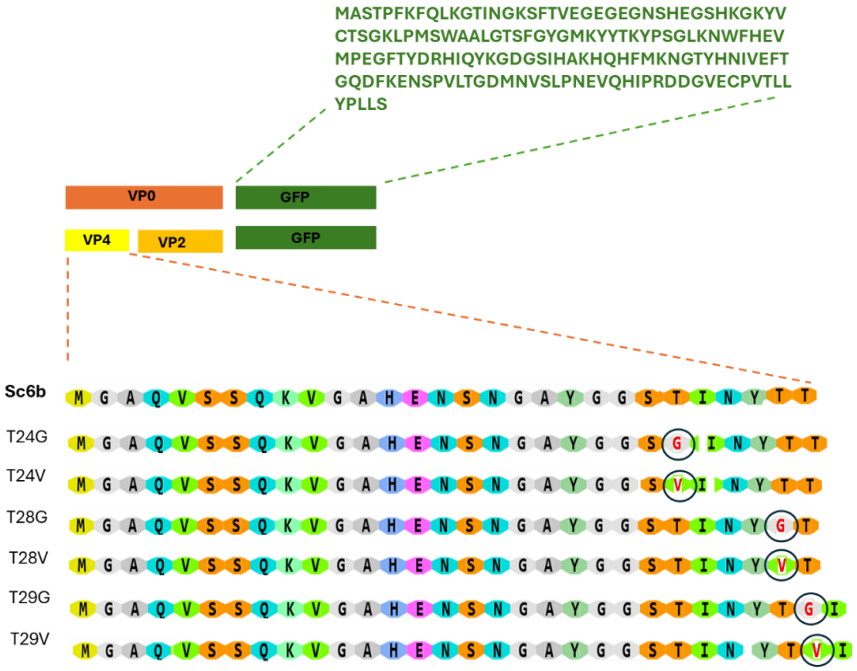

Figure 53. The site-specific mutations in the VP4 using DNA Dynamo (Blue Tractor Software) were aligned and constructed with GFP to visualize dynamics of gene expression in *vivo*.

5.4.1 The Expression of PV1 VP0 -GFP Mutants by Recombinant Baculovirus in Insect Cells

Plasmids encoding the pTriEx™-1.1 VP0-GFP construct of Poliovirus 1 Mahoney SC6b, including the VP4 site-specific mutations, were utilized to generate recombinant baculoviruses. The transfer vector and baculovirus bacmid were transfected into *Sf9* insect cells using a standard transfection, resulting in recombinant baculoviruses expressing the VP4-GFP mutations under the control of the p10 promoter. Recombinant baculoviruses specific to each mutation were obtained following transfection and subsequent viral passages, yielding high-titer stocks in *Sf9* cells.

Tnao38 cells small-scale cultures were infected with the recombinant baculoviruses and the protein expression tested via WB. An HRP-conjugated Anti-6X His tag antibody (ab1187) was employed to detect VP0-GFP **(Figure 54)**, which revealed a band of ~67kDa for all constructs, consistent with the predicted molecular weight of VP0 ~ 36kDa plus GFP ~ 26kDa and His tag ~6kDa, confirming successful expression of the correct sequences for all VP0-GFP mutants.

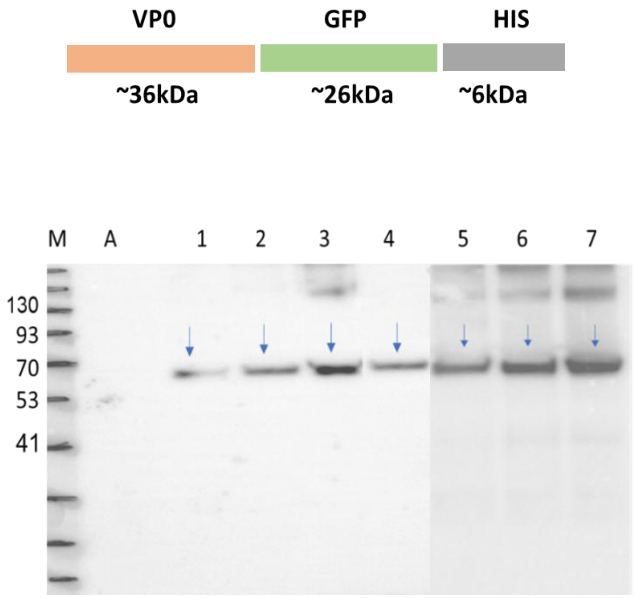

Figure 54. Western blot analysis with HRP-conjugated Anti-6X His tag antibody (ab1187). Lane A represents uninfected cells serving as a negative control, while Lane 1 contains wild-type Poliovirus of VP0-GFP. Lanes 2 to 7 contain pTriEx™-1.1 VP0-GFP with site-specific mutants in VP4 in order (2-T24G), (3-T28G), (4- T29G), (5- T24V), (6- T28V) and (7- T29V) Lanes. Molecular weight markers (M) on the left side of the membrane represent protein sizes in kilodaltons (BLUeye Pre-Stained Protein Ladder, Geneflow S6-0024).

5.4.2 Flow Cytometry for VP0-GFP Mutants

Flow cytometry (C6 Plus) was used to measure GFP intensity for each of the VP0-GFP mutations. Gene expression in the baculovirus system is dictated by the very late viral promoters used for expression and is the same for all constructs. However, protein stability could be altered by the mutations made, which would result in lower fluorescence levels when analysed on a whole cell basis.Small-scale cultures of Tnao38 cells infected with the VP0-GFP recombinant baculoviruses stock. A six-well plate was seeded with $1x10^6$ Tnao38 cells per well, infected with recombinant baculovirus stock, and incubated at 27°C for 4 days. Cells were then harvested by centrifugation. Pellets were prepared for flow cytometry by washing one time with 500ul PBS and spin down again. The pellets were resuspended in 500 ul PBS and transferred into Flow cytometry tube to measure the FITC channel.

The results show different levels of GFP were expressed among the tested constructs **(Figure 55)**. The mutant showed the highest GFP signal 29G-GFP and WT (sc6B)-VP0-GFP whereas the

29V-GFP mutant showed the lowest fluorescence although the error bars overlap for many of the constructs limiting the conclusions that can be drawn. What is clear is that fluorescence is abundant for all the constructs made but that there is some variation among them, possibly reflecting stability or trafficking changes.

(A)

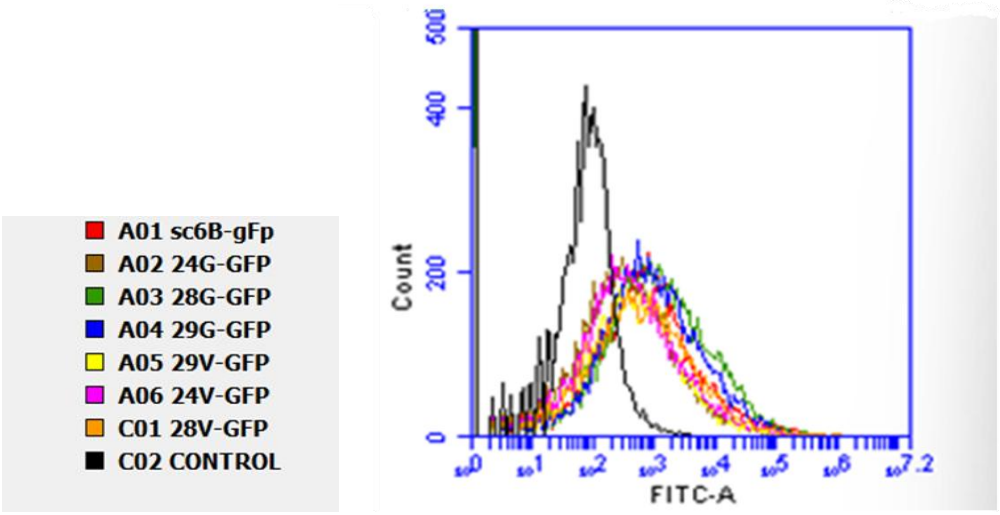

(B)

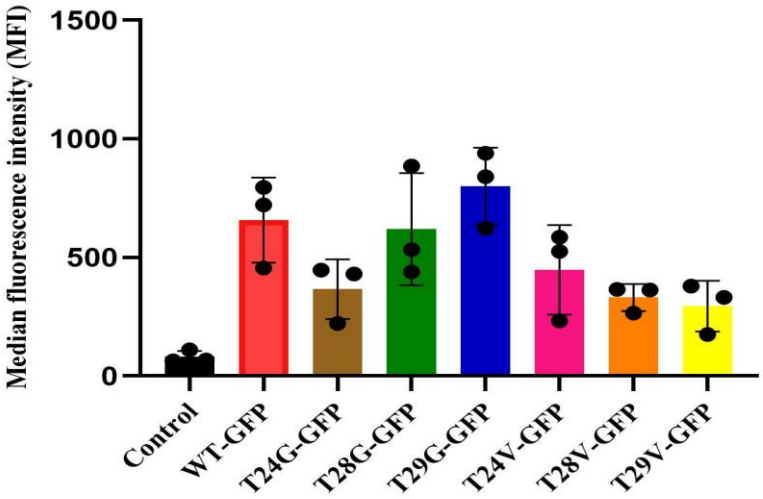

Figure 55. A) Flow cytometry analysis assessed the expression levels of GFP-cloned to VP0 in Tnao38 cells infected with WT -GFP(Sc6b-GFP) various VP0 site-mutants in VP4. Cells were analysed for fluorescence intensity in the FITC-A channel, with the black curve representing the non-infected cells control (GFP-negative). **B)** The graph illustrates the median fluorescence intensity (MFI) relative values obtained from biological triplicates for each mutant, as detected by flow cytometry in the FITC-A channel.

5.4.3 Fluorescence Microscopy for VP0-GFP Mutants

Each recombinant virus was also used for tracking VP0 expression in living Tnao38 cells using fluorescence microscopy. Monolayers of fixed Tnao38 cells on the glass-bottom dishes were infected with the VP0-GFP mutants and the culture was incubated at 27°C for up to three days. The cells were imaged directly using an EVOS fluorescent microscope and pictures were captured at 40x and 60× magnification.

Infected Tnao38 cells expressing the WT VP0-GFP **(Figure 55)** showed distinct green fluorescence predominantly localized to the cytoplasm of the infected cells. As baculovirus replication is nuclear, the nucleus of infected cells expands, pushing the cytoplasm to the poles of the cell. Typical "dumbbells" of green colour are observed in many of the cells, although some display other patterns consistent with cell distortion as a result of the infection **(Figure 56)**. Little if any GFP signal was found in the nucleus despite the size of the fusion protein being close to the nuclear pore limit of ~60kDa (Kitamura *et al.*, 2015).

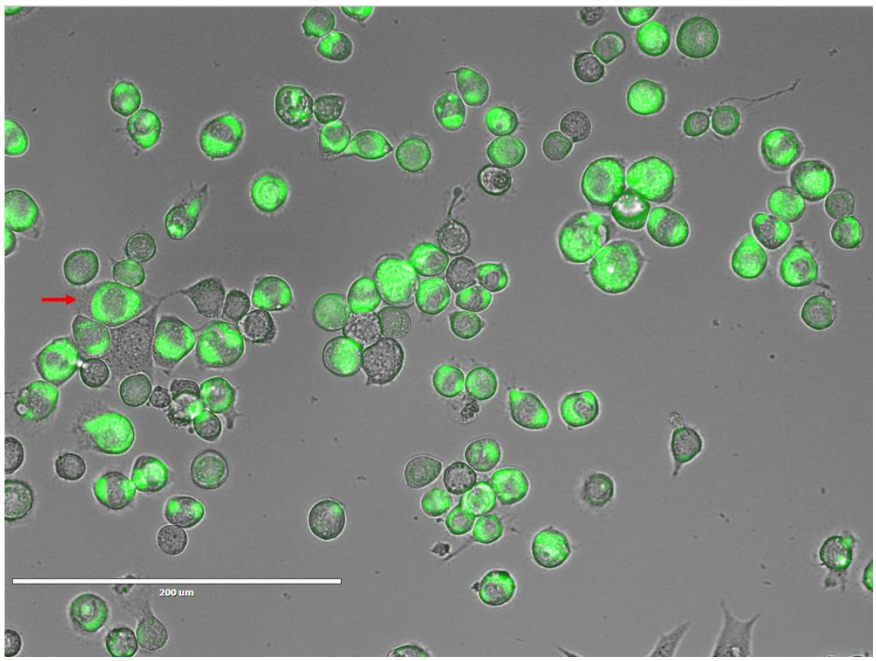

Figure 56. Fluorescence shown by the WT VP0 following expression in Tnao38 cells. The picture is an overlay of the GFP channel and the visible channel to show the pattern of fluorescence in relation to cell morphology. A typical "dumbbell" appearance is arrowed.

When the VP4 mutants were similarly analysed, considerable variation in the cellular distribution of signal was apparent **(Figure 57)**. Cells expressing 24G, 28V, 29G and 29V broadly

conformed to the WT signal although it was less uniform with some cells showing punctate patches of fluorescence and a granular appearance. Cells expressing 24V were notably different with very few cells showing the typical pattern. Instead, the pattern was amorphous with some cells (arrowed) showing a distinct granular appearance possibly related to protein binding the rough ER. To a lesser extent this was also true of 28G although the contrast with the WT pattern was less pronounced. Some cells expressing 28G also appeared to have signal in the nucleus although no Z stacks are available on the microscope used to verify this. Some of the variability apparent in the pictures taken could result from non-synchronous expression following infection. Sufficient virus is added to ensure ~100% of cells are infected (MOI ≥ 3) among the mutants analysed but it remains possible that some cells were infected as soon as the virus inoculum was added while others became infected sometime later. However, the pictures shown are typical of those taken for each mutant on repeated occasions and demonstrate significant alteration in protein distribution in the cell as a result of the mutations made.

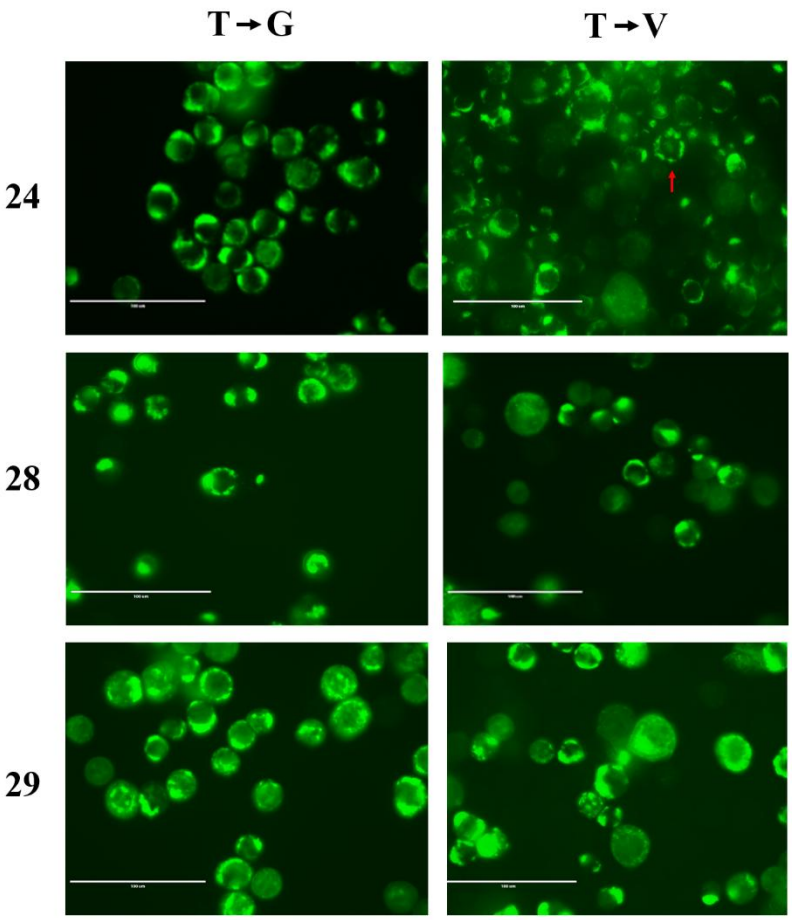

Figure 57. Fluorescence associated with individual VP4 mutations expressed as VP4-GFP fusion proteins in insect cells. The distinct presentation of some cells expressing the T24V mutation is indicated by the arrow. Scale bar is 100 μm.

An attempt was made to quantify the differences between key samples by using the cell profile function of ImageJ (Schneider *et al.*, 2012). A linear transect was drawn across the cells arrowed in **Figure 56 and 57** and the profile function invoked, measuring integrated fluorescence as a function of distance across the transect. The "dumbbell" pattern of the WT is very clear with substantial peaks either side of the non-fluorescent nucleus **(Figure 58, upper panel).** By contrast the signal from the 24V mutant was flatter and more granular, notably across the middle of the cell (**Figure 57)**.

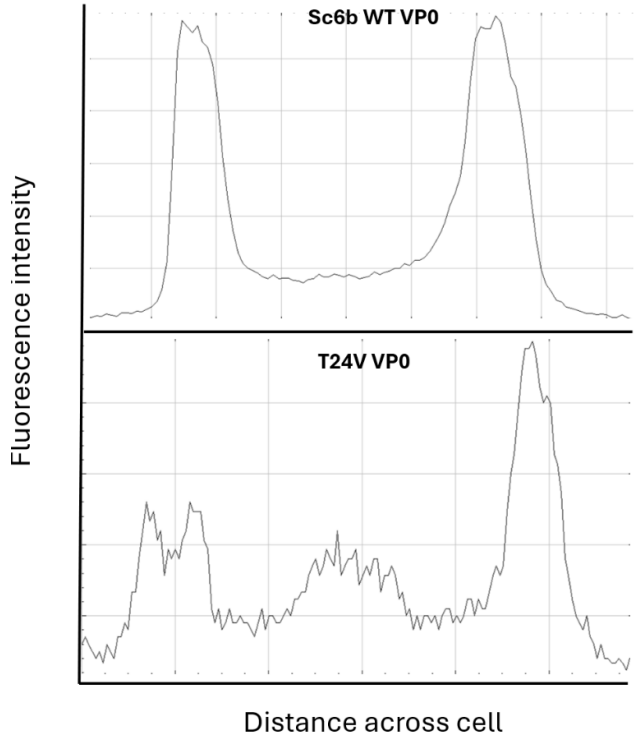

Figure 58. Image J fluorescence profile of the cells arrowed in **Figures 56 and 57**. The difference in pattern is pronounced across the middle of the cell.

Table 10. Analysis of VP4 mutants for liquid–liquid phase separation (LLPS) potential predicted via the FuzDrop server (Hardenberg *et al.*, 2020; Hatos *et al.*, 2022; Vendruscolo & Fuxreiter, 2022b).

PV1

VP4 Mutant	Mutant Sequence (AA change underlined)	pLLPS Score	Aggregation Hotspots
WT(SC6b)	MGAQVSSQKVGAHENSNGAYGGSTINYTTINYYRD SASNAASKQDFSQDPSKFTEPIKDVLIKTAPMLNS	0.910	None
T24G	MGAQVSSQKVGAHENSNGAYGGSGINYTTINYYRD SASNAASKQDFSQDPSKFTEPIKDVLIKTAPMLNS	0.916	None
T28G	MGAQVSSQKVGAHENSNGAYGGSTINYGTINYYRD SASNAASKQDFSQDPSKFTEPIKDVLIKTAPMLNS	0.942	2-10 23-29
T29G	MGAQVSSQKVGAHENSNGAYGGSTINYTGINYYRD SASNAASKQDFSQDPSKFTEPIKDVLIKTAPMLNS	0.930	4-13
T24V	MGAQVSSQKVGAHENSNGAYGGSVINYTTINYYRD SASNAASKQDFSQDPSKFTEPIKDVLIKTAPMLNS	0.955	38-49
T28V	MGAQVSSQKVGAHENSNGAYGGSTINYVTINYYRD SASNAASKQDFSQDPSKFTEPIKDVLIKTAPMLNS	0.864	None
T29V	MGAQVSSQKVGAHENSNGAYGGSTINYTVINYYRD SASNAASKQDFSQDPSKFTEPIKDVLIKTAPMLNS	0.844	None

5.5 Discussion

This chapter investigated the threonine residues at position 24, 28, and 29 in the VP4 region of PV1 Mahoney SC6b strain to assess their effect on protein expression and potentially on the antigenic form of the virus-like particle produced. Residue 28 was originally investigated as the poliovirus structure had shown a bond between its hydroxyl side chain and the myristate group present at the N-terminus (Moscufo & Chow, 1992). The data showed that substitution of Thr28 with glycine or lysine was lethal whereas substitution with serine or valine was tolerated, albeit with defects in particle assembly, infectivity and thermal inactivation. Later, this conclusion was modified to a specific role in virus entry following the generation of the 135S particle (Moscufo *et al.*, 1993). Further analysis of mutants in which Thr28 was substituted with glycine or valine led to the finding that the non-viable T 4028G particles did not bind to host cell membranes, unlike the wild-type and the viable mutants. In addition, membrane channel activity was altered in a number of mutant viruses, as was the cytoplasmic delivery of the viral genome (Danthi *et al.*, 2003). Based on this literature I hypothesized that the apparent "locking" of these assembled particles might affect the flexibility of the capsid and restrict its tendency to form in the H antigenic conformation. I was also interested to study these mutants, previously studied only by reverse genetics, in the context of VLP expression. The construction of the mutants was done in two poliovirus P1 backgrounds, the WT SC6b and the C-terminally modified -0 mutant, the latter of which expresses at a much higher level as described in Chapter 4. A novel addition was to express each mutant as VP0-GFP fusion proteins for an examination of cellular distribution.

The WB analysis of the mutants in all backgrounds confirmed expression but, in agreement with the original data the level of VP1 (the band probed) was poor for T28G **(Figure 46, 50)**, possibly confirming a role in conformational stability. It is notable that the original data was done with permissive cells as the substrate, so CD155 engagement would have occurred but for the data here no CD155 is present, implying an effect directly on stability. In the VLP system T24V also displayed instability (low expression) consistent with lethality described in the original studies (Danthi *et al.*, 2003). Disappointingly, examination of the H and N antigenic forms of VLPs through flow cytometry demonstrated marked alterations in H-form expression but minimal to no change in the N form. It is possible the lack of N-antigenicity is the result of the fixation step during Fluorescence-Activated Cell Scanning (FACS) preparation, although this is no different to the fixation done in the preparation of IPV, which is then subject to H/N ELISA (Kumar *et al.*, 2022). More work would be needed to establish a better N reactivity assay before the mutants are analyzed again.

An interesting observation is that the effects of mutations in the context of VLP expression is paralleled to a degree when they are expressed solely within VP0. Fluorescence profiles for 24V and 28G were noticeable different from the remaining mutants, with a tendency to aggregate in expressing cells. As noted in the **Introduction**, VP4 fulfills the criteria for a protein that undergoes liquid-liquid phase separation (LLPS). To assess the role of these single residue substitutions on this property, each mutant sequence was submitted to the Fuzzdrop server and the LLPS score, and hotspots of aggregation were tabulated **(Table 10)**. Remarkably, 24V and 28G give the highest LLPS scores and have extensive hotspots for aggregation whereas all other mutants score lower and in some cases have no propensity at all for aggregation. This provides the first data for PV that correlates predicted protein behavior with biological outcomes and could be a useful way of designing further mutants that might address the H/N question, specifically in regard to VP4 function.

The findings of this chapter contribute to the literature indicating that minor alterations in capsid proteins of PV can significantly affect VLP assembly, production, and antigenic characteristics and establishes a foundation for further studies focused on improving poliovirus VLPs for enhanced antigen stability, and maybe immunogenicity.

Chapter 6 General Discussion

The work in this thesis investigated novel sequence changes to enhance the production, solubility, and antigenicity of poliovirus virus-like particles (VLPs). Expression in both *E. coli* and insect cell systems were used, with the first making progress but failing to demonstrate VLP assembly but the second showing that mutation of the P1 sequence was not only tolerated but was beneficial in some cases. The overall objective was to create an efficient and affordable platform to produce PV VLPs as next-generation vaccines, an objective which, at the start of these studies had still not been demonstrated in the literature. However, across three experimental chapters, several recurring challenges emerged that limited this broad effort to develop VLP-based vaccines for poliovirus. Despite picornavirus-like particles being identified since the early 1990s, it is only recently that VLP synthesis has become efficient, for PV and for other *Picornaviridae* family members. This has paralleled the drift in the use of expression systems from eukaryotic expression, e.g. through the use of recombinant vaccinia viruses, to yeast and prokaryotic expression (Ren *et al.*, 2024). A finding that stimulated the early sections of these was the claim that virus-like particles of Foot-and-Mouth Disease Virus, a member of the *picornaviridae*, could be synthesised in *E. coli* system following use of SUMO fusion proteins. The Small Ubiquitin-like Modifier (SUMO) fusion system has been employed to enhance the solubility of viral proteins (Lee *et al.*, 2009) and following its removal FMDV VLPs were shown to assemble after expression in *E. coli* and that such VLPs elicited a strong protective immunological response following immunisation (Guo *et al.*, 2013). More recently the assembly FMDV VLP in vitro was investigated after no SUMO tagged VP1, VP2 and VP3 were expressed in *E.coli* and extracted from inclusion bodies (Wang *et al.*, 2023b).

In the work described here, PV VP0, VP3, and VP1 were produced in *E. coli* as SUMO fusion proteins and an autoinduction system, which was found to be more efficient than IPTG based induction. The proteins could be purified but a consistent barrier to PV capsid protein production was their intrinsic tendency to aggregate into inclusion bodies (Ponte-Sucre *et al.*, 2021). Although solubilisation was achieved the amount of protein in solution was low and became even lower with each subsequent biochemical step. Viral capsid proteins are known to be difficult to express in soluble form in bacteria, due to their complex folding requirements and propensity for aggregation and although SUMO fusion improved the outcome, as it has in other contexts (Malakhov *et al.*, 2004; Lee *et al.*, 2009), its effectiveness was limited for PV proteins. Despite improved expression in BL21-AI cells under varied induction conditions, VP0 and VP1 remained largely insoluble, and SUMO cleavage was inefficient under denaturing conditions (Marblestone *et al.*, 2006a). A related problem was the level of contamination with nucleic acid which made the extracts viscous and difficult to resuspend. This was particularly true of VP0, and it is

interesting to note that recent structural improvements have recorded that" VP4 dynamically interacts with RNA" following capsid expansion (Karunatilaka *et al.*, 2021b). This suggests that VP0 could be the prime effector of RNA packaging and that, subject to methods to improve solubility, SUMO-VP0 could be a suitable model for further experimental work in this area. In all. the findings in this thesis highlight the challenges that remain for the production of the PV capsid proteins in *E. coli* systems and the need for more work to generate the high levels of soluble PV proteins required for onward VLP assembly.

In contrast, the baculovirus system provided a more favourable platform for expressing modified P1 sequences. Baculovirus expression vectors are widely used for picornavirus VLP production, but improvements are often limited to promoter strength and codon optimization (Fox *et al.*, 2017a). In this study, the findings presented novel mutations not previously reported in any VLP system. The first modifications targeted the N-myristoylation site of VP4 and led to measurable improvements in P1 expression without disrupting protein processing or VLP assembly. Although earlier work suggested that myristoylation was required for PV assembly (Ansardi *et al.*, 1992a), that observation has not held in several studies since. Founded on the idea that the insect cell N-myristoyltransferase (NMT) may not efficiently recognize mammalian derived substrate sequences, several alternate Myr substrates were assessed.Structural predictions indicated that these modifications did not perturb overall folding, reinforcing the feasibility of sequence engineering at the N-terminus of VP4 for enhanced expression(Ramljak *et al.*, 2018a). Importantly, the data showed that these modifications did not compromise VLP assembly, supporting their potential for vaccine applications.

The last chapter focused single-residue substitutions in VP4 and their consequences for VLP assembly and antigenicity. Mutations at threonine at position 24 and 28 produced profound effects on expression, stability, and antigenic profile, in line with previous studies implicating these residues in either capsid flexibility, genome release, or membrane interactions (Danthi *et al.*, 2003; Moscufo *et al.*, 1993; Moscufo & Chow, 1992). This thesis work is the first to my knowledge to return to mutations studied solely via reverse genetics, where functional virus particles are the final readout, to assess their role only in VLP assembly. The findings highlighted the critical role of VP4 in maintaining capsid stability and recapitulated some of the phenotypes observed in infectious virus, including aggregation and altered antigenicity, thereby validating VLPs as a useful surrogate model for studying such mutations. Computational analyses revealed that destabilizing substitutions (T24V, T28G) correlated with elevated LLPS scores, indicating a mechanistic link between amino acid sequence, phase separation propensity, and particle stability. This represents the first application of LLPS prediction tools to PV capsid proteins and provides a conceptual framework for rationally predicting aggregation-prone variants. While antigenicity

assays provided valuable insights, the lack of a robust N-antigen capture antibody limited definitive conclusions about the preservation of protective conformations. This remains a critical gap, as the generation of N-antigenic VLPs is essential for PV vaccine development.

Taken together, the results across chapters underscore both the promise and limitations of recombinant systems for poliovirus VLP production. *E. coli* expression provides cost efficiency and scalability but suffers from insolubility and refolding challenges, whereas baculovirus systems yield higher expression and more consistent assembly, albeit with complexities related to post-translational modifications. During this work, the field was also progressed by others with the most recent findings suggesting that yeast expression, an intermediate between bacterial expression and complex eukaryotic cells appearing to provide the most efficient PV VLP production to date (Sherry *et al.*, 2020; Hong *et al.*, 2024). Subject to successful scale-up these systems do appear to be capable of making vaccine qulaity material for clinical use. Beyond the immediate findings, several broader implications arise. First, the demonstration that VP4 modifications influence LLPS provides a new conceptual framework for understanding capsid protein behaviour during assembly, an area of growing interest in virology. Second, the combined use of predictive modeling (AlphaFold, LLPS algorithms) and experimental validation highlights the value of integrating computational and empirical approaches to guide rational design of capsid proteins. Finally, and notwithstanding the recent advances noted above, the research reinforces the central challenge in PV VLP development: achieving high yield, soluble expression of properly folded and antigenically correct particles, a goal that will likely require iterative cycles of sequence optimization, expression testing, and antigenicity validation.

In *E. coli*, potential directions may should prioritize strategies that minimize inclusion body formation such as codon harmonization, chaperone co-expression, or cell-free protein synthesis (Mühlmann *et al.*, 2017; Sergeev *et al.*, 2024). Expressing PV VLPs in insect cells offers a suitable environment for expressing myristoylated and properly folded capsid proteins but challenges remain in achieving consistent solubility and neutralizing conformations. Future studies should assess the behaviour of these mutants in poliovirus-infected mammalian cells, once the required materials become available, to clarify their physiological relevance. Additional efforts should refine these approaches and evaluate structural stability, antigenicity, and immunogenicity in preclinical models to advance the development of PV VLPs as vaccine candidates.

References

Adeyemi, O. O., Nicol, C., Stonehouse, N. J., & Rowlands, D. J. (2017). Increasing Type 1 Poliovirus Capsid Stability by Thermal Selection. https://doi.org/10.1128/JVI.01586-16

Aguado-Garcia, D., Olvera, A., Brander, C., Sanchez-Merino, V., & Yuste, E. (2022). Evaluation of the Thermal Stability of a Vaccine Prototype Based on Virus-like Particle Formulated HIV-1 Envelope. Vaccines, 10(4). https://doi.org/10.3390/vaccines10040484

Alibolandi, M., & Mirzahoseini, H. (2011). Chemical Assistance in Refolding of Bacterial Inclusion Bodies. Biochemistry Research International, 2011, 631607. https://doi.org/10.1155/2011/631607

Ansardi, D. C., Porter, D. C., & Morrow, C. D. (1991). Coinfection with recombinant vaccinia viruses expressing poliovirus P1 and P3 proteins results in polyprotein processing and formation of empty capsid structures. Journal of Virology, 65(4), 2088–2092. https://doi.org/10.1128/JVI.65.4.2088-2092.1991

Avanzino, B. C., Jue, H., Miller, C. M., Cheung, E., Fuchs, G., & Fraser, C. S. (2018). Molecular mechanism of poliovirus Sabin vaccine strain attenuation. Journal of Biological Chemistry, 293(40), 15471–15482. https://doi.org/10.1074/JBC.RA118.004913

Azevedo, F., Pereira, H., & Johansson, B. (2017). Colony PCR. Methods in Molecular Biology (Clifton, N.J.), 1620, 129–139. https://doi.org/10.1007/978-1-4939-7060-5_8

Bahar, M. W., Porta, C., Fox, H., Macadam, A. J., Fry, E. E., & Stuart, D. I. (2021). Mammalian expression of virus-like particles as a proof of principle for next generation polio vaccines. Npj Vaccines, 6(1). https://doi.org/10.1038/S41541-020-00267-3,

Baicus, A. (2012). History of polio vaccination. World J Virol, 1(4), 108–114. https://doi.org/10.5501/wjv.v1.i4.108

Baj, A., Colombo, M., Headley, J. L., McFarlane, J. R., Liethof, M. ann, & Toniolo, A. (2015). Post-poliomyelitis syndrome as a possible viral disease. International Journal of Infectious Diseases, 35, e107–e116. https://doi.org/10.1016/j.ijid.2015.04.018

Balke, I., & Zeltins, A. (2019). Use of plant viruses and virus-like particles for the creation of novel vaccines. Advanced Drug Delivery Reviews, 145, 119–129. https://doi.org/10.1016/j.addr.2018.08.007

Basavappa, R., Filman, D. J., Syed, R., Flore, O., Icenogle, J. P., & Hogle, J. M. (1994). Role and mechanism of the maturation cleavage of VP0 in poliovirus assembly: Structure of the empty capsid assembly intermediate at 2.9 Å resolution. Protein Science, 3(10), 1651–1669. https://doi.org/10.1002/PRO.5560031005

Basavappa, R., Gómez-Yafal, A., & Hogle, J. M. (1998). The poliovirus empty capsid specifically recognizes the poliovirus receptor and undergoes some, but not all, of the transitions associated with cell entry. Journal of virology, 72(9), 7551–7556. https://doi.org/10.1128/JVI.72.9.7551-7556.1998

Belnap, D. M., McDermott, B. M., Filman, D. J., Cheng, N., Trus, B. L., Zuccola, H. J., Racaniello, V. R., Hogle, J. M., & Steven, A. C. (2000). Three-dimensional structure of poliovirus receptor bound to poliovirus. Proceedings of the National Academy of Sciences of the United States of America, 97(1), 73–78. https://doi.org/10.1073/PNAS.97.1.73

Berrow, N. S., Alderton, D., Sainsbury, S., Nettleship, J., Assenberg, R., Rahman, N., Stuart, D. I., & Owens, R. J. (2007). A versatile ligation-independent cloning method suitable for high-throughput expression screening applications. Nucleic Acids Research, 35(6), 45. https://doi.org/10.1093/nar/gkm047

Bhatwa, A., Wang, W., Hassan, Y. I., Abraham, N., Li, X. Z., & Zhou, T. (2021). Challenges Associated With the Formation of Recombinant Protein Inclusion Bodies in Escherichia coli and Strategies to Address Them for Industrial Applications. Frontiers in Bioengineering and Biotechnology, 9, 630551. https://doi.org/10.3389/fbioe.2021.630551

Bissett, S. L., & Roy, P. (2024). Multi-Gene Recombinant Baculovirus Expression Systems: From Inception to Contemporary Applications. Viruses 2024, Vol. 16, Page 492, 16(4), 492. https://doi.org/10.3390/V16040492

Blake, I. M., Pons-Salort, M., Molodecky, N. A., Diop, O. M., Chenoweth, P., Bandyopadhyay, A. S., Zaffran, M., Sutter, R. W., & Grassly, N. C. (2018). Type 2 Poliovirus Detection after Global Withdrawal of Trivalent Oral Vaccine. New England Journal of Medicine, 379(9), 834–845. https://doi.org/10.1056/NEJMOA1716677,

Blondel, B., Colbère-Garapin, F., Couderc, T., Wirotius, A., & Guivel-Benhassine, F. (2005). Poliovirus, Pathogenesis of Poliomyelitis, and Apoptosis. Current Topics in Microbiology and Immunology, 289, 25–56. https://doi.org/10.1007/3-540-27320-4_2

Blondel, B., Duncan, G., Couderc, T., Delpeyroux, F., Pavio, N., & Colbère-Garapin, F. (1998). Molecular aspects of poliovirus biology with a special focus on the interactions with nerve cells. Journal of NeuroVirology, 4(1), 1–26. https://doi.org/10.3109/13550289809113478,

Brachelente, S., Galli, A., & Cervelli, T. (2023). Yeast and Virus-like Particles: A Perfect or Imperfect Couple? Applied Microbiology 2023, Vol. 3, Pages 805-825, 3(3), 805–825. https://doi.org/10.3390/APPLMICROBIOL3030056

Brandenburg, B., Lee, L. Y., Lakadamyali, M., Rust, M. J., & Zhuang, X. (2007a). Imaging poliovirus entry in live cells. PLoS Biol, 5(7), 183. https://doi.org/10.1371/journal.pbio.0050183

Bravo, L. C., Carlos, J. C., Gatchalian, S. R., Montellano, M. E. B., Tabora, C. F. C. B., Thierry-Carstensen, B., Tingskov, P. N., Sørensen, C., Wachmann, H., Bandyopadhyay, A. S., Nielsen, P. I., & Kusk, M. V. (2020). Immunogenicity and safety of an adjuvanted inactivated polio vaccine, IPV-Al, compared to standard IPV: A phase 3 observer-blinded, randomised, controlled trial in infants vaccinated at 6, 10, 14 weeks and 9 months of age. Vaccine, 38(3), 530–538. https://doi.org/10.1016/j.vaccine.2019.10.064

Breindl, M. (1971). The Structure of Heated Poliovirus Particles. In J. gen. Virol (Vol. 97).

Brosius, J., Erfle, M., & Storella, J. (1985). Spacing of the -10 and -35 regions in the tac promoter. Effect on its in vivo activity. Journal of Biological Chemistry, 260(6), 3539–3541. https://doi.org/10.1016/s0021-9258(19)83655-4

Burrill, C. P., Westesson, O., Schulte, M. B., Strings, V. R., Segal, M., & Andino, R. (2013a). Global RNA Structure Analysis of Poliovirus Identifies a Conserved RNA Structure Involved in Viral Replication and Infectivity. Journal of Virology, 87(21), 11670–11683. https://doi.org/10.1128/JVI.01560-13,

Butt, T. R., Edavettal, S. C., Hall, J. P., & Mattern, M. R. (2005). SUMO fusion technology for difficult-to-express proteins. Protein Expression and Purification, 43(1), 1. https://doi.org/10.1016/J.PEP.2005.03.016

Buyel, J. F. (2024). Towards a seamless product and process development workflow for recombinant proteins produced by plant molecular farming. Biotechnology Advances, 75. https://doi.org/10.1016/j.biotechadv.2024.108403

Canto, T. (2016). Transient expression systems in plants: Potentialities and constraints. Advances in Experimental Medicine and Biology, 896, 287–301. https://doi.org/10.1007/978-3-319-27216-0_18,

CE, S., PE, T., MJ, T., PT, T., GN, V., PV, N., JY, W., & S, K. (1987). Yeast-recombinant hepatitis B vaccine. Efficacy with hepatitis B immune globulin in prevention of perinatal hepatitis B virus transmission. JAMA, 257(19), 2612–2616. https://doi.org/10.1001/JAMA.257.19.2612

Cervera, L., Gutiérrez-Granados, S., Martínez, M., Blanco, J., Gòdia, F., & Segura, M. M. (2013). Generation of HIV-1 Gag VLPs by transient transfection of HEK 293 suspension cell cultures using an optimized animal-derived component free medium. Journal of Biotechnology, 166(4), 152–165. https://doi.org/10.1016/J.JBIOTEC.2013.05.001

Chambers, A. C., Aksular, M., Graves, L. P., Irons, S. L., Possee, R. D., & King, L. A. (2018a). Overview of the Baculovirus Expression System. In Current Protocols in Protein Science (Vol. 91, Issue 1, pp. 5.4.1-5.4.6). Blackwell Publishing Inc. https://doi.org/10.1002/cpps.47

Chambers, A. C., Aksular, M., Graves, L. P., Irons, S. L., Possee, R. D., & King, L. A. (2018b). Overview of the Baculovirus Expression System. In Current Protocols in Protein Science (Vol. 91, Issue 1, pp. 5.4.1-5.4.6). Blackwell Publishing Inc. https://doi.org/10.1002/cpps.47

Chow, M., Newman, J. F. E., Filman, D., Hogle, J. M., Rowlands, D. J., & Brown, F. (1987a). Myristylation of picornavirus capsid protein VP4 and its structural significance. Nature, 327(6122), 482–486. https://doi.org/10.1038/327482a0

Chung, Y. H., Church, D., Koellhoffer, E. C., Osota, E., Shukla, S., Rybicki, E. P., Pokorski, J. K., & Steinmetz, N. F. (2022). Integrating plant molecular farming and materials research for next-generation vaccines. Nature Reviews Materials, 7(5), 372–388. https://doi.org/10.1038/S41578-021-00399-5,

Combelas, N., Holmblat, B., Joffret, M.-L., Colbère-Garapin, F., & Delpeyroux, F. (2011). Recombination between Poliovirus and Coxsackie A Viruses of Species C: A Model of Viral Genetic Plasticity and Emergence. Viruses, 3, 1460–1484. https://doi.org/10.3390/v3081460

Corbic Ramljak, I., Stanger, J., Real-Hohn, A., Dreier, D., Wimmer, L., Redlberger-Fritz, M., Fischl, W., Klingel, K., Mihovilovic, M. D., Blaas, D., & Kowalski, H. (2018a). Cellular N-myristoyltransferases play a crucial picornavirus genus-specific role in viral assembly, virion maturation, and infectivity. https://doi.org/10.1371/journal.ppat.1007203

Crisci, E., Bárcena, J., & Montoya, M. (2012). Virus-like particles: The new frontier of vaccines for animal viral infections. Veterinary Immunology and Immunopathology, 148(3–4), 211–225. https://doi.org/10.1016/J.VETIMM.2012.04.026

Curry, S., Chow, M., & Hogle, J. M. (1996). The Poliovirus 135S Particle Is Infectious. JOURNAL OF VIROLOGY, 70(10), 7125–7131. https://journals.asm.org/journal/jvi

Cutts, F. T., Franceschi, S., Goldie, S., Castellsague, X., de Sanjose, S., Garnett, G., Edmunds, W. J., Claeys, P., Goldenthal, K. L., Harperi, D. M., & Markowitz, L. (2007). Human papillomavirus and HPV vaccines: A review. In Bulletin of the World Health Organization (Vol. 85, Issue 9, pp. 719–726). https://doi.org/10.2471/BLT.06.038414

Danthi, P., Tosteson, M., Li, Q., & Chow, M. (2003). Genome Delivery and Ion Channel Properties Are Altered in VP4 Mutants of Poliovirus. Journal of Virology, 77(9), 5266–5274. https://doi.org/10.1128/jvi.77.9.5266-5274.2003

de Marco, A. (2025). Recent advances in recombinant production of soluble proteins in E. coli. Microbial Cell Factories, 24(1), 1–12. https://doi.org/10.1186/S12934-025-02646-8/METRICS

Deressa, W., Kayembe, P., Neel, A. H., Mafuta, E., Seme, A., & Alonge, O. (2020). Lessons learned from the polio eradication initiative in the Democratic Republic of Congo and Ethiopia: analysis of implementation barriers and strategies. BMC Public Health, 20(4), 1–15. https://doi.org/10.1186/S12889-020-09879-9/TABLES/3

Donovan, R. S., Robinson, C. W., & Glick, B. R. (1996). Review: Optimizing inducer and culture conditions for expression of foreign proteins under the control of the lac promoter. In Journal of Industrial Microbiology (Vol. 16). https://academic.oup.com/jimb/article/16/3/145/5988682

Dorji, T., Nopsopon, T., Tamang, S. T., & Pongpirul, K. (2021). Human papillomavirus vaccination uptake in low-and middle-income countries: a meta-analysis. EClinicalMedicine, 34. https://doi.org/10.1016/j.eclinm.2021.100836

Dotzauer, A. (2012). Innate and adaptive immune responses against picornaviruses and their counteractions: An overview. World Journal of Virology, 1(3), 91. https://doi.org/10.5501/wjv.v1.i3.91

Duizer, E., Ruijs, W. L., van der Weijden, C. P., & Timen, A. (2017). Response to a wild poliovirus type 2 (WPV2)-shedding event following accidental exposure to WPV2, the

Netherlands, April 2017. Eurosurveillance, 22(21). https://doi.org/10.2807/1560-7917.ES.2017.22.21.30542

Dumont, J., Euwart, D., Mei, B., Estes, S., & Kshirsagar, R. (2016). Human cell lines for biopharmaceutical manufacturing: history, status, and future perspectives. Critical Reviews in Biotechnology, 36(6), 1110–1122. https://doi.org/10.3109/07388551.2015.1084266,

Elvin, C. M., Thompson, P. R., Argall, M. E., Philip Hendr, N., Stamford, P. J., Lilley, P. E., & Dixon, N. E. (1990). Modified bacteriophage lambda promoter vectors for overproduction of proteins in Escherichia coli. Gene, 87(1), 123–126. https://doi.org/10.1016/0378-1119(90)90503-J

EMD Chemicals Inc (2011). TB250 pTriExTM System Manual. Darmstadt, Germany.

Farazi, T. A., Waksman, G., & Gordon, J. I. (2001). The Biology and Enzymology of Protein N-Myristoylation* □ S. Journal of Biological Chemistry, 276, 39501–39504. https://doi.org/10.1074/jbc.R100042200

Felberbaum, R. S. (2015). The baculovirus expression vector system: A commercial manufacturing platform for viral vaccines and gene therapy vectors. Biotechnology Journal, 10(5), 702–714. https://doi.org/10.1002/BIOT.201400438

Feng, Q., Langereis, M. A., Lork, M., Nguyen, M., Hato, S. V., Lanke, K., Emdad, L., Bhoopathi, P., Fisher, P. B., Lloyd, R. E., & van Kuppeveld, F. J. M. (2014). Enterovirus 2A pro Targets MDA5 and MAVS in Infected Cells . Journal of Virology, 88(6), 3369–3378. https://doi.org/10.1128/JVI.02712-13/ASSET/CD82FE97-0B13-4808-AA1A-EA88D1AB9E22/ASSETS/GRAPHIC/ZJV9990987800007.JPEG

Ferguson, M., Minor, P. D., Magrath, D. I., Yi-Hua, Q., Spitz, M., & Schild, G. C. (1984). Neutralization Epitopes on Poliovirus Type 3 Particles: an Analysis Using Monoclonal Antibodies (Vol. 65).

Fontana, D., Kratje, R., Etcheverrigaray, M., & Prieto, C. (2015). Immunogenic virus-like particles continuously expressed in mammalian cells as a veterinary rabies vaccine candidate. Vaccine, 33(35), 4238–4246. https://doi.org/10.1016/J.VACCINE.2015.03.088

Fox, H., Knowlson, S., Minor, P. D., & Macadam, A. J. (2017a). Genetically Thermo-Stabilised, Immunogenic Poliovirus Empty Capsids; a Strategy for Non-replicating Vaccines. PLoS Pathogens, 13(1). https://doi.org/10.1371/JOURNAL.PPAT.1006117

Francis, D. M., & Page, R. (2010). Strategies to Optimize Protein Expression in E. coli. Current Protocols in Protein Science, 61(1), 5241. https://doi.org/10.1002/0471140864.PS0524S61

Fricks, C. E., & Hogle, J. M. (1990). Cell-induced conformational change in poliovirus: externalization of the amino terminus of VP1 is responsible for liposome binding. Journal of Virology, 64(5), 1934–1945. https://doi.org/10.1128/JVI.64.5.1934-1945.1990,

Fuenmayor, J., Gòdia, F., & Cervera, L. (2017). Production of virus-like particles for vaccines. New Biotechnology, 39(Pt B), 174–180. https://doi.org/10.1016/j.nbt.2017.07.010

García-Fraga, B., da Silva, A. F., López-Seijas, J., & Sieiro, C. (2015). Optimized expression conditions for enhancing production of two recombinant chitinolytic enzymes from different prokaryote domains. Bioprocess and Biosystems Engineering, 38(12). https://doi.org/10.1007/s00449-015-1485-5

Gassler, T., Heistinger, L., Mattanovich, D., Gasser, B., & Prielhofer, R. (2019). CRISPR/Cas9-mediated homology-directed genome editing in Pichia pastoris. Methods in Molecular Biology, 1923, 211–225. https://doi.org/10.1007/978-1-4939-9024-5_9,

Gelfand, H. M., Potash, L., LeBlanc, D. R., & Fox, J. P. (1959). INTRAFAMILIAL AND INTERFAMILIAL SPREAD OF LIVING VACCINE STRAINS OF POLIOVIRUSES. Journal of the American Medical Association, 170(17), 2039–2048. https://doi.org/10.1001/jama.1959.03010170001001

Gerloff, N., Sun, H., Mandelbaum, M., Maher, C., Nix, W. A., Zaidi, S., Shaukat, S., Seakamela, L., Nalavade, U. P., Sharma, D. K., Oberste, M. S., & Vega, E. (2018a). Diagnostic assay development for poliovirus eradication. Journal of Clinical Microbiology, 56(2). https://doi.org/10.1128/JCM.01624-17/FORMAT/EPUB

Gerloff, N., Sun, H., Mandelbaum, M., Maher, C., Nix, W. A., Zaidi, S., Shaukat, S., Seakamela, L., Nalavade, U. P., Sharma, D. K., Oberste, M. S., & Vega, E. (2018b). Diagnostic assay development for poliovirus eradication. Journal of Clinical Microbiology, 56(2). https://doi.org/10.1128/JCM.01624-17/FORMAT/EPUB

Gnügge, R., & Rudolf, F. (2017). Saccharomyces cerevisiae Shuttle vectors. Yeast, 34(5), 205–221. https://doi.org/10.1002/YEA.3228

Goeddel, D. V, Kleid, D. G., Bolivar, F., Heyneker, H. L., Yansura, D. G., Crea, R., Hirosef, T., Kraszewskit, A., Itakuraf, K., & Riggstt, A. D. (1979). Expression in Escherichia coli of chemically synthesized genes for human insulin (plasmid construction/lac operon/fused proteins/radioimmunoassay/peptide purification). In Biochemistry (Vol. 76, Issue 1). https://www.pnas.org

Gonzalez, H., Khademi, M., Borg, K., & Olsson, T. (2012). Intravenous immunoglobulin treatment of the post-polio syndrome: Sustained effects on quality of life variables and cytokine expression after one year follow up. Journal of Neuroinflammation, 9. https://doi.org/10.1186/1742-2094-9-167,

Goujon, M., McWilliam, H., Li, W., Valentin, F., Squizzato, S., Paern, J., & Lopez, R. (2010). A new bioinformatics analysis tools framework at EMBL-EBI. Nucleic Acids Research, 38(SUPPL. 2). https://doi.org/10.1093/nar/gkq313

Gronenborn, B. (1976). Overproduction of phage Lambda repressor under control of the lac promotor of Escherichia coli. MGG Molecular & General Genetics, 148(3), 243–250. https://doi.org/10.1007/BF00332898/METRICS

Guo, H. C., Sun, S. Q., Jin, Y., Yang, S. L., Wei, Y. Q., Sun, D. H., Yin, S. H., Ma, J. W., Liu, Z. X., Guo, J. H., Luo, J. X., Yin, H., Liu, X. T., & Liu, D. X. (2013a). Foot-and-mouth disease virus-like particles produced by a SUMO fusion protein system in Escherichia coli induce potent protective immune responses in guinea pigs, swine and cattle. Veterinary Research, 44(1). https://doi.org/10.1186/1297-9716-44-48

Guzman, L.-M., Belin, D., Carson, M. J., & Beckwith, J. (1995). Tight Regulation, Modulation, and High-Level Expression by Vectors Containing the Arabinose P BAD Promoter. JOURNAL OF BACTERIOLOGY, 177(14), 4121–4130. https://journals.asm.org/journal/jb

Haldimann, A., Daniels, L. L., & Wanner, B. L. (1998). Use of New Methods for Construction of Tightly Regulated Arabinose and Rhamnose Promoter Fusions in Studies of the Escherichia coli Phosphate Regulon. JOURNAL OF BACTERIOLOGY, 180(5), 1277–1286. https://journals.asm.org/journal/jb

Hardenberg, M., Horvath, A., Ambrus, V., Fuxreiter, M., & Vendruscolo, M. (2020). Widespread occurrence of the droplet state of proteins in the human proteome. Proceedings of the National Academy of Sciences of the United States of America, 117, 33254–33262. https://doi.org/10.1073/PNAS.2007670117

Harjulehto-Mervaala, T., Aro, T., Hiilesmaa, V. K., Saxen, H., Hovi, T., & Saxen, L. (1993). Oral Polio Vaccination during Pregnancy: No Increase in the Occurrence of Congenital Malformations. In American Journal erf Epidemiology (Vol. 138, Issue 6). https://academic.oup.com/aje/article/138/6/407/104920

Harutyunyan, V., Quddus, A., Pallansch, M., Zipursky, S., Woods, D., Ottosen, A., Vertefeuille, J., & Lewis, I. (2023). Global oral poliovirus vaccine stockpile management as an essential preparedness and response mechanism for type 2 poliovirus outbreaks following global oral poliovirus vaccine type 2 withdrawal. Vaccine, 41(Suppl 1), A70–A78. https://doi.org/10.1016/j.vaccine.2022.02.058

Hashimoto, Y., Zhang, S., & Blissard, G. W. (2010). Ao38, a new cell line from eggs of the black witch moth, Ascalapha odorata (Lepidoptera: Noctuidae), is permissive for AcMNPV infection and produces high levels of recombinant proteins. BMC Biotechnology, 10(1), 1–16. https://doi.org/10.1186/1472-6750-10-50/TABLES/2

Hatos, A., Tosatto, S. C. E., Vendruscolo, M., & Fuxreiter, M. (2022). FuzDrop on AlphaFold: visualizing the sequence-dependent propensity of liquid-liquid phase separation and aggregation of proteins. Nucleic Acids Research, 50, W337–W344. https://doi.org/10.1093/nar/gkac386

Hellen, C. U. T., Kräusslich, H. G., & Wimmer, E. (1989). Proteolytic Processing of Polyproteins in the Replication of RNA Viruses. Biochemistry, 28(26), 9881–9890. https://doi.org/10.1021/BI00452A001/ASSET/BI00452A001.FP.PNG_V03

Herniou, E. A., Olszewski, J. A., Cory, J. S., & O'Reilly, D. R. (2003). The Genome Sequence and Evolution of Baculoviruses. In Annual Review of Entomology (Vol. 48, pp. 211–234). https://doi.org/10.1146/annurev.ento.48.091801.112756

Hillebrandt, N., Vormittag, P., Bluthardt, N., Dietrich, A., & Hubbuch, J. (2020). Integrated Process for Capture and Purification of Virus-Like Particles: Enhancing Process Performance by Cross-Flow Filtration. Frontiers in Bioengineering and Biotechnology, 8. https://doi.org/10.3389/FBIOE.2020.00489,

Hindiyeh, M., Li, Q.-H., Basavappa, R., Hogle, J. M., & Chow, M. (1999). Poliovirus Mutants at Histidine 195 of VP2 Do Not Cleave VP0 into VP2 and VP4. Journal of Virology, 73(11), 9072–9079. https://doi.org/10.1128/JVI.73.11.9072-

9079.1999/ASSET/5695DB65-D256-4844-A942-4C0CA8D7A5A2/ASSETS/GRAPHIC/JV1190794007.JPEG

Hirano, M., Ando, R., Shimozono, S., Sugiyama, M., Takeda, N., Kurokawa, H., Deguchi, R., Endo, K., Haga, K., Takai-Todaka, R., Inaura, S., Matsumura, Y., Hama, H., Okada, Y., Fujiwara, T., Morimoto, T., Katayama, K., & Miyawaki, A. (2022). A highly photostable and bright green fluorescent protein. Nature Biotechnology, 40(7), 1132–1142. https://doi.org/10.1038/S41587-022-01278-2,

Hird, T. R., & Grassly, N. C. (2012). Systematic Review of Mucosal Immunity Induced by Oral and Inactivated Poliovirus Vaccines against Virus Shedding following Oral Poliovirus Challenge. 8(4). https://doi.org/10.1371/journal.ppat.1002599

Hogle, J. M. (2002). Poliovirus cell entry: Common structural themes in viral cell entry pathways. Annual Review of Microbiology, 56(Volume 56, 2002), 677–702. https://doi.org/10.1146/ANNUREV.MICRO.56.012302.160757/CITE/REFWORKS

Hogle, J. M., Chow, M., & Filman, D. J. (1985). Three-dimensional structure of poliovirus at 2.9 Å resolution. Science, 229(4720), 1358–1365. https://doi.org/10.1126/SCIENCE.2994218

Hong, Q., Liu, J., Wei, Y., & Wei, X. (2023). Application of Baculovirus Expression Vector System (BEVS) in Vaccine Development. Vaccines, 11(7). https://doi.org/10.3390/VACCINES11071218,

Hong, Q., Wang, S., Wang, X., Han, W., Chen, T., Liu, Y., Cheng, F., Qin, S., Zhao, S., Liu, Q., Cong, Y., & Huang, Z. (2024a). Vaccine Potency and Structure of Yeast-Produced Polio Type 2 Stabilized Virus-like Particles. Vaccines, 12(9). https://doi.org/10.3390/vaccines12091077

Hopkins, R. F., & Esposito, D. (2009). A rapid method for titrating baculovirus stocks using the Sf-9 Easy Titer cell line. BioTechniques, 47(3), 785–788. https://doi.org/10.2144/000113238/SUPPL_FILE/IBTN_A_12359248_SM0001.PDF

Hsieh, J. -H, Shih, K. -Y, Kung, H. -F, Shiang, M., Lee, L. -Y, Meng, M. -H, Chang, C. -C, Lin, H. -M, Shih, S. -C, Lee, S. -Y, Chow, T. -Y, Feng, T. -Y, Kuo, T. -T, & Choo, K. -B. (1988). Controlled fed-batch fermentation of recombinant Saccharomyces cerevisiae to produce hepatitis B surface antigen. Biotechnology and Bioengineering, 32(3), 334–340.https://doi.org/10.1002/BIT.260320310;REQUESTEDJOURNAL:JOURNAL:10970290;PAGE:STRING:ARTICLE/CHAPTER

ICTV (no date) Picornaviridae. Available at: https://ictv.global/report/chapter/picornaviridae/picornaviridae (Accessed: 4 July 2025).

ICTV. (2025). Species List: Baculoviridae .Available at: https://ictv.global/report/chapter/baculoviridae/taxonomy/baculoviridae

IHR. (2025, July 28). Statement of the Forty-second meeting of the Polio IHR Emergency Committee. https://www.who.int/news/item/28-07-2025-statement-of-the-forty-second-meeting-of-the-polio-ihr-emergency-committee

Jeong, H., & Seong, B. L. (2017). Exploiting virus-like particles as innovative vaccines against emerging viral infections. Journal of Microbiology, 55(3), 220–230. https://doi.org/10.1007/S12275-017-7058-3,

Jiang, P., Liu, Y., Ma, H.-C., Paul, A. v., & Wimmer, E. (2014). Picornavirus Morphogenesis. Microbiology and Molecular Biology Reviews: MMBR, 78(3), 418. https://doi.org/10.1128/MMBR.00012-14

Joe, C. C. D., Chatterjee, S., Lovrecz, G., Adams, T. E., Thaysen-Andersen, M., Walsh, R., Locarnini, S. A., Smooker, P., & Netter, H. J. (2020). Glycoengineered hepatitis B virus-like particles with enhanced immunogenicity. Vaccine, 38(22), 3892–3901. https://doi.org/10.1016/j.vaccine.2020.03.007

Judy, E., & Kishore, N. (2019). A look back at the molten globule state of proteins: thermodynamic aspects. https://doi.org/10.1007/s12551-019-00527-0

Jumper, J., Evans, R., Pritzel, A., Green, T., Figurnov, M., Ronneberger, O., Tunyasuvunakool, K., Bates, R., Žídek, A., Potapenko, A., Bridgland, A., Meyer, C., Kohl, S. A. A., Ballard, A. J., Cowie, A., Romera-Paredes, B., Nikolov, S., Jain, R., Adler, J., … Hassabis, D. (2021). Highly accurate protein structure prediction with AlphaFold. Nature, 596(7873), 583–589. https://doi.org/10.1038/S41586-021-03819-2,

Karunatilaka, K. S., Filman, D. J., Strauss, M., Loparo, J. J., & Hogle, J. M. (2021a). Real-time imaging of polioviral rna translocation across a membrane. MBio, 12(1), 1–16. https://doi.org/10.1128/MBIO.03695-20,

Karunatilaka, K. S., Filman, D. J., Strauss, M., Loparo, J. J., & Hogle, J. M. (2021b). Real-time imaging of polioviral rna translocation across a membrane. MBio, 12(1), 1–16. https://doi.org/10.1128/MBIO.03695-20,

Kastan, J. P., Tremblay, M. W., Brown, M. C., Trimarco, J. D., Dobrikova, E. Y., Dobrikov, M. I., & Gromeier, M. (2021). Enterovirus 2Apro cleavage of the ythdf M6A readers implicates YTHDF3 as a mediator of type I interferon-driven Jak/Stat signaling. MBio, 12(2). https://doi.org/10.1128/MBIO.00116-21,

Kaur, J., Kumar, A., & Kaur, J. (2018a). Strategies for optimization of heterologous protein expression in E. coli: Roadblocks and reinforcements. In International Journal of Biological Macromolecules (Vol. 106, pp. 803–822). Elsevier B.V. https://doi.org/10.1016/j.ijbiomac.2017.08.080

Kew, O. M., Sutter, R. W., De Gourville, E. M., Dowdle, W. R., & Pallansch, M. A. (2005). Vaccine-derived polioviruses and the endgame strategy for global polio eradication. Annual Review of Microbiology, 59(Volume 59, 2005), 587–635. https://doi.org/10.1146/ANNUREV.MICRO.58.030603.123625/CITE/REFWORKS

Kidd, D. (1996). Poliomyelitis. Postgraduate Medical Journal, 72(853), 641–647. https://doi.org/10.1136/PGMJ.72.853.641

Kilpatrick, D. R., Nottay, B., Yang, C. F., Yang, S. J., Mulders, M. N., Holloway, B. P., Pallansch, M. A., & Kew, O. M. (1996). Group-specific identification of polioviruses by PCR using primers containing mixed-base or deoxyinosine residues at positions of

codon degeneracy. Journal of Clinical Microbiology, 34(12), 2990–2996. https://doi.org/10.1128/JCM.34.12.2990-2996.1996,

Kingston, N. J., Snowden, J. S., Grehan, K., Hall, P. K., Hietanen, E. V., Passchier, T. C., Polyak, S. J., Filman, D. J., Hogle, J. M., Rowlands, D. J., & Stonehouse, N. J. (2024). Mechanism of enterovirus VP0 maturation cleavage based on the structure of a stabilised assembly intermediate. PLoS Pathogens, 20(9 September). https://doi.org/10.1371/JOURNAL.PPAT.1012511,

Kishore *et al.* (2017). Myristoylation: An important Protein Modification in the immune Response. 8, 1. https://doi.org/10.3389/fimmu.2017.00751

Kitamura, A., Nakayama, Y., & Kinjo, M. (2015). Efficient and dynamic nuclear localization of green fluorescent protein via RNA binding. Biochemical and Biophysical Research Communications, 463(3), 401–406. https://doi.org/10.1016/j.bbrc.2015.05.084

Konopka-Anstadt, J. L., Campagnoli, R., Vincent, A., Shaw, J., Wei, L., Wynn, N. T., Smithee, S. E., Bujaki, E., Te Yeh, M., Laassri, M., Zagorodnyaya, T., Weiner, A. J., Chumakov, K., Andino, R., Macadam, A., Kew, O., & Burns, C. C. (2020). Development of a new oral poliovirus vaccine for the eradication end game using codon deoptimization. Npj Vaccines, 5(1). https://doi.org/10.1038/S41541-020-0176-7,

Kotecha, A., Seago, J., Scott, K., Burman, A., Loureiro, S., Ren, J., Porta, C., Ginn, H. M., Jackson, T., Perez-Martin, E., Siebert, C. A., Paul, G., Huiskonen, J. T., Jones, I. M., Esnouf, R. M., Fry, E. E., Maree, F. F., Charleston, B., & Stuart, D. I. (2015). Structure-based energetics of protein interfaces guides foot-and-mouth disease virus vaccine design. Nature Structural and Molecular Biology, 22(10), 788–794. https://doi.org/10.1038/NSMB.3096,

Kotton, C. N. (2008). Vaccination and immunization against travel-related diseases in immunocompromised hosts. Expert Review of Vaccines, 7(5), 663–672.

Kumar, P., Bird, C., Holland, D., Joshi, S. B., & Volkin, D. B. (2022). Current and next-generation formulation strategies for inactivated polio vaccines to lower costs, increase coverage, and facilitate polio eradication. Human Vaccines and Immunotherapeutics, 18(7). https://doi.org/10.1080/21645515.2022.2154100,

Kurup, V. M., & Thomas, J. (2020). Edible Vaccines: Promises and Challenges. Molecular Biotechnology, 62(2), 79–90. https://doi.org/10.1007/S12033-019-00222-1,

Laurens, M. B. (2019). RTS,S/AS01 vaccine (MosquirixTM): an overview. Human Vaccines & Immunotherapeutics, 16(3), 480. https://doi.org/10.1080/21645515.2019.1669415

Lee, C.-D., Yan, Y.-P., Liang, S.-M., & Wang, T.-F. (2009). Production of FMDV virus-like particles by a SUMO fusion protein approach in Escherichia coli. https://doi.org/10.1186/1423-0127-16-69

Lee, S. E., Greene, S. A., Burns, C. C., Tallis, G., Wassilak, S. G. F., & Bolu, O. (2025). Progress Toward Poliomyelitis Eradication — Worldwide, January 2021–March 2023. MMWR. Morbidity and Mortality Weekly Report, 72(19), 517–522. https://doi.org/10.15585/MMWR.MM7219A3

Lee, Y. M. H., & Chow, M. (1992a). Myristate modification does not function as a membrane association signal during poliovirus capsid assembly. Virology, 187(2), 814–820. https://doi.org/10.1016/0042-6822(92)90485-8

Lee, Y. T., Ko, E. J., Lee, Y., Kim, K. H., Kim, M. C., Lee, Y. N., & Kang, S. M. (2018). Intranasal vaccination with M2e5x virus-like particles induces humoral and cellular immune responses conferring cross-protection against heterosubtypic influenza viruses. PLoS ONE, 13(1). https://doi.org/10.1371/JOURNAL.PONE.0190868,

Li, Q., Yafal, A. G., Lee, Y. M., Hogle, J., & Chow, M. (1994). Poliovirus neutralization by antibodies to internal epitopes of VP4 and VP1 results from reversible exposure of these sequences at physiological temperature. Journal of Virology, 68(6), 3965. https://doi.org/10.1128/JVI.68.6.3965-3970.1994

Li, X. Y., Das, I., Lepletier, A., Addala, V., Bald, T., Stannard, K., Barkauskas, D., Liu, J., Aguilera, A. R., Takeda, K., Braun, M., Nakamura, K., Jacquelin, S., Lane, S. W., Teng, M. W. L., Dougall, W. C., & Smyth, M. J. (2018). CD155 loss enhances tumor suppression via combined host and tumor-intrinsic mechanisms. Journal of Clinical Investigation, 128(6), 2613–2625. https://doi.org/10.1172/JCI98769

Li, Y., Jin, L., & Chen, T. (2020). The Effects of Secretory IgA in the Mucosal Immune System. https://doi.org/10.1155/2020/2032057

Li, Z., Ma, Y., Nan, X., Dong, H., Tang, J., Yin, S., Sun, S., Bao, E., & Guo, H. (2024a). Production of virus-like particles of FMDV by 3C protease cleaving precursor polyprotein P1 in vitro. 108, 542. https://doi.org/10.1007/s00253-024-13376-z

Liu, Y., Hill, M. G., Klose, T., Chen, Z., Watters, K., Bochkov, Y. A., Jiang, W., Palmenberg, A. C., & Rossmann, M. G. (2016). Atomic structure of a rhinovirus C, a virus species linked to severe childhood asthma. Proceedings of the National Academy of Sciences of the United States of America, 113(32), 8997–9002. https://doi.org/10.1073/pnas.1606595113

Lonberg Holm, K., Gosser, L. B., & Kauer, J. C. (1975). Early alteration of poliovirus in infected cells and its specific inhibition. Journal of General Virology, 27(3), 329–342. https://doi.org/10.1099/0022-1317-27-3-329,

Lünsdorf, H., Gurramkonda, C., Adnan, A., Khanna, N., & Rinas, U. (2011). Virus-like particle production with yeast: Ultrastructural and immunocytochemical insights into Pichia pastoris producing high levels of the Hepatitis B surface antigen. Microbial Cell Factories, 10. https://doi.org/10.1186/1475-2859-10-48,

Malakhov, M. P., Mattern, M. R., Malakhova, O. A., Drinker, M., Weeks, S. D., & Butt, T. R. (2004). SUMO fusions and SUMO-specific protease for efficient expression and purification of proteins. Journal of Structural and Functional Genomics, 5(1–2), 75–86. https://doi.org/10.1023/B:JSFG.0000029237.70316.52/METRICS

Marblestone, J. G., Edavettal, S. C., Lim, Y., Lim, P., Zuo, X., & Butt, T. R. (2006a). Comparison of SUMO fusion technology with traditional gene fusion systems: Enhanced expression and solubility with SUMO. Protein Science : A Publication of the Protein Society, 15(1), 182. https://doi.org/10.1110/PS.051812706

Marblestone, J. G., Edavettal, S. C., Lim, Y., Lim, P., Zuo, X., & Butt, T. R. (2006b). Comparison of SUMO fusion technology with traditional gene fusion systems: Enhanced expression and solubility with SUMO. Protein Science, 15(1), 182–189. https://doi.org/10.1110/ps.051812706

Marc, D., Drugeon, G., Haenni, A. L., Girard, M., & der Werf, S. Van. (1989). Role of myristoylation of poliovirus capsid protein VP4 as determined by site-directed mutagenesis of its N-terminal sequence. The EMBO Journal, 8(9), 2661–2668. https://doi.org/10.1002/J.1460-2075.1989.TB08406.X

Mardanova, E. S., Vasyagin, E. A., & Ravin, N. V. (2024). Virus-like Particles Produced in Plants: A Promising Platform for Recombinant Vaccine Development. Plants, 13(24). https://doi.org/10.3390/PLANTS13243564,

Marsian, J., Fox, H., Bahar, M. W., Kotecha, A., Fry, E. E., Stuart, D. I., Macadam, A. J., Rowlands, D. J., & Lomonossoff, G. P. (2017a). Plant-made polio type 3 stabilized VLPs-A candidate synthetic polio vaccine. Nature Communications, 8(1). https://doi.org/10.1038/s41467-017-00090-w

Marsian, J., Fox, H., Bahar, M. W., Kotecha, A., Fry, E. E., Stuart, D. I., Macadam, A. J., Rowlands, D. J., & Lomonossoff, G. P. (2017b). Plant-made polio type 3 stabilized VLPs-A candidate synthetic polio vaccine. Nature Communications, 8(1). https://doi.org/10.1038/s41467-017-00090-w

Martin, A., Wychowski, C., Couderc, T., Crainic, R., Hogle, J., & Girard, M. (1988). Engineering a poliovirus type 2 antigenic site on a type 1 capsid results in a chimaeric virus which is neurovirulent for mice. The EMBO Journal, 7(9), 2839–2847. https://doi.org/10.1002/J.1460-2075.1988.TB03140.X,

Martín-Belmonte, F., López-Guerrero, J. A., Carrasco, L., & Alonso, M. A. (2000). The Amino-Terminal Nine Amino Acid Sequence of Poliovirus Capsid VP4 Protein Is Sufficient To Confer N-Myristoylation and Targeting to Detergent-Insoluble Membranes †. https://doi.org/10.1021/bi992132e

Maurer-Stroh, S., & Eisenhaber, F. (2004a). Myristoylation of viral and bacterial proteins. In Trends in Microbiology (Vol. 12, Issue 4, pp. 178–185). https://doi.org/10.1016/j.tim.2004.02.006

Mehndiratta, M. M., Mehndiratta, P., & Pande, R. (2014). Poliomyelitis: Historical Facts, Epidemiology, and Current Challenges in Eradication. The Neurohospitalist, 4(4), 223–229. https://doi.org/10.1177/1941874414533352,

Melnick, J. L. (1996). Current Status of Poliovirus Infections. In CLINICAL MICROBIOLOGY REVIEWS (Vol. 9, Issue 3, pp. 293–300).

Mendelsohn, C. L., Wimmer, E., & Racaniello, V. R. (1989). Cellular receptor for poliovirus: Molecular cloning, nucleotide sequence, and expression of a new member of the immunoglobulin superfamily. Cell, 56(5), 855–865. https://doi.org/10.1016/0092-8674(89)90690-9,

Minor, P. (2014). The polio endgame. Human Vaccines and Immunotherapeutics, 10(7), i–iii. https://doi.org/10.4161/21645515.2014.981115,

Minor, P. D. (2004). Polio eradication, cessation of vaccination and re-emergence of disease. In Nature Reviews Microbiology (Vol. 2, pp. 473–482). https://doi.org/10.1038/nrmicro906

Minor, P. D., Schild, G. C., Wood, J. M., & Dandawate, C. N. (1980). The Preparation of Specific Immune Sera against Type 3 Poliovirus D-Antigen and C-Antigen and the Demonstration of Two C-Antigenic Components in Vaccine Strain Populations. In J. gen. Virol. 0980) (Vol. 5).

Mohsen, M. O., Gomes, A. C., Vogel, M., & Bachmann, M. F. (2018a). Interaction of viral capsid-derived virus-like particles (VLPs) with the innate immune system. Vaccines, 6(3). https://doi.org/10.3390/VACCINES6030037,

Molla, A., Paul, A. V., Schmid, M., Jang, S. K., & Wimmer, E. (1993). Studies on Dicistronic Polioviruses Implicate Viral Proteinase 2Apro in RNA Replication. Virology, 196(2), 739–747. https://doi.org/10.1006/viro.1993.1531

Monto, A. S. (1999). Francis Field Trial of Inactivated Poliomyelitis Vaccine: Background and Lessons for Today. 21(1). http://epirev.oxfordjournals.org/

Moscufo, N., & Chow, M. (1992). Myristate-protein interactions in poliovirus: interactions of VP4 threonine 28 contribute to the structural conformation of assembly intermediates and the stability of assembled virions. Journal of Virology, 66(12), 6849–6857. https://doi.org/10.1128/JVI.66.12.6849-6857.1992

Moscufo, N., Gomez Yafal, A., Rogove, A., Hogle, § James, & Chowi11, M. (1993). A Mutation in VP4 Defines a New Step in the Late Stages of Cell Entry by Poliovirus. JOURNAL OF VIROLOGY, 5075–5078. https://journals.asm.org/journal/jvi

Moscufo, N., Simons, J., & Chow, M. (1991). Myristoylation is important at multiple stages in poliovirus assembly. Journal of Virology, 65(5), 2372–2380. https://doi.org/10.1128/JVI.65.5.2372-2380.1991,

Mousnier, A., Bell, A. S., Swieboda, D. P., Morales-Sanfrutos, J., Pérez-Dorado, I., Brannigan, J. A., Newman, J., Ritzefeld, M., Hutton, J. A., Guedán, A., Asfor, A. S., Robinson, S. W., Hopkins-Navratilova, I., Wilkinson, A. J., Johnston, S. L., Leatherbarrow, R. J., Tuthill, T. J., Solari, R., & Tate, E. W. (2018). Fragment-derived inhibitors of human N-myristoyltransferase block capsid assembly and replication of the common cold virus. Nature Chemistry, 10(6), 599–606. https://doi.org/10.1038/S41557-018-0039-2,

Mühlmann, M., Forsten, E., Noack, S., & Büchs, J. (2017). Optimizing recombinant protein expression via automated induction profiling in microtiter plates at different temperatures. Microbial Cell Factories, 16(1), 1–12. https://doi.org/10.1186/S12934-017-0832-4/FIGURES/5

Muir, P., Nicholson, F., Jhetam, M., Neogi, S., & Banatvala, J. E. (1993). Rapid diagnosis of enterovirus infection by magnetic bead extraction and polymerase chain reaction detection of enterovirus RNA in clinical specimens. Journal of Clinical Microbiology, 31(1), 31–38. https://doi.org/10.1128/JCM.31.1.31-38.1993,

Murdin, A. D., Lu, T. H., Murray, M. G., & Wimmer, E. (1992). Poliovirus antigenic hybrids simultaneously expressing antigenic determinants from all three serotypes. Journal of General Virology, 73(3), 607–611. https://doi.org/10.1099/0022-1317-73-3-607,

Muslin, C., Joffret, M.-L., Pelletier, I., Blondel, B., & Delpeyroux, F. (2015). Evolution and Emergence of Enteroviruses through Intra-and Inter-species Recombination: Plasticity and Phenotypic Impact of Modular Genetic Exchanges in the 5' Untranslated Region. https://doi.org/10.1371/journal.ppat.1005266

Nathanson, N. (2008). Chapter 1 The Pathogenesis of Poliomyelitis: What We Don't Know. Advances in Virus Research, 71, 1–50. https://doi.org/10.1016/S0065-3527(08)00001-8

Nazir, A., Shad, M., Rehman, H. M., Azim, N., & Sajjad, M. (2024). Application of SUMO fusion technology for the enhancement of stability and activity of lysophospholipase from Pyrococcus abyssi. World Journal of Microbiology and Biotechnology, 40(6). https://doi.org/10.1007/s11274-024-03998-w

Nkowane, B. M., Wassilak, S. G. F., Orenstein, W. A., Bart, K. J., Schonberger, L. B., Hinman, A. R., & Kew, O. M. (1987). Vaccine-Associated Paralytic Poliomyelitis: United States: 1973 Through 1984. JAMA, 257(10), 1335–1340. https://doi.org/10.1001/JAMA.1987.03390100073029

Nolan, J. P., Wilmer, B. H., & Melnick, J. L. (1955). Poliomyelitis: its highly invasive nature and narrow stream of infection in a community of high socioeconomic level. The New England Journal of Medicine, 253(22), 945–954. https://doi.org/10.1056/NEJM195512012532201

Nooraei, S., Bahrulolum, H., Hoseini, Z. S., Katalani, C., Hajizade, A., Easton, A. J., & Ahmadian, G. (2021). Virus-like particles: preparation, immunogenicity and their roles as nanovaccines and drug nanocarriers. Journal of Nanobiotechnology, 19(1). https://doi.org/10.1186/S12951-021-00806-7,

Ogra, P. L., Karzon, D. T., Righthand, F., & MacGillivray, M. (1968). Immunoglobulin Response in Serum and Secretions after Immunization with Live and Inactivated Poliovaccine and Natural Infection. New England Journal of Medicine, 279, 893–900. https://doi.org/10.1056/nejm196810242791701

Ogra, P. L., Sinks, L. F., & Karzon, D. T. (1971a). Poliovirus antibody response in patients withacute leukemia. The Journal of Pediatrics, 79, 444–449. https://doi.org/10.1016/S0022-3476(71)80154-3

Paffenbarger, R. S., Bodian, D., Hyde, R. T., Potter, M. M., Jensen, O., Gharpure, P. V., Cosco, N. P., Hultin, J. V., & Rubinstein, H. M. (1961). Poliomyelitis immune status in ecologically diverse populations, in relation to virus spread, clinical incidence, and virus disappearance. American Journal of Epidemiology, 74, 311–325. https://doi.org/10.1093/oxfordjournals.aje.a120222

Palmer, I., & Wingfield, P. T. (2012). Preparation and extraction of insoluble (Inclusion-body) proteins from Escherichia coli. Current Protocols in Protein Science, 1. https://doi.org/10.1002/0471140864.ps0603s70

Panjwani, A., Asfor, A. S., & Tuthill, T. J. (2016). The conserved N-terminus of human rhinovirus capsid protein VP4 contains membrane pore-forming activity and is a target for neutralizing antibodies. Journal of General Virology, 97(12), 3238–3242. https://doi.org/10.1099/JGV.0.000629,

Panjwani, A., Strauss, M., Gold, S., Wenham, H., Jackson, T., Chou, J. J., Rowlands, D. J., Stonehouse, N. J., Hogle, J. M., & Tuthill, T. J. (2014a). Capsid Protein VP4 of Human Rhinovirus Induces Membrane Permeability by the Formation of a Size-Selective Multimeric Pore. PLoS Pathogens, 10(8). https://doi.org/10.1371/JOURNAL.PPAT.1004294,

Park, J., & LaBaer, J. (2006). Recombinational Cloning. Current Protocols in Molecular Biology, 74(1), 3.20.1-3.20.22. https://doi.org/10.1002/0471142727.MB0320S74

Patwardhan, P., & Resh, M. D. (2010). Myristoylation and Membrane Binding Regulate c-Src Stability and Kinase Activity. Molecular and Cellular Biology, 30(17), 4094–4107. https://doi.org/10.1128/MCB.00246-10,

Paul, A. V., Schultz, A., Pincus, S. E., Oroszlan, S., & Wimmer, E. (1987). Capsid protein VP4 of poliovirus is N-myristoylated. Proceedings of the National Academy of Sciences of the United States of America, 84(22), 7827–7831. https://doi.org/10.1073/PNAS.84.22.7827

Perez, L., & Carrasco, L. (1993). Entry of Poliovirus into Cells Does Not Require a Low-pH Step. In JOURNAL OF VIROLOGY (pp. 4543–4548).

Pfeiffer, J. K. (2010). Innate host barriers to viral trafficking and population diversity: Lessons learned from poliovirus. Advances in Virus Research, 77(C), 85. https://doi.org/10.1016/B978-0-12-385034-8.00004-1

Pliaka, V., Kyriakopoulou, Z., & Markoulatos, P. (2014). Risks associated with the use of live-attenuated vaccine poliovirus strains and the strategies for control and eradication of paralytic poliomyelitis. Http://Dx.Doi.Org/10.1586/Erv.12.28, 11(5), 609–628. https://doi.org/10.1586/ERV.12.28

Ponte-Sucre, A., Korea Dae-Hee Lee, S., Korea, S., Zhou, T., X-z, L., Bhatwa, A., Wang, W., Hassan, Y. I., Abraham, N., & Li, X.-Z. (2021). Challenges Associated With the Formation of Recombinant Protein Inclusion Bodies in Escherichia coli and Strategies to Address Them for Industrial Applications. https://doi.org/10.3389/fbioe.2021.630551

Porta, C., Xu, X., Loureiro, S., Paramasivam, S., Ren, J., Al-Khalil, T., Burman, A., Jackson, T., Belsham, G. J., Curry, S., Lomonossoff, G. P., Parida, S., Paton, D., Li, Y., Wilsden, G., Ferris, N., Owens, R., Kotecha, A., Fry, E., … Jones, I. M. (2013). Efficient production of foot-and-mouth disease virus empty capsids in insect cells following down regulation of 3C protease activity. Journal of Virological Methods, 187(2), 406–412. https://doi.org/10.1016/j.jviromet.2012.11.011

Primer Design tool for In-Fusion®. (n.d.). Https://Www.Takara-Bio.Co.Jp/Research/Infusion_primer/Infusion_primer_form.Php.

Priyamvada, L., Kallemeijn, W. W., Faronato, M., Wilkins, K., Goldsmith, C. S., Cotter, C. A., Ojeda, S., Solari, R., Moss, B., Tate, E. W., & Satheshkumar, P. S. (2022). Inhibition of

vaccinia virus L1 N-myristoylation by the host N-myristoyltransferase inhibitor IMP-1088 generates non-infectious virions defective in cell entry. PLoS Pathogens, 18(10). https://doi.org/10.1371/JOURNAL.PPAT.1010662,

Puckette, M., Clark, B. A., Smith, J. D., Turecek, T., Martel, E., Gabbert, L., Pisano, M., Hurtle, W., Pacheco, J. M., Barrera, J., Neilan, J. G., & Rasmussen, M. (2017). Foot-and-Mouth Disease (FMD) Virus 3C Protease Mutant L127P: Implications for FMD Vaccine Development. Journal of Virology, 91(22). https://doi.org/10.1128/JVI.00924-17,

Pushko, P., Pumpens, P., & Grens, E. (2013). Development of virus-like particle technology from small highly symmetric to large complex virus-like particle structures. Intervirology, 56(3), 141–165. https://doi.org/10.1159/000346773,

Pushko, P., Tumpey, T. M., van Hoeven, N., Belser, J. A., Robinson, R., Nathan, M., Smith, G., Wright, D. C., & Bright, R. A. (2007). Evaluation of influenza virus-like particles and Novasome adjuvant as candidate vaccine for avian influenza. Vaccine, 25(21), 4283–4290. https://doi.org/10.1016/j.vaccine.2007.02.059

Putnak JR, Phillips BA. 1982.Poliovirus empty capsid morphogenesis: evidence for conformational differences between self- and extract-assembled empty capsids. J Virol41.https://doi.org/10.1128/jvi.41.3.792-800.1982

Racaniello, V. R. (1996). Early events in poliovirus infection: Virus-receptor interactions. Proceedings of the National Academy of Sciences of the United States of America, 93(21), 11378–11381. https://doi.org/10.1073/PNAS.93.21.11378,

Racaniello, V. R. (2006). One hundred years of poliovirus pathogenesis. In Virology (Vol. 344, Issue 1, pp. 9–16). https://doi.org/10.1016/j.virol.2005.09.015

Ramljak, I. C., Stanger, J., Real-Hohn, A., Dreier, D., Wimmer, L., Redlberger-Fritz, M., Fischl, W., Klingel, K., Mihovilovic, M. D., Blaas, D., & Kowalski, H. (2018a). Cellular N-myristoyltransferases play a crucial picornavirus genus-specific role in viral assembly, virion maturation, and infectivity. PLoS Pathogens, 14(8). https://doi.org/10.1371/journal.ppat.1007203

Ramljak, I. C., Stanger, J., Real-Hohn, A., Dreier, D., Wimmer, L., Redlberger-Fritz, M., Fischl, W., Klingel, K., Mihovilovic, M. D., Blaas, D., & Kowalski, H. (2018b). Cellular N-myristoyltransferases play a crucial picornavirus genus-specific role in viral assembly, virion maturation, and infectivity. https://doi.org/10.1371/journal.ppat.1007203

Rao, D. M., Horton, E. R., Barrington, C. L., Briney, C. A., Henriksen, J. C., Martinez-Seidel, F., Morrison, E. J., Sterling, E. M., Provencio, E. D., Harris, M., Allen, E., Hesselberth, J. R., & Rissland, O. S. (2025). Systematic identification and characterization of eukaryotic and viral 2A peptide-bond-skipping sequences. Cell Reports, 44(7). https://doi.org/10.1016/j.celrep.2025.115822

Reinheimer, C., Friedrichs, I., Rabenau, H. F., & Doerr, H. W. (2012). Deficiency of immunity to poliovirus type 3: a lurking danger? https://doi.org/10.1186/1471-2334-12-24

Ren, M., Abdullah, S. W., Pei, C., Guo, H., & Sun, S. (2024). Use of virus-like particles and nanoparticle-based vaccines for combating picornavirus infections. Veterinary Research, 55(1), 128. https://doi.org/10.1186/S13567-024-01383-X,

Rocque, W. J., McWherter, C. A., Wood, D. C., & Gordon, J. I. (1993). A comparative analysis of the kinetic mechanism and peptide substrate specificity of human and Saccharomyces cerevisiae myristoyl-CoA:Protein N-myristoyltransferase. Journal of Biological Chemistry, 268(14), 9964–9971. https://doi.org/10.1016/s0021-9258(18)82159-7

Rombaut, B., & Jore, J. P. M. (1997). Immunogenic, non-infectious polio subviral particles synthesized in Saccharomyces cerevisiae. Journal of General Virology, 78(8), 1829–1832. https://doi.org/10.1099/0022-1317-78-8-1829,

Rombaut, B., Boeye, A., Ferguson, M., Minor, P. D., Mosser, A., & Rueckert, R. (1990). Creation of an antigenic site in poliovirus type 1 by assembly of 14 S subunits. Virology, 174(1), 305–307. https://doi.org/10.1016/0042-6822(90)90080-B

Rombaut, B., Vrijsen, R., Brioen, P., & Boeyé, A. (1982). A pH-dependent antigenic conversion of empty capsids of poliovirus studied with the aid of monoclonal antibodies to N and H antigen. Virology, 122(1), 215-218.

Rosano, G. L., & Ceccarelli, E. A. (2014a). Recombinant protein expression in Escherichia coli: Advances and challenges. In Frontiers in Microbiology (Vol. 5, Issue APR). Frontiers Research Foundation. https://doi.org/10.3389/fmicb.2014.00172

Rosano, G. L., & Ceccarelli, E. A. (2014b). Recombinant protein expression in Escherichia coli: Advances and challenges. In Frontiers in Microbiology (Vol. 5, Issue APR). Frontiers Research Foundation. https://doi.org/10.3389/fmicb.2014.00172

Rose, C., Andrews, W., Ferguson, M., McKeating, J., Almond, J., & Evans, D. (1994). The construction and characterization of poliovirus antigen chimeras presenting defined regions of the human T lymphocyte marker CD4. Journal of General Virology, 75(5), 969–977. https://doi.org/10.1099/0022-1317-75-5-969,

Rossmann, M. G. (1994). Viral cell recognition and entry. In Protein Science (Vol. 3, pp. 1712–1725). Cambridge University Press.

Rybicki, E. P. (2020). Plant molecular farming of virus-like nanoparticles as vaccines and reagents. Wiley Interdisciplinary Reviews: Nanomedicine and Nanobiotechnology, 12(2). https://doi.org/10.1002/WNAN.1587,

Sailaja, G., Skountzou, I., Quan, F. S., Compans, R. W., & Kang, S. M. (2007). Human immunodeficiency virus-like particles activate multiple types of immune cells. Virology, 362(2), 331–341. https://doi.org/10.1016/j.virol.2006.12.014

Saleem, A. F., Mach, O., Quadri, F., Khan, A., Bhatti, Z., Rehman, N. U., Zaidi, S., Weldon, W. C., Oberste, S. M., Salama, M., Sutter, R. W., & Zaidi, A. K. M. (2015). Immunogenicity of poliovirus vaccines in chronically malnourished infants: A randomized controlled trial in Pakistan. Vaccine, 33(24), 2757–2763. https://doi.org/10.1016/j.vaccine.2015.04.055

Schlager, B., Straessle, A., & Hafen, E. (2012). Use of anionic denaturing detergents to purify insoluble proteins after overexpression. BMC biotechnology, 12(1), 95.

Schneider, C. A., Rasband, W. S., & Eliceiri, K. W. (2012). NIH Image to ImageJ: 25 years of image analysis. Nature Methods, 9(7), 671–675. https://doi.org/10.1038/NMETH.2089,

Seaton, K. E., & Smith, C. D. (2008). N-Myristoyltransferase isozymes exhibit differential specificity for human immunodeficiency virus type 1 Gag and Nef. Journal of General Virology, 89(1), 288–296. https://doi.org/10.1099/VIR.0.83412-0,

Sergeev, E. L. ; P. ;, Golovina, D. I. ;, Pometun, A. A., Atroshenko, D. L., Sergeev, E. P., Golovina, D. I., & Pometun, A. A. (2024). Citation: Atroshenko, D Additivities for Soluble Recombinant Protein Expression in Cytoplasm of fermentation Additivities for Soluble Recombinant Protein Expression in Cytoplasm of Escherichia coli. https://doi.org/10.3390/fermentation10030120

Shah, P. N. M., Filman, D. J., Karunatilaka, K. S., Hesketh, E. L., Groppelli, E., Strauss, M., & Hogle, J. M. (2020). Cryo-em structures reveal two distinct conformational states in a picornavirus cell entry intermediate. PLoS Pathogens, 16(9). https://doi.org/10.1371/JOURNAL.PPAT.1008920,

Shahmahmoodi, S., Mamishi, S., Aghamohammadi, A., Aghazadeh, N., Tabatabaie, H., Gooya, M. M., Zahraei, S. M., Mousavi, T., Yousefi, M., Farrokhi, K., Mohammadpour, M., Ashrafi, M. R., Nategh, R., & Parvaneh, N. (2010). Vaccine-associated Paralytic Poliomyelitis in Immunodeficient Children, Iran, 1995–2008 - Volume 16, Number 7—July 2010 - Emerging Infectious Diseases journal - CDC. Emerging Infectious Diseases, 16(7), 1133–1136. https://doi.org/10.3201/EID1607.091606

Sherry, L., Bahar, M. W., Porta, C., Fox, H., Grehan, K., Nasta, V., Duyvesteyn, H. M. E., De Colibus, L., Marsian, J., Murdoch, I., Ponndorf, D., Kim, S.-R., Shah, S., Carlyle, S., Swanson, J. J., Matthews, S., Nicol, C., Lomonossoff, G. P., Macadam, A. J., … Rowlands, D. J. (2025). Recombinant expression systems for production of stabilised virus-like particles as next-generation polio vaccines. Nature Communications, 16(1), 831. https://doi.org/10.1038/S41467-025-56118-Z

Sherry, L., Grehan, K., Snowden, J. S., Knight, M. L., Adeyemi, O. O., Rowlands, D. J., & Stonehouse, N. J. (2020). Comparative Molecular Biology Approaches for the Production of Poliovirus Virus-Like Particles Using Pichia pastoris. https://doi.org/10.1128/mSphere.00838-19

Sherry, L., Swanson, J. J., Grehan, K., Xu, H., Uchida, M., Jones, I. M., Stonehouse, N. J., & Rowlands, D. J. (2023). Protease-Independent Production of Poliovirus Virus-like Particles in Pichia pastoris: Implications for Efficient Vaccine Development and Insights into Capsid Assembly. Microbiology Spectrum, 11(1). https://doi.org/10.1128/SPECTRUM.04300-22/SUPPL_FILE/SPECTRUM.04300-22-S0001.PDF

Sievers, F., Wilm, A., Dineen, D., Gibson, T. J., Karplus, K., Li, W., Lopez, R., McWilliam, H., Remmert, M., Söding, J., Thompson, J. D., & Higgins, D. G. (2011). Fast, scalable generation of high-quality protein multiple sequence alignments using Clustal Omega. Molecular Systems Biology, 7. https://doi.org/10.1038/msb.2011.75

Simmonds, P., Gorbalenya, A. E., Harvala, H., Hovi, T., Knowles, N. J., Lindberg, A. M., Oberste, M. S., Palmenberg, A. C., Reuter, G., Skern, T., Tapparel, C., Wolthers, K. C., Woo, P. C. Y., & Zell, R. (2020). Recommendations for the nomenclature of enteroviruses and rhinoviruses. Archives of Virology, 165(3), 793–797. https://doi.org/10.1007/S00705-019-04520-6,

Singh, A., Upadhyay, V., Upadhyay, A. K., Singh, S. M., & Panda, A. K. (2015). Protein recovery from inclusion bodies of Escherichia coli using mild solubilization process. In Microbial Cell Factories (Vol. 14). BioMed Central Ltd. https://doi.org/10.1186/s12934-015-0222-8

Skerra A. (1994). Use of the tetracycline promoter for the tightly regulated production of a murine antibody fragment in Escherichia coli. Gene, 151(1-2), 131–135. https://doi.org/10.1016/0378-1119(94)90643-2

Slack, J., & Arif, B. M. (2007a). The Baculoviruses Occlusion-Derived Virus: Virion Structure and Function. Advances in Virus Research, 69, 99. https://doi.org/10.1016/S0065-3527(06)69003-9

Smith, G. E., Summers, M. D., & Fraser, M. J. (1983). Production of human beta interferon in insect cells infected with a baculovirus expression vector. Molecular and Cellular Biology, 24, 434–443. https://doi.org/10.1128/MCB.3.12.2156-2165.1983

Snyder, J. P., Slavik, M. A., Harvey, P. L., Del Rio Guerra, R., Mainou, B. A., Sette, A. W., Kirkpatrick, B., Grifoni, A., & Crothers, J. W. (2025). Oral live attenuated polio vaccines induce enhanced T-cell responses with broad antigen recognition compared to inactivated polio vaccines. MedRxiv, 2025.05.20.25328004. https://doi.org/10.1101/2025.05.20.25328004

Spice, A. J., Aw, R., Bracewell, D. G., & Polizzi, K. M. (2020). Synthesis and Assembly of Hepatitis B Virus-Like Particles in a Pichia pastoris Cell-Free System. Frontiers in Bioengineering and Biotechnology, 8, 494686. https://doi.org/10.3389/FBIOE.2020.00072/BIBTEX

Studier, F. W. (2005). Protein production by auto-induction in high density shaking cultures. Protein Expression and Purification, 41(1), 207–234. https://doi.org/10.1016/j.pep.2005.01.016

Studier, F. W., & Moffatt, B. A. (1986). Use of bacteriophage T7 RNA polymerase to direct selective high-level expression of cloned genes. Journal of Molecular Biology, 189(1), 113–130. https://doi.org/10.1016/0022-2836(86)90385-2

Sułek, M., & Szuster-Ciesielska, A. (2025). The Bioengineering of Insect Cell Lines for Biotherapeutics and Vaccine Production: An Updated Review. Vaccines 2025, Vol. 13, Page 556, 13(6), 556. https://doi.org/10.3390/VACCINES13060556

Sutter, R. W., Kew, O. M., Cochi, S. L., & Aylward, R. B. (2018). Poliovirus Vaccine–Live. Plotkin's Vaccines, 866-917.e16. https://doi.org/10.1016/B978-0-323-35761-6.00048-1

Taha, E. A., Lee, J., & Hotta, A. (2022). Delivery of CRISPR-Cas tools for in vivo genome editing therapy: Trends and challenges. Journal of Controlled Release, 342, 345–361. https://doi.org/10.1016/j.jconrel.2022.01.013

Tanaka, T., Ames, J. B., Harvey, T. S., Stryer, L., & Ikura, M. (1995). Sequestration of the membrane-targeting myristoyl group of recoverin in the calcium-free state. Nature, 376(6539), 444–447. https://doi.org/10.1038/376444A0,

Tano, Y., Shimizu, H., Martin, J., Nishimura, Y., Simizu, B., & Miyamura, T. (2007). Antigenic characterization of a formalin-inactivated poliovirus vaccine derived from live-

attenuated Sabin strains. Vaccine, 25(41), 7041–7046. https://doi.org/10.1016/J.VACCINE.2007.07.060

Terpe, K. (2006). Overview of bacterial expression systems for heterologous protein production: From molecular and biochemical fundamentals to commercial systems. In Applied Microbiology and Biotechnology (Vol. 72, Issue 2, pp. 211–222). https://doi.org/10.1007/s00253-006-0465-8

Thomassen, Y. E., van, A. G., C T van Oijen, M. G., Wijffels, R. H., van der Pol, L. A., M Bakker, W. A., Lee Ho, P., & Butantan, I. (2013). Next Generation Inactivated Polio Vaccine Manufacturing to Support Post Polio-Eradication Biosafety Goals. https://doi.org/10.1371/journal.pone.0083374

Tokmakov, A. A., Kurotani, A., Takagi, T., Toyama, M., Shirouzu, M., Fukami, Y., & Yokoyama, S. (2012). Multiple post-translational modifications affect heterologous protein synthesis. Journal of Biological Chemistry, 287(32), 27106–27116. https://doi.org/10.1074/jbc.M112.366351

Tosteson, M. T., Wang, H., Naumov, A., & Chow, M. (2004a). Poliovirus binding to its receptor in lipid bilayers results in particle-specific, temperature-sensitive channels. Journal of General Virology, 85(6), 1581–1589. https://doi.org/10.1099/VIR.0.19745-0,

Uchida, M. (2019). Studies of Poliovirus Virus Like Particle assembly in foreign expression systems. PhD thesis. University of Reading. https://centaur.reading.ac.uk/88011/1/14015411_Uchida_thesis.pdf

Uma, M., Rao, P. P., Nagalekshmi, K., & Hegde, N. R. (2016). Expression and purification of polioviral proteins in E. coli, and production of antisera as reagents for immunological assays. Protein Expression and Purification, 128, 115. https://doi.org/10.1016/J.PEP.2016.08.014

Urakawa, T., Ferguson, M., Minor, P. D., Cooper, J., Sullivan, M., Almond, J. W., & Bishop, D. H. L. (1989). Synthesis of immunogenic, but non-infectious, poliovirus particles in insect cells by a baculovirus expression vector. Journal of General Virology, 70(6), 1453–1463. https://doi.org/10.1099/0022-1317-70-6-1453

Vallejo, L. F., & Rinas, U. (2004). Strategies for the recovery of active proteins through refolding of bacterial inclusion body proteins. In Microbial Cell Factories (Vol. 3). https://doi.org/10.1186/1475-2859-3-11

van Oosten, L., Altenburg, J. J., Nowee, G., Kenbeek, D., Neef, T., Rouw, T., Tegelbeckers, V. I. P., van der Heijden, J., Mentink, S., Willemsen, W., Hausjell, C. S., Kuijpers, L., van der Pol, L., Roldão, A., Correia, R., van den Born, E., Wijffels, R. H., Martens, D. E., van Oers, M. M., & Pijlman, G. P. (2025). Engineered thermoswitch in the baculovirus expression vector system for production of virus-like particle vaccines with minimized baculovirus contaminants. Trends in Biotechnology. https://doi.org/10.1016/j.tibtech.2025.04.004

Vaughn, J. L., Goodwin, R. H., Tompkins, G. J., & McCawley, P. (1977). The establishment of two cell lines from the insect Spodoptera frugiperda (Lepidoptera; Noctuidae). In Vitro, 13(4), 213–217. https://doi.org/10.1007/BF02615077

Vendruscolo, M., & Fuxreiter, M. (2022a). Sequence Determinants of the Aggregation of Proteins Within Condensates Generated by Liquid-liquid Phase Separation: Sequence code of aggregation in protein condensates. Journal of Molecular Biology, 434(1). https://doi.org/10.1016/j.jmb.2021.167201

Wahid, R., Cannon, M. J., & Chow, M. (2005a). Virus-Specific CD4 + and CD8 + Cytotoxic T-Cell Responses and Long-Term T-Cell Memory in Individuals Vaccinated against Polio . Journal of Virology, 79(10), 5988–5995. https://doi.org/10.1128/JVI.79.10.5988-5995.2005,

Wahid, R., Cannon, M. J., & Chow, M. (2005b). Virus-Specific CD4+ and CD8+ Cytotoxic T-Cell Responses and Long-Term T-Cell Memory in Individuals Vaccinated against Polio. Journal of Virology, 79(10), 5988. https://doi.org/10.1128/JVI.79.10.5988-5995.2005

Wang, B., Dai, T., Sun, W., Wei, Y., Ren, J., Zhang, L., Zhang, M., & Zhou, F. (2021). Protein N-myristoylation: functions and mechanisms in control of innate immunity. Cellular and Molecular Immunology, 18(4), 878–888. https://doi.org/10.1038/S41423-021-00663-2,

Wang, R., Zhang, C., Zhang, Y., Wu, J., Zhang, Y., Zhang, L., Yu, R., & Liu, Y. (2023a). Synergetic interaction of capsid proteins for virus-like particles assembly of foot-and-mouth disease virus (serotype O) from the inclusion bodies. Protein Expression and Purification, 204. https://doi.org/10.1016/j.pep.2023.106231

Wang, X., Peng, W., Ren, J., Hu, Z., Xu, J., Lou, Z., Li, X., Yin, W., Shen, X., Porta, C., Walter, T. S., Evans, G., Axford, D., Owen, R., Rowlands, D. J., Wang, J., Stuart, D. I., Fry, E. E., & Rao, Z. (2012). A sensor-adaptor mechanism for enterovirus uncoating from structures of EV71. *Nature structural & molecular biology*, *19*(4), 424–429. https://doi.org/10.1038/nsmb.2255

Wien, M. W., Chow, M., & Hogle, J. M. (1996). Poliovirus: new insights from an old paradigm. Structure, 4, 763–767.

Wimmer E. (1982). Genome-linked proteins of viruses. Cell, 28(2), 199–201. https://doi.org/10.1016/0092-8674(82)90335-x

Wimmer, E., Hellen, C. U. T., & Cao, X. (1993a). Genetics of poliovirus. Annual Review of Genetics, 27(Volume 27,), 353–436. https://doi.org/10.1146/ANNUREV.GE.27.120193.002033/CITE/REFWORKS

Woof, J. M., & Russell, M. W. (2011). Structure and function relationships in IgA. Mucosal Immunology. https://doi.org/10.1038/mi.2011.39

Wu, T., Li, S. W., Zhang, J., Ng, M. H., Xia, N. S., & Zhao, Q. (2012). Hepatitis E vaccine development: A 14-year odyssey. Human Vaccines and Immunotherapeutics, 8(6), 823–827. https://doi.org/10.4161/HV.20042,

Xiao, C., Bator-Kelly, C. M., Rieder, E., Chipman, P. R., Craig, A., Kuhn, R. J., Wimmer, E., & Rossmann, M. G. (2005). The crystal structure of coxsackievirus A21 and its interaction with ICAM-1. Structure, 13(7), 1019–1033. https://doi.org/10.1016/j.str.2005.04.011

Xiao, Y., Chen, H. Y., Wang, Y., Yin, B., Lv, C., Mo, X., Yan, H., Xuan, Y., Huang, Y., Pang, W., Li, X., Yuan, Y. A., & Tian, K. (2016a). Large-scale production of foot-and-mouth

disease virus (serotype Asia1) VLP vaccine in Escherichia coli and protection potency evaluation in cattle. BMC Biotechnology, 16(1). https://doi.org/10.1186/s12896-016-0285-6

Xiao, Y., Zhang, S., Yan, H., Geng, X., Wang, Y., Xu, X., Wang, M., Zhang, H., Huang, B., Pang, W., Yang, M., & Tian, K. (2021). The High Immunity Induced by the Virus-Like Particles of Foot-and-Mouth Disease Virus Serotype O. Frontiers in Veterinary Science, 8. https://doi.org/10.3389/fvets.2021.633706

Xu, X., Ren, S., Chen, X., Ge, J., Xu, Z., Huang, H., Sun, H., Gu, Y., Zhou, T., Li, J., & Xu, H. (2014). Generation of hepatitis B virus PreS2-S antigen in Hansenula polymorpha. Virologica Sinica, 29(6), 403. https://doi.org/10.1007/S12250-014-3508-9

Xu, Y., Ma, S., Huang, Y., Chen, F., Chen, L., Ding, D., Zheng, Y., Li, H., Xiao, J., Feng, J., & Peng, T. (2019). Virus-like particle vaccines for poliovirus types 1, 2, and 3 with enhanced thermostability expressed in insect cells. Vaccine, 37(17), 2340–2347. https://doi.org/10.1016/j.vaccine.2019.03.031

Yafal, A. G., Kaplan, G., Racaniello, V. R., & Hogle, J. M. (1993). Characterization of poliovirus conformational alteration mediated by soluble cell receptors. Virology, 197(1), 501–505. https://doi.org/10.1006/viro.1993.1621

Yeh, M. Te, Smith, M., Carlyle, S., Konopka-Anstadt, J. L., Burns, C. C., Konz, J., Andino, R., & Macadam, A. (2023). Genetic stabilization of attenuated oral vaccines against poliovirus types 1 and 3. Nature, 619(7968), 135–142. https://doi.org/10.1038/S41586-023-06212-3,

Ypma-Wong, M. F., Dewalt, P. G., Johnson, V. H., Lamb, J. G., & Semler, B. L. (1988). Protein 3CD is the major poliovirus proteinase responsible for cleavage of the p1 capsid precursor. Virology, 166(1), 265–270. https://doi.org/10.1016/0042-6822(88)90172-9,

Yu, S. C., Lee, I. K., Kong, H. S., Shin, S. H., Hwang, S. Y., Ahn, Y. J., Park, J. H., Kim, B. Y., & Song, Y. C. (2025). Foot-and-Mouth Disease Virus-like Particles Produced in E. coli as Potential Antigens for a Novel Vaccine. Veterinary Sciences, 12(6). https://doi.org/10.3390/VETSCI12060539,

Zahid, M., Lünsdorf, H., & Rinas, U. (2015). Assessing stability and assembly of the hepatitis B surface antigen into virus-like particles during down-stream processing. Vaccine, 33(31), 3739–3745. https://doi.org/10.1016/J.VACCINE.2015.05.066,

Zhai, L., Yadav, R., Kunda, N. K., Anderson, D., Bruckner, E., Miller, E. K., Basu, R., Muttil, P., & Tumban, E. (2019). Oral immunization with bacteriophage MS2-L2 VLPs protects against oral and genital infection with multiple HPV types associated with head & neck cancers and cervical cancer. Antiviral Research, 166, 56–65. https://doi.org/10.1016/j.antiviral.2019.03.012

Zimina, A., Viktorova, E. G., Moghimi, S., Nchoutmboube, J., & Belov, G. A. (2021). Interaction of Poliovirus Capsid Proteins with the Cellular Autophagy Pathway. Viruses, 13(8), 1587. https://doi.org/10.3390/V13081587